Washington University in St. Louis
Washington University Open Scholarship

Arts & Sciences Electronic Theses and Dissertations | Arts & Sciences

Summer 8-15-2015

Peripheral and Central Mechanisms of Temporal Pattern Recognition

Christa Ann Baker
Washington University in St. Louis

Follow this and additional works at: https://openscholarship.wustl.edu/art_sci_etds

 Part of the Biology Commons

Recommended Citation
Baker, Christa Ann, "Peripheral and Central Mechanisms of Temporal Pattern Recognition" (2015). *Arts & Sciences Electronic Theses and Dissertations*. 570.
https://openscholarship.wustl.edu/art_sci_etds/570

This Dissertation is brought to you for free and open access by the Arts & Sciences at Washington University Open Scholarship. It has been accepted for inclusion in Arts & Sciences Electronic Theses and Dissertations by an authorized administrator of Washington University Open Scholarship. For more information, please contact digital@wumail.wustl.edu.

WASHINGTON UNIVERSITY IN ST. LOUIS

Division of Biology and Biomedical Sciences
Neurosciences

Dissertation Examination Committee:
Bruce A. Carlson, Chair
Dennis L. Barbour
Timothy E. Holy
Jeanne M. Nerbonne
Barani Raman

Peripheral and Central Mechanisms of Temporal Pattern Recognition

by

Christa Ann Baker

A dissertation presented to the
Graduate School of Arts & Sciences
of Washington University in
partial fulfillment of the
requirements for the degree
of Doctor of Philosophy

August 2015
St. Louis, Missouri

© 2015, Christa A. Baker

Table of Contents

List of Figures

Chapter 1

Chapter 2

Chapter 3

Chapter 4

List of Tables

Chapter 2

List of Abbreviations

AMPA	2-amino-3-(3-hydroxy-5-methyl-isoxazol-4-yl)propanoic acid
BCA	bulbar command-associated nucleus
C_m	membrane capacitance
CN	command nucleus
DFA	discriminant function analysis
DP	dorsal posterior thalamic nucleus
DSI	direction-selectivity index
EGTA	ethylene glycol tetraacetic acid
EL	exterolateral nucleus
ELa	anterior exterolateral nucleus
ELL	electrosensory lateral line lobe
ELp	posterior exterolateral nucleus
EMN	electromotor neurons
EOD	electric organ discharge
FFT	fast Fourier transform
GABA	γ-Aminobutyric acid
HEPES	4-(2-Hydroxyethyl)piperazine-1-ethanesulfonic acid
IG	isthmic granule nucleus
KO	knollenorgan
IPI	interpulse interval
MCA	mesencephalic command-associated nucleus
MRN	medullary relay nucleus

MS-222	tricaine methanesulfonate
MV	medioventral nucleus
nELL	nucleus of the electrosensory lateral line lobe
OB	olfactory bulb
PCN	precommand nucleus
PSP	post-synaptic potential
R_m	input resistance
RP	resting potential
SDF	spike-density function
SL	standard length
slem	sublemniscal nucleus
SPE	subpræeminential nucleus
tel	telencephalon
τ_m	membrane time constant
val	valvula cerebellum
V_m	membrane potential
VP	ventroposterior nucleus

Acknowledgements

I am grateful to the many people who helped make this thesis possible. First I would like to thank my advisor, Bruce Carlson, who has taught me to be a conscientious scientist and an effective communicator. I would also like to thank him for introducing me to the field of neuroethology, which has had a significant impact on how I think about and approach neuroscience, and for the opportunity to spend the past six years doing fun and exciting science. I am also indebted to current and past members of the Carlson Lab for their many contributions. Special thanks to Dr. Andrew George for troubleshooting help when I was a newborn electrophysiologist, Dr. Ariel Lyons-Warren for much-needed lunch breaks, Dr. Tsunehiko Kohashi for his scientific insights and camaraderie over the years, and Dr. Alejandro Vélez and Kimberley Sukhum for helpful feedback and discussions. I would like to thank the members of my thesis committee for advice and input that contributed greatly to my scientific development.

I would like to acknowledge the DBBS Neuroscience program, with a special thank you to Sally Vogt. Sally has been a wonderful resource over the years. She always has an ear to listen and a smile to encourage.

I am especially grateful to Dr. David Ryugo for introducing me to neuroscience and for his dedicated mentorship. I would not be a neuroscientist today without his influence.

I cannot thank my parents enough for their unwavering support and encouragement of everything that I do. I would also like to thank my friends, too numerous to mention here, for making my years as a grad student about more than just work. Special thanks to the Mighty Homunculi softball team for all the beautiful evenings in Forest Park, and to the Intelligent Designers flag football team for all the intramural championships.

Finally, a very special thank you to Kasey Wagoner. His undying patience, optimism, and sense of humor have made the (many) failures less painful and the (few) successes more rewarding. Kasey has been instrumental in encouraging both halves of my work/life balance, and he has enriched both immensely. He now knows far more about neuroscience than he ever cared to. For that, you are welcome Kasey.

The work herein was supported by the Cognitive, Computational, and Systems Neuroscience (CCSN) pathway, the National Institute on Deafness and Other Communication Disorders (F31-DC012452 to Christa Baker and F30-DC011197 to Ariel Lyons-Warren), the National Science Foundation (IOS-0818390, IOS-1050701, and IOS-1255396 to Bruce Carlson), the Uehara Memorial Foundation, and the Japan Society for the Promotion of Science (G2205 to Tsunehiko Kohashi).

ABSTRACT OF THE DISSERTATION

Peripheral and Central Mechanisms of Temporal Pattern Recognition

by

Christa Ann Baker

Doctor of Philosophy in Biology and Biomedical Sciences

Neurosciences

Washington University in St. Louis, 2015

Associate Professor Bruce A. Carlson, Chair

Encoding information into the timing patterns of action potentials, or spikes, is a strategy used broadly in neural circuits. This type of coding scheme requires downstream neurons to be sensitive to the temporal patterns of presynaptic inputs. Indeed, neurons with temporal filtering properties have been found in a wide range of sensory pathways. However, how such response properties arise was previously not well understood. The goal of my dissertation research has been to elucidate how temporal filtering by single neurons contributes to the behavioral ability to recognize timing patterns in communication signals.

I have addressed this question using mormyrid weakly electric fish, which vary the time intervals between successive electric pulses to communicate. Fish detect these signals with sensory receptors in their skin. In the majority of species, these receptors fire a single spike in response to each electric pulse. Spiking receptors faithfully encode the interpulse intervals in communication signals into interspike intervals, which are then decoded by interval-selective midbrain neurons. Using *in vivo* intracellular recordings from awake fish during sensory stimulation, I found that short-term depression and temporal summation play important roles in

establishing single-neuron interval selectivity. Moreover, the combination of short-term depression and temporal summation in the circuit resulted in greater diversity of interval tuning properties across the population of neurons, which would increase the population's ability to detect temporally patterned communication signals. Indeed, I found that the responses of single interval-selective neurons were sensitive to subtle variation in the timing patterns of a specific communication display produced by different individuals.

A subset of mormyrid species has sensory receptors that produce spontaneously oscillating potentials. How the electrosensory system of these species established sensitivity to temporally patterned communication signals was completely unknown. Using *in vivo* extracellular recordings, I demonstrated that these receptors encode sensory stimuli into phase resets, which is the first clear instance of information coding by oscillatory phase reset. Furthermore, the ongoing oscillations conferred enhanced sensitivity to fast temporal patterns that are only found in the communication signals of a large group of fish. Behavioral playback experiments provided further support for the hypothesis that oscillating receptors are specialized for detecting communication signals produced by a group of conspecifics, which is a novel role for a sensory receptor. These findings demonstrate that temporal pattern sensitivity, which was previously thought to be a central processing problem, can also arise from peripheral filtering through a novel oscillatory phase reset mechanism.

Chapter 1

Multiplexed temporal coding of electric communication signals in mormyrid fishes

This chapter contains a previously published manuscript:

Baker C.A., Kohashi T., Lyons-Warren A.M., Ma X., and Carlson B.A. (2013) Multiplexed temporal coding of electric communication signals in mormyrid fishes. *The Journal of Experimental Biology* 216:2365-2379.

Author contributions for the above citation:

C.A.B., T.K., A.M. L.-W., X.M., and B.A.C. contributed to the writing of the manuscript.

ABSTRACT

The coding of stimulus information into patterns of spike times occurs widely in sensory systems. Determining how temporally coded information is decoded by central neurons is essential to understanding how brains process sensory stimuli. Mormyrid weakly electric fishes are experts at time coding, making them an exemplary organism for addressing this question. Mormyrids generate brief, stereotyped electric pulses. Pulse waveform carries information about sender identity, and it is encoded into submillisecond-to-millisecond differences in spike timing between receptors. Mormyrids vary the time between pulses to communicate behavioral state, and these intervals are encoded into the sequence of interspike intervals within receptors. Thus, the responses of peripheral electroreceptors establish a temporally multiplexed code for communication signals, one consisting of spike timing differences between receptors and a second consisting of interspike intervals within receptors. These signals are processed in a dedicated sensory pathway, and recent studies have shed light on the mechanisms by which central circuits can extract behaviorally relevant information from multiplexed temporal codes. Evolutionary change in the anatomy of this pathway is related to differences in electrosensory perception, which appears to have influenced the diversification of electric signals and species. However, it remains unknown how this evolutionary change relates to differences in sensory coding schemes, neuronal circuitry, and central sensory processing. The mormyrid electric communication pathway is a powerful model for integrating mechanistic studies of temporal coding with evolutionary studies of correlated differences in brain and behavior to investigate neural mechanisms for processing temporal codes.

INTRODUCTION

Neurons transmit information with trains of action potentials, or spikes. The relationship between spikes and the information they represent is referred to as a neural code (Perkel and Bullock, 1968). Information can be encoded in the spike trains of single neurons or in the activity of a population of neurons. Scientists trying to understand a neural code are faced with two challenges: first, how is stimulus information encoded by the circuit, and second, how is this information decoded by postsynaptic neurons? The study of sensory systems in a wide range of animal models has revealed a variety of neural codes (Churchland and Sejnowski, 1992; Rieke et al., 1997), including rate codes, place codes, population codes, and sparse codes. Here we focus on temporal codes, in which the precise timing of action potentials carries information (Lestienne, 2001; Theunissen and Miller, 1995). Temporal codes have been implicated in the processing of somatosensory (Jones et al., 2004), olfactory (Laurent, 1997), gustatory (Di Lorenzo et al., 2009), visual (Victor and Purpura, 1996), auditory (Decharms and Merzenich, 1996), vestibular (Sadeghi et al., 2007), mechanosensory lateral line (Goulet et al., 2012), and electrosensory stimuli (Carlson, 2008b).

A sensory system can employ multiple types of codes (Ainsworth et al., 2012). For instance, the barn owl auditory system computes two sound localization cues, using a rate code for interaural level differences and a temporal code for interaural timing differences (Konishi, 1993). In addition, central circuits often convert information from one type of code to another (Groh, 2001). For example, the temporal code of the barn owl is converted into a place code within the hindbrain (Carr and Konishi, 1990). Finally, information about multiple stimulus features can be transmitted simultaneously through a single pathway by encoding information about each feature at different timescales of neural activity. Such a coding scheme is called

temporal multiplexing and it is found in visual, olfactory, auditory, electrosensory, and hippocampal pathways (Friedrich et al., 2004; Middleton et al., 2011; Panzeri et al., 2010). Temporal multiplexing is an efficient way for neural circuits to increase information transmission without requiring additional neurons.

The rich sensory coding literature provides numerous examples of temporal coding. However, with notable exceptions (i.e. coding for interaural timing differences in birds, reptiles, and mammals), we still know relatively little about the circuitry and synaptic mechanisms by which temporal codes are decoded by central neurons. Mormyrid weakly electric fishes represent an ideal system for addressing this problem because: (1) they employ two different temporal codes in a single circuit (temporal multiplexing); (2) the circuit is accessible for *in vivo* and *in vitro* electrophysiology and imaging; (3) spike timing can be easily manipulated in behaviorally relevant ways both *in vivo* and *in vitro*; (4) the behavioral significance of the multiplexed temporal codes is clear; and (5) evolutionary change in this circuit allows for a comparative approach that links changes in neural circuitry to differences in behavior. From the perspective of the central nervous system, there is no difference between the electrosense and other modalities – all stimuli are represented as patterns of spiking. Therefore, the mechanisms by which mormyrids process temporally coded information are relevant to understanding basic principles for how any neural circuit can solve this problem.

ELECTRIC SIGNALS IN MORMYRID FISHES COMMUNICATE SENDER IDENTITY AND BEHAVIORAL STATE

Two components of electrocommunication: EOD and IPI

Mormyrids produce an electric organ discharge (EOD) to communicate and actively sense their environment (Hopkins, 1986). These fish have three types of electroreceptors in their skin: mormyromasts are used for active sensing, ampullary receptors for passive sensing, and knollenorgans for communication (Bell, 1989; Bennett, 1965; Szabo and Fessard, 1974; Zakon, 1986). Communication in mormyrids consists of the discrete EOD produced with variable interpulse intervals (IPIs; Fig. 1). The EOD waveform is species-specific, and in some species it provides additional identifying information such as sex, maturity and dominance status (reviewed in Carlson, 2002a). EOD waveforms can vary in polarity, number of phases, duration of each phase, inflection, rise/fall times, and total duration (Hopkins, 1980; Hopkins, 1981). The number of phases varies from one to four, and the duration ranges from <200 μs in some species to >30 ms in others (Arnegard et al., 2010; Carlson et al., 2011; Sullivan et al., 2000).

Signaling fish vary IPIs to communicate their behavioral state, such as dominance, submission, aggression, and courtship. IPIs can range from just under 10 ms to several seconds (Carlson, 2002a; Hopkins, 1986). Several temporal patterns of IPI sequences have been identified: irregular random patterns, regularized patterns, pauses in signaling called cessations, and bursts of short-interval pulses (reviewed in Carlson, 2002a). Carlson and Hopkins (2004b) demonstrated at least three categorically distinct burst signals in *Brienomyrus brachyistius* called scallops, accelerations, and rasps, with each signal hypothesized to play different behavioral roles. Wong and Hopkins (2007) reported an additional signal in *B. brachyistius* called a creak.

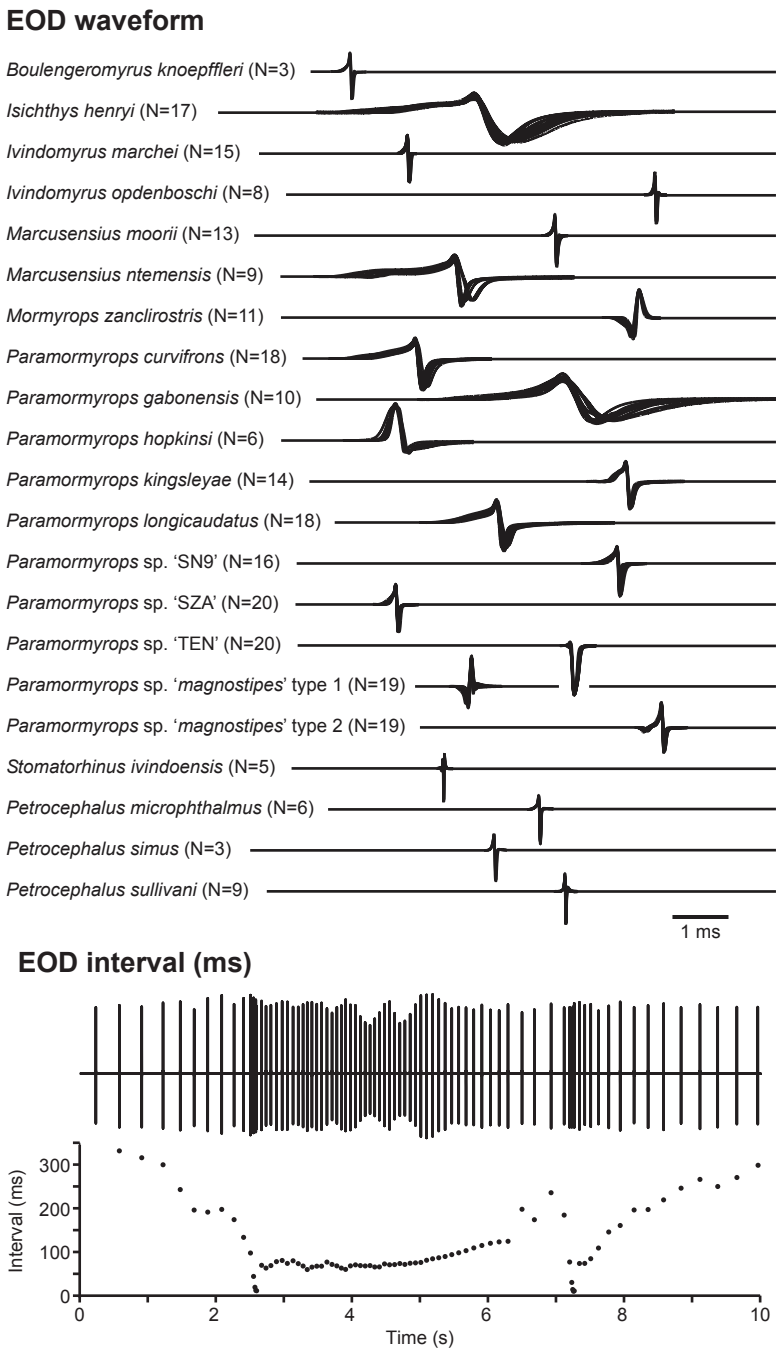

Figure 1. Mormyrid electrocommunication consists of a fixed electric organ discharge (EOD) produced at variable interpulse intervals (IPIs). Top: EOD waveforms recorded from the 21 known species within the Ivindo River of Gabon reveal that the waveforms are species-specific and span a wide range of durations (modified from Carlson et al., 2011). In each case, EOD waveforms from different individuals of the same species are normalized to the same peak-to-peak height, superimposed, and aligned to the head-positive peak (except for *Paramormyrops* sp. 'TEN', for which waveforms are aligned to the head-negative peak). Bottom: 10 s of a raw electrical recording from an isolated *Brienomyrus brachyistius*. The spike-like nature of the EODs is evident, and the amplitude changes throughout the recording as a result of the fish moving with respect to the recording electrode. Below, the raw recording has been converted into a plot that illustrates the sequence of IPIs over time.

Like rasps, creaks appear to function as a male courtship signal. Wong and Hopkins (2007) also described electrical duetting during courtship and spawning in *B. brachyistius*, in which males and females alternately generate rasps and bursts, respectively.

Additional IPI patterns include preferred latency or echo responses, in which a fish emits its own EOD at a defined interval after the EOD of another fish, and preferred latency avoidance, in which fish avoid a specific range of latencies (Arnegard and Carlson, 2005; Bauer and Kramer, 1974; Bell et al., 1974; Heiligenberg, 1976; Kramer, 1974; Kramer, 1978; Lucker and Kramer, 1981; Russell et al., 1974). The social significance of these signals is not known, though hypotheses include jamming avoidance, active jamming, dominance/submission, and sexual recognition. Other IPI patterns may serve functions such as schooling, group cohesion, and adult-young interactions (Arnegard and Carlson, 2005; Hopkins, 1977; Moller, 1976; Westby and Kirschbaum, 1978).

Electric signal generation

The EOD is produced by an electric organ located at the base of the tail (reviewed in Bass, 1986a; Bennett, 1971; Caputi et al., 2005). Individual cells, called electrocytes, act as batteries in series such that when they are activated synchronously their action potentials summate to produce the EOD. The morphology and physiology of the electrocytes determine EOD waveform (reviewed in Hopkins, 1999), and steroid hormones act directly on the electrocytes to establish EOD sex differences (Bass, 1986b; Bass and Volman, 1987; Freedman et al., 1989).

EOD production is controlled by a central electromotor command network (Fig. 2) composed of the command nucleus (CN), medullary relay nucleus (MRN), and bulbar command-

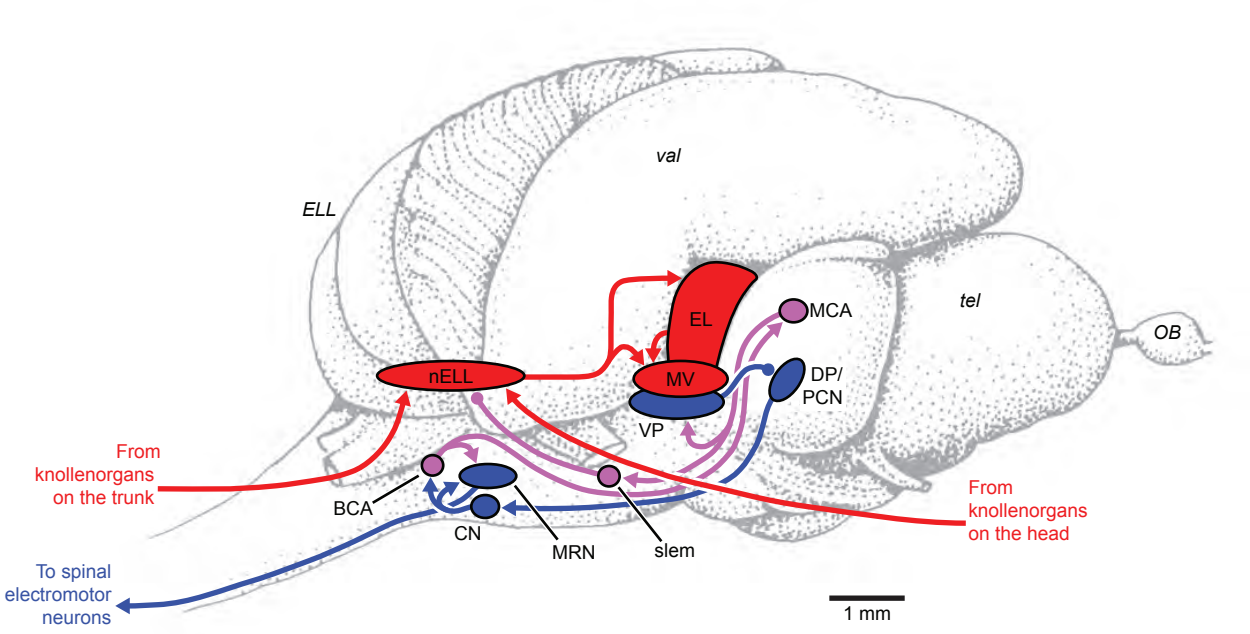

Figure 2. Neuroanatomy of the knollenorgan electrosensory (red), electromotor (blue), and corollary discharge (purple) pathways. Excitatory connections are indicated by arrows and inhibitory connections by punctate terminals. Knollenorgan electroreceptors project somatotopically to the hindbrain nucleus of the electrosensory lateral line lobe (nELL), which projects to two nuclei of the torus semicircularis: the exterolateral nucleus (EL) and the medioventral nucleus (MV). Each EOD command originates in the command nucleus (CN). CN projects to the medullary relay nucleus (MRN), which in turn innervates the electromotor neurons in the spinal cord that innervate the electric organ. CN output is influenced by excitation from the precommand nucleus (PCN) and the dorsal posterior thalamic nucleus (DP), both of which receive inhibition from the ventroposterior nucleus (VP). When CN initiates an EOD, it sends a copy of this signal to the bulbar command-associated nucleus (BCA), which projects to MRN and to the mesencephalic command-associated nucleus (MCA), which mediates inhibition of the motor pathway through VP, and inhibition of the KO sensory pathway through the sublemniscal nucleus (slem). *ELL*, electrosensory lateral line lobe; *OB*, olfactory bulb; *tel*, telencephalon; *val*, valvula of the cerebellum.

associated nucleus (BCA) (Bell et al., 1983; Grant et al., 1986). MRN projects to the electromotor neurons (EMNs) in the spinal cord, which innervate the electrocytes of the electric organ (Bennett et al., 1967; Grant et al., 1986). Neurons in CN, MRN, and EMN are extensively connected by gap junctions both within and between nuclei to promote synchronous activation of electrocytes (Bennett et al., 1967; Bennett et al., 1963; Elekes et al., 1985; Elekes and Szabo, 1985; Grant et al., 1986). EOD production is primarily influenced by excitatory inputs to CN from the midbrain precommand nucleus (PCN) and the dorsal posterior thalamic nucleus (DP) (Bell et al., 1983; Carlson, 2002b; Carlson, 2003; Carlson and Hopkins, 2004a; von der Emde et al., 2000).

The electromotor command network also gives rise to a corollary discharge pathway that provides motor-related inputs to electrosensory pathways. This corollary discharge is initiated in BCA, which projects to the paratrigeminal command-associated nucleus and mesencephalic command-associated nucleus (MCA) (Bell et al., 1983; Carlson, 2002b). MCA in turn projects to the sublemniscal nucleus (slem), which delivers inhibition onto neurons in the electrosensory hindbrain that blocks responses to the fish's own EOD (Bell and Grant, 1989). DP and PCN also receive corollary discharge-mediated inhibition from the dorsal portion of the ventroposterior nucleus (VP) of the torus semicircularis, which receives input from MCA (Carlson, 2002b; Carlson, 2003; Carlson and Hopkins, 2004a; von der Emde et al., 2000). This recurrent inhibition appears to regulate EOD output (Carlson and Hopkins, 2004a).

Playback experiments reveal the behavioral significance of EOD waveform and IPI patterns

Electric signals are easy to record, manipulate, and play back, allowing investigators to present modified versions of natural signals to identify the specific signal components relevant to any given behavior. Such studies reveal that mormyrids vary in their ability to discriminate temporal variation in EOD waveform (Carlson et al., 2011). There are two subfamilies of mormyrids, the Mormyrinae and Petrocephalinae (Fig. 3) (Sullivan et al., 2000). A specific lineage of mormyrines called 'clade A' can detect small phase shifts in the EOD waveform, as small as 2 μs in *Pollimyrus adspersus* (Paintner and Kramer, 2003). By contrast, most non-clade A species are unable to detect even maximal phase shifts in the EOD waveform, and this perceptual difference is related to key anatomical differences in their peripheral and central electrosensory systems (Carlson et al., 2011).

The functional significance of EOD waveform variation for electric communication has been addressed in several behavior studies on clade A species, which suggest a key role for the EOD in species recognition and mate choice (Arnegard et al., 2006; Feulner et al., 2009; Hopkins and Bass, 1981; Machnik and Kramer, 2008; Markowski et al., 2008). In species with sex differences in EODs, the male EOD is always longer than the female EOD (Carlson and Arnegard, 2011; Hopkins, 1986). In *Marcusenius macrolepidotus*, EOD duration correlates with male body length, and longer EODs elicit more male aggression than shorter EODs, suggesting that the EOD in this species may be an honest indicator of size (Hanika and Kramer, 2005). *Pollimyrus isidori* and *Gnathonemus petersii* can be trained to distinguish individual differences in EOD waveform (Graff and Kramer, 1992), and *M. macrolepidotus* appear to recognize familiar individuals on this basis (Hanika and Kramer, 2005).

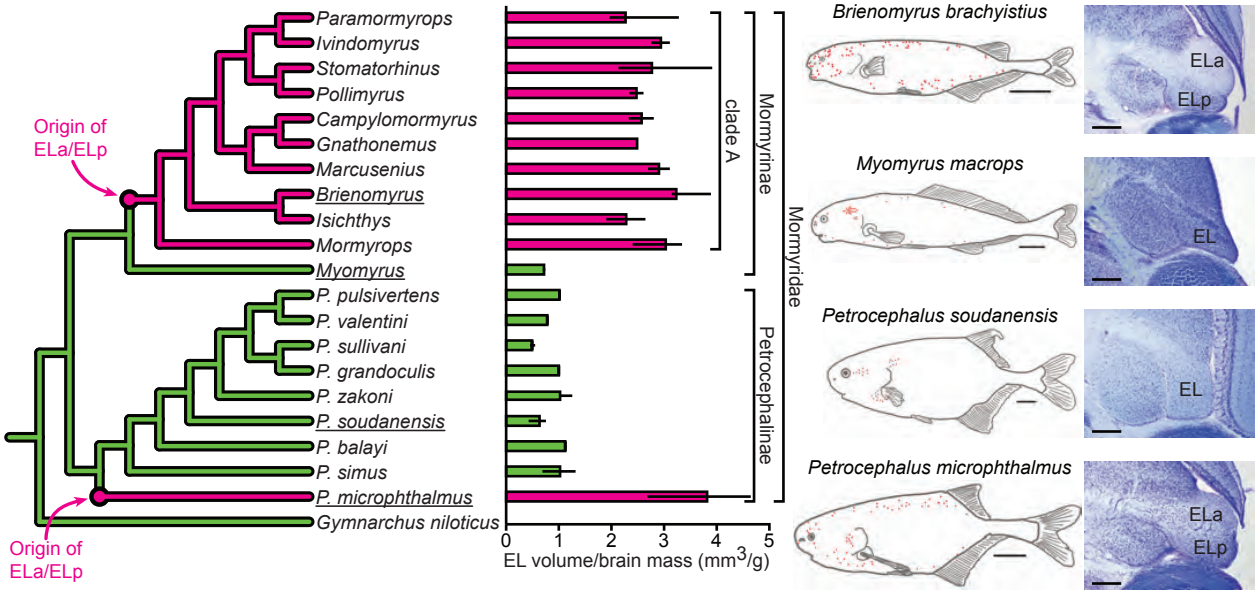

Figure 3. Evolutionary change in the knollenorgan electrosensory system (modified from Carlson et al., 2011). The cladogram on the left illustrates the transition from a relatively small exterolateral nucleus (EL, green) to an enlarged EL with separate anterior and posterior subdivisions (ELa/ELp, magenta). Normalized EL sizes of each branch are shown to the right (median ± range). A parsimonious reconstruction suggests that ELa/ELp evolved twice, once in the lineage leading to clade A within the subfamily Mormyrinae and once in the lineage leading to *Petrocephalus microphthalmus* within the subfamily Petrocephalinae. The locations of knollenorgans on the body surface (red dots) and 50 µm horizontal sections of the midbrain highlighting EL and ELa/ELp from four different species are shown at the far right (these species are underlined in the cladogram). Scale bars are 1 mm for the fish outlines, and 300 µm for the brain sections.

Playback experiments have also revealed the critical role of IPIs in social behavior. *G. petersii* display more aggression towards a playback electrode delivering IPI patterns recorded from attacking fish than from resting fish (Kramer, 1979). In addition, *G. petersii* approached a playback electrode more often when a natural sequence of IPIs was presented than when a randomized sequence of the same IPIs was presented (Teyssedre and Serrier, 1986). Therefore, the precise serial ordering of IPIs, and not just overall IPI distribution, appears to carry important information. Species differences in IPI patterns may even mediate species recognition in some cases (Kramer and Kuhn, 1994). IPIs may be particularly important for species recognition in non-clade A species that cannot detect EOD waveform variation (Carlson and Arnegard, 2011).

PERIPHERAL CODING OF COMMUNICATION SIGNALS: TWO TEMPORAL CODES, ONE CIRCUIT

Electrocommunication signals are detected by peripheral sensory receptors called knollenorgans (KOs) (Derbin and Szabo, 1968; Franz, 1921). The locations of KOs on the body surface are remarkably diverse (Fig. 3). In clade A species, KOs are widely distributed across the head, back, and underbelly of the fish (Carlson et al., 2011; Harder, 1968). In one clade A genus, *Mormyrus*, KOs are also found on the side of the body (Harder, 1968). In most petrocephaline species, however, KOs are clustered into distinct rosettes, with one rosette near the eye, one near the gill, and one near the base of the pectoral fin (Carlson et al., 2011; Harder, 1968; Lavoué et al., 2004; Lavoué et al., 2010). Two petrocephaline species are exceptional in having a broad distribution of KOs similar to clade A (Carlson et al., 2011; Lavoué et al., 2010). Finally, the only non-clade A mormyrine genus, *Myomyrus*, is unique in having an intermediate pattern, with

a single rosette near the back of the head and a relatively sparse distribution of receptors across the head, back, and underbelly (Carlson et al., 2011).

Each KO consists of a canal in the epidermis that opens into a chamber lined with flattened epithelial cells (Derbin and Szabo, 1968). The canal is filled with a plug of loose epithelial cells, which adds a series capacitance to the organ (Zakon, 1986). This capacitance, along with the parallel resistive properties of the surrounding skin, makes the organ AC-coupled, establishing tuning to the high frequencies that characterize the power spectra of EODs (Bennett, 1965; Lyons-Warren et al., 2012a). Inside the chamber are one to ten sensory cells (up to 40 in petrocephaline rosettes) (Derbin and Szabo, 1968; Harder, 1968; Szabo, 1965). A single myelinated afferent fiber branches to innervate all sensory cells within a KO (Derbin and Szabo, 1968; Jørgensen, 2005).

Our understanding of KO stimulus encoding is limited to studies of broadly distributed KOs in clade A species, which generate spike-like potentials in response to electrosensory stimuli (Bennett, 1965). The rosette-type KOs of petrocephalines do not appear to spike; instead, they continuously oscillate at up to 3 kHz (Harder, 1968). How rosette-type KOs encode electric signals remains unknown.

Clade A KOs are tuned to frequencies roughly matching the power spectrum of the species-specific EOD (Hopkins, 1981), and their sensitivity increases with increasing pulse duration (Lyons-Warren et al., 2012a). Variation in duration tuning among KOs may establish a population code for pulse duration at low intensities, when signaling fish are at a distance (Lyons-Warren et al., 2012a). At higher intensities, however, when signaling fish are close by and most of the receptors are responsive, a temporal code is used for encoding duration (Hopkins and Bass, 1981; Lyons-Warren et al., 2012a).

KOs spike with a latency of ~100 ms in response to positive changes in voltage across the skin, or inward current (Bennett, 1965). Because they are AC-coupled, KOs respond both to the onset of positive voltage steps and to the offset of negative voltage steps. Since each KO faces "out" towards the surrounding water, KOs on opposite sides of the body point in opposite directions. Thus, for any given electrical potential, KOs on one side of the body will receive an inward current whereas KOs on the other side of the body will receive an outward current, and this results in differences in spike timing between receptors on opposite sides of the body. For instance, in response to a positive voltage step applied to one side of the body, ipsilateral KOs will spike at the onset, whereas contralateral KOs will spike at the offset. These observations led Hopkins and Bass (1981) to propose a start-stop temporal code for EOD waveform, in which KOs on one side of the body respond to the start of a signal, KOs on the opposite side of the body respond to the end of the signal, and the difference in spike timing between them encodes signal duration. More complex, multiphasic signals, such as natural EODs, would result in different subsets of KOs responding to different stimulus edges, depending on stimulus intensity at the receptor pore (Fig. 4). Therefore, spike timing differences, in the submillisecond-to-millisecond range, between KOs represent the EOD waveform.

KO afferents follow stimulation rates up to 500 Hz, corresponding to interspike intervals of 2 ms (Bell and Grant, 1989). The shortest IPI observed in signaling fish is just below 10 ms (Carlson, 2002a; Hopkins, 1986), meaning KOs faithfully represent the timing of each EOD with a single, phase-locked spike. Therefore, interspike intervals, on the order of tens of milliseconds to seconds, within each KO represent the IPIs in electrocommunication signals.

The responses of peripheral receptors thus establish two distinct temporal codes for electrocommunication signals: differences in spike timing between KOs code for EOD

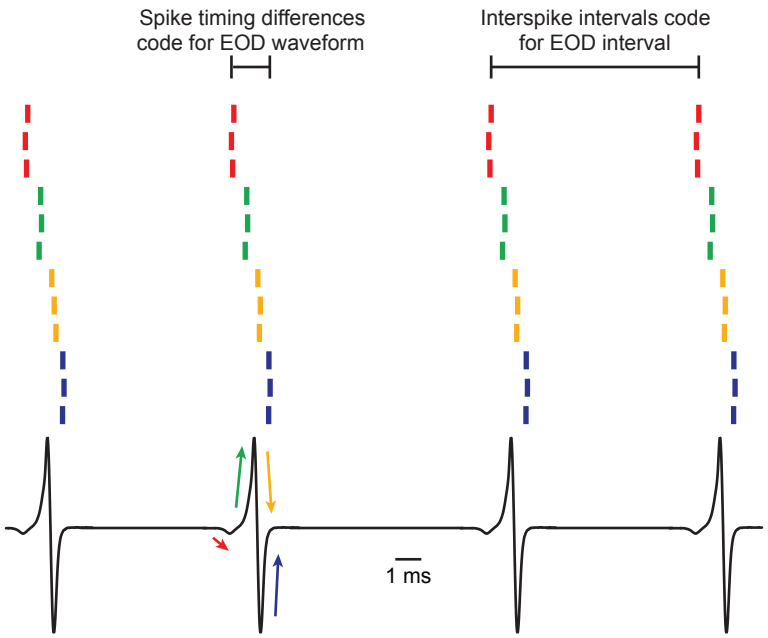

Figure 4. Temporal multiplexing of electrocommunication signals by knollenorgans. This schematic representation shows a train of EOD stimuli at the bottom, with the responses of different knollenorgans to these stimuli above. Each row represents a different knollenorgan and each tick mark indicates the timing of an individual spike. The location of each knollenorgan on the body surface with respect to the electric field determines which edge of the EOD waveform it will respond to, and the spikes are color-coded for the edge (arrows) to which the knollenorgan is responding. Spike timing differences between different knollenorgans represent EOD waveform, whereas interspike intervals within each knollenorgan represent EOD intervals.

waveform, and interspike intervals within KOs code for IPI (Fig. 4). Both of these temporal codes are similar to those used in other sensory systems. For example, sound localization, echolocation, localization of tactile stimuli, and visual motion detection rely on response timing differences between different sensory receptors, and timing sequences within a stimulus are used for the discrimination of tactile texture, and the pitch, timbre, and rhythm of speech (Cariani, 2001). Whereas the importance of temporal coding in sensory systems is clear, our understanding of how these temporal codes are processed is still developing.

The use of different time scales and different temporal coding schemes to encode multiple features of communication signals by KOs is a textbook example of temporal multiplexing (Panzeri et al., 2010). Another example of multiplexing occurs in the zebrafish olfactory bulb, where mitral cells represent general odor category in the precise phase-locking of spikes to oscillatory field potentials, and specific odor identity in non-phase-locked spike rates (Friedrich et al., 2004). Analyzing mitral cell output with low temporal resolution provides information about precise odor identity, whereas analyzing with higher temporal resolution provides information about broad odor category. Temporal filtering of mitral cell output in the telencephalon therefore allows for the extraction of odor identity without distorting the code for odor category (Blumhagen et al., 2011). We will see that a similar computation is performed in the KO pathway.

A SENSORY PATHWAY DEVOTED TO COMMUNICATION BEHAVIOR

Electrocommunication signals are processed by a dedicated sensory pathway (Fig. 2). KO afferent fibers conduct at 40 m/s to the ipsilateral nucleus of the electrosensory lateral line lobe (nELL) in the hindbrain (Enger et al., 1976a), where corollary discharge inhibition blocks

responses to the fish's own EOD (Bell and Grant, 1989; Zipser and Bennett, 1976). That is, each time an EOD motor command is generated, nELL neurons receive inhibition that prevents them from responding to sensory input. In this manner, the KO pathway is dedicated to processing communication signals: responses to the fish's own EOD never get past the hindbrain (Carlson, 2008a).

The axons of nELL neurons project bilaterally through the lateral lemniscus to the midbrain torus semicircularis (Fig. 2), homologue of the mammalian inferior colliculus (Nieuwenhuys et al., 1998). These axons conduct at 15 m/sec (Amagai et al., 1998; Enger et al., 1976a; Enger et al., 1976b). The main projection from nELL is to the exterolateral nucleus (EL), although en route the ascending axons give off small branches that terminate in the medioventral nucleus (MV) (Amagai et al., 1998; Enger et al., 1976a; Enger et al., 1976b; Friedman and Hopkins, 1998).

The structure of the mormyrid EL can take one of two forms (Fig. 3). In clade A, EL is subdivided into anterior (ELa) and posterior (ELp) regions (Xu-Friedman and Hopkins, 1999). In most petrocephalines and in the non-clade A mormyrine genus *Myomyrus*, however, the EL is a relatively small, homogeneous structure lacking any apparent subdivisions (Carlson et al., 2011). A subdivided ELa/ELp has been found in one non-clade A species, *Petrocephalus microphthalmus* (Carlson et al., 2011). Interestingly, this species also has broadly distributed KOs typical of clade A, and it is the only known petrocephaline with the ability to discriminate variation in EOD waveform.

Virtually nothing is currently known about the circuitry and physiology of EL, whereas we are starting to understand quite a bit about ELa/ELp (Fig. 5). The axons of nELL neurons terminate in ELa, which contains two cell types: large GABAergic inhibitory interneurons and

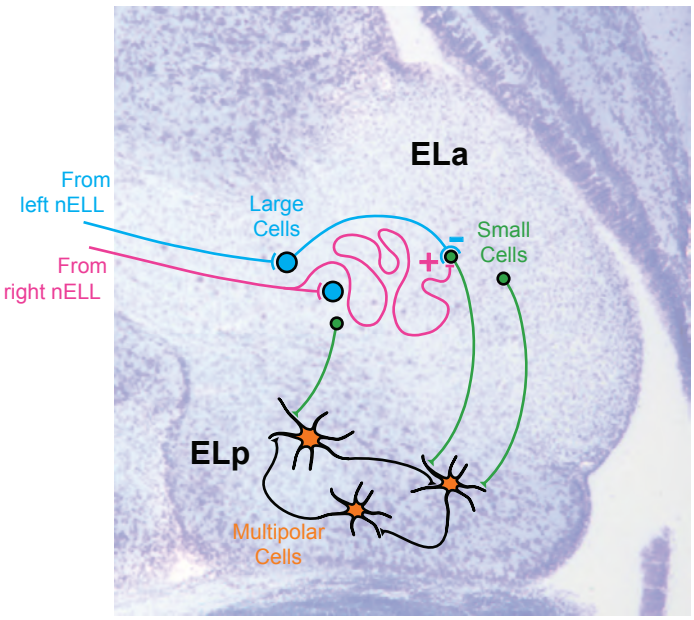

Figure 5. ELa and ELp microcircuitry overlaid on a horizontal Nissl section through the midbrain of *Brienomyrus brachyistius* (schematic cells are not to scale). As nELL axons enter ELa, they synapse directly onto adendritic large cells before following a convoluted path to synapse onto adendritic small cells. Large cells are entirely intrinsic to ELa, providing inhibitory input onto small cells via a large calyx-like terminal. Small cells are hypothesized to act as time comparators that integrate inhibition from one side of the body with excitation from the opposite side of the body to recode the peripheral spike timing differences that code for EOD waveform. ELa small cells project to multipolar cells in ELp. The microcircuitry within ELp is less well understood, although there are extensive excitatory and inhibitory interactions among the multipolar cells. Temporal filtering of small cell outputs by the circuit in ELp establishes tuning to the peripheral spike timing differences that code for IPI.

small excitatory projection neurons (Friedman and Hopkins, 1998; George et al., 2011; Mugnaini and Maler, 1987a; Szabo et al., 1975). Local circuitry within ELa performs the first stages of EOD waveform analysis (Lyons-Warren et al., 2012b; Xu-Friedman and Hopkins, 1999). ELa sends its only outputs to the adjacent ELp, where the first stages of IPI analysis occurs (Carlson, 2009). ELp projects to the isthmic granule nucleus (IG), which in turn projects back to ELp and to the valvula cerebellum (Finger et al., 1981; Haugede-Carre, 1979). The role of the feedback projection from IG to ELp is not yet understood. The IG-valvula connection is thought to be the main pathway by which electrocommunication information reaches the cerebellum (Russell and Bell, 1978). Horseradish peroxidase injections into ELp also retrogradely labeled small perilemniscal neurons in the caudal midbrain and neurons in the rostral midbrain in an area ventral to the torus longitudinalis (Finger et al., 1981), although the functions of these putative inputs to ELp are not known.

ELp also projects bilaterally to the subpræeminential nucleus (SPE) and ipsilaterally to the inferior olive and MV (Haugede-Carre, 1979). MV therefore receives a direct projection from the nELL, as well as an indirect projection via EL (Fig. 2). MV projects to the optic tectum (Wullimann and Northcutt, 1990), homologue of the mammalian superior colliculus (Nieuwenhuys et al., 1998). The function of the MV-optic tectum pathway is currently unknown; however, the optic tecta of many taxa contain spatial maps of multiple sensory modalities. Therefore, one hypothesis is that MV plays a role in localizing signaling fish (Friedman and Hopkins, 1998). MV may also provide a minor projection to the KO region of the valvula cerebellum (Finger et al., 1981). Responses to electrosensory stimuli can be recorded in the telencephalon (Prechtl et al., 1998), and at least some of these responses are likely mediated by the KO pathway. It remains unknown how electrosensory information from KOs may reach the

telencephalon, although a projection from the valvula cerebellum has been described (Wullimann and Rooney, 1990). Clearly, much remains to be learned about the processing of electrocommunication signals after ELp.

The KO pathway contains several anatomical specializations characteristic of time-coding circuits. First, the channel for processing communication signals is dedicated to this task and it remains segregated from other electrosensory pathways. Second, the timing of sensory events is encoded by precisely time-locked spikes in KO receptors, nELL axons, and ELa large cells (Amagai et al., 1998; Bennett, 1965; Friedman and Hopkins, 1998). Third, both nELL and ELa contain large adendritic neurons (Amagai et al., 1998; Szabo and Ravaille, 1976). Larger neurons are required to maintain axons with large diameters, which conduct impulses with greater velocity than axons of smaller diameter (Waxman, 1980). The heavy myelination of nELL axons further aids in increasing conduction velocity. In addition, larger neurons have lower input resistance and greater ability to generate current, thereby resulting in neurons that are less susceptible to voltage fluctuations caused by stray currents (Carr and Friedman, 1999). However, larger neurons require a larger synaptic current, which is achieved by large synaptic terminals and gap junctions onto the large cells of both nELL and ELa (Bell and Russell, 1978; Mugnaini and Maler, 1987a; Mugnaini and Maler, 1987b; Szabo and Ravaille, 1976; Szabo et al., 1983). Larger synaptic endings also transmit with lower temporal jitter (Trussell, 2008), and electric coupling through gap junctions further helps preserve timing information by reducing transmission time. Another, although less well understood, specialization common to time-coding pathways is an abundance of calcium-binding proteins (Carr and Friedman, 1999). These proteins may decrease presynaptic levels of calcium soon after synaptic transmission to shorten postsynaptic potentials, or to prevent the buildup of harmful loads of calcium as a byproduct of

large synaptic currents (Friedman and Kawasaki, 1997). The large cells of nELL and ELa are immunoreactive to the calcium-binding proteins calretinin and calbindin, with precise staining patterns varying across species (Friedman and Kawasaki, 1997). Additional specializations that contribute to timing preservation in auditory pathways include AMPA-receptor splice variants with exceptionally fast kinetics and high calcium permeability, voltage-gated potassium channels, and large, fast inhibitory postsynaptic currents (Trussell, 1997), although similar features have not yet been found in the KO pathway.

SENSORY FILTERING AND TEMPORAL SHARPENING

Sensory-evoked spikes are relayed by KO afferents to the ipsilateral nELL (Fig. 2), where they terminate with large club endings onto large, adendritic, spherical neurons via mixed chemical-electrical synapses (Bell and Grant, 1989; Bell and Russell, 1978; Denizot et al., 1987; Mugnaini and Maler, 1987b; Szabo and Ravaille, 1976; Szabo et al., 1983). Each KO afferent contacts three to eleven nELL cells, and an estimated three to four afferents converge onto each nELL cell (Bell and Grant, 1989).

In addition to excitation from KO afferents, nELL cells receive GABAergic inhibitory input from the slem via small boutons that terminate on the soma and axon initial segment (Bell et al., 1981; Denizot et al., 1987; Mugnaini and Maler, 1987b; Szabo et al., 1983). The slem receives input from MCA and thereby mediates corollary discharge-driven inhibition of nELL neurons (Fig. 2), which blocks sensory responses for a brief window of time immediately after production of the fish's own EOD (Zipser and Bennett, 1976). The effects of this corollary discharge-driven inhibition can be seen downstream of the nELL, as stimuli delivered during a period of about 3 ms starting immediately after the production of each EOD do not elicit

electrosensory responses in the EL or KO region of the valvula (Amagai, 1998; Bennett and Steinbach, 1969; Russell and Bell, 1978; Szabo et al., 1979; Zipser and Bennett, 1976). Behavioral studies have confirmed that fish are less sensitive to electrosensory stimuli occurring within 1.5 ms after the fish's own EOD (Moller, 1970).

Broad somatotopy is evident in the KO projections to nELL, such that afferents arising from the dorsal surface of the skin terminate ventrally, and those from the ventral surface terminate dorsally (Bell and Russell, 1978; Maler et al., 1973a; Maler et al., 1973b). Further, afferents from the head project to the rostral nELL, and those from the tail project to the caudal nELL. Accordingly, the latency of potentials in response to sensory stimulation is shortest in the rostral nELL and longest in the caudal nELL. A matching latency gradient is present in the corollary discharge potentials recorded at different locations within the nELL (Bell and Grant, 1989). Thus, the corollary discharge is effective at blocking KO responses to the fish's own EOD, with anatomical adjustments accounting for differences in conduction time from KOs on different parts of the body. The duration of mormyrid EODs spans a wide range across species (Fig. 1), and it remains to be determined whether the window of corollary discharge-driven inhibition varies in relation to species differences in EOD duration. Another open question is whether nELL projections to the midbrain incorporate compensatory delays to account for the differences in latency from KOs on the tail compared to those on the head.

The nELL has been considered to simply relay spike times from peripheral receptors to the midbrain. However, comparing the microcircuitry within nELL with other sensory pathways suggests that the temporal codes established by KOs may be sharpened in nELL. First, the convergence of multiple time-locked inputs has been proposed to enhance temporal precision by reducing jitter in the postsynaptic neuron (Carr et al., 1986a; Kawasaki et al., 1988). Such a

mechanism has been implicated in the sharpening of phase-locking in auditory pathways (Joris et al., 1994; Sullivan and Konishi, 1984). When *n* correlated inputs converge onto a single neuron, the jitter of the response of the postsynaptic neuron should be reduced by $1/\sqrt{n}$ (Calvin, 1983). This hypothesis was tested in the mouse auditory brainstem by Xu-Friedman and Regehr (2005), who found that convergence of multiple inputs onto single postsynaptic neurons reduces jitter, with the degree of jitter reduction determined by the number, strength, and timing of inputs. The spherical soma and long, thin initial segment of nELL cells may also contribute to enhancing their temporal precision. An electron-dense undercoating thought to represent the spike-initiation zone occurs distally on the initial segment (Mugnaini and Maler, 1987b). Thus, synaptic currents must traverse a region of low input resistance (large adendritic soma) followed by a region of high input resistance ("uncoated" proximal initial segment) before reaching the spike initiation zone. This may provide a mechanism to "discard" synaptic inputs not arriving in sufficient synchrony with other inputs (Maler et al., 1981). Neurons with similar morphology have been found in the time coding pathways of multiple, distantly related species of wave-type weakly electric fish (Carr et al., 1986b; Kawasaki and Guo, 1996; Maler et al., 1981). Further, convergence of multiple synaptic inputs onto such neurons is associated with postsynaptic reductions in temporal jitter (Carr et al., 1986a). Thus, convergence of multiple inputs onto spherical somas with long initial segments and distal spike-initiation zones could represent a general adaptation for temporal coding.

DETERMINING SENDER IDENTITY: A CIRCUIT FOR PROCESSING SUBMILLISECOND SPIKE TIMING DIFFERENCES

In species with an ELa/ELp, the axons of nELL cells project bilaterally to the ELa (Figs. 2, 5), with ~60% of the axons arising contralaterally and ~40% arising ipsilaterally (Amagai et al., 1998; Bell et al., 1981; Bell and Grant, 1989; Enger et al., 1976b; Friedman and Hopkins, 1998; Szabo et al., 1983). At least some of the nELL cells bifurcate, giving rise to bilateral ELa projections (Friedman and Hopkins, 1998). The nELL-ELa projections show no obvious somatotopy (Bell and Maler, 2005; Friedman and Hopkins, 1998). In addition to incoming nELL axons, ELa contains large GABAergic inhibitory interneurons and small projection neurons (Friedman and Hopkins, 1998; Mugnaini and Maler, 1987a). The large cells of *Brienomyrus brachyistius* are adendritic, measure 9-18 μm in diameter, and are predominately located in the medial portion of ELa, where incoming nELL axons enter the nucleus (Friedman and Hopkins, 1998; George et al., 2011). Interestingly, the large cells of *Gnathonemus petersii* have dendrites (Mugnaini and Maler, 1987a), indicating important species differences in ELa microcircuitry. In both species, small cells are adendritic, measure 3-7 μm in diameter, and are distributed throughout ELa (Amagai et al., 1998; Friedman and Hopkins, 1998; George et al., 2011; Mugnaini and Maler, 1987a).

As nELL axons enter ELa, they first contact one to three large cells with large, cup-like endings giving rise to mixed chemical-electrical synapses (Mugnaini and Maler, 1987a; Szabo et al., 1983). Each nELL axon then follows a long and tortuous path, traveling for up to an additional 7 mm after the first synapse onto a large cell (Friedman and Hopkins, 1998). As an nELL axon winds through the ELa, it makes small en passant mixed chemical-electrical excitatory endings onto dozens of small cells, although the majority of these endings are made by

the last 1-2 mm of the axon (Friedman and Hopkins, 1998; Xu-Friedman and Hopkins, 1999). Large cells project directly to small cells with a more restricted terminal field, giving rise to large GABAergic calyceal synapses that envelop the small cell somas (Friedman and Hopkins, 1998; George et al., 2011; Mugnaini and Maler, 1987a). Sensory stimulation elicits a time-locked action potential in both nELL axons and large cells at a latency of ~2.5-3 ms and with low jitter following a stimulus edge, reflecting the "on" or "off" responses of KOs (Amagai et al., 1998; Friedman and Hopkins, 1998). Taken together, these findings suggest that small cells receive delayed excitatory input via an nELL axon, and time-locked inhibitory input via a large cell (Fig. 5).

ELa small cells are hypothesized to perform analysis of the small spike timing differences between peripheral receptors that represent EOD waveform. Several lines of evidence support this hypothesis. First, ELa is the first station in the KO pathway where information from opposite sides of the body converges (Szabo et al., 1983), and small cells appear to be the only cells in ELa that receive inputs from different receptive fields (Friedman and Hopkins, 1998; Xu-Friedman and Hopkins, 1999). Second, small cells are adendritic, and time comparator neurons in other circuits are typically adendritic or have minimally branching dendritic arbors (Carr et al., 1986a; Carr and Konishi, 1990; Grothe, 2003; Matsushita and Kawasaki, 2004). Third, variation in nELL axon lengths to small cells function as delay lines (Friedman and Hopkins, 1998), similar to the delay lines found in certain sound localization circuits (Carr, 1993). Fourth, the large calyceal ending onto small cells presumably makes the inhibitory transmission fast and reliable, as seen in the excitatory calyx of Held in the mammalian auditory system (Nicol and Walmsley, 2002). Fifth, anatomical specializations for preserving timing information disappear at small cells (Friedman and Kawasaki, 1997; Xu-

Friedman and Hopkins, 1999). Finally, ELp neurons that receive input from small cells are tuned to pulse waveform (Amagai, 1998).

These various lines of evidence led Friedman and Hopkins (1998) to propose a delay-line anti-coincidence detection mechanism for small cell encoding of stimulus duration. In this model, each small cell receives inhibition elicited by one edge of a stimulus pulse and delayed excitation elicited by the other edge (Fig. 6). A given small cell will respond only if the excitatory and inhibitory inputs are not coincident, i.e. if the two inputs are separated in time. The relative timing of these inputs is determined by the duration of the stimulus pulse as well as the length of the axonal delay to the small cell. For short stimulus durations, inhibition in response to the trailing stimulus edge will block the delayed excitation in response to the leading edge, but for longer durations, the delayed excitation will arrive before the inhibition (Fig. 6). Therefore, this model predicts that each small cell will only respond to stimuli longer than a certain minimum duration, and variation in axonal delay across the population of small cells will establish variation in this minimum duration (Fig. 6). Under this model, then, small cells would recode peripheral timing differences into a population code, with the number of responding small cells increasing with increasing stimulus pulse duration.

Unfortunately, small cells are extremely difficult to record from so that direct tests of this model have not yet been possible (Amagai et al., 1998; Friedman and Hopkins, 1998; Xu-Friedman and Hopkins, 1999). However, we recently developed a novel fluorescence-based method for obtaining targeted extracellular recordings from small cell axons (Lyons-Warren et al., in press). Preliminary results suggest that variably delayed excitation and precisely timed inhibition in response to different stimulus edges are indeed important in establishing small cell responses, but that multiple excitatory inputs to small cells, as well as relatively short axonal

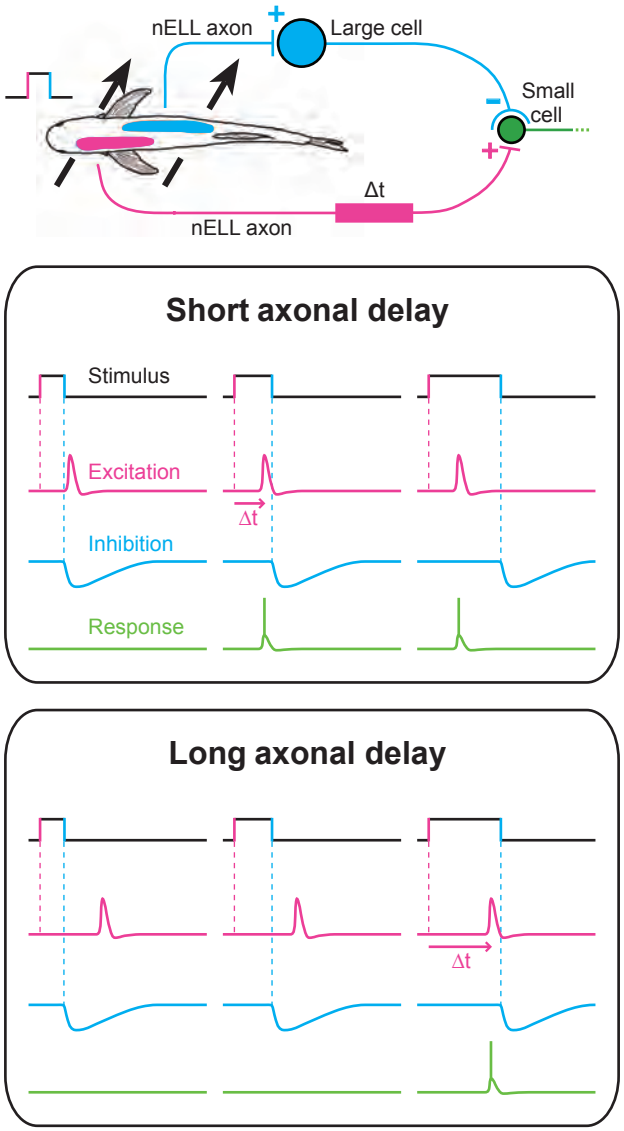

Figure 6. Friedman-Hopkins model for small cell duration tuning (modified from Xu-Friedman and Hopkins, 1999). Knollenorgans on one side of the body surface (pink) respond to the upward edge of a square pulse, and this gives rise to an excitatory input to a small cell via an nELL axonal delay line (Δt). Knollenorgans on the other side of the body surface (blue) respond to the downward edge, and this gives rise to an inhibitory input to the small cell via an ELa large cell. This is just one example of many possible receptive field organizations of the excitatory and inhibitory inputs to small cells. The responses of small cells to stimuli of different durations are determined by the length of the excitatory axonal delay (below). For short duration stimuli, inhibition in response to stimulus offset blocks the delayed excitation in response to stimulus onset. For pulses that are longer than the excitatory delay, however, the delayed excitation arrives before the inhibition, and the small cell responds. Different small cells receive excitatory input with different delays, establishing variation in the minimum pulse duration that can elicit a response. As a result, increasing pulse duration leads to the progressive recruitment of small cells with longer axonal delays, and pulse duration is reflected in the total number of responding cells.

delays to some cells, make for more complicated patterns of tuning than predicted by the Friedman-Hopkins model (Lyons-Warren et al., 2012b). This scenario would result in a distributed population code, with the identity of responsive small cells, and not just total number, reflecting EOD waveform (Fig. 7). This would represent a novel mechanism for recoding submillisecond timing differences, distinct from avian sound localization pathways that use delay-line coincidence detection to convert a temporal code into a place code, as well as mammalian sound localization pathways that use binaural excitation combined with monaural inhibition to convert a temporal code into a rate code (Köppl, 2009; Schnupp and Carr, 2009).

Small cell axons project topographically to ELp, with medial small cells projecting medially and lateral small cells projecting laterally (Friedman and Hopkins, 1998). The anatomy of ELp indicates that it is a region of substantial local processing. First, ELp neurons, with somatic diameters of 6-14 μm, exhibit widely branching dendritic arbors spanning up to 200 μm in diameter (George et al., 2011; Xu-Friedman and Hopkins, 1999), suggesting extensive synaptic integration. Second, ELp contains inhibitory GABAergic interneurons (George et al., 2011). Third, in addition to their extrinsic projections, the axons of individual ELp neurons give rise to collaterals that project throughout the nucleus (George et al., 2011; Xu-Friedman and Hopkins, 1999). Fourth, ELp neurons exhibit a range of response latencies to sensory stimulation: some neurons respond in a time-locked manner 7-9 ms after a stimulus, whereas others respond with variable latencies of 12-20 ms, longer than would be expected from a direct excitatory input from ELa (Amagai, 1998). Fifth, multiple phases of excitation and inhibition can often be seen in intracellular recordings from ELp neurons (Carlson, 2009; George et al., 2011; Xu-Friedman and Hopkins, 1999). Finally, paired whole-cell recordings *in vitro* reveal extensive synaptic connections among ELp neurons (Ma et al., 2013).

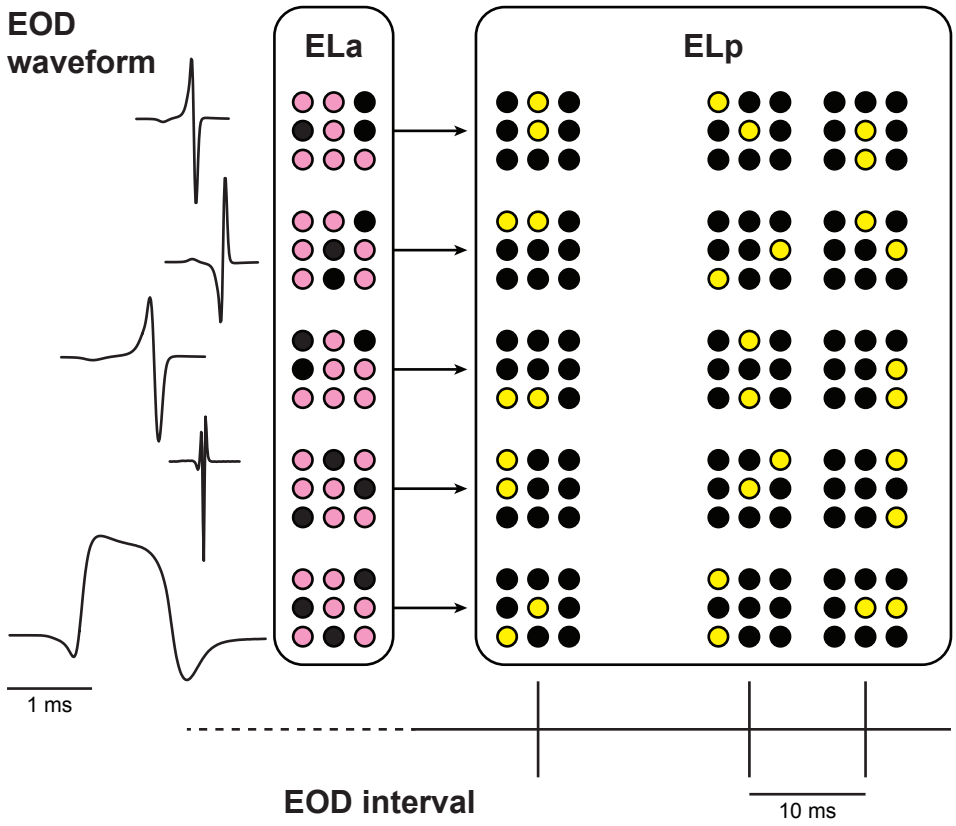

Figure 7. Multiplexed temporal codes are converted into distributed population codes in ELa/ELp. EOD waveform is represented by the pattern of responsive neurons across the population of small cells in ELa, and both EOD waveform and EOD interval are represented by the pattern of responsive neurons across the population of multipolar cells in ELp. Five different EOD waveforms are shown, from top to bottom: *Brienomyrus brachyistius* EOD, reversed polarity *B. brachyistius* EOD, elongated *B. brachyistius* EOD, *Stomatorhinus ivindoensis* EOD, *Paramormyrops* sp. 'VAD' EOD. Nine model small cells are shown and for each of the five EOD waveforms, pink indicates responding cells and black indicates non-responding cells. Each EOD waveform results in a unique pattern of responsiveness across the population of small cells. This information is sent to ELp, where multipolar cells respond selectively to EOD waveform as well as EOD interval. Nine model multipolar cells are shown and for the five EOD waveforms and three different EOD intervals (from left to right: long, medium, and short), yellow indicates responding cells and black indicates non-responding cells. Each possible combination of EOD waveform and EOD interval results in a unique pattern of responsive neurons across the population of multipolar cells.

Extracellular single unit recordings in ELp suggest two cell types based on responses to single pulses (Amagai, 1998). Type I cells respond with high probability at latencies of 7-9 ms and their responses increase with increasing stimulus duration, being minimally affected by stimulus polarity or amplitude. In contrast, Type II cells have a low response probability, weaker time locking, latencies >12 ms, selectivity for a limited range of stimulus durations and intensities, and strong preferences for stimulus polarity. The sensitivity of ELp neurons to stimulus pulse duration, amplitude, and polarity reveals that the information necessary for identifying signaling fish, as well as determining their distance, location, and orientation are present in the spike timing differences of KOs.

DETERMINING THE BEHAVIORAL STATE OF THE SENDER: MULTIPLE MECHANISMS FOR TEMPORAL FILTERING OF INTERSPIKE INTERVALS

In addition to pulse waveform, ELp neurons are also tuned to IPI (Fig. 8), owing to temporal filtering of incoming small cell spike trains (Carlson, 2009; George et al., 2011). Thus, stimulus information encoded into interspike intervals in the periphery is retained during the processing of spike timing differences in ELa. Low-pass tuning describes preferential responses to long intervals (low frequencies), high-pass tuning describes preferential responses to short intervals (high frequencies), band-pass tuning describes preferential responses to intermediate intervals, and band-stop tuning describes preferential responses to short and long, but not intermediate, intervals. Low-pass and high-pass tuning curves vary widely in shape, and band-pass and band-stop tuning curves vary widely in best/worst interval and bandwidth (Carlson, 2009; George et al., 2011). As a result, diversity of interval tuning across the population of ELp neurons results in the recoding of IPIs into a distributed population code in which IPI is reflected

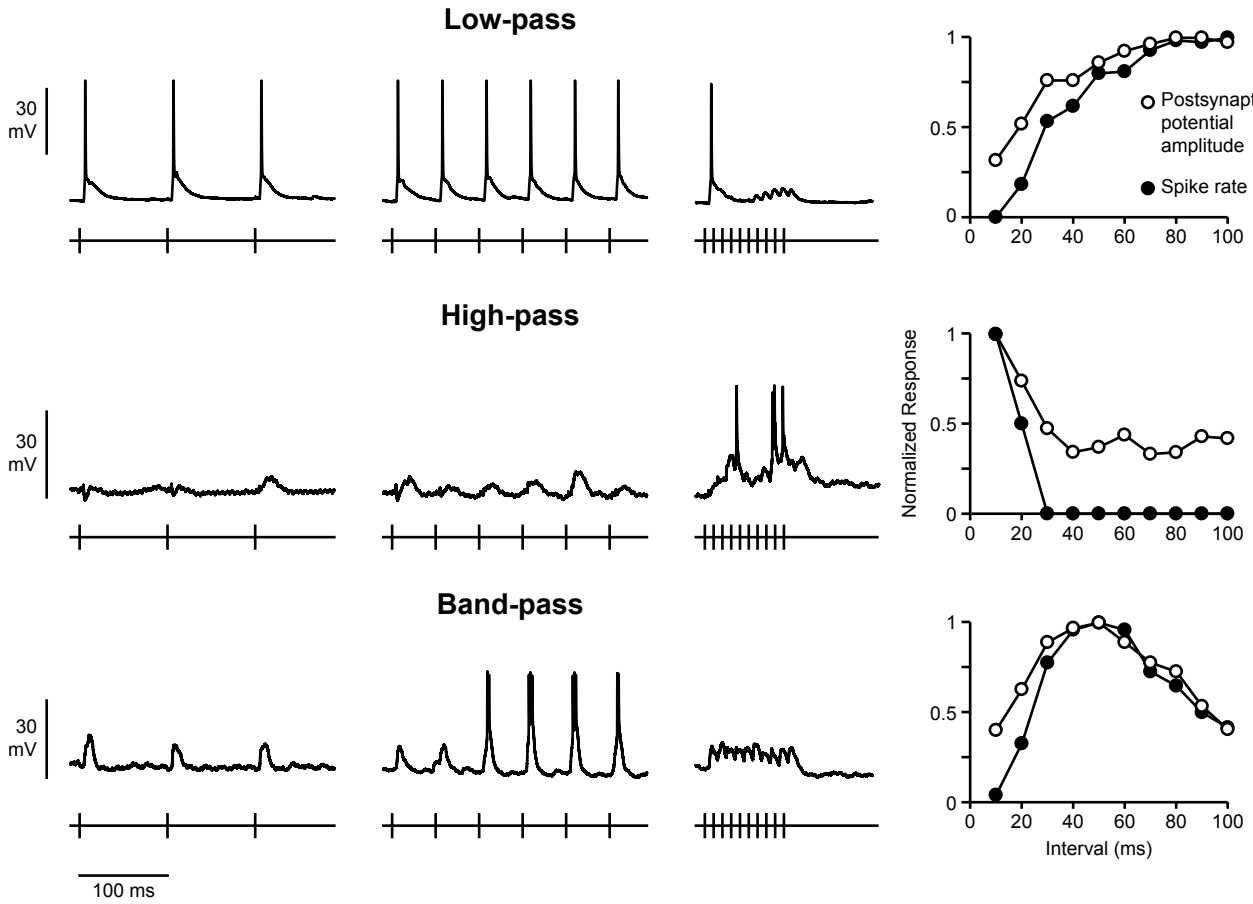

Figure 8. IPI tuning of ELp neurons in response to electrosensory stimulation *in vivo.* Data from three different neurons are shown (data from Carlson, 2009). Intracellular recordings show responses to, from left to right, 100, 50, and 10 ms IPIs, with stimulus trains shown underneath each recording trace. On the far right, tuning curves show the normalized average spike rate and postsynaptic potential amplitude as a function of stimulus IPI in response to 10 repetitions of each stimulus (details on stimulus presentation and tuning curve generation can be found in Carlson, 2009).

in the identity of responsive neurons, much like the population code of EOD waveform in ELa. Thus, both temporal codes, spike timing differences that code for EOD waveform and interspike intervals that code for IPI, are sequentially converted into distributed population codes in this circuit. The resulting sensitivity of ELp neurons to EOD waveform and IPI means that both components are represented in the identities of responsive neurons (Fig. 7).

Some ELp neurons are also responsive to changes in IPI, with response magnitude depending on whether IPIs are increasing or decreasing (Carlson, 2009). This preference arises from hysteresis, or the degree to which responses to particular IPIs are affected by preceding IPIs. Some neurons in each tuning class exhibit a large amount of hysteresis, whereas others exhibit little to none. Thus, the responses among ELp neurons can provide information about the direction of IPI change as well as the specific IPI sequence, resulting in selective responses to communication signals such as scallops, rasps, and accelerations (Carlson, 2009).

GABAergic inhibition plays an important role in IPI tuning. Blocking $GABA_A$, but not glycine, receptors caused increases in the amplitude, latency to maximum depolarization, and duration of synaptic responses to single pulse stimulation (George et al., 2011). These effects occurred regardless of the neurons' IPI tuning, demonstrating that neurons of all tuning classes receive inhibition. Furthermore, blocking inhibition caused a general shift towards high-pass tuning: the majority of low-pass, band-pass, and band-stop neurons switched to high-pass tuning, and most high-pass neurons experienced a sharpening of their high-pass tuning. Therefore, the interaction of excitation and inhibition is essential in establishing IPI tuning diversity among ELp neurons.

Similar selectivity of central neurons to temporal patterns of sensory stimulation has been documented in several auditory and electrosensory pathways (Edwards et al., 2002; Fortune and

Rose, 1997b; Grothe, 1994; Huetz et al., 2009; Marsat and Maler, 2010; Pluta and Kawasaki, 2010; Rose and Capranica, 1983). Given the prevalence of temporal coding across sensory systems, an understanding of central mechanisms for temporal filtering in these systems should provide fundamental insight into general issues in sensory processing. A variety of synaptic mechanisms have been proposed to give rise to temporal filtering properties in single neurons (Fig. 9). Temporal summation, in which responses evoked by successive stimuli overlap in time, has been hypothesized to produce interval tuning (Edwards et al., 2007; Rose et al., 2011). Temporal summation of excitation can cause increased responses to short intervals, whereas temporal summation of inhibition can cause decreased responses to short intervals (Fig. 9). Short-term synaptic plasticity, or a change in synaptic strength with repeated stimulation, has also been implicated in interval tuning (Buonomano, 2000; Edwards et al., 2007; Edwards et al., 2008; Fortune and Rose, 2000; Klyachko and Stevens, 2006; Rose and Fortune, 1999; Zucker and Regehr, 2002). Short-term synaptic plasticity occurs on the timescale of tens of milliseconds to several minutes, and can result in increases or decreases in synaptic strength, called facilitation and depression, respectively (Zucker and Regehr, 2002). Facilitation of excitation or depression of inhibition at short stimulation intervals could produce high-pass responses, whereas facilitation of inhibition or depression of excitation could produce low-pass responses (Fig. 9). Finally, differences in the relative timing of excitatory and inhibitory inputs has also been hypothesized to underlie interval tuning (Edwards et al., 2008; Grothe, 1994). If inhibition is delayed with respect to excitation, then repeated stimulation at short intervals could cause excitation to overlap with inhibition evoked by previous stimuli, resulting in an attenuation of response characteristic of low-pass tuning (Fig. 9). This scenario requires the latency of excitation and inhibition to be fixed during repeated stimulation. By contrast, high-pass tuning

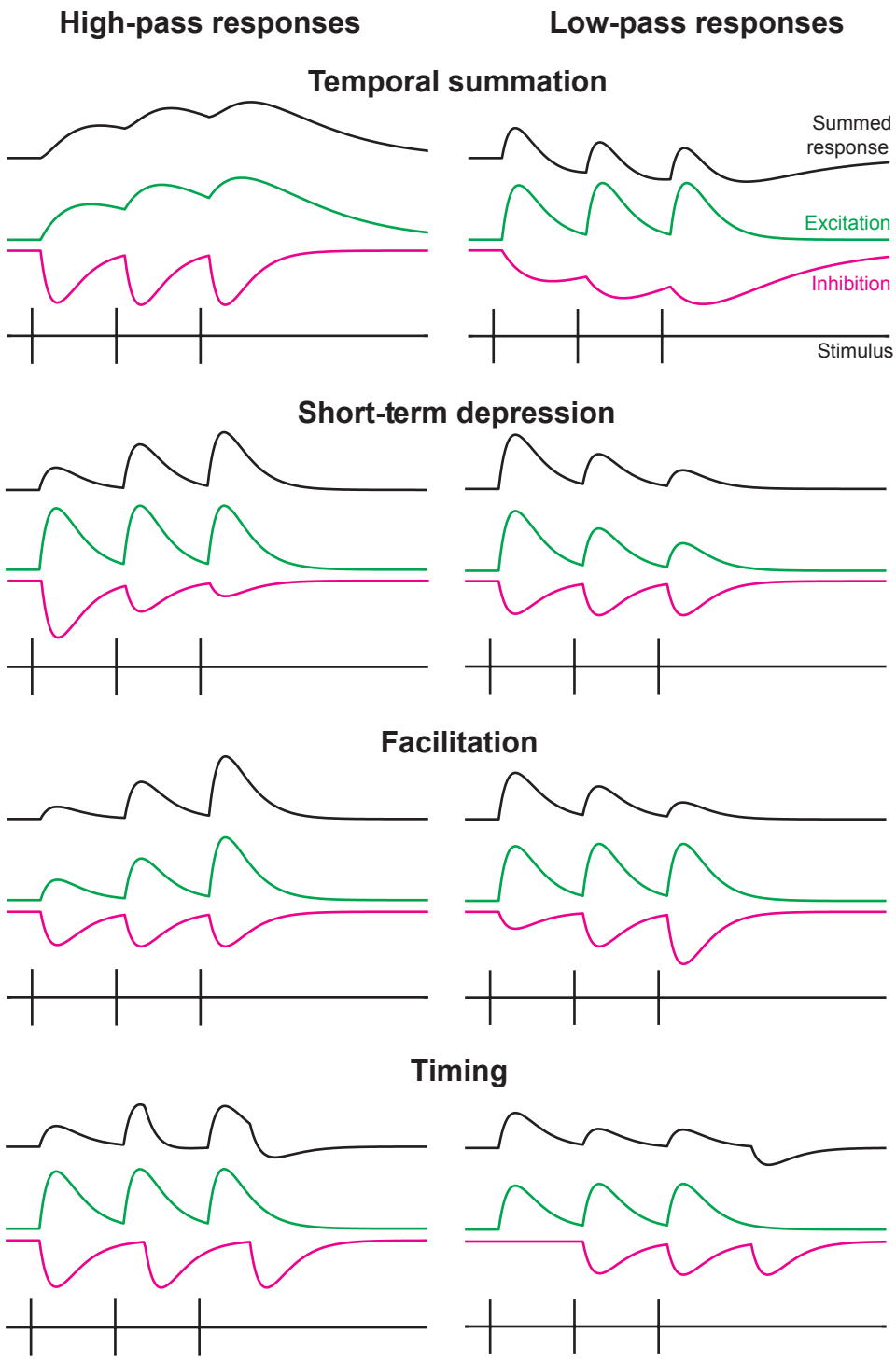

Figure 9. Multiple synaptic mechanisms can establish IPI tuning. Different excitatory (green) and inhibitory (magenta) responses to short-interval stimulation (ticks) can give rise to different summated synaptic responses (black). In this simple model, summed responses are determined by subtracting the inhibitory response from the excitatory response. Temporal summation, in which synaptic responses to successive stimuli overlap in time, can establish IPI tuning. When excitation lasts longer than the stimulation interval, temporal summation leads to an increase in response characteristic of high-pass

tuning. Conversely, temporal summation of inhibition occurs when inhibition lasts longer than the stimulation interval, causing a decrease in response characteristic of low-pass tuning. Short-term synaptic depression, or a decrease in synaptic strength with repeated stimulation, of inhibition can produce high-pass tuning, and depression of excitation can produce low-pass tuning. Facilitation, or an increase in synaptic strength with repeated stimulation, of excitation can result in high-pass tuning, whereas facilitation of inhibition can result in low-pass tuning. Finally, the relative timing of excitation and inhibition can establish interval-tuned responses. If excitation and inhibition occur near-coincidently, the response to a single stimulus would be small. Increasing latency of inhibition with repeated stimulation could result in high-pass tuning. On the other hand, if the latencies of excitation and inhibition were fixed, and inhibition was delayed with respect to excitation, stimulation at short intervals could cause excitation to coincide with inhibition elicited by previous stimuli, resulting in low-pass tuning.

could result if the latency to excitation or inhibition changes with repeated stimulation. For instance, if excitation and inhibition occur near-simultaneously in response to a single pulse, the resulting synaptic response would be small. If, however, repeated stimulation increased inhibitory latency, then larger responses giving rise to high-pass tuning could result (Fig. 9).

In ELp, *in vitro* whole-cell recordings have revealed that temporal summation of excitation and inhibition plays a major role in establishing single-neuron tuning to temporal patterns of presynaptic input, and computational modeling reveals that all major classes of IPI tuning can be established by just this one mechanism (George et al., 2011). However, this study also revealed that the IPI tuning of a small subset of ELp neurons may be influenced by short-term synaptic depression (George et al., 2011). Somewhat surprisingly, *in vivo* and *in vitro* studies currently underway have uncovered widespread short-term depression in both excitatory and inhibitory pathways to ELp neurons (Baker et al., 2012). Differences in the relative magnitude and time course of depression in excitatory and inhibitory pathways may contribute to interval tuning as well as directional sensitivity to changes in interval. Short-term depression is also prevalent in avian and mammalian auditory time-coding pathways (MacLeod, 2011).

In addition to synaptic mechanisms, intrinsic membrane properties of postsynaptic neurons can contribute to temporal filtering (Hutcheon and Yarom, 2000; Mehaffey et al.,

2008b). First, the membrane itself passively filters high-frequency fluctuations in membrane potential. In ELp, membrane time constants are widely distributed between 5 and 25 ms (Kohashi et al., 2012), suggesting that short IPIs within the behaviorally relevant range are differentially filtered. Further, neurons with longer time constants would be more affected by temporal summation, and they would be able to integrate over multiple non-coincident inputs. Such a scenario could give rise to the longer latency and more highly variable responses of the Type II ELp neurons described by Amagai (1998). Second, voltage-gated channels in the postsynaptic cell can shape synaptic responses (O'Donnell and Nolan, 2011). The significance of low-threshold voltage-sensitive channels in temporal coding is particularly well described in auditory brainstem neurons where timing information is highly preserved (Brown and Kaczmarek, 2011; Kuba, 2007; Trussell, 1999). Calcium-activated potassium channels (Ellis et al., 2007) as well as voltage-sensitive channels (Carlson and Kawasaki, 2006; Fortune and Rose, 1997a; Fortune and Rose, 2003; Mehaffey et al., 2008a) are suggested to shape frequency tuning and stimulus selectivity in response to electrosensory stimuli in wave-type electric fish. Current studies are investigating the contribution of similar mechanisms to interval tuning in ELp (Kohashi et al., 2012). The diversity of interval tuning and hysteresis among ELp neurons is likely due to complex interactions between temporal summation, short-term synaptic plasticity, and intrinsic membrane properties. Having multiple such "free parameters" may establish a higher dimensionality of "coding space" in which to represent multiple behaviorally relevant stimulus features in a single circuit.

Finally, although current evidence points to extensive processing of communication signals within ELp, many questions about the nature of these local circuit interactions remain. Excitatory and inhibitory network interactions among IPI-tuned neurons could act in several

ways to shape IPI tuning (Fig. 10). For example, combining inputs from one low- and one high-pass neuron onto a single postsynaptic neuron can establish band-pass, band-stop, or all-pass tuning, depending on the excitatory/inhibitory nature of the inputs. Furthermore, sharpening of low- or high-pass tuning can result when excitatory and inhibitory inputs converge.

SENSORY MULTIPLEXING AND THE EVOLUTION OF SIGNALS AND SPECIES

Evolutionary change in nervous systems can have profound effects on processes that influence species diversification (Carlson, 2012; Carlson and Arnegard, 2011). Communication signals play an essential role in mate choice. As a result, signal divergence can establish reproductive isolation between populations, thereby reinforcing this divergence and promoting speciation (Hoskin and Higgie, 2010). For signal divergence to result in reproductive isolation, however, receivers must have the perceptual ability to detect signal variation. The evolution of novel perceptual abilities can therefore open up new dimensions of signal variation for mate choice, which can drive increased rates of species diversification and signal evolution (Carlson, 2012; Carlson and Arnegard, 2011). For example, if two populations of the same species become geographically isolated, their mating signals may diverge over time due to processes such as genetic drift, local adaptation to different environments, or reproductive character displacement. If receivers can detect the difference, then members of the two populations will be less likely to mate if they later come into contact, and selection may then act to drive further signal divergence to prevent hybridization. Indeed, the evolution of distributed KOs and ELa/ELp in clade A (Fig. 3) established the novel ability to discriminate temporal variation in EOD waveform, which fueled dramatic increases in the rates of species diversification and EOD evolution (Carlson et al., 2011). A similar process may have resulted from evolutionary change in the auditory system

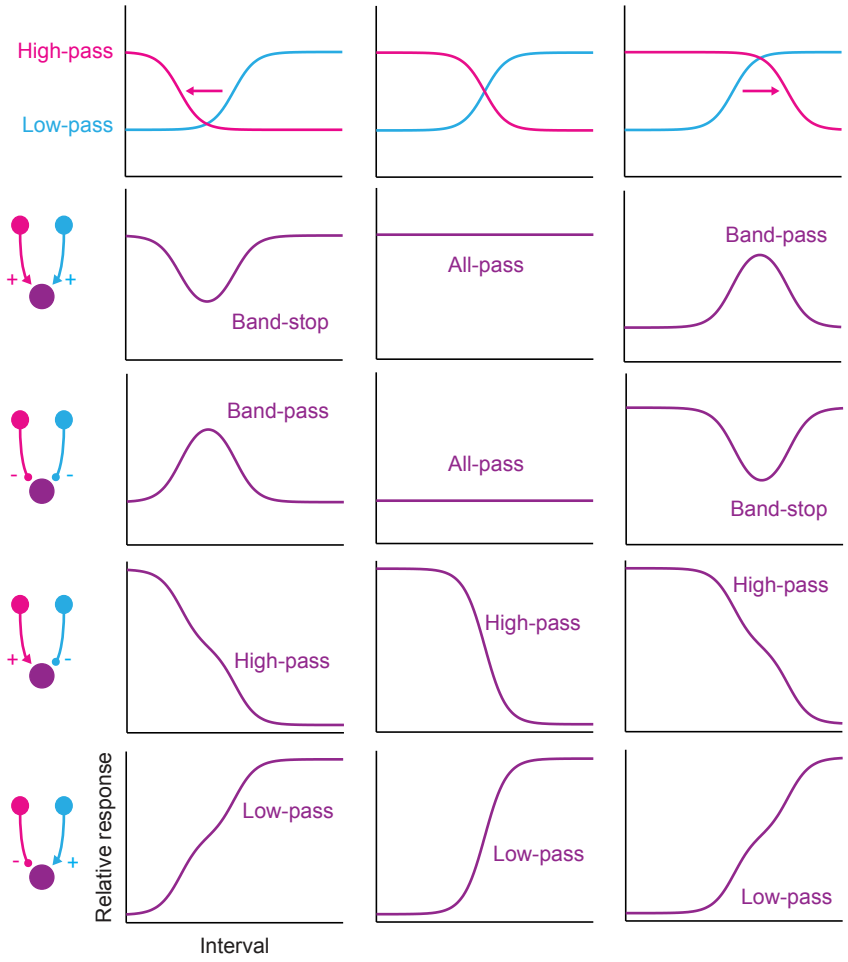

Figure 10. Convergence of high- and low-pass tuning can establish diverse temporal filters. The tuning curves of model neurons (purple) that receive synaptic inputs from one high-pass (magenta) and one low-pass (blue) neuron are shown. Excitatory connections are indicated by '+' and inhibitory connections are indicated by '-', and the tuning of each postsynaptic neuron is determined by a simple addition of '+' tuning curves and subtraction of '-' tuning curves. A variety of different types of interval tuning, including high-pass, low-pass, band-pass, band-stop, and all-pass, can be created by different combinations of high-pass and low-pass excitation and inhibition.

of frogs (Ryan, 1986) and the visual system of cichlid fishes (Seehausen et al., 2008; Terai et al., 2006). Importantly, the evolution of EOD waveform coding established temporal multiplexing in the KO electrosensory system (Fig. 4), thereby adding increased dimensionality to electrocommunication. This evolutionary change and its effects on mormyrid diversity underscore a primary advantage of temporal multiplexing: increased information transmission within a single channel.

FUTURE DIRECTIONS

Evolutionary change in nervous systems provides a powerful tool for employing comparative approaches to study neural mechanisms of behavior, as it allows for a direct comparison between differences in behavior with differences in neural circuitry (Carlson, 2012). However, we have only scratched the surface in understanding evolutionary change in the KO sensory system. How do the rosette KOs of non-clade A species encode electric signals? How does EL process these signals? Does EL have the large cells and small cells of ELa, the multipolar cells of ELp, or completely different cell types? Are there axonal delay lines in EL?

Many important questions remain about the coding of electrocommunication signals in clade A species. For example, how is information about signaler location and orientation (Schluger and Hopkins, 1987) extracted from the spatiotemporal pattern of KO responses? How are signals from multiple fish differentiated? How is signal coding affected by changes in the relative positions of sender and receiver? What are the roles of MV and the ELp-IG feedback loop in processing communication signals? How do downstream targets, including the cerebellum and optic tectum, process information from ELp and MV, and how do they modulate the fish's own EOD production? The answers to these questions will contribute to our

understanding of not only mormyrid electrocommunication, but to sensory processing of temporally coded information in general.

REFERENCES

Ainsworth, M., Lee, S., Cunningham, M. O., Traub, R. D., Kopell, N. J. and Whittington, M. A. (2012). Rates and rhythms: a synergistic view of frequency and temporal coding in neuronal networks. *Neuron* **75**, 572-83.

Amagai, S. (1998). Time coding in the midbrain of mormyrid electric fish. II. Stimulus selectivity in the nucleus exterolateralis pars posterior. *J Comp Physiol A* **182**, 131-43.

Amagai, S., Friedman, M. A. and Hopkins, C. D. (1998). Time coding in the midbrain of mormyrid electric fish. I. Physiology and anatomy of cells in the nucleus exterolateralis pars anterior. *J Comp Physiol A* **182**, 115-30.

Arnegard, M. E. and Carlson, B. A. (2005). Electric organ discharge patterns during group hunting by a mormyrid fish. *Proc Biol Sci* **272**, 1305-14.

Arnegard, M. E., Jackson, B. S. and Hopkins, C. D. (2006). Time-domain signal divergence and discrimination without receptor modification in sympatric morphs of electric fishes. *J Exp Biol* **209**, 2182-98.

Arnegard, M. E., McIntyre, P. B., Harmon, L. J., Zelditch, M. L., Crampton, W. G., Davis, J. K., Sullivan, J. P., Lavoue, S. and Hopkins, C. D. (2010). Sexual signal evolution outpaces ecological divergence during electric fish species radiation. *Am Nat* **176**, 335-56.

Baker, C. A., Ma, X. and Carlson, B. A. (2012). Differences in short-term synaptic depression of excitatory and inhibitory pathways contribute to temporal pattern recognition. In *10th International Congress of Neuroethology*. College Park, MD.

Bass, A. H. (1986a). Electric organs revisited: Evolution of a vertebrate communication and orientation organ. In *Electroreception*, (ed. T. H. Bullock and W. Heiligenberg), pp. 13-70. New York: John Wiley and Sons.

Bass, A. H. (1986b). Species differences in electric organs of mormyrids: substrates for species-typical electric organ discharge waveforms. *J Comp Neurol* **244**, 313-330.

Bass, A. H. and Volman, S. F. (1987). From behavior to membranes: testosterone-induced changes in action potential duration in electric organs. *Proc Natl Acad Sci USA* **84**, 9295-9298.

Bauer, R. and Kramer, B. (1974). Agonistic behavior in mormyrid fish: latency-relationship between the electric discharges of *Gnathonemus petersii* and *Mormyrus rume*. *Experientia* **30**, 51-52.

Bell, C. C. (1989). Sensory coding and corollary discharge effects in mormyrid electric fish. *Journal of Experimental Biology* **146**, 229-253.

Bell, C. C., Finger, T. E. and Russell, C. J. (1981). Central connections of the posterior lateral line lobe in mormyrid fish. *Exp Brain Res* **42**, 9-22.

Bell, C. C. and Grant, K. (1989). Corollary discharge inhibition and preservation of temporal information in a sensory nucleus of mormyrid electric fish. *J Neurosci* **9**, 1029-44.

Bell, C. C., Libouban, S. and Szabo, T. (1983). Pathways of the electric organ discharge command and its corollary discharges in mormyrid fish. *J Comp Neurol* **216**, 327-38.

Bell, C. C. and Maler, L. (2005). Central neuroanatomy of electrosensory systems in fish. In *Electroreception*, (ed. T. H. Bullock C. D. Hopkins A. N. Popper and R. R. Fay). New York: Springer Science & Business Media.

Bell, C. C., Myers, J. P. and Russell, C. J. (1974). Electric organ discharge patterns during dominance related behavioral displays in *Gnathonemus petersii* (Mormyridae). *J Comp Physiol* **92**, 201-228.

Bell, C. C. and Russell, C. J. (1978). Termination of electroreceptor and mechanical lateral line afferents in the mormyrid acousticolateral area. *J Comp Neurol* **182**, 367-82.

Bennett, M. V. (1965). Electroreceptors in mormyrids. *Cold Spring Harb Symp Quant Biol* **30**, 245-62.

Bennett, M. V., Pappas, G. D., Aljure, E. and Nakajima, Y. (1967). Physiology and ultrastructure of electrotonic junctions. II. Spinal and medullary electromotor nuclei in mormyrid fish. *J Neurophysiol* **30**, 180-208.

Bennett, M. V. L. (1971). Electric organs. In *Fish Physiology*, eds. W. S. Hoar and D. J. Randall), pp. 347-491. London: Academic Press.

Bennett, M. V. L., Aljure, E., Nakajima, Y. and Pappas, G. D. (1963). Electrotonic junctions between teleost spinal neurons: electrophysiology and ultrastructure. *Science* **141**, 262-264.

Bennett, M. V. L. and Steinbach, A. B. (1969). Influence of electric organ control system on electrosensory afferent pathways in Mormyrids. In *Neurobiology of Cerebellar Evolution and Development*, (ed. R. Llinas), pp. 207-14. Chicago, Ill.: American Medical Association.

Blumhagen, F., Zhu, P., Shum, J., Scharer, Y. P., Yaksi, E., Deisseroth, K. and Friedrich, R. W. (2011). Neuronal filtering of multiplexed odour representations. *Nature* **479**, 493-8.

Brown, M. R. and Kaczmarek, L. K. (2011). Potassium channel modulation and auditory processing. *Hearing Research* **279**, 39-42.

Buonomano, D. V. (2000). Decoding temporal information: A model based on short-term synaptic plasticity. *J Neurosci* **20**, 1129-41.

Calvin, W. H. (1983). A stone's throw and its launch window: timing precision and its implications for language and hominid brains. *J Theor Biol* **104**, 121-35.

Caputi, A. A., Carlson, B. A. and Macadar, O. (2005). Electric organs and their control. In *Electroreception*, (ed. T. H. Bullock C. D. Hopkins A. N. Popper and R. R. Fay), pp. 410-451. New York: Springer Science & Business Media, Inc.

Cariani, P. A. (2001). Temporal coding of sensory information in the brain. *Acoust Sci & Tech* **22**, 77-84.

Carlson, B. A. (2002a). Electric signaling behavior and the mechanisms of electric organ discharge production in mormyrid fish. *J Physiol Paris* **96**, 405-19.

Carlson, B. A. (2002b). Neuroanatomy of the mormyrid electromotor control system. *J Comp Neurol* **454**, 440-55.

Carlson, B. A. (2003). Single-unit activity patterns in nuclei that control the electromotor command nucleus during spontaneous electric signal production in the mormyrid Brienomyrus brachyistius. *J Neurosci* **23**, 10128-36.

Carlson, B. A. (2008a). Reafferent control in electric communication. In *Encyclopedia of Neuroscience*, eds. M. D. Binder N. Hirokawa U. Windhorst and M. C. Hirsch), pp. 3368-3373. New York: Springer.

Carlson, B. A. (2008b). Temporal coding in electroreception. In *Encyclopedia of Neuroscience*, (ed. M. D. Binder N. Hirokawa U. Windhorst and M. C. Hirsch), pp. 4039-4044. New York: Springer.

Carlson, B. A. (2009). Temporal-pattern recognition by single neurons in a sensory pathway devoted to social communication behavior. *J Neurosci* **29**, 9417-28.

Carlson, B. A. (2012). Diversity matters: The importance of comparative studies and the potential for synergy between neuroscience and evolutionary biology. *Archives of Neurology* **69**, 987-993.

Carlson, B. A. and Arnegard, M. E. (2011). Neural innovations and the diversification of African weakly electric fishes. *Commun Integr Biol* **4**, 720-5.

Carlson, B. A., Hasan, S. M., Hollmann, M., Miller, D. B., Harmon, L. J. and Arnegard, M. E. (2011). Brain evolution triggers increased diversification of electric fishes. *Science* **332**, 583-6.

Carlson, B. A. and Hopkins, C. D. (2004a). Central control of electric signaling behavior in the mormyrid Brienomyrus brachyistius: segregation of behavior-specific inputs and the role of modifiable recurrent inhibition. *Journal of Experimental Biology* **207**, 1073-84.

Carlson, B. A. and Hopkins, C. D. (2004b). Stereotyped temporal patterns in electrical communication. *Anim Behav* **68**, 867-878.

Carlson, B. A. and Kawasaki, M. (2006). Stimulus selectivity is enhanced by voltage-dependent conductances in combination-sensitive neurons. *J Neurophysiol* **96**, 3362-3377.

Carr, C. E. (1993). Processing of temporal information in the brain. *Annu Rev Neurosci* **16**, 223-43.

Carr, C. E. and Friedman, M. A. (1999). Evolution of time coding systems. *Neural Comput* **11**, 1-20.

Carr, C. E., Heiligenberg, W. and Rose, G. J. (1986a). A time-comparison circuit in the electric fish midbrain. I. Behavior and physiology. *J Neurosci* **6**, 107-19.

Carr, C. E. and Konishi, M. (1990). A circuit for detection of interaural time differences in the brain stem of the barn owl. *J Neurosci* **10**, 3227-46.

Carr, C. E., Maler, L. and Taylor, B. (1986b). A time-comparison circuit in the electric fish *Eigenmannia* midbrain II. Functional morphology. *J Neurosci* **6**, 1372-1383.

Churchland, P. S. and Sejnowski, T. J. (1992). The Computational Brain. Cambridge, MA: MIT Press.

Decharms, D. C. and Merzenich, M. M. (1996). Primary cortical representation of sounds by the coordination of action potential timing. *Nature* **381**, 610-613.

Denizot, J. P., Clausse, S., Elekes, K., Geffard, M., Grant, K., Libouban, S., Ravaille-Veron, M. and Szabo, T. (1987). Convergence of electrotonic club endings, GABA- and serotoninergic terminals on second order neurons of the electrosensory pathway in mormyrid fish, *Gnathonemus petersii* and *Brienomyrus niger* (Teleostei). *Cell Tissue Res* **249**, 301-309.

Derbin, C. and Szabo, T. (1968). Ultrastructure of an electroreceptor (knollenorgan) in the mormyrid fish *Gnathonemus petersii*. I. *J Ultrastruct Res* **22**, 469-484.

Di Lorenzo, P., Chen, J.-Y. and Victor, J. D. (2009). Quality time; Representation of a multidimensional sensory domain through temporal coding. *J Neurosci* **29**, 9227-9238.

Edwards, C. J., Alder, T. B. and Rose, G. J. (2002). Auditory midbrain neurons that count. *Nature Neuroscience* **5**, 934-936.

Edwards, C. J., Leary, C. J. and Rose, G. J. (2007). Counting on inhibition and rate-dependent excitation in the auditory system. *J Neurosci* **27**, 13384-92.

Edwards, C. J., Leary, C. J. and Rose, G. J. (2008). Mechanisms of long-interval selectivity in midbrain auditory neurons: roles of excitation, inhibition, and plasticity. *J Neurophysiol* **100**, 3407-16.

Elekes, K., Ravaille, M., Bell, C. C., Libouban, S. and Szabo, T. (1985). The mormyrid brainstem II. The medullary electromotor relay nucleus: an ultrastructural horseradish peroxidase study. *Neuroscience* **15**, 417-430.

Elekes, K. and Szabo, T. (1985). The mormyrid brainstem III. Ultrastructure and synaptic organization of the medullary 'pacemaker' nucleus. *Neuroscience* **15**, 431-444.

Ellis, L. D., Mehaffey, W. H., Harvey-Girard, E., Turner, R. W., Maler, L. and Dunn, R. J. (2007). SK channels provide a novel mechanism for the control of frequency tuning in electrosensory neurons. *Journal of Neuroscience* **27**, 9491-9502.

Enger, P. S., Libouban, S. and Szabo, T. (1976a). Fast conducting electrosensory pathway in the mormyrid fish, Gnathonemus petersii. *Neurosci Lett* **2**, 133-6.

Enger, P. S., Libouban, S. and Szabo, T. (1976b). Rhombo-mesencephalic connections in the fast conducting electrosensory system of the mormyrid fish, Gnathonemus petersii. An HRP study. *Neurosci Lett* **3**, 239-43.

Feulner, P. G., Plath, M., Engelmann, J., Kirschbaum, F. and Tiedemann, R. (2009). Electrifying love: electric fish use species-specific discharge for mate recognition. *Biol Lett* **5**, 225-8.

Finger, T. E., Bell, C. C. and Russell, C. J. (1981). Electrosensory pathways to the valvula cerebelli in mormyrid fish. *Exp Brain Res* **42**, 23-33.

Fortune, E. S. and Rose, G. J. (1997a). Passive and active membrane properties contribute to the temporal filtering properties of midbrain neurons in vivo. *J Neurosci* **17**, 3815-25.

Fortune, E. S. and Rose, G. J. (1997b). Temporal filtering properties of ampullary electrosensory neurons in the torus semicircularis of Eigenmannia: evolutionary and computational implications. *Brain Behav Evol* **49**, 312-23.

Fortune, E. S. and Rose, G. J. (2000). Short-term synaptic plasticity contributes to the temporal filtering of electrosensory information. *J Neurosci* **20**, 7122-30.

Fortune, E. S. and Rose, G. J. (2003). Voltage-gated Na+ channels enhance the temporal filtering properties of electrosensory neurons in the torus. *J Neurophysiol* **90**, 924-9.

Franz, V. (1921). Zur mikroskopischen Anatomie der Mormyriden. *Zool Jahrb Anat Abt* **1**, 119-129.

Freedman, E. G., Olyarchuk, J., Marchaterre, M. A. and Bass, A. H. (1989). A temporal analysis of testosterone-induced changes in electric organs and electric organ discharges of mormyrid fishes. *J Neurobiol* **20**, 619-34.

Friedman, M. A. and Hopkins, C. D. (1998). Neural substrates for species recognition in the time-coding electrosensory pathway of mormyrid electric fish. *J Neurosci* **18**, 1171-85.

Friedman, M. A. and Kawasaki, M. (1997). Calretinin-like immunoreactivity in mormyrid and gymnarchid electrosensory and electromotor systems. *J Comp Neurol* **387**, 341-57.

Friedrich, R. W., Habermann, C. J. and Laurent, G. (2004). Multiplexing using synchrony in the zebrafish olfactory bulb. *Nat Neurosci* **7**, 862-71.

George, A. A., Lyons-Warren, A. M., Ma, X. and Carlson, B. A. (2011). A diversity of synaptic filters are created by temporal summation of excitation and inhibition. *J Neurosci* **31**, 14721-34.

Goulet, J., van Hemmen, J., Jung, S., Chagnaud, B., Scholze, B. and Engelman, J. (2012). Temporal precision and reliability in the velocity regime of a hair-cell sensory system: the mechanosensory lateral line of goldfish, *Carassius auratus*. *J Neurophysiol* **107**, 2581-2593.

Graff, C. and Kramer, B. (1992). Trained weakly electric fishes *Pollimyrus isidori* and *Gnathonemus petersii* (Mormyridae, Teleostei) discriminate between waveforms of electric pulse discharges. *Ethol* **90**, 279-292.

Grant, K., Bell, C. C., Clausse, S. and Ravaille, M. (1986). Morphology and physiology of the brainstem nuclei controlling the electric organ discharge in mormyrid fish. *J Comp Neurol* **245**, 514-30.

Groh, J. M. (2001). Converting neural signals from place codes to rate codes. *Biol Cybern* **85**, 159-65.

Grothe, B. (1994). Interaction of excitation and inhibition in processing of pure tone and amplitude-modulated stimuli in the medial superior olive of the mustached bat. *J Neurophysiol* **71**, 706-21.

Grothe, B. (2003). New roles for synaptic inhibition in sound localization. *Nature Reviews Neuroscience* **4**, 1-11.

Hanika, S. and Kramer, B. (2005). Intra-male variability of its communication signal in the weakly electric fish, *Marcusenius macrolepidotus* (South African form), and possible functions. *Behavior* **142**, 145-166.

Harder, W. (1968). Die beziehungen zwischen electrorezeptoren, elektrischem organ, seitenlinienorganen und nervensystem bei den mormyridae (Teleostei, Pisces). *Zeitschrift fur vergleichende Physiologie* **59**, 272-318.

Haugede-Carre, F. (1979). The mesencephalic exterolateral posterior nucleus of the mormyrid fish Bryenomyrus niger: efferent connections studied by the HRP method. *Brain Res* **178**, 179-84.

Heiligenberg, W. (1976). Electrolocation and jamming avoidance in the mormyrid fish *Brienomyrus*. *J Comp Physiol* **109**, 357-372.

Hopkins, C. D. (1977). Electric communication. Bloomington: Indiana Univ. Press.

Hopkins, C. D. (1980). Evolution of electric communication channels of mormyrids. *Behav Ecol Sociobiol* **7**, 1-13.

Hopkins, C. D. (1981). On the diversity of electric signals in a community of mormyrid electric fish in West Africa. *Amer Zool* **21**, 211-222.

Hopkins, C. D. (1986). Behavior of Mormyridae. In *Electroreception*, (ed. T. H. Bullock and W. Heiligenberg), pp. 527-576. New York: John Wiley & Sons.

Hopkins, C. D. (1999). Design features for electric communication. *J Exp Biol* **202**, 1217-28.

Hopkins, C. D. and Bass, A. H. (1981). Temporal coding of species recognition signals in an electric fish. *Science* **212**, 85-7.

Hoskin, C. J. and Higgie, M. (2010). Speciation via species interactions: the divergence of mating traits within species. *Ecology Letters* **13**, 409-420.

Huetz, C., Philibert, B. and Edeline, J.-M. (2009). A Spike-timing code for discriminating conspecific vocalizations in the thalamocortical system of anesthetized and awake guinea pigs. *J Neurosci* **29**, 334-350.

Hutcheon, B. and Yarom, Y. (2000). Resonance, oscillation, and the intrinsic frequency preferences of neurons. *Trends in Neurosciences* **23**, 216-222.

Jones, L. M., Depireux, D. A., Simons, D. J. and Keller, A. (2004). Robust temporal coding in the trigeminal system. *Science* **304**, 1986-1989.

Jørgensen, J. M. (2005). Morphology of electroreceptive sensory organs. In *Electroreception* (ed. T. H. Bullock, C. D. Hopkins, A. N. Popper and R. R. Fay), pp. 47-67. New York, NY: Springer Science & Business Media.

Joris, P. X., Carney, L. H., Smith, P. H. and Yin, T. C. (1994). Enhancement of neural synchronization in the anteroventral cochlear nucleus. I. Responses to tones at the characteristic frequency. *J Neurophysiol* **71**, 1022-36.

Kawasaki, M. and Guo, Y. (1996). Neuronal circuitry for comparison of timing in the electrosensory lateral line lobe of the African wave-type electric fish *Gymnarchus niloticus*. *Journal of Neuroscience* **16**, 380-391.

Kawasaki, M., Rose, G. and Heiligenberg, W. (1988). Temporal hyperacuity in single neurons of electric fish. *Nature* **336**, 173-6.

Klyachko, V. A. and Stevens, C. F. (2006). Excitatory and feed-forward inhibitory hippocampal synapses work synergistically as an adaptive filter of natural spike trains. *PLoS Biol* **4**, e207.

Kohashi, T., Ma, X. and Carlson, B. A. (2012). Passive and active membrane properties contribute to temporal selectivity for communication signals in mormyrid electric fish. In *10th International Congress of Neuroethology*. College Park, MD.

Konishi, M. (1993). Listening with two ears. *Sci Am* **268**, 66-73.

Köppl, C. (2009). Evolution of sound localization in land vertebrates. *Curr Biol* **19**, R635-R639.

Kramer, B. (1974). Electric organ discharge interaction during interspecific agonistic behavior in freely swimming mormyrid fish. *J Comp Physiol* **93**, 203-235.

Kramer, B. (1978). Spontaneous discharge rhythms and social signalling in the weakly electric fish *Pollimyrus isidori* (Cuvier et Valenciennes) (Mormyridae, Teleostei). *Behav Ecol Sociobiol* **4**, 61-74.

Kramer, B. (1979). Electric and motor responses of the weakly electric fish, *Gnathonemus petersii* (Mormyridae), to play-back of social signals. *Behav Ecol Sociobiol* **6**, 67-79.

Kramer, B. and Kuhn, B. (1994). Species recognition by the sequence of discharge intervals in weakly electric fishes of the genus *Campylomormyrus* (Mormyridae, Teleostei). *Anim Behav* **48**, 435-445.

Kuba, H. (2007). Cellular and molecular mechanisms of avian auditory coincidence detection. *Neuroscience Research* **59**, 370-376.

Laurent, G. (1997). Olfactory processing: Maps, times, and codes. *Curr. Opin. Neurobiol.* **7**, 547-553.

Lavoué, S., Hopkins, C. D. and Toham, A. K. (2004). The *Petrocephalus* (Pisces, Osteoglossomorpha, Mormyridae) of Gabon, Central Africa, with the description of a new species. *Zoosystema* **26**, 511-535.

Lavoué, S., Sullivan, J. P. and Arnegard, M. E. (2010). African weakly electric fishes of the genus *Petrocephalus* (Osteoglossomorpha: Mormyridae) of Odzala National Park, Republic of the Congo (Lékoli River, Congo River basin) with description of five new species. *Zootaxa* **2600**, 1-52.

Lestienne, R. (2001). Spike timing, synchronization and information processing on the sensory side of the central nervous system. *Prog Neurobiol* **65**, 545-91.

Lucker, H. and Kramer, B. (1981). Development of a sex difference in the preferred latency response in the weakly electric fish, *Pollimyrus isidori* (Cuvier et Valenciennes) (Mormyridae, Teleostei). *Behav Ecol Sociobiol* **9**, 103-109.

Lyons-Warren, A. M., Hollmann, M. and Carlson, B. A. (2012a). Sensory receptor diversity establishes a peripheral population code for stimulus duration at low intensities. *J Exp Biol* **215**, 2586-600.

Lyons-Warren, A. M., Kohashi, T., Mennerick, S. and Carlson, B. A. (2012b). It's not a coincidence: A novel mechanism for processing submillisecond spike timing differences. In *10th International Congress of Neuroethology*. College Park, MD.

Lyons-Warren, A. M., Kohashi, T., Mennerick, S. and Carlson, B. A. (2013). Retrograde fluorescent labeling allows for targeted extracellular single-unit recording from identified neurons *in vivo*. *J Vis Exp* **76**, e3921.

Ma, X., Kohashi, T. and Carlson, B. A. (2013) Extensive excitatory network interactions shape temporal processing of communication signals in a model sensory system. *J. Neurophysiol*., doi:10.1152/jn.00145.2013.

Machnik, P. and Kramer, B. (2008). Female choice by electric pulse duration: attractiveness of the males' communication signal assessed by female bulldog fish, Marcusenius pongolensis (Mormyridae, Teleostei). *J Exp Biol* **211**, 1969-77.

MacLeod, K. M. (2011). Short-term synaptic plasticity and intensity coding. *Hearing Research* **279**, 13-21.

Maler, L., Karten, H. J. and Bennett, M. V. L. (1973a). The central connections of the anterior lateral line nerve of *Gnathonemus petersii*. *J Comp Neurol* **151**, 67-84.

Maler, L., Karten, H. J. and Bennett, M. V. L. (1973b). The central connections of the posterior lateral line nerve of *Gnathonemus petersii*. *J Comp Neurol* **151**, 57-66.

Maler, L., Sas, E. K. B. and Rogers, J. (1981). The cytology of the posterior lateral line lobe of high frequency weakly electric fish (Gymnotidae): Dendritic differentiation and synaptic specificity in a simple cortex. *J Comp Neurol* **195**, 87-139.

Markowski, B., Baier, B. and Kramer, B. (2008). Differentiation in electrical pulse waveforms in a pair of sibling Dwarf Stonebashers *Pollimyrus castelnaui* and *P. marianne*: possible mechanisms and functions (Mormyridae, Teleostei). *Behaviour* **145**, 115-135.

Marsat, G. and Maler, L. (2010). Neural heterogeneity and efficient population codes for communication signals. *J Neurophysiol* **104**, 2543-2555.

Matsushita, A. and Kawasaki, M. (2004). Unitary giant synapses embracing a single neuron at the convergent site of time-coding pathways of an electric fish, *Gymnarchus niloticus*. *Journal of Comparative Neurology* **472**, 140-155.

Mehaffey, W. H., Ellis, L. D., Krahe, R., Dunn, R. J. and Chacron, M. J. (2008a). Ionic and neuromodulatory regulation of burst discharge controls frequency tuning. *Journal of Physiology-Paris* **102**, 195-208.

Mehaffey, W. H., Maler, L. and Turner, R. W. (2008b). Intrinsic frequency tuning in ELL pyramidal cells varies across electrosensory maps. *J Neurophysiol* **99**, 2641-55.

Middleton, J., Yu, N., Longtin, A. and Maler, L. (2011). Routing the flow of sensory signals using plastic responses to bursts and isolated spikes: experiment and theory. *J Neurosci* **31**, 2461-2473.

Moller, P. (1970). 'Communication' in weakly electric fish, *Gnathonemus niger* (mormyridae) I. Variation of electric organ discharge (EOD) frequency elicited by controlled electric stimuli. *Anim Behav* **18**, 768-786.

Moller, P. (1976). Electric signals and schooling behavior in a weakly electric fish, Marcusenius cyprinoides L. (Mormyriformes). *Science* **193**, 697-9.

Mugnaini, E. and Maler, L. (1987a). Cytology and immunocytochemistry of the nucleus extrolateralis anterior of the mormyrid brain: possible role of GABAergic synapses in temporal analysis. *Anat Embryol (Berl)* **176**, 313-36.

Mugnaini, E. and Maler, L. (1987b). Cytology and immunocytochemistry of the nucleus of the lateral line lobe in the electric fish Gnathonemus petersii (Mormyridae): evidence suggesting that GABAergic synapses mediate an inhibitory corollary discharge. *Synapse* **1**, 32-56.

Nicol, M. J. and Walmsley, B. (2002). Ultrastructural basis of synaptic transmission between endbulbs of Held and bushy cells in the rat cochlear nucleus. *J Physiol* **539**, 713-23.

Nieuwenhuys, R., ten Donkelaar, H. J. and Nicholson, C. (1998). The meaning of it all. In *The Central Nervous System of Vertebrates*, vol. 3 (ed. R. Nieuwenhuys H. J. ten Donkelaar and C. Nicholson), pp. 2135-2195. Berlin: Springer-Verlag.

O'Donnell, C. and Nolan, M. F. (2011). Tuning of synaptic responses: an organizing principle for optimization of neural circuits. *Trends Neurosci* **34**, 51-60.

Paintner, S. and Kramer, B. (2003). Electrosensory basis for individual recognition in a weakly electric, mormyrid fish, *Pollimyrus adspersus* (Gunther, 1866). *Behav Ecol Sociobiol* **55**, 197-208.

Panzeri, S., Brunel, N., Logothetis, N. K. and Kayser, C. (2010). Sensory neural codes using multiplexed temporal scales. *Trends Neurosci* **33**, 111-20.

Perkel, D. and Bullock, T. H. (1968). Neuronal coding. *Neurosci Res Prog Bull* **6**, 221-348.

Pluta, S. R. and Kawasaki, M. (2010). Temporal selectivity in midbrain electrosensory neurons identified by modal variation in active sensing. *J Neurophysiol* **104**, 498-507.

Prechtl, J. C., von der Emde, G., Wolfart, J., Karamursel, S., Akoev, G. N., Andrianov, Y. N. and Bullock, T. H. (1998). Sensory processing in the pallium of a mormyrid fish. *Journal of Neuroscience* **18**, 7381-7393.

Rieke, F., Warland, D., de Ruyter van Steveninck, R. and Bialek, W. (1997). Spikes: Exploring the Neural Code. Cambridge, MA: The MIT Press.

Rose, G. and Capranica, R. R. (1983). Temporal selectivity in the central auditory system of the leopard frog. *Science* **219**, 1087-1089.

Rose, G. J. and Fortune, E. S. (1999). Frequency-dependent PSP depression contributes to low-pass temporal filtering in Eigenmannia. *J Neurosci* **19**, 7629-39.

Rose, G. J., Leary, C. J. and Edwards, C. J. (2011). Interval-counting neurons in the anuran auditory midbrain: factors underlying diversity of interval tuning. *J Comp Physiol A Neuroethol Sens Neural Behav Physiol* **197**, 97-108.

Russell, C. J. and Bell, C. C. (1978). Neuronal responses to electrosensory input in mormyrid valvula cerebelli. *J Neurophysiol* **41**, 1495-1510.

Russell, C. J., Myers, J. P. and Bell, C. C. (1974). The echo response in *Gnathonemus petersii* (Mormyridae). *J Comp Physiol* **92**, 181-200.

Ryan, M. J. (1986). Neuroanatomy influences speciation rates among anurans. *Proc Natl Acad Sci USA* **83**, 1379-1382.

Sadeghi, S. G., Chacron, M. J., Taylor, M. C. and Cullen, K. E. (2007). Neural variability, detection thresholds, and information transmission in the vestibular system. *J Neurosci* **27**, 771-81.

Schluger, J. H. and Hopkins, C. D. (1987). Electric fish approach stationary signal sources by following electric current lines. *J Exp Biol* **130**, 359-67.

Schnupp, J. W. H. and Carr, C. E. (2009). On hearing with more than one ear: lessons from evolution. *Nat Neurosci* **12**, 692-697.

Seehausen, O., Terai, Y., Magalhaes, I. S., Carleton, K. L., Mrosso, H. D. J., Miyagi, R., van der Sluijs, I., Schneider, M. V., Maan, M. E., Tachida, H. et al. (2008). Speciation through sensory drive in cichlid fish. *Nature* **455**, 620-627.

Sullivan, J. P., Lavoue, S. and Hopkins, C. D. (2000). Molecular systematics of the African electric fishes (Mormyroidea: teleostei) and a model for the evolution of their electric organs. *J Exp Biol* **203**, 665-83.

Sullivan, W. E. and Konishi, M. (1984). Segregation of stimulus phase and intensity coding in the cochlear nucleus of the barn owl. *J Neurosci* **4**, 1787-99.

Szabo, T. (1965). Sense organs of the lateral line system in some electric fish of the Gymnotidae, Mormyridae and Gymnarchidae. *J Morphol* **117**, 229-49.

Szabo, T., Enger, P. S. and Libouban, S. (1979). Electrosensory systems in the mormyrid fish, Gnathonemus petersii : special emphasis on the fast conducting pathway. *J Physiol (Paris)* **75**, 409-20.

Szabo, T. and Fessard, A. (1974). Physiology of electroreceptors. In *Handbook of Sensory Physiology, Vol. III Pt. 3*, (ed. A. Fessard), pp. 59-124. Berlin, Heidelberg, New York: Springer-Verlag.

Szabo, T. and Ravaille, M. (1976). Synaptic structure of the lateral line lobe nucleus in mormyrid fish. *Neurosci Lett* **2**, 127-131.

Szabo, T., Ravaille, M., Libouban, S. and Enger, P. S. (1983). The mormyrid rhombencephalon: I. Light and EM investigations on the structure and connections of the lateral line lobe nucleus with HRP labelling. *Brain Res* **266**, 1-19.

Szabo, T., Sakata, H. and Ravaille, M. (1975). An electrotonically coupled pathway in the central nervous system of some teleost fish, Gymnotidae and Mormyridae. *Brain Res* **95**, 459-74.

Terai, Y., Seehausen, O., Sasaki, T., Takahashi, K., Mizoiri, S., Sugawara, T., Sato, T., Watanabe, M., Konijnendijk, N., Mroso, H. D. J. et al. (2006). Divergent selection on opsins drives incipient speciation in Lake Victoria cichlids. *PLOS Biology* **4**, e433.

Teyssedre, C. and Serrier, J. (1986). Temporal spacing of signals in communication, studied in weakly-electric mormyrid fish (Teleostei, Pisces). *Behav Processes* **12**, 77-98.

Theunissen, F. and Miller, J. P. (1995). Temporal encoding in nervous systems: a rigorous definition. *J Comput Neurosci* **2**, 149-62.

Trussell, L. O. (1997). Cellular mechanisms for preservation of timing in central auditory pathways. *Curr Opin Neurobiol* **7**, 487-92.

Trussell, L. O. (1999). Synaptic mechanisms for coding timing in auditory neurons. *Annu Rev Physiol* **61**, 477-496.

Trussell, L. O. (2008). Central synapses that preserve auditory timing. In *The Senses: A Comprehensive Reference*, eds. A. I. Basbaum A. Kaneko G. M. Shepherd and G. Westheimer), pp. 587-602. San Diego, CA: Academic.

Victor, J. D. and Purpura, K. P. (1996). Nature and precision of temporal coding in visual cortex: a metric-space analysis. *J Neurophysiol* **76**, 1310-1326.

von der Emde, G., Sena, L. G., Niso, R. and Grant, K. (2000). The midbrain precommand nucleus of the mormyrid electromotor network. *J Neurosci* **20**, 5483-95.

Waxman, S. G. (1980). Determinants of conduction velocity in myelinated nerve fibers. *Muscle Nerve* **3**, 141-50.

Westby, G. W. M. and Kirschbaum, F. (1978). Emergence and development of the electric organ discharge in the mormyrid fish, *Pollimyrus isidori*. *J Comp Physiol A* **127**, 45-49.

Wong, R. Y. and Hopkins, C. D. (2007). Electrical and behavioral courtship displays in the mormyrid fish Brienomyrus brachyistius. *J Exp Biol* **210**, 2244-52.

Wullimann, M. F. and Northcutt, R. G. (1990). Visual and electrosensory circuits of the diencephalon in mormyrids: an evolutionary perspective. *J Comp Neurol* **297**, 537-52.

Wullimann, M. F. and Rooney, D. J. (1990). A direct cerebello-telencephalic projection in an electrosensory mormyrid fish. *Brain Res* **520**, 354-7.

Xu-Friedman, M. A. and Hopkins, C. D. (1999). Central mechanisms of temporal analysis in the knollenorgan pathway of mormyrid electric fish. *J Exp Biol* **202**, 1311-8.

Xu-Friedman, M. A. and Regehr, W. G. (2005). Dynamic-clamp analysis of the effects of convergence on spike timing. I. Many synaptic inputs. *J Neurophysiol* **94**, 2512-25.

Zakon, H. H. (1986). The electroreceptive periphery. In *Electroreception*, (ed. T. H. Bullock and W. Heiligenberg), pp. 103-156. New York: John Wiley & Sons.

Zipser, B. and Bennett, M. V. (1976). Interaction of electrosensory and electromotor signals in lateral line lobe of a mormyrid fish. *J Neurophysiol* **39**, 713-21.

Zucker, R. S. and Regehr, W. G. (2002). Short-term synaptic plasticity. *Annu Rev Physiol* **64**, 355-405.

Chapter 2

Short-term depression, temporal summation, and onset inhibition shape interval tuning in midbrain neurons

This chapter contains a previously published manuscript:

Baker C.A. and Carlson B.A. (2014) Short-term depression, temporal summation, and onset inhibition shape interval tuning in midbrain neurons. *The Journal of Neuroscience* 34:14272-14287.

Author contributions for the above citation:

C.A.B. and B.A.C. designed research; C.A.B. performed research; C.A.B. analyzed data; C.A.B. and B.A.C. wrote the manuscript.

ABSTRACT

A variety of synaptic mechanisms can contribute to single-neuron selectivity for temporal intervals in sensory stimuli. However, it remains unknown how these mechanisms interact to establish single-neuron sensitivity to temporal patterns of sensory stimulation *in vivo.* Here we address this question in a circuit that allows us to control the precise temporal patterns of synaptic input to interval-tuned neurons in behaviorally relevant ways. We obtained *in vivo* intracellular recordings under multiple levels of current-clamp from midbrain neurons in the mormyrid weakly electric fish *Brienomyrus brachyistius* during stimulation with electrosensory pulse trains. To reveal the excitatory and inhibitory inputs onto interval-tuned neurons, we then estimated the synaptic conductances underlying responses. We found short-term depression in excitatory and inhibitory pathways onto all interval-tuned neurons. Short-interval selectivity was associated with excitation that depressed less than inhibition at short intervals, as well as temporally summating excitation. Long-interval selectivity was associated with long-lasting onset inhibition. We investigated tuning after separately nullifying the contributions of temporal summation and depression, and found the greatest diversity of interval-selectivity among neurons when both mechanisms were at play. Furthermore, eliminating the effects of depression decreased sensitivity to directional changes in interval. These findings demonstrate that variation in depression and summation of excitation and inhibition helps establish tuning to behaviorally relevant intervals in communication signals, and that depression contributes to neural coding of interval sequences. This work reveals for the first time how the interplay between short-term plasticity and temporal summation mediates the decoding of temporal sequences in awake, behaving animals.

INTRODUCTION

Many circuits contain neurons tuned to particular timing sequences in sensory stimuli (Rose and Capranica, 1983; Grothe, 1994; Fortune and Rose, 1997a; Edwards et al., 2002; Sakai et al., 2009; Pluta and Kawasaki, 2010; Goel and Buonomano, 2014). Single-neuron temporal tuning reflects a combination of presynaptic tuning, synaptic filtering, and postsynaptic filtering. Two synaptic mechanisms that have been implicated in establishing temporal filtering *in vivo* are short-term depression (Fortune and Rose, 2000) and temporal summation (Rose et al., 2011). However, it is difficult to precisely determine the relative contributions of various synaptic filtering mechanisms to interval tuning *in vivo* because temporal filtering by presynaptic neurons makes the relationship between stimulus intervals and presynaptic input patterns unknown. *In vitro* slice recordings, which allow precise control of presynaptic stimulation, have also revealed that short-term plasticity (Klyachko and Stevens, 2006) and temporal summation (George et al., 2011) act as temporal filters of synaptic input. However, *in vitro* preparations sever connections between neurons thereby disrupting the natural spatiotemporal pattern of inputs. Furthermore, pharmacologically blocking inhibition may release presynaptic excitatory inputs from their natural inhibition, making it difficult to isolate the relative contributions of excitation and inhibition to single-neuron temporal selectivity under natural conditions.

Here we study the interactions of excitation and inhibition in interval-tuned neurons *in vivo* in a circuit that allows precise control of presynaptic timing. Mormyrid electric fish are ideal for studying synaptic mechanisms of temporal filtering because the interspike intervals of presynaptic inputs onto interval-tuned neurons precisely follow the interpulse intervals in sensory stimuli. Moreover, these intervals can be varied in ways that fish would naturally experience. Mormyrids vary the intervals between successive electric organ discharges (EODs)

to communicate (see Carlson, 2002 for review). Natural interpulse intervals (IPIs) range from approximately ten to hundreds of milliseconds (Hopkins, 1986), and the ability to accurately detect and decode rapidly changing temporal patterns of EODs is essential for social interactions (Carlson, 2002).

Electric communication signals are processed by a dedicated sensory pathway (Xu-Friedman and Hopkins, 1999; Baker et al., 2013). Electroreceptors in the skin fire one time-locked spike in response to each EOD (Bennett, 1965). This spike pattern is relayed to the hindbrain nucleus of the electrosensory lateral line lobe, which in turn projects to the anterior exterolateral nucleus (ELa) of the midbrain torus semicircularis. ELa sends its only output to the adjacent posterior exterolateral nucleus (ELp) while preserving the IPIs of the sensory stimulus (Carlson, 2009). ELp neurons respond selectively to particular IPIs and thus act as temporal filters of afferent spike patterns (Carlson, 2009).

In the current study, we present electrosensory stimulation to awake, behaving fish, record responses of single ELp neurons to IPI trains under multiple levels of current-clamp, and estimate the excitatory and inhibitory synaptic conductances underlying IPI tuning. This method maintains the intact neural circuit and allows direct comparison of the strength and time course of excitation and inhibition to study the relative contributions of short-term synaptic plasticity and temporal summation in establishing interval selectivity.

MATERIALS AND METHODS

Animals. We used a total of 45 *Brienomyrus brachyistius* (5.0-9.0 cm in standard length) of both sexes in this study. We acquired the fish through the aquarium trade and housed them in groups with a 12h:12h light:dark cycle, water conductivity of 200-400 μS/cm, and temperature of 25-29° C. We fed the fish live black worms four times per week. All procedures were in accordance with the guidelines established by the National Institutes of Health and were approved by the Institutional Animal Care and Use Committee at Washington University in St. Louis.

Surgery. The surgical procedure has been described previously (Carlson, 2009; Lyons-Warren et al., 2013b). Briefly, fish were anesthetized in a solution of 300 mg/L tricaine methanesulfonate (MS-222) and paralyzed with an intramuscular injection of 100 μL of 3 mg/mL gallamine triethiodide (Flaxedil). We then respired the fish with 100 mg/L MS-222. Before surgery, we applied a drop of 0.4% lidocaine local anesthetic to the incision site. Next we glued a head post to the skull and performed a craniotomy to expose ELp. Following surgery, we switched respiration to freshwater and allowed the fish to recover from anesthesia before beginning the recording session. We monitored the fish's anesthetized state with a pair of electrodes external to the electric organ to record the fictive EOD generated by the electromotor neurons (Carlson, 2009). The fictive EOD is silenced during anesthesia; the return of fictive discharges at regular intervals signals that the fish has recovered. At the end of the recording session, the fish was anesthetized with 100 mg/L MS-222 respiration until no fictive EOD could be recorded, and then the fish was killed by freezing.

Intracellular whole-cell recordings. We obtained intracellular whole-cell current-clamp recordings following previously published methods (Rose and Fortune, 1996; Carlson, 2009).

We filled glass micropipettes of 20-40 MΩ resistance with a tip solution containing the following (in mM): 100 CH_3CO_2K, 2 KCl, 1 $MgCl_2$, 5 EGTA, 10 HEPES, 20 KOH, and 43 biocytin. We filled the pipette shank with the same solution except that we replaced biocytin with D-mannitol (Carlson, 2009). Initial seals were >1 GΩ. Intracellular recordings were amplified 10x and low-pass filtered (cut-off frequency=10 kHz) through an Axopatch 200B amplifier (Molecular Devices) and digitized at a sampling rate of 97.7 kHz (Tucker-Davis Technologies; model RX8). We saved recordings using custom-made software for Matlab 7 (Mathworks).

Stimulus presentation. We delivered electrosensory stimuli through electrodes positioned at the perimeter of the recording chamber. For transverse stimulation to the fish, stimuli were delivered between three vertically oriented electrodes on one side of the chamber and three vertically oriented electrodes on the other side of the chamber. For longitudinal stimulation to the fish, stimuli were delivered between two vertically oriented electrodes on the front of the chamber and two vertically oriented electrodes on the back of the chamber (Lyons-Warren et al., 2013b). Stimuli consisted of monophasic square electric pulses. After establishing a recording, we first stimulated with single pulses while varying pulse duration (0.5-1.5 ms), intensity (1-100 mV/cm), polarity (normal or reversed), and orientation (transverse or longitudinal to the fish) to identify the combination of features that elicited maximal postsynaptic potential (PSP) responses from a given neuron. We then delivered all stimuli to that neuron using this combination of features, varying only the interpulse intervals (as in Carlson, 2009). We discarded responses to stimulus pulses delivered 2-5 ms after a fictive EOD, since a corollary discharge at the level of the hindbrain blocks sensory responses occurring within this window (Bell and Grant, 1989).

Data analysis. We removed spikes from recording traces using a linear extrapolation method (Hedwig and Knepper, 1992). First, we smoothed the derivative of the recorded trace using a moving average filter with width of 0.5 ms. We defined spike start as the point where the smoothed derivative first exceeded the prestimulus mean + 4SD, and spike end as the point where the smoothed derivative decreased below the prestimulus mean - 1SD. We chose four SD for the spike start to avoid identifying fast PSPs as spikes, and one SD for the spike end to ensure capturing as much of the spike as possible. If the smoothed derivative did not cross the spike end threshold, we used the first minimum in the smoothed derivative up to 8 ms after the spike start as the spike end. Such a wide window was necessary to accommodate variation in neurons' responses, which depend not only on intrinsic membrane properties but also where on the membrane the patch recording is located. To remove the spikes, we linearly extrapolated the membrane potential between spike start and spike end.

We averaged responses to 10 repetitions of each stimulus presented. Next we determined the membrane's resting potential (RP) by averaging the potential over a 50 ms window immediately preceding the stimulus. We measured the PSP amplitude by finding the maximum potential in a window starting 3 ms after stimulus pulse offset and ending immediately before the onset of the next pulse. We chose 3 ms as the start of the measurement window because the latency of electrosensory responses in ELa, the primary input to ELp, is ~3 ms (Amagai, 1998; Carlson, 2009). If the maximum potential occurred after delivery of the next pulse, we increased the measurement window by 3 ms while ignoring the stimulus artifact. We subtracted the RP from the maximum potential to yield the PSP amplitude. For presentation purposes, we removed the stimulus artifact by linearly extrapolating the membrane potential from the time of pulse onset to 0.5 ms after pulse offset.

We assessed tuning to interpulse intervals (IPIs) in 72 neurons using scanning IPI stimuli. We presented two scan stimuli; one consisted of a sequence of decreasing then increasing intervals (200 to 10 ms IPIs followed by 10 to 200 ms IPIs; see Fig. 1), and the other consisted of a sequence of increasing then decreasing intervals. These IPI scan stimuli are similar to frequency sweeps used to quantify response properties of the central auditory systems of many animals (e.g., Carrasco and Lomber, 2011; Williams and Fuzessery, 2012; Geis and Borst, 2013). We measured the PSPs elicited by each pulse in the two scan stimuli, and then averaged the PSPs in response to the same IPI. We also evaluated IPI tuning in nine neurons using trains of 10 pulses delivered at constant IPI ranging from 10 to 100 ms. We averaged responses to the 2^{nd}-10^{th} pulses in the train to obtain the neuron's response to each IPI (Carlson, 2009; George et al., 2011; Ma et al., 2013). We collected both scanning IPI and constant IPI tuning curves from two neurons, and in both cases the scanning and constant IPI tuning curves were in agreement with one another.

High-pass neurons respond best to short intervals, low-pass neurons respond best to long intervals, band-pass neurons respond best to intermediate intervals, and band-stop neurons respond best to short and long, but not intermediate, intervals (Carlson, 2009). To generate tuning curves, we normalized responses to each IPI by dividing by the maximum response (Fig. 1). If PSPs to all IPIs were negative (i.e., below the neuron's resting potential), we multiplied all PSPs by -1 before normalizing by the maximum response. If the normalized responses to all IPIs remained above 0.85, we classified the neuron as all-pass (Carlson, 2009; George et al., 2011; Ma et al., 2013). Otherwise, we fit tuning curves with both Gaussian and sigmoidal functions to characterize IPI tuning (Groh et al., 2003). If the r^2 values of both the Gaussian and the sigmoidal fits were < 0.5, we classified the neuron's tuning as complex. Since Gaussian and sigmoidal

curves can fit low- and high-pass tuning curves equally well, we used an $r^2_{sigmoid}/r^2_{Gaussian}$ ratio of 0.85 as a cutoff for comparing the goodness of sigmoid and Gaussian fits (Groh et al., 2003). If at least one r^2 was ≥ 0.5, we used the ratio of the r^2 values to determine tuning. If $r^2_{sigmoid}/r^2_{Gaussian} \geq 0.85$, we classified the neuron as high-pass if the ratio of the sigmoid slope to the sigmoid amplitude was negative, and low-pass if this ratio was positive. If $r^2_{sigmoid}/r^2_{Gaussian} < 0.85$, we classified the neuron as band-pass if the Gaussian amplitude was positive and band-stop if the Gaussian amplitude was negative. For tuning curves in which all PSPs were originally negative, we classified tuning as the opposite of the result of the fits to account for the reversed sign.

From the scanning IPI stimuli used to assess tuning, we also quantified the degree of sensitivity to direction of IPI change. Changes in IPI are common characteristics of mormyrid electric communication signals (Carlson, 2002; Carlson and Hopkins, 2004; Wong and Hopkins, 2007). To quantify the degree of sensitivity to direction of IPI change, we calculated a scan direction-selectivity index (DSI). We started by normalizing the PSPs elicited by a scan stimulus to the maximum PSP. If the maximum potential in response to a particular IPI was below the neuron's resting potential, we set the response to that IPI to 0. This step was necessary to limit the range of the DSI from 0 to 1. For a single scan stimulus, we next found the difference between the PSP evoked by a given IPI when presented during the decreasing portion of the scan, and that evoked by the same IPI when presented during the increasing portion of the scan. We took the sum of the absolute values of these differences across all IPIs and divided by the total number of IPIs (n=12 IPIs). We then averaged the DSI across the two scan stimuli (increasing then decreasing scan, and decreasing then increasing scan). When the PSPs in response to each IPI are identical regardless of scan direction, the DSI equals 0 (no directional

selectivity), and when the PSPs in response to each IPI are equal to the maximum response in one direction and zero in the other direction, the DSI equals 1 (maximal directional selectivity).

To investigate the influence of temporal summation on IPI tuning and scan directional selectivity, we removed its effects from our PSP measurements. From the maximum potential evoked by each stimulus pulse, we subtracted the minimum potential that occurred between the time of the maximum potential and the time of the stimulus pulse. The results provide an estimate of the membrane potential changes evoked only by each pulse while minimizing the lingering effects of responses to previous pulses. To assess the validity of this method, we compared the results to measurements of true summation for the second PSP in 10 ms and 100 ms IPI trains. To measure true summation, we subtracted the change in membrane potential of the single-pulse response at the time of the second PSP from the amplitude of the second PSP. We then normalized the second PSP amplitudes resulting from each summation removal method to the first PSP amplitude in the train. We compared the results of the two methods in 40 neurons for which responses to both 10 ms and 100 ms IPIs were available. Our summation removal method resulted in three outlier neurons in which the 10 ms IPI PSPs were greatly overestimated, and one outlier neuron in which the 100 ms IPI PSPs were greatly overestimated relative to the true summation removal method. After removing these outliers, we found a linear correlation between the normalized PSPs using our summation removal method and the normalized PSPs using the true summation removal method at 10 ms IPIs ($y=0.54x+0.88$, $r^2=0.24$, $F_{(1,34)}=11$, $p=0.0025$) as well as 100 ms IPIs ($y=0.46x+0.66$, $r^2=0.28$, $F_{(1,34)}=13$, $p=0.00099$). Based on these results, we performed our summation removal method on the PSPs used to determine each neuron's IPI tuning and scan directional selectivity to determine the contribution of temporal summation to these two properties. We did not include the four outlier neurons in this analysis.

In general, our summation removal method (median normalized PSP=1.25, range=0-4.2) tended to modestly overestimate 10 ms IPI PSPs relative to the true summation removal method (median normalized PSP=0.93, range=-0.09-4.0; Wilcoxon matched-pairs test, $Z_{(36)}$=2.3, p=0.03). There was no difference between the results of the two methods for 100 ms IPIs (Wilcoxon matched-pairs test, $Z_{(36)}$=1.7, p=0.084). Therefore, our method of removing summation may overestimate PSP amplitudes at short intervals but not long intervals. The net effect of this error would be a tendency to exaggerate the high-pass nature of summation-removed responses. Since we found that minimizing the effects of summation reduced the number of high-pass neurons (see Fig. 8), the possibility that we overestimated neurons' high-pass characteristics means that there may have actually been fewer high-pass responses if we could have more accurately assessed tuning without summation. Thus, this error is conservative, as accounting for this modest overestimation could only lend added support to our conclusion that temporal summation is important for producing high-pass responses (see Results).

Synaptic conductance estimation. We estimated the synaptic conductances underlying neural responses following established methods (i.e., Wehr and Zador, 2003; Priebe and Ferster, 2005; Higley and Contreras, 2006; Monier et al., 2008; Gittelman et al., 2009), which are based on solving the membrane equation

$$C_m \frac{dV_m}{dt} = g_e(V_m - V_e) + g_i(V_m - V_i) + g_{leak}(V_m - V_{rest}) + I_{inj}, \qquad (2.1)$$

where C_m is the membrane capacitance, dV_m/dt is the change in membrane potential over time, V_{rest} is the resting membrane potential, I_{inj} is the injected current, V_e and V_i are the excitatory and inhibitory reversal potentials, respectively, and g_e, g_i, and g_{leak} are the excitatory, inhibitory, and leak conductances, respectively.

We first measured the input resistance (R_m) and membrane time constant (τ_m) by fitting a double exponential to each neuron's response to a 100 ms, -0.10 nA current pulse, as described by Gittelman et al. (2009). We then used these values to calculate the membrane capacitance ($C_m = \tau_m/R_m$).

Next we obtained intracellular recordings of responses to single stimulus pulses, constant IPI trains (10 ms and 100 ms IPIs), and scanning IPI trains (10-200 ms IPIs) at multiple levels of current clamp (0 to -0.20 nA). We estimated the capacitive current (I_{cap}) according to

$$I_{cap} = C_m \frac{dV_m}{dt}. \tag{2.2}$$

Using the equation

$$V_m = \frac{1}{g_T}(I_{inj} - I_{cap}) + V_{rev}, \tag{2.3}$$

where V_m is the membrane potential, g_T is the total conductance, and V_{rev} is the synaptic reversal potential, we created plots of ($I_{inj} - I_{cap}$) vs. V_m for the different levels of current clamp at each time point in the recording. The inverse of the slope of the best-fit line at each time point yields g_T. The baseline g_T represents g_{leak}, and was found by taking the inverse of the median slope of best fits over the 50 ms prestimulus period. We then calculated the synaptic conductance (g_{syn}) throughout the recording as g_T - g_{leak}.

Next we defined a baseline (I_{inj} - I_{cap}) vs. V_m curve, with y-intercept equal to the median of the y-intercepts of the best fits during the prestimulus period, and slope equal to the inverse of g_{leak}. The intersection of the baseline curve with the best-fit line at each time point during the recording yields V_{rev} at that time point. Following the simplification that the synaptic current is 0 nA at V_{rev}, equations for g_e and g_i can be written as

$$g_e = g_{syn} \frac{(V_i - V_{rev})}{(V_i - V_e)} \tag{2.4}$$

and

$$g_i = g_{syn} \frac{(V_e - V_{rev})}{(V_e - V_i)} . \tag{2.5}$$

We used a V_e of 0 mV and a V_i of -106 mV, which was the calculated reversal potential for potassium based on our intracellular electrode solution and extracellular Hickman's ringer solution.

Because this method is based on the cell's I-V linearity, spikes necessarily violate this linearity and cause error in conductance estimation that cannot be overcome through spike removal (Guillamon et al., 2006). Therefore, we discarded current-clamp levels containing spikes. However, if fewer than three current-clamp levels were spike-free for a given neuron, we removed spikes by ignoring the portion of the recording trace from 2 ms before spike start to 2 ms after spike end before averaging across ten stimulus repetitions. Spike start and end criteria were as described for spike removal. If this process resulted in gaps (due to the presence of spikes in all repetitions) or large edge effects (due to throwing out portions of some repetitions), we excluded the file from synaptic conductance estimation. If fewer than three current-clamp levels passed these criteria, we excluded the neuron from synaptic conductance estimation. An additional inclusion criterion required a RP of at least -40 mV at 0 nA current injection.

Recordings from 48 of 83 neurons passed our inclusion criteria. The excluded recordings contained neurons from all tuning classes, and there were no differences in the tuning distributions of excluded vs. included neurons ($X^2_{(5)}$=6.3, p>0.25). Furthermore, there were no differences between included and excluded recordings in terms of resting membrane potential (Student's t-test, $t_{(81)}$=1.9, p=0.068), membrane time constant (Student's t-test, $t_{(81)}$=-1.8,

p=0.077), or input resistance (Student's t-test, $t_{(81)}$=-0.87, p=0.39). We therefore conclude that our inclusion criteria did not bias the tuning or the passive membrane properties of the neurons analyzed in this study.

We median filtered synaptic conductances with a filter width of 1 ms. To assess the goodness of the linear fits giving rise to the conductance estimates, we calculated the skewness of the linear r^2 distribution for each estimate according to

$$skewness(X) = \frac{n}{(n-1)(n-2)} \sum_{i=1}^{n} \left(\frac{X_i - \overline{X}}{\sigma} \right)^3 , \qquad (2.6)$$

where n is the number of points, $\overline{X}$ is the mean, and σ is the standard deviation of the r^2 distribution. Distributions clustered near 1 had negative skewness values, whereas distributions clustered near 0 had positive skewness values. If the skewness was >-1, we used only those conductance values at points where the r^2 of the I-V fits were greater than the median r^2. Skewness values ranged from -40 to 0.9 across all conductance estimates, with 20% of estimates having skewness values $\leq$-1.

In several neurons (n=10 neurons), the median-filtered synaptic reversal potential decreased below the inhibitory reversal potential, most likely due to a poor space clamp. In these cases, we set g_e = 0 nS and $g_i = g_{syn}$ at the points where $V_{rev} < V_i$, since the responses at these points were most likely dominated by inhibition.

Conductance estimations are based on a linear, isopotential neuron. While this method may cause slight underestimation of conductance magnitudes, it should not affect the time course (Wehr and Zador, 2003). We have tried to minimize these effects by comparing excitatory and inhibitory conductances within the same neuron and by normalizing conductance magnitudes before comparisons across neurons. Further, although cable attenuation may cause inhibitory

conductances to be slightly more underestimated than excitatory conductances (Wehr and Zador, 2003), we focused on differences between neuron types. Therefore, our comparisons should hold despite any systematic errors in estimation. Another potential source of error in our estimates would be the presence of voltage-gated conductances. Although we have no definitive evidence for voltage-gated conductances in ELp, we have tried to minimize potential effects by limiting our analysis to points in which the current-voltage relationship was roughly linear.

To quantify synaptic conductances, we measured the peak magnitudes evoked by stimulus pulses as the maximum conductance in a window starting 3 ms after stimulus pulse offset to immediately before onset of the next pulse. To determine onset and offset latencies of responses to single pulses, we first smoothed conductances using a median filter with width of 2 ms. Then the point at which the filtered conductance exceeded the prestimulus mean + 3SD defined the onset, and the point at which the filtered conductance decreased below the prestimulus mean + 1SD defined the offset. In some cases, two phases of conductance increases were present. If the filtered conductance crossed the onset threshold 5 ms or less after the offset of the first phase, we recorded the onset and offset of a second phase. We measured conductance duration by subtracting conductance onset from offset; in neurons with two phases, we measured the duration as the offset of the second phase minus onset of the first phase. For presentation purposes, we removed the stimulus artifact by linearly extrapolating the conductance estimates from the time of stimulus onset to 0.5 ms after stimulus offset.

To estimate the dynamics of short-term depression, we removed the effects of temporal summation from conductance estimates. From each conductance peak elicited by a stimulus pulse we subtracted the minimum conductance that occurred between the time of the peak and the time of the preceding peak, starting with the second pulse in a train. The results provide an

estimate of the conductance changes evoked only by each pulse while minimizing the lingering effects of responses to previous pulses. To assess the validity of this method, we compared the results to measurements of true summation for the second conductance peak in 10 ms IPI trains. To measure true summation, we subtracted the conductance value of the single-pulse response that occurred at the time of the second conductance peak elicited by the 10 ms IPI train from the second conductance peak. We then normalized the second conductance amplitudes resulting from each summation removal method to the amplitude of the first peak conductance in the train. We found a linear correlation between the results of the two methods for 10 ms IPI excitatory ($y=0.79x+0.13$, $r^2=0.68$, $F_{(1,40)}=85$, $p<0.000001$) and inhibitory ($y=0.72x+0.16$, $r^2=0.54$, $F_{(1,40)}=46$, $p<0.000001$) conductances.

To quantify the time course and degree of response decay (estimated conductances) or depression (estimated conductances with effects of summation removed) evoked by 10 ms IPI stimulus trains, we first normalized peak conductances to the conductance evoked by the first pulse. We then fit the normalized conductances with a single exponential function described by

$$y = ae^{\frac{-t}{\tau}} + b, \tag{2.7}$$

where t is the time of stimulus pulses. For our normalized data that by definition equal 1 at t=0 ms, we can simplify this equation to

$$y = a(e^{\frac{-t}{\tau}} - 1) + 1. \tag{2.8}$$

The coefficient (a) of the best fit gives a measure of the magnitude of decay/depression and the time constant (τ) gives a measure of the time course of decay/depression. We restricted τ to between 0 and 90 ms, corresponding to the range of stimulus times used. We restricted a to between 0 and 1. If a fit resulted in a=0, indicating no decay, we did not use the corresponding τ. This situation occurred in two band-pass neurons; however, after the effects of summation were

removed, a was greater than 0. Since we limited the data in the fit to the stimulus times used, the resulting a and τ reflect the decay/depression observed during the presented stimuli, and not necessarily steady-state values. Conductances that decay or depress faster will have a smaller τ, and conductances that decay or depress to a greater degree will have a larger a.

To study the effects of depression, we estimated what synaptic conductance responses would be in the absence of plasticity by convolving conductances evoked by single-pulse stimuli with IPI trains. First, for single-pulse conductances in which points with poor linear I-V fits were discarded, we linearly interpolated between the remaining points to recover a trace with the original uniform sampling rate. Next we defined the single-pulse conductances as the time point at which the stimulus occurred until the end of the recording (200 ms). We then convolved the single-pulse conductances with a 10-ms IPI train. To quantify the time course and degree of the resulting summation of conductances, we fit a single exponential described by

$$y = a(1 - e^{\frac{-t}{\tau}}) + b \tag{2.9}$$

to the normalized peak responses to a 10 ms IPI train, where t is the time of stimulus pulses. For our normalized data that by definition equal 1 at t=0 ms, the offset term b is equal to 1. The coefficient (a) and time constant (τ) of the best fit give a measure of the degree and time course, respectively, of temporal summation. We restricted τ to between 0 and 90 ms based on the stimulus times used, and we restricted a to between 0 and the maximum normalized conductance minus 1.

To estimate IPI tuning in the absence of plasticity, we convolved single-pulse conductances with the same IPI stimuli used to characterize tuning in each neuron. We then put these conductances into the membrane equation to estimate the membrane potential that would

result. We measured PSPs from the estimated membrane potential and characterized IPI tuning as described for recorded potentials.

Statistics. We performed all statistical tests in Statistica 6.1 (StatSoft, Inc.). Parametric tests included Student's *t*-test, paired *t*-test, one-way ANOVA, and repeated-measures ANOVA. Nonparametric tests included Wilcoxon matched-pairs test and observed vs. expected frequency χ^2.

RESULTS

We obtained intracellular whole-cell recordings from 83 ELp neurons during presentation of electrosensory pulse trains with IPIs ranging from 10-200 ms (Fig. 1). Recordings from 48 neurons yielded conductance estimates that fit our inclusion criteria (see Materials and Methods). Their tuning curves were classified as high-pass (*n*=15 neurons), low-pass (*n*=23 neurons), band-pass (*n*=4 neurons), band-stop (*n*=3 neurons), complex (*n*=2 neurons), or all-pass (*n*=1 neuron). We did not consider complex or all-pass tuned neurons in any subsequent analysis. We have included band-pass and band-stop neurons in population data to give an accurate representation of the diversity of responses of ELp neurons. However, we focused our analysis primarily on responses from high- and low-pass neurons since the majority of ELp neurons fall into one of these two categories (Carlson, 2009; George et al., 2011; Kohashi and Carlson, 2014).

High- and low-pass neurons responded differently to short-interval stimulation. At short IPIs, high-pass neurons exhibited increased synaptic response amplitudes, whereas low-pass neurons exhibited decreased response amplitudes (Fig. 1) (Carlson, 2009). In some cases, the responses of high- and low-pass neurons to long-interval stimuli also varied depending on the direction of interval change, as we describe in detail later. A variety of synaptic mechanisms have been shown to give rise to such temporal sensitivity (Baker et al., 2013), including temporal summation (George et al., 2011; Rose et al., 2011), short-term depression (Fortune and Rose, 2000; Klyachko and Stevens, 2006), and facilitation (Klyachko and Stevens, 2006). The relative timing of excitatory and inhibitory inputs has also been hypothesized to play a role (Grothe, 1994; Edwards et al., 2008). Here we address the extent to which these various synaptic mechanisms interact to generate temporal filtering of behaviorally relevant synaptic input patterns in an intact sensory midbrain circuit.

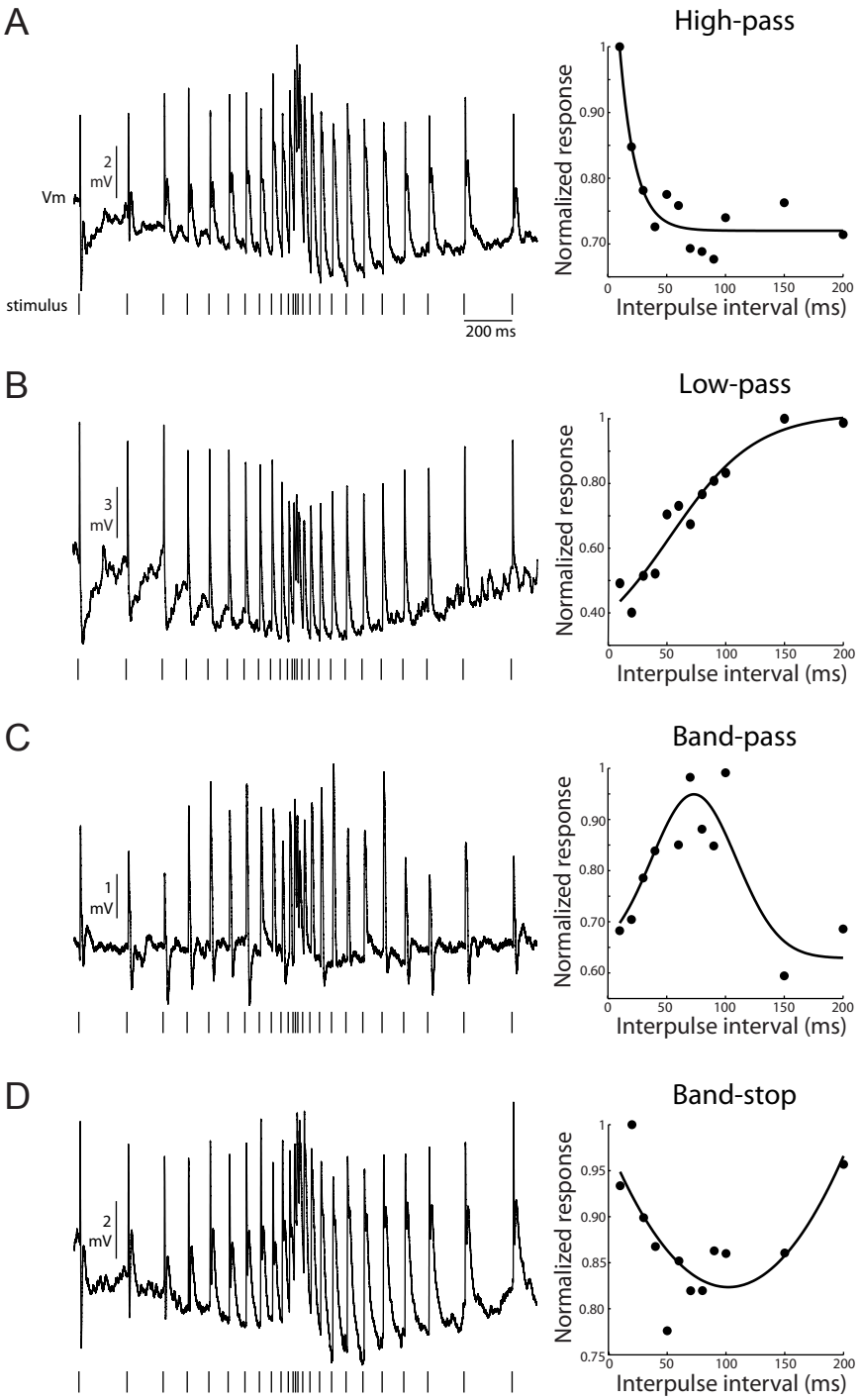

Figure 1. ELp neurons vary in their tuning to stimulus interval. Recorded membrane potential (V_m) in response to a scan of decreasing then increasing interpulse intervals (IPIs) (left) and tuning curve (right) for a high-pass (A), low-pass (B), band-pass (C), and band-stop (D) neuron. Tick marks below the recording traces indicate stimulus times. Tuning curves were generated by averaging postsynaptic potential (PSP) amplitudes in response to the same IPI during a decreasing-increasing train and an increasing-decreasing train, then normalizing by the maximum average response. These curves were then fit with both a Gaussian and a sigmoidal function. Neurons were classified as high-pass or low-pass if

$r^2_{sigmoid}/r^2_{Gaussian} \geq 0.85$, and as band-pass or band-stop if this ratio was < 0.85 (see Materials and Methods). The sigmoidal (high- and low-pass) or Gaussian (band-pass and band-stop) fit is shown for each neuron.

Excitatory and inhibitory synaptic conductances experience rate-dependent decreases in magnitude

The increased PSP amplitudes at short intervals that characterize high-pass responses could result from weakened inhibition or strengthened excitation. Conversely, the decreased PSP amplitudes at short intervals that characterize low-pass responses could result from strengthened inhibition or weakened excitation. To reveal the excitatory and inhibitory conductances evoked by IPIs ranging from 10 to 200 ms, we recorded intracellular responses of seven high-pass and ten low-pass neurons to electrosensory pulse trains of increasing and decreasing IPIs at multiple levels of holding current (Fig. 2A), and then estimated the underlying synaptic conductances (Fig. 2B,C). We found that the peak magnitude of both excitatory (Fig. 2D) and inhibitory (Fig. 2E) conductances decreased at short intervals in all neurons, with the shortest intervals resulting in the smallest conductances.

Excitation was significantly more reduced at short IPIs in low-pass neurons compared to high-pass neurons (Fig. 2D; repeated-measures ANOVA, interaction between tuning and IPI, $F_{(11,15)}$=6.3, p<0.000001). In contrast to excitation, inhibition was similarly reduced in the two groups of neurons during short IPIs (Fig. 2E; repeated-measures ANOVA, interaction between tuning and IPI, $F_{(11,15)}$=0.38 p=0.96). Notably, the amplitudes of inhibitory conductances were reduced compared to single-pulse responses even at the longest IPI tested (200 ms) in both groups of neurons.

Since the differences between high- and low-pass neurons were greatest at the shortest intervals tested, we next sought to characterize synaptic conductance dynamics during a train of

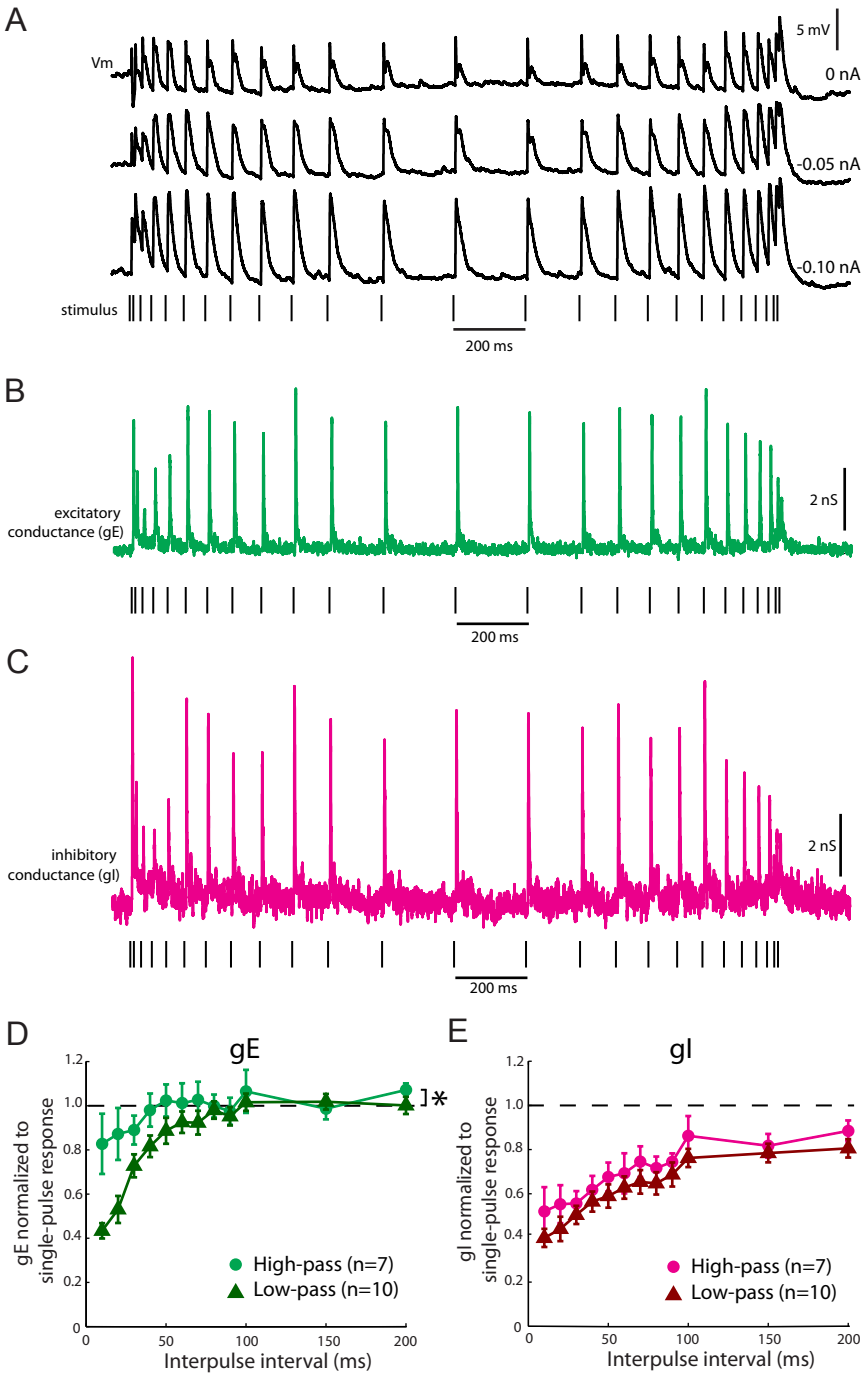

Figure 2. Excitatory and inhibitory conductances decrease at short intervals in response to IPI scans. (A) The membrane potential (V_m) recorded from a high-pass neuron during a decreasing-increasing IPI scan under three levels of current-clamp. (B-C) The excitatory (gE) (B) and inhibitory (gI) (C) synaptic conductances estimated from the potentials recorded in (A). Notice that the peak amplitudes decrease at short IPIs. (D-E) Average peak excitatory (D) and inhibitory conductances (E) normalized to single-pulse responses for high- and low-pass neurons. Error bars represent SEM. * p<0.000001, repeated-measures ANOVA, interaction between tuning and IPI.

10 electrosensory pulses at a constant 10 ms IPI, which corresponds to approximately the minimum IPI a single fish produces (Hopkins, 1986). We then compared these responses to the synaptic conductances evoked by 100 ms IPIs. In 42 ELp neurons, we recorded intracellular responses at multiple levels of holding current (Fig. 3A) and estimated the underlying synaptic conductances (Fig. 3B). A plot of normalized PSPs evoked by 10 ms IPIs reveals the diversity of responses of ELp neurons, with the PSPs of some neurons increasing or decreasing to various degrees (Fig. 3D). The synaptic conductance estimates resulting from these PSPs revealed widespread reduction of the magnitudes of both excitation and inhibition in neurons of all tuning classes (Fig. 3E,F). These decreases were rate-dependent, with greater conductance decreases during 10 ms IPIs compared to 100 ms IPIs (Fig. 3C,G-I).

Inhibition depresses more than excitation in high-pass neurons

We next investigated how the dynamics of decreasing excitation and inhibition related to IPI tuning. In general, high-pass neurons received inhibitory inputs that decreased more than excitatory inputs during the 10 ms IPI train (Fig. 4B,C; repeated-measures ANOVA, interaction between excitation/inhibition and pulse time, $F_{(9,11)}$=4.7, p=0.000031). To quantify the degree and time course of the decay of conductance magnitudes during 10 ms IPI trains, we fit the normalized peak conductances evoked by the stimulus train with a single exponential function (see Materials and Methods). The resulting time constant (τ) gives a measure of how quickly the conductance decreased, with smaller τ indicating faster decay. The amplitude (a), or coefficient, of the fit gives a measure of the magnitude of decay, with larger a indicating decay to a greater degree.

The greater decrease in inhibition compared to excitation in high-pass neurons was due to

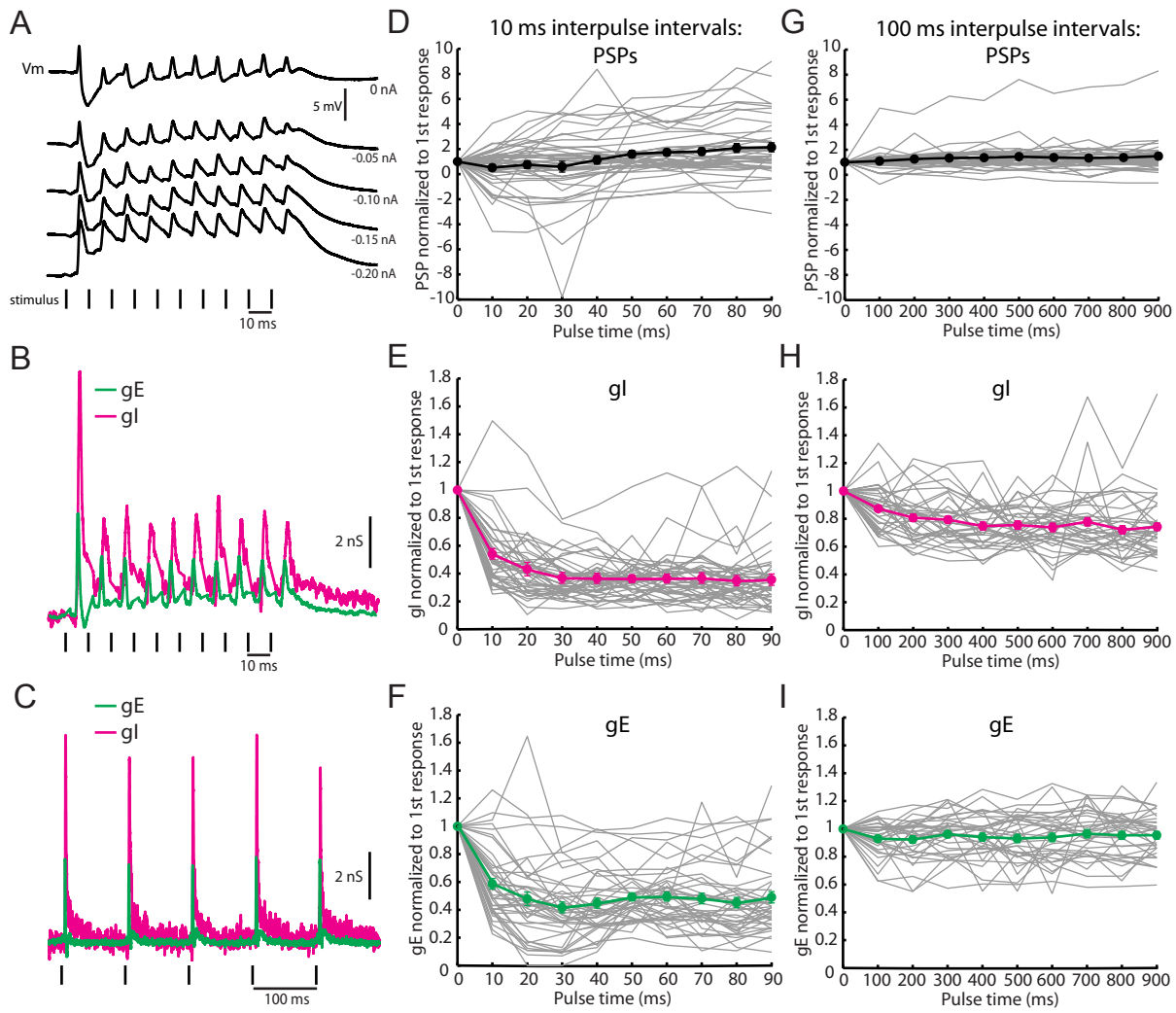

Figure 3. Interval-tuned neurons receive excitatory and inhibitory inputs that decrease to varying degrees during 10 ms IPIs. (A) The membrane potentials (V_m) recorded from a low-pass ELp neuron in response to a 10 ms IPI train under multiple levels of current-clamp. (B) Estimated excitatory (gE) and inhibitory (gI) conductances underlying the responses in (A). (C) Estimated synaptic conductances of the same neuron in (A-B) in response to a 100 ms IPI train. (D-F) Plots of normalized postsynaptic potential (PSP) (D), inhibitory conductance (E), and excitatory conductance (F) amplitudes evoked by a 10 ms IPI train versus stimulus time. Plots for each individual neuron (*n*=42 neurons) are shown in gray, and the averages + SEM are shown in black (PSPs), magenta (gI), and green (gE). (G-I) Same as in (D-F) for the responses of 34 ELp neurons to 100 ms IPI trains.

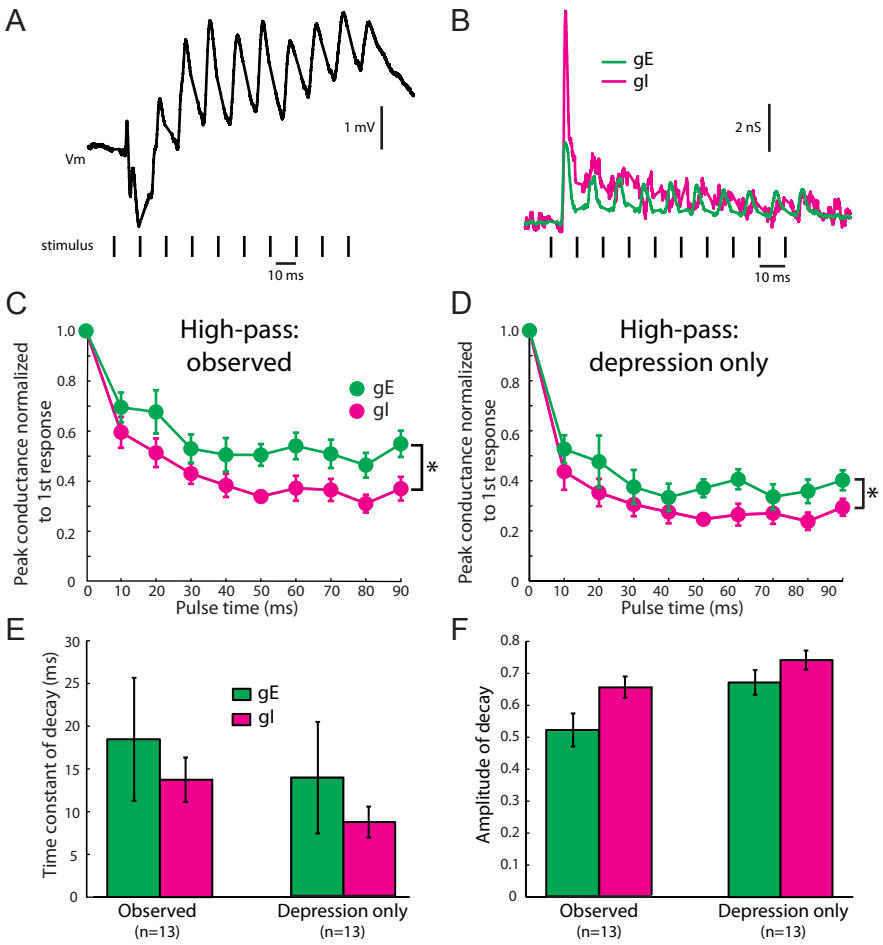

Figure 4. Excitation depresses less than inhibition at short intervals in high-pass neurons. (A) The membrane potential (V_m) recorded from a representative high-pass neuron in response to a 10 ms IPI train. (B) The excitatory (gE) and inhibitory (gI) synaptic conductances underlying the responses shown in (A). (C) Normalized synaptic conductances during a 10 ms IPI train in high-pass neurons (n=13 neurons). * p<0.0001, repeated-measures ANOVA, interaction between excitation/inhibition and pulse time. (D) Normalized synaptic conductances during the 10 ms IPI train after removing the effects of temporal summation (see Materials and Methods) for high-pass neurons. * p<0.01, repeated-measures ANOVA, interaction between excitation/inhibition and pulse time. (E-F) Bar graphs of average time constants (E) and amplitudes (F) of exponential fits to normalized observed and summation-removed ("depression only") conductances during 10 ms IPI trains in high-pass neurons. Error bars represent SEM.

inhibition that tended to decay faster (smaller τ in Fig. 4E) and to a greater degree (larger a in Fig. 4F) than excitation. However, conductances rarely returned to baseline levels between the peaks evoked by each pulse in the 10 ms IPI train (Fig. 4B), indicating that temporal summation of conductance changes to previous pulses likely influenced the peak conductances. Therefore, to determine the extent to which summation affected the degree and time course of conductance changes, we removed the effects of summation from the 2^{nd}-10^{th} peak conductances by subtracting the minimum conductance value occurring between the measured peak and the preceding peak. We then normalized these summation-removed peak values by the peak elicited by the first pulse in the train and fit these data with single exponential functions (see Materials and Methods). The results provide an estimate of the actual short-term depression of excitation and inhibition, with the confounding effects of temporal summation removed.

Inhibition depressed more than excitation in high-pass neurons (Fig. 4D; repeated-measures ANOVA, interaction between excitation/inhibition and pulse time, $F_{(9,11)}$=3.0, p=0.0036). Accordingly, inhibition tended to depress faster (smaller τ in Fig. 4E) and to a greater degree (larger a in Fig. 4F) than excitation. Six of 13 high-pass neurons (46%) received excitation that depressed more slowly and to a lesser degree than inhibition, five neurons (39%) received excitation that depressed to a lesser degree than inhibition, and the remaining two neurons (15%) received excitation that depressed more slowly than inhibition. Therefore, all high-pass neurons fit a depression model for high-pass tuning: with inhibition depressing more quickly and/or to a greater degree than excitation, depolarization of the neurons' membrane potentials increased with repeated stimulation (Fig. 4A).

These data also suggest a role for temporal summation of excitation in establishing high-pass responses. The differences between excitation and inhibition were greater for the

normalized observed conductances (Fig. 4C) than for the normalized conductances after summation was removed (Fig. 4D). This finding indicates that temporal summation must have contributed to the observed differences in excitation and inhibition shown in Figure 4C. Most likely, the slower depression of excitation (Fig. 4E) allowed for greater summation of excitation compared to inhibition during short IPIs, leading to excitation that decreased less overall than inhibition (Fig. 4C).

Excitation depresses more than inhibition in most, but not all, low-pass neurons

In general, low-pass neurons received excitatory and inhibitory inputs that decreased similarly during 10 ms IPIs (Fig. 5B,C; repeated-measures ANOVA, interaction between excitation/inhibition and pulse time, $F_{(9,20)}$=1.5, p=0.15). Excitation tended to decrease more quickly (smaller τ in Fig. 5E) than inhibition, although excitation and inhibition decreased with similar amplitudes of decay (Fig. 5F) in low-pass neurons. However, we found that low-pass neurons varied in the relative balance of excitatory and inhibitory decreases. Seven of 22 low-pass neurons (32%) received excitation that decreased more quickly ($\tau_e < \tau_i$) and to a greater degree than inhibition ($a_e > a_i$). Six neurons (27%) received excitation that decreased more quickly than inhibition, and three neurons (14%) received excitation that decreased to a greater degree than inhibition. The remaining six low-pass neurons (27%), however, received excitation that decreased more slowly ($\tau_e > \tau_i$) and to a lesser degree than inhibition ($a_e < a_i$).

After removing the effects of temporal summation, we found that excitation and inhibition tended to depress similarly in low-pass neurons during 10 ms IPIs (Fig. 5D; repeated-measures ANOVA, interaction between excitation/inhibition and pulse time, $F_{(9,20)}$=1.3, p=0.23). Accordingly, the depression time constants (Fig. 5E) and amplitudes (Fig. 5F) were similar for

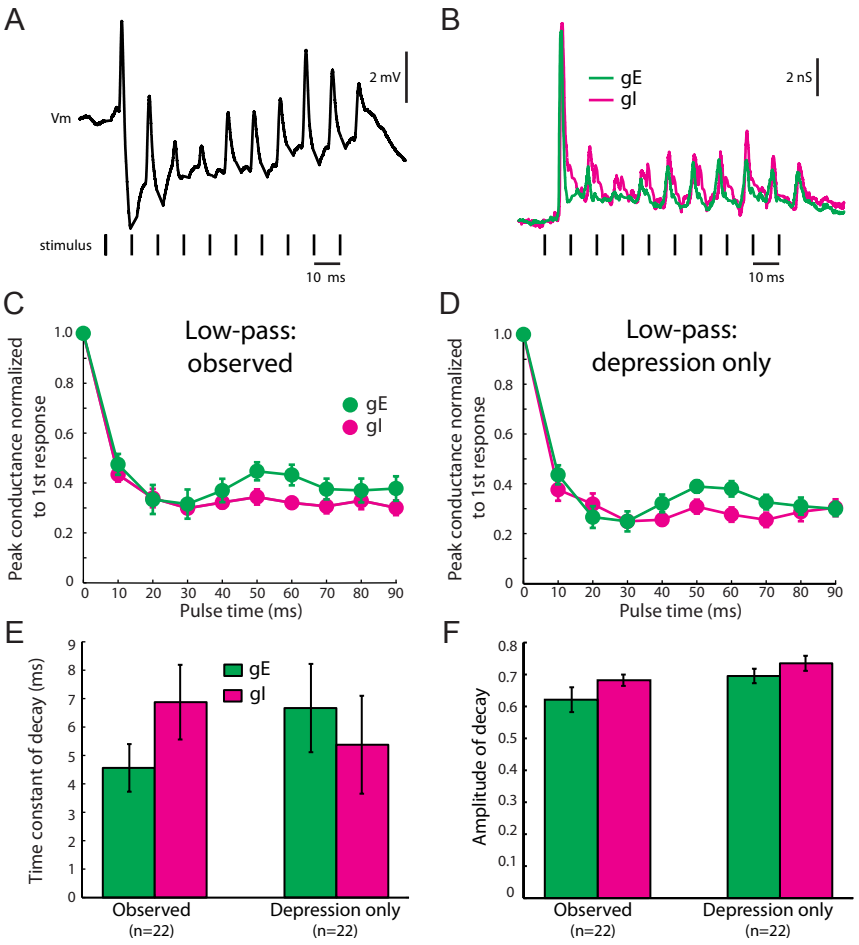

Figure 5. Excitation and inhibition depress similarly at short intervals in low-pass neurons. (A) The membrane potential (V_m) recorded from a representative low-pass neuron in response to a 10 ms IPI train. (B) The excitatory (gE) and inhibitory (gI) synaptic conductances underlying the responses shown in (A). (C) Normalized synaptic conductances during a 10 ms IPI train in low-pass neurons (*n*=22 neurons). (D) Normalized synaptic conductances during the 10 ms IPI train after removing the effects of temporal summation (see Materials and Methods) in low-pass neurons. (E-F) Bar graphs of average time constants (E) and amplitudes (F) of exponential fits to normalized observed and summation-removed ("depression only") conductances during 10 ms IPI trains in low-pass neurons. Error bars represent SEM.

excitation and inhibition in low-pass neurons. However, low-pass neurons actually varied in the balance of relative depression of excitation and inhibition. Three of 22 low-pass neurons (14%) received excitation that depressed more quickly and to a greater degree than inhibition, six neurons (27%) received excitation that depressed more quickly than inhibition, and five neurons (23%) received excitation that depressed to a greater degree than inhibition. Therefore, almost two-thirds of low-pass neurons fit a depression model for low-pass tuning: since excitation depressed to a greater degree and/or more quickly than inhibition, the neurons' membrane potentials decreased with repeated stimulation (Fig. 5A). The remaining eight neurons (36%), however, received excitation and inhibition that were inconsistent with this depression model for low-pass tuning. In these neurons, excitation depressed more slowly and to a lesser degree than inhibition. Factors other than differences in depression of excitatory and inhibitory pathways must therefore contribute to low-pass tuning in this group of neurons.

Temporal summation of excitation contributes to high-pass tuning

A previous *in vitro* and computational study of ELp neurons demonstrated a role for temporal summation of excitation and inhibition in establishing IPI tuning (George et al., 2011). Indeed, removing the effects of summation from observed conductance values revealed that summation of excitation contributed to differences in excitatory and inhibitory decreases during short-interval responses in high-pass neurons (compare Fig. 4D with Fig. 4C). Temporal summation of excitatory or inhibitory conductances will occur if the durations of the respective conductance changes are longer than the stimulation interval. Therefore, excitation that lasts longer than inhibition would result in greater temporal summation of excitation at short intervals, which could contribute to high-pass responses. Likewise, inhibition that lasts longer than

excitation would result in greater summation of inhibition, which could contribute to low-pass responses at short intervals (Baker et al., 2013).

A neuron's membrane capacitance will cause PSPs to last longer than the underlying conductance changes, which will lead to further temporal summation. To investigate the role of the initial durations of excitation and inhibition in establishing interval tuning, we collected responses to single electrosensory stimulus pulses. Comparing the PSPs evoked by single pulses to those evoked by 10 ms IPI trains in high-pass neurons supports a role for temporal summation of excitation in producing larger-amplitude synaptic responses at short intervals (Fig. 6A). A single stimulus pulse elicits two depolarizing phases separated by a hyperpolarization. This kind of response was frequently observed in high-pass neurons. The initial depolarization evoked by the second pulse in the 10 ms train overlaps in time with the later depolarization evoked by the first pulse, resulting in a greater depolarization. In this way, temporal summation of depolarizing PSPs contributes to establishing high-pass responses.

To study the contributions of excitation and inhibition to these responses, we estimated the synaptic conductances underlying single-pulse responses in 13 high-pass neurons. We found that high-pass neurons received excitatory and inhibitory inputs of similar durations (Fig. 6D; paired t-test, $t_{(12)}$=-0.11, p=0.91). These balanced durations indicate that the two conductances should summate at a similar range of IPIs, such that summation of excitation and inhibition partially counteract each other.

Interestingly, the amplitude of inhibition in response to single pulses was significantly larger than excitation in high-pass neurons (Fig. 6E; paired t-test, $t_{(12)}$=-2.8, p=0.016). Stronger inhibition than excitation in response to the onset of a stimulus train would serve to initially limit

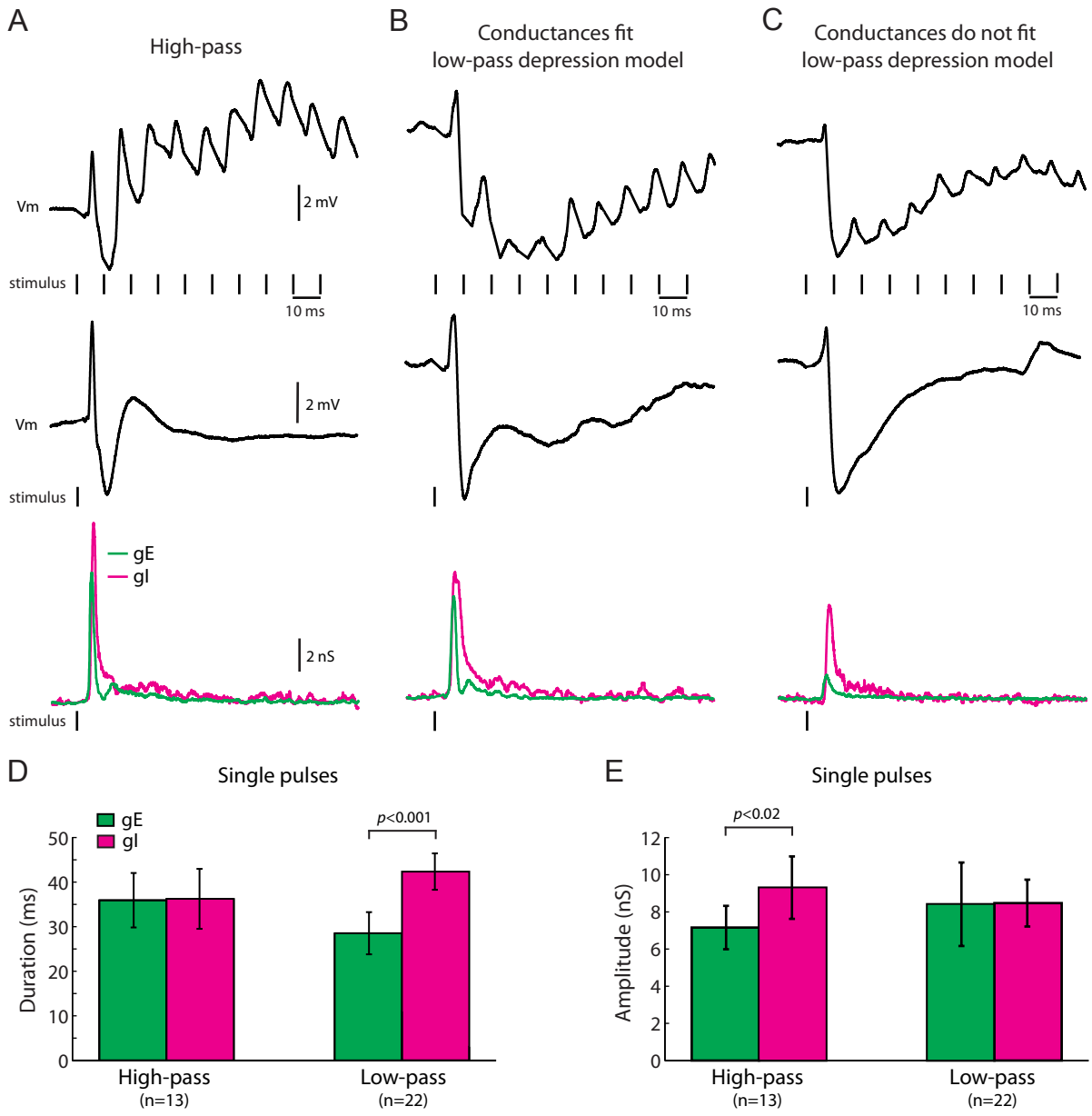

Figure 6. Temporal summation of excitation contributes to high-pass responses, whereas long onset inhibition contributes to low-pass responses. (A) Membrane potential (V_m) recordings in response to a 10 ms IPI train (top) and a single stimulus pulse (middle), and excitatory (gE) and inhibitory (gI) synaptic conductances (bottom) underlying the single-pulse PSPs for a representative high-pass neuron. (B) Same as in (A) for a low-pass neuron whose 10 ms IPI conductances fit a depression model for low-pass tuning. (C) Same as in (A) for a low-pass neuron whose 10 ms IPI conductances do not fit a depression model for low-pass tuning. (D-E) Bar graphs of the average durations (D) and amplitudes (E) of excitatory and inhibitory conductances elicited by single pulses in high- and low-pass neurons. Error bars represent SEM. *P*-values are shown for significant differences between excitation and inhibition resulting from paired t-tests.

excitatory postsynaptic responses. However, in response to short-interval stimulus trains, this strong inhibition will depress more than excitation (Fig. 4D), leading to high-pass tuning due to increased relative excitation that is further enhanced by the effects of temporal summation (Fig. 6A).

Long-lasting onset inhibition contributes to low-pass tuning

Comparing the PSPs in response to 10 ms IPI trains to those elicited by single pulses in low-pass neurons reveals a potential role for long inhibition in establishing decreased synaptic responses at short intervals (Fig. 6B,C). Single pulses evoked an initial long-lasting hyperpolarization that drastically reduced the baseline potential on top of which subsequent PSPs occurred, resulting in a net hyperpolarization. The time course of recovery of PSPs during the stimulus train roughly followed the time course of the single-pulse hyperpolarization (Fig. 6B,C). These effects were seen in low-pass neurons that fit a low-pass depression model, i.e., excitation depressed faster and/or to a greater degree than inhibition in response to 10 ms IPIs (Fig. 6B). These same effects were also observed in low-pass neurons whose 10 ms IPI conductances did not fit a depression model (Fig. 6C). Synaptic conductance estimates of single-pulse responses in 22 low-pass neurons revealed that inhibition lasted significantly longer than excitation in low-pass neurons (Fig. 6D; paired t-test, $t_{(22)}$=-3.9, p=0.00083). There was no difference in the amplitudes of excitatory and inhibitory single-pulse conductances in low-pass neurons (Fig. 6E; paired t-test, $t_{(22)}$=-0.05, p=0.96).

On average, inhibition lasted ~10 ms longer than excitation in low-pass neurons (Fig. 6D), indicating that inhibitory conductances should summate at slightly longer IPIs than excitatory conductances. This longer inhibition did not translate into greater effects of

summation on inhibitory vs. excitatory conductances at 10 ms IPIs, however (Fig. 5). Further, notice that after the long-lasting hyperpolarization in response to the first pulse in a 10 ms IPI train, PSPs of low-pass neurons gradually recovered instead of continuing to hyperpolarize as would occur due to summation if this long-lasting inhibition followed each pulse (Fig. 6B,C). It is likely that the strong depression of both excitation and inhibition in low-pass neurons (Fig. 5D,F) acts to limit the extent of temporal summation. Therefore, it appears that long-lasting onset inhibition that reduces excitatory responses to subsequent pulses is an important contributor to low-pass tuning, regardless of whether differences in short-term depression of excitation and inhibition enhance this tuning.

Passive membrane properties do not play a major role in establishing interval tuning

Differences in the effects of temporal summation between high- and low-pass neurons could be influenced by passive membrane properties (Fortune and Rose, 1997b). We estimated the membrane time constant, capacitance, and input resistance of each neuron by fitting a double exponential to responses to a 100 ms, -0.10 nA current step (see Materials and Methods). We found no differences in the membrane time constant (Student's *t*-test, $t_{(33)}$=-0.49, p=0.63; mean=7.5 $\pm$ 0.6 ms), membrane capacitance (Student's t-test, $t_{(33)}$=-0.087, p=0.93; mean=74 $\pm$ 6 pF), or input resistance (Student's t-test, $t_{(33)}$=0.48, p=0.63; mean=119 $\pm$ 11 MΩ) between high- and low-pass neurons. Therefore, differences in the observed effects of summation between high- and low-pass neurons are influenced primarily by the properties of their inputs and not by the passive properties of their membranes.

Differences in the relative timing of excitation and inhibition do not contribute to interval tuning

The relative timing of excitation and inhibition has been proposed to play a role in interval tuning (Grothe, 1994; Edwards et al., 2008; Baker et al., 2013). We compared the times of the excitatory and inhibitory peak conductances in response to each pulse in a 10 ms IPI train. Inhibitory conductances reached their maximum significantly later (by ~0.6 ms) than excitatory conductances (repeated-measures ANOVA, effect of excitation/inhibition, $F_{(1)}$=7.0, p=0.012) with no systematic differences between tuning groups (effect of tuning, $F_{(1)}$=0.001, p=0.98; interaction between tuning and excitation/inhibition, $F_{(1,31)}$=0.31, p=0.58; interaction between tuning and pulse time, $F_{(9,15)}$=0.40, p=0.93). The latency of PSPs evoked by 10 ms IPI trains tended to increase with repeated stimulation (repeated-measures ANOVA, effect of pulse time, $F_{(9)}$=2.0, p=0.039), but there were no differences between high- and low-pass neurons (effect of tuning, $F_{(1)}$=0.89, p=0.35; interaction between pulse time and tuning, $F_{(9,33)}$=0.29, p=0.98). While the relative timing of inputs certainly contributes to an individual neuron's responses, we did not find evidence that systematic variation in relative timing plays a major role in establishing different patterns of interval tuning in ELp.

Short-term depression is essential for diversity in interval tuning

By subtracting the effects of temporal summation from excitatory and inhibitory conductances, we have demonstrated that summation of excitation contributes to producing high-pass responses (Fig. 4). To provide an estimate of what responses would occur in the absence of depression, we convolved single-pulse conductances with 10 ms IPI trains, and then used the membrane equation to estimate the resulting membrane potentials (see Materials and Methods).

The results allowed us to investigate how temporal summation alone (without depression) would influence the responses of ELp neurons (Fig. 7). The membrane potentials resulting from convolved conductances typically decreased drastically with repeated stimulation (Fig. 7A). Convolutions of synaptic conductances resulted in excitation and inhibition that gradually increased due to temporal summation (Fig. 7B), with the extent of summation varying across neurons.

Without depression, excitation would summate significantly more than inhibition at 10 ms IPIs in high-pass neurons (Fig. 7C; repeated-measures ANOVA, interaction between excitation/inhibition and pulse time, $F_{(9,11)}$=2.7, p=0.0078). In contrast, inhibition would summate significantly more than excitation in low-pass neurons (Fig. 7D; repeated-measures ANOVA, interaction between excitation/inhibition and pulse time, $F_{(9,11)}$=35, p<0.001). However, the magnitude of the difference in summation of excitation vs. inhibition was far greater for low-pass neurons than for high-pass neurons (compare Fig. 7D with Fig. 7C), reflecting the longer onset inhibition of low-pass neurons (Fig. 6D).

To quantify the time course and degree of summation of the convolved conductances, we fit an exponential function to the normalized responses (see Materials and Methods). The resulting time constant of the fit is smaller for convolved conductances that summate faster, and the resulting amplitude of the fit is greater for convolved conductances that summate to a greater extent.

Convolved excitatory conductances tended to summate more quickly (smaller τ in Fig. 7E) than inhibitory conductances in high-pass neurons, although the two conductances reached a similar level of summation (Fig. 7F). In contrast, inhibition tended to summate to a greater extent (larger a in Fig. 7F) than excitation in low-pass neurons, even though the two inputs summated

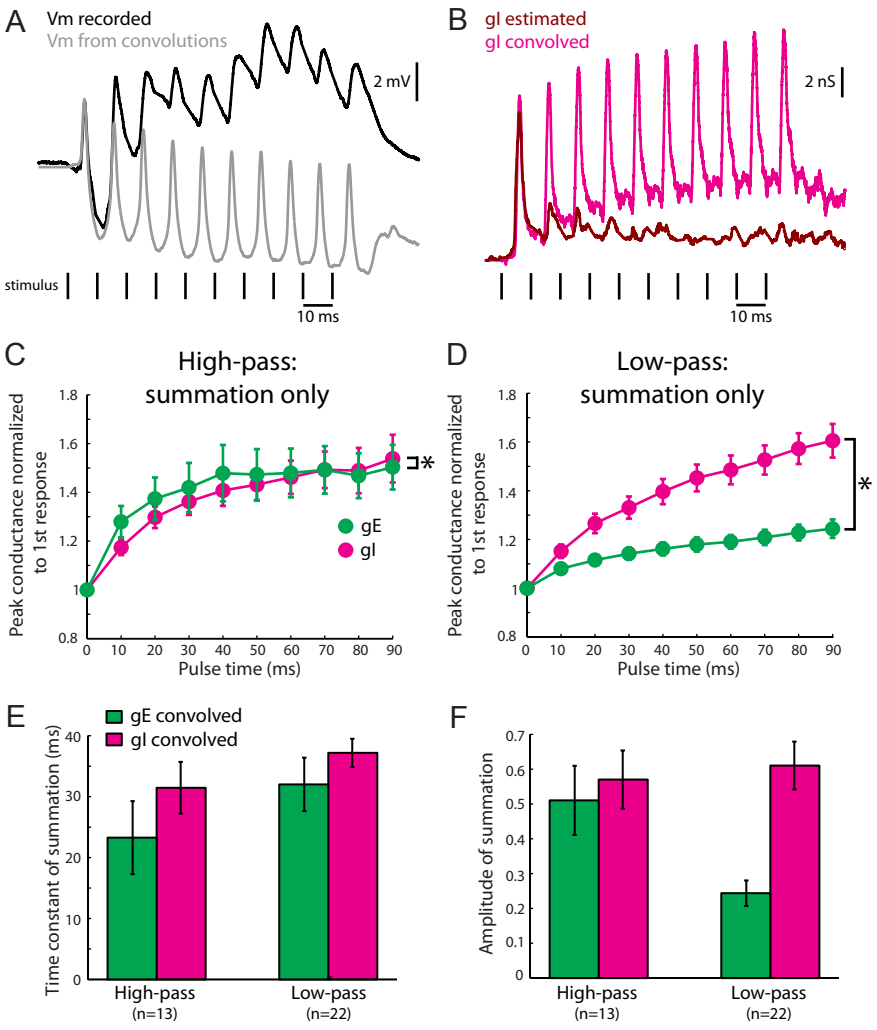

Figure 7. Convolutions of single-pulse conductances reveal that, without depression, excitation would summate more than inhibition in high-pass neurons, whereas inhibition would summate more than excitation in low-pass neurons. (A) The recorded membrane potential ("V_m recorded") and the membrane potential resulting from conductance convolutions ("V_m from convolutions") of a high-pass neuron in response to a 10 ms IPI stimulus train. (B) The estimated ("gI estimated") and convolved ("gI convolved") inhibitory conductances of the same neuron in (A) in response to a 10 ms IPI train. (C-D) Normalized convolved synaptic conductances during a 10 ms IPI train for high-pass (C) and low-pass (D) neurons. * $p<0.01$, repeated-measures ANOVA, interaction between excitation/inhibition and pulse time. (E-F) Bar graphs of the average time constants (E) and amplitudes (F) of single exponential fits to normalized convolved excitatory and inhibitory conductances. Error bars represent SEM.

with similar time courses (Fig. 7E). These results are in line with the findings of the single-pulse balance of excitation and inhibition in the two groups of neurons. Low-pass neurons experienced longer inhibition that, in the absence of depression, would summate more than excitation. High-pass neurons received excitatory and inhibitory inputs of similar durations that, in the absence of depression, would summate roughly equally. However, summation of onset inhibition that is of larger magnitude than onset excitation (see Fig. 6E) would lead to inhibition-dominated responses in high-pass neurons.

Depression and temporal summation both contribute to diversity of IPI tuning

We have shown that both temporal summation and depression of excitation and inhibition contribute to the increasing synaptic response amplitudes of high-pass neurons and the decreasing synaptic response amplitudes of low-pass neurons at short intervals. Next we sought to evaluate the relative contributions of each mechanism in generating the diversity of IPI tuning observed among ELp neurons. To reveal the contribution of depression to IPI tuning, we convolved single-pulse conductances with the same IPI stimuli used to characterize tuning in each neuron and then used the membrane equation to estimate the resulting membrane potentials. We then measured the PSPs of the estimated membrane potentials in response to each stimulus pulse, and generated tuning curves as described in Materials and Methods. The results provide an estimate of each neuron's tuning in the absence of depression.

The averaged tuning curves of the responses without depression in both tuning groups decreased sharply at short intervals, with PSPs at the shortest intervals dropping below neurons' resting potentials ("summation only" curves in Fig. 8A,B). The results therefore reveal the importance of short-term depression in establishing high-pass tuning. After removing the effects

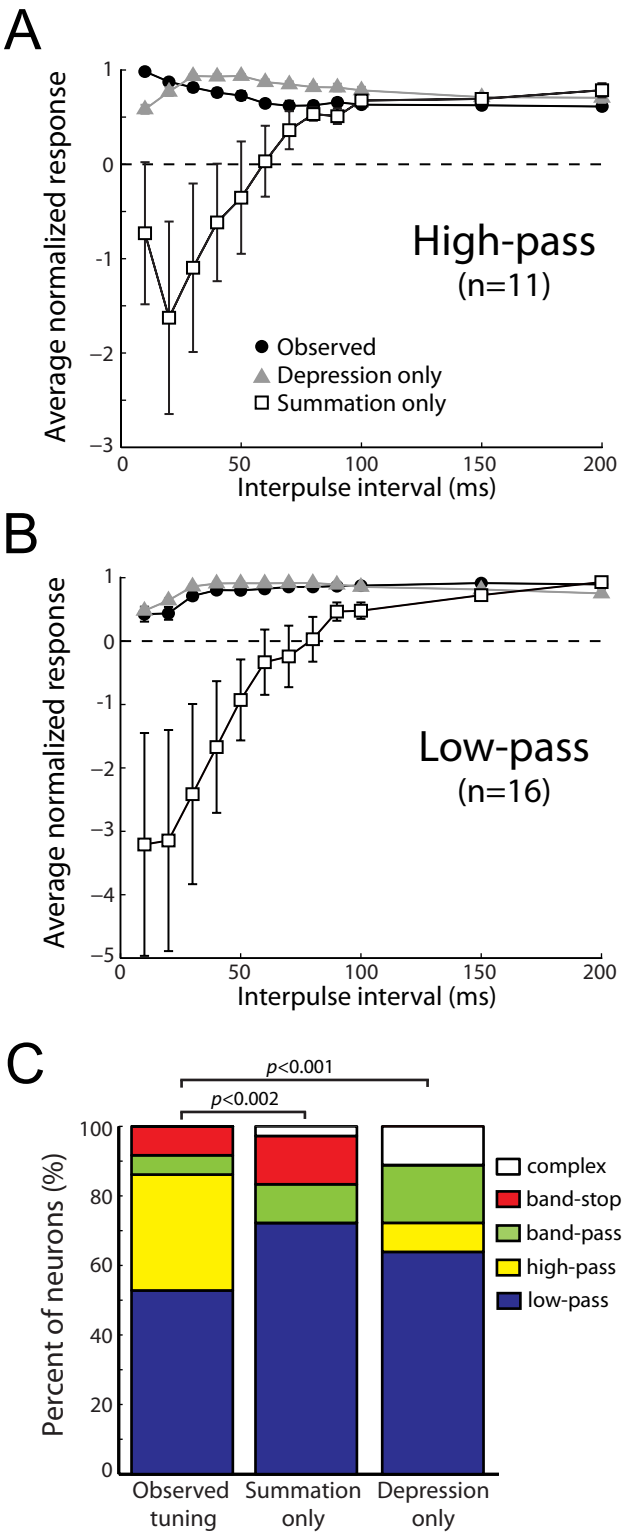

Figure 8. With temporal summation alone or depression alone, tuning among the population of ELp neurons would shift toward low-pass. (A-B) Tuning curves of observed PSPs, PSPs after summation removal ("depression only"), and PSPs estimated from conductance convolutions ("summation only") in response to IPI stimuli from high-pass (A) and low-pass (B) neurons. Error bars represent SEM. (C) The

percentage of neurons (n=36 neurons) classified as each tuning type using the observed PSPs, the PSPs estimated from conductance convolutions, and the PSPs after summation removal. Reported p-values are the results of X^2 observed vs. expected frequency tests.

of depression, no neurons were classified as high-pass. The majority (n=7/12 neurons; 58%) of high-pass neurons became low-pass, three (25%) neurons became band-pass, and the remaining two neurons (17%) became band-stop after removing depression. In contrast, the majority (n=14/19 neurons; 74%) of low-pass neurons were still classified as low-pass after removing depression. Of the remaining low-pass neurons, three (16%) became band-stop, one (5%) became band-pass, and one (5%) became complex after removing depression. These results suggest that without depression, the balance of excitation and inhibition would produce primarily low-pass responses. Thus, removing the effects of depression caused a significant shift toward low-pass tuning and away from high-pass tuning among the population of ELp neurons (Fig. 8C; $X^2_{(4)}$=18, p<0.0013).

To evaluate the contribution of temporal summation to producing the observed diversity of IPI tuning, we minimized its effects by removing lingering effects of responses to previous pulses from PSP amplitudes. From the maximum membrane potential evoked by each pulse in an IPI train, we subtracted the minimum membrane potential within a window starting with the stimulus pulse offset and ending with the peak potential evoked by that pulse (see Materials and Methods). We found that temporal summation was critical for establishing high-pass responses (compare “observed” with “depression only” curves in Fig. 8A). Without summation, only one (8%) of 12 high-pass neurons was classified as being high-pass. Five high-pass neurons (42%) were classified as band-pass tuned, three (25%) were classified as low-pass tuned, and three (25%) were classified as complex tuned. Compared to high-pass neurons, removing the effects of summation in low-pass neurons had minimal effects on tuning (compare “observed” with

"depression only" curves in Fig. 8B). The majority (17/19 neurons; 89%) of low-pass neurons remained low-pass tuned, with one (5%) neuron becoming high-pass tuned and one (5%) neuron becoming band-pass tuned. Without the effects of summation, tuning shifted toward low-pass and away from high-pass (Fig. 8C; $X^2_{(8)}=19$, $p<0.00095$).

Taken together, these results suggest that temporal summation and depression each contribute to establishing multiple tuning types, but that the greatest diversity of tuning occurs when summation and depression are both acting. Summation and depression are equally effective at producing low-pass responses, suggesting an inherent bias toward producing low-pass responses in the initial balance of excitation and inhibition as well as the degree of depression of inputs. A combination of summation and depression is essential for establishing high-pass tuning and generating a greater diversity of IPI tuning among the population of ELp neurons.

Depression increases sensitivity to directional changes in IPI

The responses of some ELp neurons are sensitive to the direction of interval change (Fig. 9A,B) (Carlson, 2009). In the low-pass neuron shown in Figure 9, the amplitude of the PSPs evoked by the shortest and the longest intervals delivered depends upon the direction of interval change (Fig. 9C). To determine how depression and summation contribute to this directional sensitivity, we calculated a scan direction-selectivity index (DSI) for recorded PSPs ("observed"), PSPs estimated from convolved conductances ("summation only"), and summation-removed PSPs ("depression only") in response to IPI scans (see Materials and Methods). The scan DSI ranges from 0 (no direction-selectivity) to 1 (maximum direction-selectivity). ELp neurons exhibited a range of DSI (range=0.07-0.33), with no differences among

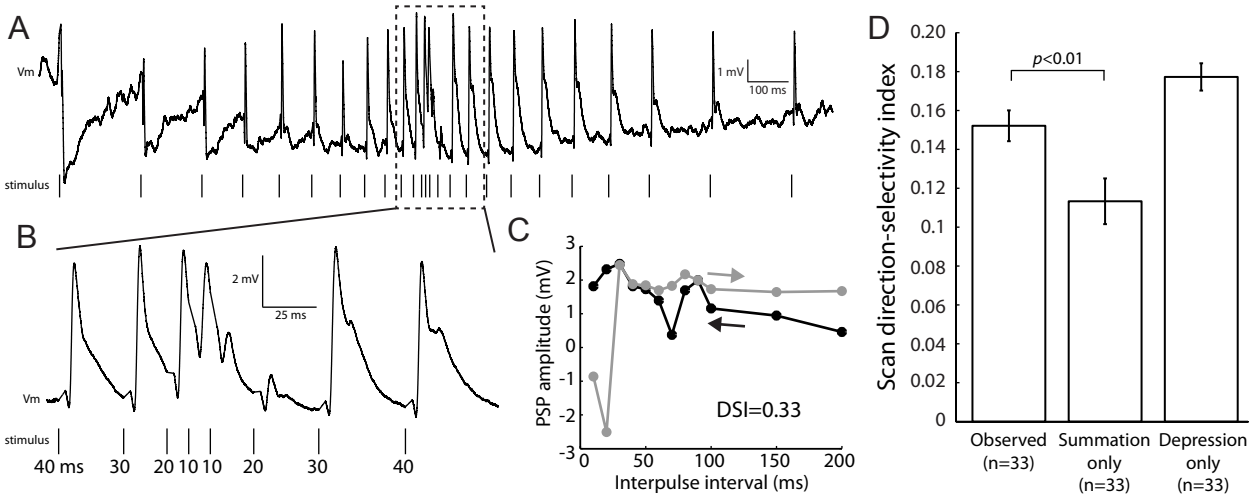

Figure 9. Depression increases selectivity for direction of interval change. (A) The membrane potential (V_m) recorded from a low-pass neuron in response to a decreasing then increasing IPI scan stimulus. (B) Close-up of the responses to short intervals of the recording trace in (A). Numbers below the stimulus tick marks indicate the IPI in ms. (C) A plot of the PSP amplitudes of the neuron in (A) versus IPI for the decreasing (black) and increasing (grey) portion of the scan stimulus. The scan direction-selectivity index (DSI) for this neuron was 0.33. (D) Bar graph of the average scan DSI for observed PSPs, PSPs estimated from conductance convolutions ("summation only"), and PSPs after summation removal ("depression only"). Because there were no differences in DSI among high-pass, low-pass, band-pass, and band-stop neurons, neurons from all tuning groups were combined. The reported *p*-value is the result of a Tukey post-hoc test following a repeated-measures ANOVA.

the tuning groups (one-way ANOVA, $F_{(3)}$=0.56, p=0.64). Therefore, we combined high-pass, low-pass, band-pass, and band-stop neurons to investigate the effects of depression and summation. We limited our analysis only to neurons in which the results of our summation removal method were linearly correlated with those of the true summation removal method at both 10 ms and 100 ms IPIs (see Materials and Methods).

Minimizing the effects of depression and summation significantly affected the scan DSI (repeated-measures ANOVA, $F_{(2)}$=13, p=0.00002). The DSI of the PSPs resulting from summation only (without depression) was significantly smaller than that of the observed PSPs (Fig. 9D; Tukey post-hoc test, p=0.0085). This decrease in DSI was mostly due to the summating effects of inhibition that drove the estimated PSPs below neurons' resting potentials. In contrast, there was no difference between the DSIs of the observed PSPs and the PSPs resulting from depression only (without summation) (Fig. 9D; Tukey post-hoc test, p=0.12). These results suggest that short-term depression contributes to the sensitivity of ELp neurons to changes in IPI.

DISCUSSION

Our findings provide insight into the interactions between excitation and inhibition that contribute to behaviorally relevant interval tuning *in vivo* (Table 1). The strong responses of high-pass neurons at short intervals resulted from a combination of inhibition that depressed more than excitation, and temporal summation of excitation (Fig. 10B). By contrast, the weak responses of low-pass neurons at short intervals resulted from long-lasting inhibition, with an additional contribution from excitation that depressed more than inhibition in the majority of neurons (Fig. 10C,D). Without short-term depression, low-pass tuning would dominate in ELp and neurons would be less sensitive to IPI sequences. On the other hand, without temporal summation, tuning would also shift toward low-pass but sensitivity to interval change would be unaffected. Therefore, the combination of short-term depression and temporal summation produces a more diverse range of interval tuning than either mechanism alone. Furthermore, depression in ELp increases the circuit's ability to code for changing IPI sequences. Thus, both mechanisms working together enhance the ability of the circuit to detect communication signals, which are characterized both by their IPIs and by directional changes in IPIs (Carlson, 2002). Our results provide the first description of how different synaptic mechanisms can interact *in vivo* to establish neurons that code for behaviorally relevant stimulus intervals.

Low-pass neurons received inhibition that was longer than excitation, whereas high-pass neurons received inhibition and excitation of similar durations. The duration of conductance changes can be affected not just by receptor/channel kinetics, but also by the relative timing and locations of synaptic inputs along the dendritic tree. Multiple, slightly asynchronous inhibitory inputs arriving at different locations on the postsynaptic membrane might give rise to weaker, but longer-lasting conductance changes than a few synchronous inputs arriving at the same

Mechanism	High-pass responses	Low-pass responses
Short-term depression	More depression of inhibition	More depression of excitation (usually, but not always)
Temporal summation	More summation of excitation	More summation of inhibition
Onset duration	Equal for excitation and inhibition	Longer inhibition
Onset strength	Stronger inhibition	Equal for excitation and inhibition

Table 1. Mechanisms contributing to excitatory-inhibitory integration underlying high-pass and low-pass tuning.

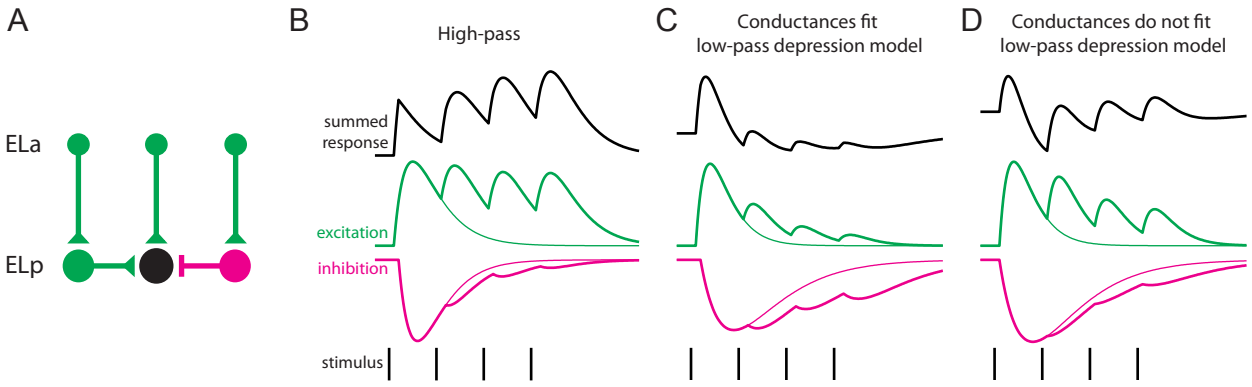

Figure 10. Schematic of ELp circuitry and synaptic mechanisms contributing to interval tuning. (A) An ELp neuron (black) receives excitatory (green) inputs from ELa and from other ELp neurons, as well as inhibitory (magenta) inputs from other ELp neurons. (B) High-pass tuning is associated with excitation that depresses less than inhibition, leading to more temporal summation of excitation than inhibition. Excitation and inhibition elicited by the first stimulus pulse are indicated by thin lines. The summed response is the result of adding excitatory and inhibitory traces. (C) The majority of low-pass neurons fit a depression model in which excitation depresses more than inhibition. Onset inhibition that lasts longer than onset excitation also contributes to low-pass responses. (D) A subset of low-pass neurons does not fit a depression model for low-pass tuning; instead, excitation depresses less than inhibition. Onset inhibition that lasts longer than onset excitation contributes to these neurons' low-pass responses.

location. Multiple studies have reported the effects of spatiotemporal activation of excitatory dendritic inputs on somatic potentials (i.e., Branco et al., 2010; Oviedo and Reyes, 2012; Abbas et al., 2013). Many additional parameters could affect the duration of conductance changes, including vesicle release dynamics, the distribution, density, and subunit composition of postsynaptic receptors, and ion channel kinetics (Euler and Denk, 2001; Farrant and Nusser, 2005).

Differences in the degrees of depression of excitation and inhibition also contributed to interval tuning. In addition to GABAergic inhibition from local interneurons (George et al., 2011), ELp neurons receive excitation from ELa small cells (Friedman and Hopkins, 1998; Lyons-Warren et al., 2013a) and from other ELp neurons (Ma et al., 2013) (Fig. 10A). A feedback projection from the isthmic granule nucleus also terminates onto ELp neurons (Haugedé-Carré, 1979); however, the nature of this input is unknown. Nevertheless, the large dendritic arborizations of ELp neurons and the relatively high probability of excitatory connections between pairs of ELp neurons suggest that they integrate a large number of inputs (Xu-Friedman and Hopkins, 1999; George et al., 2011; Ma et al., 2013). Recently, paired *in vitro* recordings revealed short-term depression at single excitatory connections between ELp neurons, with no differences in the amount of depression in relation to presynaptic or postsynaptic IPI tuning (Ma et al., 2013).

Therefore, three hypotheses for the origin of the observed differences in depression of excitation and inhibition arise. First, since excitatory connections between ELp neurons depressed similarly regardless of IPI tuning (Ma et al., 2013), inhibitory synapses could depress to varying degrees onto different neurons. Differences in depression of inhibition onto a presynaptic excitatory input could then create apparent differences in excitatory depression.

A second hypothesis is that all local ELp connections depress uniformly, but excitatory synapses from ELa depress with varying dynamics. Any variation in inhibitory depression would then reflect differences in the inputs from ELa onto inhibitory neurons. Paired intracellular recordings of ELp neurons along with their inhibitory or ELa inputs would be necessary to characterize depression at these two types of synapses. Multiple studies have reported that the same output neuron can form synapses whose type and degree of short-term plasticity depends on the target cell (see Blackman et al., 2013 for review). The observed range of time courses and degrees of depression of both excitation and inhibition onto ELp neurons could result from diversity in depression of ELa inputs as well as diversity in depression of local inhibitory connections.

A third hypothesis for differences in the degree of depression of excitation and inhibition is based on local ELp network interactions. Excitatory connections are more likely to occur between ELp neurons of the same tuning class, and single excitatory connections between ELp neurons depress to similar degrees regardless of presynaptic or postsynaptic IPI tuning (Ma et al., 2013). Since the spike output of high-pass neurons increases with short-interval stimulation (Carlson, 2009), the convergence of many excitatory high-pass inputs onto a high-pass neuron could keep the excitatory conductance higher during repeated stimulation, even with depression. Furthermore, the majority of low-pass neurons received excitatory inputs that depressed more than inhibitory inputs at short intervals. Since the spike output of low-pass neurons decreases with short-interval stimulation (Carlson, 2009), the convergence of many excitatory low-pass inputs onto a low-pass ELp neuron could cause a rapid reduction in excitatory conductance during repetitive stimulation. Thus, the observed depression of synaptic conductances in ELp

neurons may reflect the compounding effect of depression at many synapses within the local ELp circuitry.

ELp neurons exhibit large, spiny dendritic arbors that can span up to 200 μm in diameter (Xu-Friedman and Hopkins, 1999; George et al., 2011). Passive electrical properties owing to morphology, as well as active dendritic conductances, can influence linear and non-linear synaptic integration along dendrites (Magee, 2000; Gulledge et al., 2005; London and Hausser, 2005). We have not yet looked in detail for morphological differences between ELp neurons of different tuning types, but previous anatomical studies have not revealed any obvious morphological classes of ELp neurons (George et al., 2011; Ma et al., 2013). We did not find any differences in passive membrane properties with respect to IPI tuning in this study. Furthermore, we minimized possible contributions from active conductances by obtaining recordings in hyperpolarized current-clamp levels, and by limiting our conductance estimates to portions of the responses in which the current-voltage relationship was linear. However, active dendritic processing could be another factor that might further shape IPI tuning beyond the synaptic mechanisms we described. Calcium imaging and glutamate- or GABA-uncaging experiments would be necessary to reveal possible contributions of active dendritic processing to IPI tuning.

Neurons sensitive to temporal patterns in sensory stimuli have been identified in the auditory midbrains of frogs (Alder and Rose, 1998) and bats (Grothe, 1994), cat auditory cortex (Sakai et al., 2009), and the electrosensory midbrain of wave-type weakly electric fish (Fortune and Rose, 1997a), which evolved an electrosensory system independently from the mormyrid fish we studied. Interval-selective neurons in frog midbrains are tuned to the intervals between successive sound pulses (Alder and Rose, 1998), which vary across (but not within) distinct types of communication calls (Allen, 1973). Short-interval tuning in these neurons appears to

arise from interactions between inhibition and enhancement of excitation, whereas long-interval tuning can arise from different combinations of mechanisms: the relative timing of excitation and inhibition, depression of excitation, or summation or enhancement of excitation, without a role for inhibition (Edwards et al., 2008; Rose et al., 2011). Neurons that are selective for slow beat rates (2-8 Hz) in wave-type electric fish midbrains get their temporal sensitivity through depression of excitation as well as passive electrical filtering and voltage-dependent conductances (Rose and Fortune, 1999; Fortune and Rose, 2000). Whether inhibition also contributes to this tuning remains unknown.

In contrast to frog auditory and wave-type electric fish neurons, ELp neurons are involved in decoding intervals ranging from approximately ten up to hundreds of milliseconds (Hopkins, 1986). Mormyrid electric communication signals typically consist of a decrease then increase in IPI, with distinct signals differing in the precise temporal sequence of IPIs (Carlson and Hopkins, 2004). Therefore, neural representations of the IPIs present in the wide range of signals used as well as the direction of IPI change is necessary for discriminating signals with different social functions. The combination of temporal summation and depression results in greater diversity of IPI tuning and sensitivity to direction of IPI change than either mechanism alone. Detecting direction of changing temporal patterns may not be as important for distinguishing frog communication signals or sinusoidal beat rates in wave-type electric fish, such that those circuits may be able to employ fewer synaptic mechanisms to achieve the required temporal sensitivity.

Although excitatory-inhibitory interactions, short-term synaptic plasticity, and temporal summation have all been implicated in interval tuning, our study is the first to reveal how these multiple synaptic mechanisms interact in midbrain sensory neurons to establish behaviorally

relevant interval tuning *in vivo*. It remains to be seen how variations in the balance of depression and summation in excitatory and inhibitory pathways arise in ELp neurons. Future studies of IPI tuning in ELp will seek to identify the contribution of network dynamics and local dendritic computations to this behaviorally relevant information processing.

REFERENCES

Abbas SY, Hamade KC, Yang EJ, Nawy S, Smith RG, Pettit DL (2013) Directional summation in non-direction selective retinal ganglion cells. PLOS Comput Biol 9:e1002969.

Alder TB, Rose GJ (1998) Long-term temporal integration in the anuran auditory system. Nat Neurosci 1:519-523.

Allen DM (1973) Some relationships of vocalization to behavior in the pacific treefrog, *Hyla regilla*. Herpetologica 29:366-371.

Amagai S (1998) Time coding in the midbrain of mormyrid electric fish. II. Stimulus selectivity in the nucleus exterolateralis pars posterior. J Comp Physiol A 182:131-143.

Baker CA, Kohashi T, Lyons-Warren AM, Ma X, Carlson BA (2013) Multiplexed temporal coding of electric communication signals in mormyrid fishes. J Exp Biol 216:2365-2379.

Bell CC, Grant K (1989) Corollary discharge inhibition and preservation of temporal information in a sensory nucleus of mormyrid electric fish. J Neurosci 9:1029-1044.

Bennett MV (1965) Electroreceptors in mormyrids. Cold Spring Harb Symp Quant Biol 30:245-262.

Blackman AV, Abrahamsson T, Costa RP, Lalanne T, Sjostrom PJ (2013) Target-cell-specific short-term plasticity in local circuits. Front Synaptic Neurosci 5:11.

Branco T, Clark BA, Hausser M (2010) Dendritic discrimination of temporal input sequences in cortical neurons. Science 329:1671-1675.

Carlson BA (2002) Electric signaling behavior and the mechanisms of electric organ discharge production in mormyrid fish. J Physiol Paris 96:405-419.

Carlson BA (2009) Temporal-pattern recognition by single neurons in a sensory pathway devoted to social communication behavior. J Neurosci 29:9417-9428.

Carlson BA, Hopkins CD (2004) Stereotyped temporal patterns in electrical communication. Anim Behav 68:867-878.

Carrasco A, Lomber SG (2011) Neuronal activation times to simple, complex, and natural sounds in cat primary and nonprimary auditory cortex. J Neurophysiol 106:1166-1178.

Edwards CJ, Alder TB, Rose GJ (2002) Auditory midbrain neurons that count. Nat Neurosci 5:934-936.

Edwards CJ, Leary CJ, Rose GJ (2008) Mechanisms of long-interval selectivity in midbrain auditory neurons: roles of excitation, inhibition, and plasticity. J Neurophysiol 100:3407-3416.

Euler T, Denk W (2001) Dendritic processing. Curr Opin Neurobiol 11:415-422.

Farrant M, Nusser Z (2005) Variations on an inhibitory theme: Phasic and tonic activation of GABA(A) receptors. Nat Rev Neurosci 6:215-229.

Fortune ES, Rose GJ (1997a) Temporal filtering properties of ampullary electrosensory neurons in the torus semicircularis of Eigenmannia: evolutionary and computational implications. Brain Behav Evol 49:312-323.

Fortune ES, Rose GJ (1997b) Passive and active membrane properties contribute to the temporal filtering properties of midbrain neurons in vivo. J Neurosci 17:3815-3825.

Fortune ES, Rose GJ (2000) Short-term synaptic plasticity contributes to the temporal filtering of electrosensory information. J Neurosci 20:7122-7130.

Friedman MA, Hopkins CD (1998) Neural substrates for species recognition in the time-coding electrosensory pathway of mormyrid electric fish. J Neurosci 18:1171-1185.

Geis HRAP, Borst JGG (2013) Intracellular responses to frequency modulated tones in the dorsal cortex of the mouse inferior colliculus. Front Neural Circuits 7:7.

George AA, Lyons-Warren AM, Ma X, Carlson BA (2011) A diversity of synaptic filters are created by temporal summation of excitation and inhibition. J Neurosci 31:14721-14734.

Gittelman JX, Li N, Pollak GD (2009) Mechanisms underlying directional selectivity for frequency-modulated sweeps in the inferior colliculus revealed by in vivo whole-cell recordings. J Neurosci 29:13030-13041.

Goel A, Buonomano DV (2014) Timing as an intrinsic property of neural networks: evidence from in vivo and in vitro experiments. Philos T R Soc B 369:20120460.

Groh JM, Kelly KA, Underhill AM (2003) A monotonic code for sound azimuth in primate inferior colliculus. J Cogn Neurosci 15:1217-1231.

Grothe B (1994) Interaction of excitation and inhibition in processing of pure tone and amplitude-modulated stimuli in the medial superior olive of the mustached bat. J Neurophysiol 71:706-721.

Guillamon A, McLaughlin DW, Rinzel J (2006) Estimation of synaptic conductances. J Physiol Paris 100:31-42.

Gulledge AT, Kampa BM, Stuart GJ (2005) Synaptic integration in dendritic trees. J Neurobiol 64:75-90.

Haugedé-Carré F (1979) Mesencephalic exterolateral posterior nucleus of the mormyrid fish Bryenomyrus niger - efferent connections studied by the HRP method. Brain Res 178:179-184.

Hedwig B, Knepper M (1992) Separation of synaptic and spike activity in intracellular recordings for selective analysis. J Neurosci Methods 42:83-90.

Higley MJ, Contreras D (2006) Balanced excitation and inhibition determine spike timing during frequency adaptation. J Neurosci 26:448-457.

Hopkins CD (1986) Behavior of mormyridai. In: Electroreception (Bullock TH, Heiligenberg W, eds), pp 527-576. New York: John Wiley & Sons.

Klyachko VA, Stevens CF (2006) Excitatory and feed-forward inhibitory hippocampal synapses work synergistically as an adaptive filter of natural spike trains. PLOS Biol 4:e207.

Kohashi T, Carlson BA (2014) A fast BK-type K-ca current acts as a postsynaptic modulator of temporal selectivity for communication signals. Front Cell Neurosci 8:286.

London M, Hausser M (2005) Dendritic computation. Annu Rev Neurosci 28:503-532.

Lyons-Warren AM, Kohashi T, Mennerick S, Carlson BA (2013a) Detection of submillisecond spike timing differences based on delay-line anticoincidence detection. J Neurophysiol 110:2295-2311.

Lyons-Warren AM, Kohashi T, Mennerick S, Carlson BA (2013b) Retrograde fluorescent labeling allows for targeted extracellular single-unit recording from identified neurons *in vivo*. J Vis Exp 76:e3921.

Ma X, Kohashi T, Carlson BA (2013) Extensive excitatory network interactions shape temporal processing of communication signals in a model sensory system. J Neurophysiol 110:456-469.

Magee JC (2000) Dendritic integration of excitatory synaptic input. Nat Rev Neurosci 1:181-190.

Monier C, Fournier J, Fregnac Y (2008) In vitro and in vivo measures of evoked excitatory and inhibitory conductance dynamics in sensory cortices. J Neurosci Methods 169:323-365.

Oviedo HV, Reyes AD (2012) Integration of subthreshold and suprathreshold excitatory barrages along the somatodendritic axis of pyramidal neurons. PLOS One 7:e33831.

Pluta SR, Kawasaki M (2010) Temporal selectivity in midbrain electrosensory neurons identified by modal variation in active sensing. J Neurophysiol 104:498-507.

Priebe NJ, Ferster D (2005) Direction selectivity of excitation and inhibition in simple cells of the cat primary visual cortex. Neuron 45:133-145.

Rose G, Capranica RR (1983) Temporal selectivity in the central auditory system of the leopard frog. Science 219:1087-1089.

Rose GJ, Fortune ES (1996) New techniques for making whole-cell recordings from CNS neurons in vivo. Neurosci Res 26:89-94.

Rose GJ, Fortune ES (1999) Mechanisms for generating temporal filters in the electrosensory system. J Exp Biol 202:1281-1289.

Rose GJ, Leary CJ, Edwards CJ (2011) Interval-counting neurons in the anuran auditory midbrain: factors underlying diversity of interval tuning. J Comp Physiol A Neuroethol Sens Neural Behav Physiol 197:97-108.

Sakai M, Chimoto S, Qin L, Sato Y (2009) Neural mechanisms of interstimulus interval-dependent responses in the primary auditory cortex of awake cats. BMC Neurosci 10:10.

Wehr M, Zador AM (2003) Balanced inhibition underlies tuning and sharpens spike timing in auditory cortex. Nature 426:442-446.

Williams AJ, Fuzessery ZM (2012) Multiple mechanisms shape FM sweep rate selectivity: complementary or redundant? Front Neural Circuits 6:54.

Wong RY, Hopkins CD (2007) Electrical and behavioral courtship displays in the mormyrid fish Brienomyrus brachyistius. J Exp Biol 210:2244-2252.

Xu-Friedman MA, Hopkins CD (1999) Central mechanisms of temporal analysis in the knollenorgan pathway of mormyrid electric fish. J Exp Biol 202:1311-1318.

Chapter 3

Behavioral and single-neuron sensitivity to millisecond timing variations in electric communication signals

This chapter contains a version of a manuscript in preparation for submission:

Baker C.A., Ma L., Casareale, C.R., and Carlson B.A. Behavioral and single-neuron sensitivity to millisecond timing variations in electric communication signals. (in preparation)

Author contributions for the above citation:

C.A.B. and B.A.C. designed research; C.A.B., L.M., and C.R.C. performed research; C.A.B., L.M., and C.R.C. analyzed data; C.A.B. and B.A.C. wrote the manuscript.

ABSTRACT

In many sensory pathways, central neurons serve as temporal filters for timing patterns in communication signals. However, how a population of neurons with diverse temporal filtering properties codes for natural variation in communication signals is unknown. Here we addressed this question in the weakly electric fish *Brienomyrus brachyistius*, which varies the time intervals between successive electric organ discharges to communicate. These fish produce an individually stereotyped signal called a scallop, which consists of a distinctive pattern of approximately eight to twelve interpulse intervals. We manipulated the temporal structure of natural scallops during behavioral playback and *in vivo* electrophysiology experiments to probe the temporal specificity of scallop recognition. We found that fish's electric signaling behavior was sensitive to the precise temporal structure of scallops, such that presenting time-reversed, randomized, or jittered versions increased behavioral response thresholds. Next, using *in vivo* intracellular recordings and discriminant function analysis, we found that the responses of interval-selective midbrain neurons were also sensitive to the precise temporal structure of scallops. Subthreshold changes in membrane potential recorded from single neurons could be used to discriminate natural scallops from time-reversed and randomized sequences, but not from jittered sequences. However, spiking responses resulted in better discrimination of natural vs. jittered scallops than subthreshold responses. Pooling the responses of multiple neurons also improved discriminability. Finally, we found that the responses of single neurons were sensitive to inter-individual variation in scallop sequences. Collectively, these results demonstrate how a population of interval-selective neurons contributes to the detection of behaviorally relevant temporal patterns.

INTRODUCTION

Timing patterns in sensory stimuli carry information in the communication signals of a wide range of animals. For instance, the time intervals between successive sound pulses are species-specific in frogs and insects (Loftus-Hills and Littlejohn, 1971; Pollack, 2000). Short silent intervals during human speech play a role in phoneme discrimination (Diehl and Lindblom, 2004). Previous studies have shown that circuits process these types of temporal patterns with central neurons that are selective for particular timing intervals (Rose and Capranica, 1983; Grothe, 1994; Fortune and Rose, 1997b; Edwards et al., 2002; Sakai et al., 2009; Pluta and Kawasaki, 2010; Goel and Buonomano, 2014). These response properties have been shown to arise from synaptic mechanisms such as temporal summation and short-term synaptic plasticity (Fortune and Rose, 2000; George et al., 2011; Rose et al., 2011; Baker and Carlson, 2014), as well as from intrinsic postsynaptic membrane properties (Fortune and Rose, 1997a; Trussell, 1999; Fortune and Rose, 2003; Carlson and Kawasaki, 2006; Kohashi and Carlson, 2014). Whereas we now have a good understanding of how circuits can establish single-neuron temporal selectivity, how a population of neurons with a diverse range of temporal filtering properties contributes to the detection of natural timing patterns is unknown.

Here we investigate how a population of interval-selective midbrain neurons mediates the detection of temporally patterned communication signals. We use mormyrid weakly electric fish because the timing patterns in their communication signals have clear behavioral relevance, and because interval-selective neurons are easily accessible for *in vivo* electrophysiological recordings (e.g., Carlson, 2009; Baker and Carlson, 2014). Mormyrids vary the time intervals between successive electric pulses called electric organ discharges (EODs) to communicate (see Carlson, 2002 for review). At least three quantitatively distinct temporal patterns of pulses have

been linked to different social contexts in our study species, *Brienomyrus brachyistius* (Carlson and Hopkins, 2004). All three of these signals consist of a rapid decrease followed by a gradual increase in interpulse intervals (IPIs). One signal in particular, called a scallop, exhibits low within-individual variability, such that each individual appears to produce a distinctive scallop pattern that is slightly different from another individual's scallop (Serrier and Moller, 1989; Carlson and Hopkins, 2004). Scallops therefore present a valuable opportunity to test the specificity of temporal pattern recognition by this sensory pathway.

Electric communication signals are processed by a dedicated sensory pathway (Xu-Friedman and Hopkins, 1999; Baker et al., 2013). Sensory receptors called knollenorgans fire a single, time-locked spike in response to each EOD (Bennett, 1965). Afferents relay these spikes to the hindbrain nucleus of the electrosensory lateral line lobe (nELL), where corollary discharge inhibition blocks responses to the fish's own EODs (Bell and Grant, 1989). Axons from nELL project to the anterior exterolateral nucleus (ELa) of the midbrain torus semicircularis. ELa sends its only output to the posterior exterolateral nucleus (ELp), where sensitivity to interpulse intervals arises (Carlson, 2009). The interspike intervals in presynaptic inputs to ELp exactly match the IPIs in sensory stimuli. ELp neurons transform this temporal code for IPI into a population code, with neurons exhibiting a wide range of interval selectivity (Carlson, 2009; George et al., 2011; Ma et al., 2013; Baker and Carlson, 2014; Kohashi and Carlson, 2014).

In the present study, we measure behavioral and single-neuron responses to natural and manipulated versions of natural scallops to understand the temporal precision of signal detection. We demonstrate that fish are behaviorally sensitive to millisecond variations in natural timing patterns, and we subsequently ask whether the responses of interval-selective midbrain neurons contain the information necessary to resolve these variations in temporal patterns.

MATERIALS & METHODS

Animals. Eighty-one *B. brachyistius* ranging from 5.0-9.2 cm in standard length of both sexes contributed data to this study. Fish were housed in tanks with a 12 h light/dark cycle, water conductivity of 200-400 μS/cm, and water temperature of 25-29^{o}C. We fed the fish live black worms four times per week. Fish were obtained through the aquarium trade. All procedures were in accordance with National Institutes of Health guidelines and were approved by the Institutional Animal Use and Care Committee at Washington University in St. Louis.

Scallop stimulus generation. We chose six scallops as standard stimuli: one scallop from each of three males, and one scallop from each of three females (Fig. 1A). These stimuli were taken from scallops identified in (Carlson and Hopkins, 2004). Four of these scallops consisted of 11 interpulse intervals (IPIs; F1, F2, M2, M3), one consisted of 14 IPIs (F3), and one consisted of 10 IPIs (M1). To test the importance of the scallop's temporal structure, we generated start-shifted versions, in which we maintained the natural order of IPIs, but systematically varied the starting IPI. For instance, in a scallop with 11 IPIs, one start-shifted stimulus consisted of the second through eleventh IPIs followed by the first IPI. Another stimulus consisted of the third through eleventh IPIs followed by the first and second IPIs, and so on for all possible versions. To further test the temporal precision of scallop detection, we generated five temporal manipulations of natural scallops: time-reversed sequences, in which the IPI order of the natural scallop was reversed; randomized sequences, in which the IPI order was randomized on each stimulus presentation; and three sequences with added jitter. We generated sequences with 1, 3, or 5 ms jitter by adding a value drawn randomly from a Gaussian distribution centered at 0, with predefined standard deviation (1, 3, or 5 ms, respectively). We added an independently drawn jitter value to each pulse in the sequence on each stimulus

presentation, such that jitter values were independent across pulses within a stimulus, and across stimulus presentations.

Behavioral playback experiments. To test behavioral responses to scallops, we recorded fish's EOD output during presentation of natural and manipulated scallop sequences using previously described methods (Carlson et al., 2011). Briefly, we placed a rectangular plastic chamber (4.1 x 4.1 x 20.3 cm) in the middle of a singly housed fish's home tank (20.3 x 25.4 x 40.6 cm). Most fish entered the chamber voluntarily within ~5 min. If fish were not within the chamber after 5 min, we guided fish into the chamber with a net. Netted caps were placed over each end of the chamber to keep the fish inside during the experiment. Fish were then allowed an additional 10 minutes to acclimate to the chamber. A pair of Ag/AgCl electrodes oriented horizontally on both sides of the chamber delivered the stimulus, and a pair of Ag/AgCl electrodes oriented vertically on both ends of the chamber recorded the fish's EOD output. We delivered 20 repetitions of a single scallop stimulus consisting of bipolar square electric pulses of 2 ms duration, with 30 s between stimulus presentations to reduce habituation. We randomized stimulus order within and across fish. All stimuli were generated in Matlab 7 (Mathworks), digital-to-analog converted at a rate of 195.31 kHz (RX8, Tucker-Davis Technologies), and attenuated (PA5, Tucker-Davis Technologies) before delivery to the analog stimulus isolator (Model 2200, A-M Systems).

To record fish's EOD output, we amplified electrical activity 100 times before band-pass filtering (0.1 Hz – 20 kHz) (Model 1700, A-M Systems), digitizing at 97.7 kHz (RX8, Tucker-Davis Technologies), and saving using custom software in Matlab. We computed the spike density function (SDF) by convolving each EOD time with a Gaussian of 200 ms width (Carlson and Hopkins, 2004), and then averaging over stimulus presentations. We measured the fish's

baseline EOD rate by averaging the SDF over a window starting 0.2 s after the start of the 5 s prestimulus period and ending 0.2 s before stimulus onset.

To investigate how fish respond to natural and start-shifted scallop stimuli, we measured the maximum EOD rate that occurred in a window starting 0.1 s before stimulus onset up to 2.1 s after stimulus offset. To measure behavioral response thresholds, we defined a behavioral response from the fish as an increase in EOD rate exceeding the prestimulus mean + 3 standard deviations that occurred between 0.1 s before stimulus onset up to 2.1 s after stimulus offset. For each stimulus, we varied the intensity until we found the weakest intensity (to the nearest dB) to which the fish responded. We defined this intensity as the behavioral response threshold. The actual threshold stimulus intensity (in mV/cm) was determined using a calibration curve obtained by recording in the center of the playback chamber. We then normalized threshold intensities (in mV/cm) in response to manipulations of the same natural scallop to the threshold intensity for the natural scallop, and averaged across scallops before averaging across fish.

Whole-cell recordings. We prepared fish for *in vivo* recordings from ELp as described previously (Carlson, 2009; Lyons-Warren et al., 2013; Baker and Carlson, 2014). Briefly, fish were anesthetized in 300 mg/L tricaine methanesulfonate (MS-222) and paralyzed with an intramuscular injection of 100 µL of 0.1 mg/mL gallamine triethiodide (Flaxedil). We positioned the fish on a platform with lateral supports and respirated the fish with 100 mg/L MS-222 during surgery. We placed a drop of 0.4% lidocaine on the skin overlying the incision site, and then made an incision to uncover the skull overlying ELp. Next we glued a head post to the skull before using a dental drill and forceps to remove a rectangular piece of skull covering ELp. We placed the ground electrode on the nearby cerebellum. Following surgery, we switched respiration to freshwater and allowed the fish to recover from anesthesia. We monitored the

fish's anesthetized state with a pair of electrodes oriented parallel to the fish's electric organ to record the fictive EOD produced by the electromotor neurons (Carlson, 2009). Anesthesia silences the fictive EOD, such that the return of fictive discharges indicates that the fish has recovered from anesthesia. At the end of the recording session, the fish's respiration was switched back to 100 mg/L MS-222 until no fictive EOD could be recorded, and then the fish was killed by freezing.

We obtained intracellular, whole-cell patch recordings in current-clamp using previously published methods (Rose and Fortune, 1996; Carlson, 2009; Baker and Carlson, 2014). Briefly, we used a Flaming/Brown micropipette puller (Model P-97, Sutter Instruments Co.) to fabricate glass patch micropipettes of resistances of 20-40 MΩ. We backfilled the pipette tip with a solution containing (in mM): 100 CH_3CO_2K, 2 KCl, 1 MgCl, 5 EGTA, 10 HEPES, 20 KOH, and 43 biocytin. We filled the pipette shank with the same solution except we replaced biocytin with D-mannitol (Carlson, 2009; Baker and Carlson, 2014). Initial seals were >1 GΩ. Recordings were amplified 10 times and low-pass filtered (cutoff frequency = 10 kHz) using an Axopatch 200B amplifier (Molecular Devices), digitized at a rate of 97.7 kHz (Tucker Davis Technologies, model RX8), and saved using custom software in Matlab 7.

We delivered electrosensory stimulation using electrodes positioned around the perimeter of the recording chamber. Three vertically oriented electrodes on both sides of the chamber delivered stimulation transverse to the fish. Two vertically oriented electrodes at the front and back of the chamber delivered stimulation longitudinal to the fish (Lyons-Warren et al., 2013). We used stimuli consisting of monopolar square electric pulses. Stimuli were generated in Matlab, digital-to-analog converted at a rate of 195.31 kHz (RX8, Tucker-Davis Technologies),

and attenuated (PA5, Tucker-Davis Technologies) before delivery to the analog stimulus isolator (Model 2200, A-M Systems).

After obtaining a recording, we first varied the duration (0.2-2 ms), intensity (3-71 mV/cm), polarity (normal or reversed), and stimulus orientation (transverse or longitudinal to the fish) of a single pulse to elicit maximal postsynaptic potential (PSP) amplitudes from each neuron. All subsequent stimuli delivered during a recording then used these parameters while varying only the IPIs (Carlson, 2009; Baker and Carlson, 2014). We discarded responses to stimulus repetitions in which stimulus pulses occurred within 2-5 ms after a fictive EOD, since corollary discharge inhibition in the hindbrain blocks sensory responses within this window (Bell and Grant, 1989).

Data analysis. We removed spikes from recording traces and measured PSP amplitudes as described previously (Baker and Carlson, 2014). Briefly, to remove spikes, we first defined spike start as the point where the smoothed (moving average filter with width of 0.5 ms) derivative of the recorded potential first exceeded the prestimulus mean + 4SD, and spike end as the point where the smoothed derivative decreased below the prestimulus mean – 1SD. If the smoothed derivative did not meet our spike end criterion, we instead defined the spike end as the first minimum in the smoothed derivative up to 8 ms after the spike start. We measured the neuron's resting potential (RP) by first averaging the spike-removed traces over 10 presentations of the same stimulus, and then averaging the potential over a 50 ms window immediately preceding the stimulus. We measured PSP amplitudes by subtracting the RP from the maximum potential (after spike-removal) that occurred between 3 ms after each stimulus pulse up to the time of the next pulse. For presentation purposes, we removed the stimulus artifact from

recordings by linearly extrapolating the potential between the time of pulse onset to 0.5 ms after pulse offset.

We measured the membrane time constant (τ_m) and input resistance (R_m) by fitting each neuron's response to a 100 ms, -0.10 nA current pulse with a double exponential function, as previously described (Gittelman et al., 2009; Baker and Carlson, 2014). We then estimated membrane capacitance (C_m) according to

$$C_m = \frac{\tau_m}{R_m}. \tag{3.1}$$

Next we determined IPI tuning by collecting responses to scanning IPI stimuli consisting of IPIs ranging from 10-200 ms, and generating IPI tuning curves as previously described (Baker and Carlson, 2014). Briefly, we normalized PSP amplitudes in response to each IPI by the maximum PSP amplitude. If the normalized amplitudes to all IPIs were greater than 0.85, we classified the neuron as all-pass (i.e., no IPI tuning). Otherwise, we used sigmoidal and Gaussian fits to the tuning curves to classify IPI tuning as high-pass, low-pass, band-pass, or band-stop (Baker and Carlson, 2014). If a neuron's tuning did not fit any of these classes, we classified it as complex.

We next collected responses to natural and manipulated scallop stimuli. For each neuron, we randomly selected a natural scallop from our library. We then presented 10 repetitions each of the natural sequence, a time-reversed sequence, randomized sequences, and sequences with 1, 3, and 5 ms of added jitter. We randomized stimulus presentation order. Next we presented 10 additional repetitions of the natural scallop sequence. We repeated this procedure with another randomly selected scallop until we had presented manipulations of all six scallops, or until we lost the recording. We measured the PSPs evoked by each stimulus pulse on each repetition.

Inclusion criteria included 1) the RP remained below -40 mV throughout the recording; and 2) the RP varied $\leq$ 5 mV throughout the recording. Fifty-six of 60 neurons fit these criteria. Two of the excluded neurons were high-pass and two were low-pass. The RP, membrane capacitance, and membrane time constant of the four excluded neurons were within the range of those of the included neurons. For the 56 included neurons, there were no differences in RP (one-way ANOVA, $F_{(3)}$=0.68, p=0.57; mean -57.3 $\pm$ 0.4 mV), membrane capacitance (one-way ANOVA, $F_{(3)}$=1.1, p=0.36; mean 86.7 $\pm$ 10.2 pF), or membrane time constant (one-way ANOVA, $F_{(3)}$=0.46m p=0.71; mean 12.0 $\pm$ 1.2 ms) across IPI tuning groups.

Discriminant function analysis. To assess the degree to which the responses of single ELp neurons could be used to distinguish among natural and manipulated scallop sequences, we used discriminant function analysis (DFA). DFA defines a set of functions to group multivariate data by maximizing inter-group variance while minimizing intra-group variance (Cooley and Lohnes, 1971). These functions can then be used to assign independent data to one of the pre-defined groups. We used the PSPs evoked by the second through the last pulse in each stimulus as variables, and we used the PSPs measured on each stimulus presentation as a single observation. Occasionally our method of adding jitter resulted in a negative IPI (i.e., the jitter value to add was more negative than -1 times the natural IPI). This happened almost exclusively for 5 ms jitter sequences. In these cases, we threw out the neuron's responses to that particular stimulus repetition. Thus, we had 10 observations each for natural, time-reversed, randomized, 1 ms jitter-added, and 3 ms jitter-added sequences, and 5-10 observations for 5 ms jitter-added sequences in all neurons. We used the manipulation type as the grouping variable. To determine the discriminability of spiking responses, we performed DFA using the number of spikes in response to each stimulus pulse instead of PSP amplitude.

To determine whether ELp responses are sensitive to individual variation in scallops, we performed DFA on a neuron's responses to the four natural scallops in our library with the same number of IPIs. We used scallop ID as the grouping variable. For this analysis, we used the responses of only neurons from which we had responses to all four natural scallops as well as responses to repeated presentations of all four scallops. This allowed us to use an independent set of responses to each scallop to test the classification accuracy of the discriminant functions.

To implement DFA, we used a built-in discriminant function classifier (ClassificationDiscriminant.m) in Matlab. We also used a built-in function (mahal.m) to calculate Mahalanobis distances between each of 10 responses to the repeated natural sequence and the centroid of each manipulation group. To assess the discriminability of responses to natural, time-reversed, and randomized sequences, we assigned each of 10 responses to the repeated natural scallop to the group (natural, time-reversed, or randomized) with the smallest Mahalanobis distance. To assess the discriminability of responses to natural and jittered sequences, we assigned each of 10 responses to the natural repeated scallop to the group (natural, 1 ms jitter-added, 3 ms jitter-added, or 5 ms jitter-added) with the smallest Mahalanobis distance. To study the discriminability of responses to natural sequences from different individuals, we assigned each of 10 repetitions to the natural repeated scallop to the group with the smallest Mahalanobis distance.

Next we investigated how classification performance may be affected by pooling responses of multiple neurons together. We used only classification probabilities for the scallop for which we had responses from the largest number of neurons (M3; n=35 neurons). From the single-neuron classification probabilities, we calculated group probabilities according to

$$\sum_i \prod_k p(i \mid k), \tag{3.2}$$

where $p(i|k)$ is the probability that the responses of neuron i are classified as stimulus k. We calculated group classification probabilities for groups of two, three, four, and five neurons for classification in three instances: 1) natural vs. time-reversed and randomized scallop sequences, 2) natural vs. jittered scallop sequences, and 3) four different natural scallops. Group probabilities could be undefined if the denominator was 0. In these infrequent cases we did not record a probability for that particular group. We fit the resulting classification accuracy vs. group size with a logarithmic function according to

$$y = a\ln(x) + b\,, \tag{3.3}$$

where y is the classification probability, x is group size, and a and b are constants.

Statistics. All statistical tests were performed using Statistica (StatSoft). Parametric tests included single-sample *t*-tests, paired *t*-tests, one-way ANOVA, and repeated-measures ANOVA. Non-parametric tests included Spearman's rank test. Significance level for all tests was $p < 0.05$.

RESULTS

Fish's electric signaling behavior is sensitive to the temporal structure of scallops

To begin to understand the importance of the temporal structure of the stereotyped scallop signal, we first performed behavioral playback experiments in which we recorded fish's electric signaling activity in response to scallops. Our stimulus set consisted of one scallop recorded from each of three females, and one scallop recorded from each of three males (Fig. 1A). We measured fish's maximum electric organ discharge (EOD) rates in response to 20 repetitions of each scallop presented at the same intensity (291 mV/cm) (Fig. 1B). Response strengths depended on the scallop (repeated-measures ANOVA, $F_{(5,30)}$=2.7, p=0.039), with fish responding most strongly (mean= 20.6 $\pm$ 1.4 Hz) to the scallop consisting of the largest number of IPIs (F3, 14 IPIs) and least strongly (mean = 16.9 $\pm$ 1.4 Hz) to the scallop consisting of smallest number of IPIs (M1, 10 IPIs). Therefore, the difference in response strengths could be due to different numbers of IPIs in the natural scallops instead of slight differences in the temporal structure of each scallop.

The latency of fish's maximum EOD rate also depended on the scallop (repeated-measures ANOVA, $F_{(5,30)}$=5.5, p=0.011), and was positively correlated with the latency of the minimum IPI in each scallop (linear regression, r^2=0.72, p=0.033) (black points in Fig. 1C). A similar relationship held for responses to time-reversed sequences of natural scallops (linear regression, r^2=0.81, p=0.014) (blue points in Fig. 1C). These results reveal that the temporal structure of the scallop affects fish's electric signaling.

We further tested the relationship between the scallop timing pattern and fish's responses by presenting start-shifted versions of natural scallops. Start-shifted versions preserved the order of the IPIs in the scallop, but varied where in the signal the stimulus started. For instance, for a

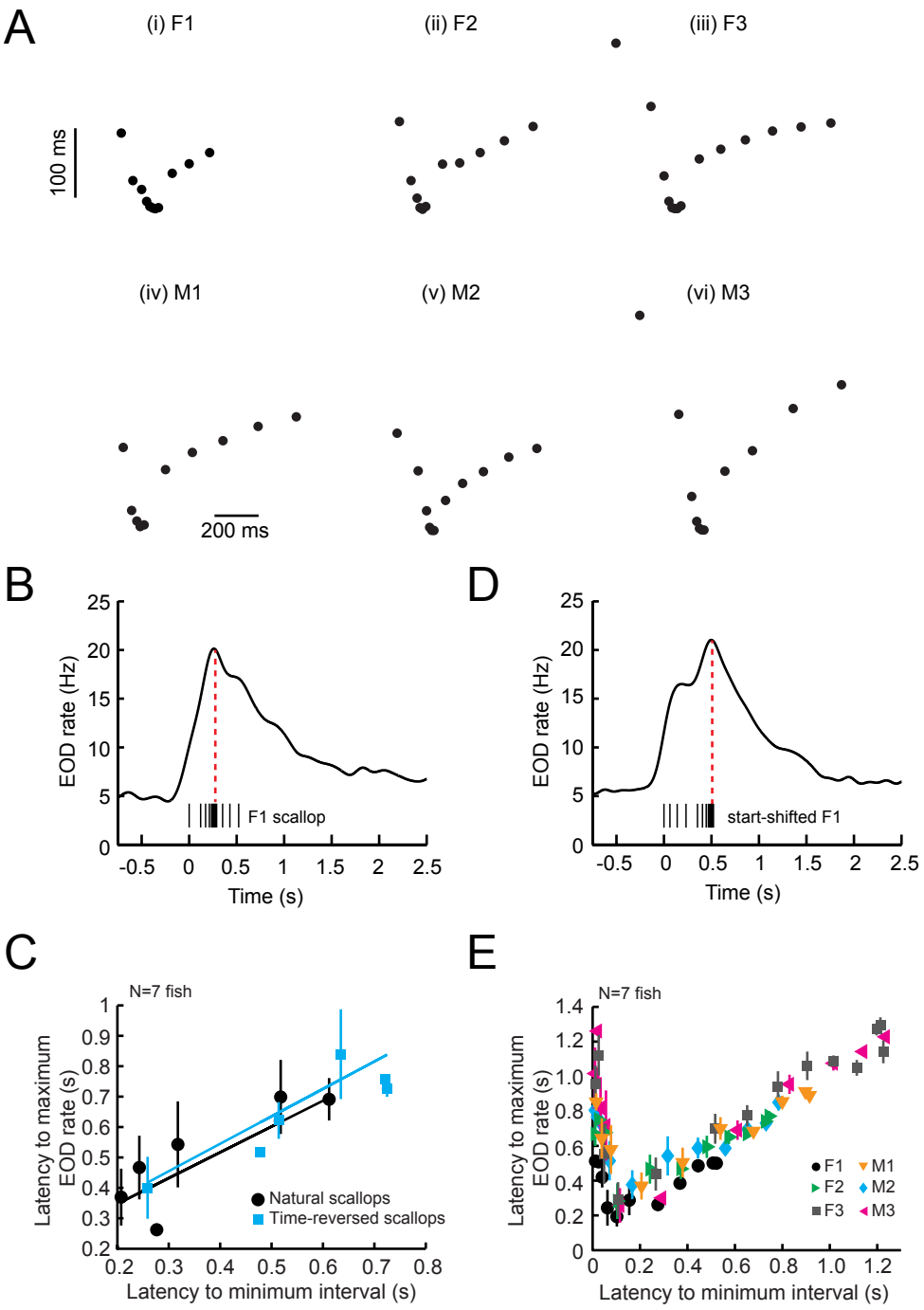

Figure 1. The timing of behavioral responses is sensitive to scallop temporal structure. (A) Our library of natural scallop patterns consisted of one sequence recorded from each of three females (F1-3) and from each of three males (M1-3). Each point represents the interpulse interval (IPI) vs. time of each electric pulse in the scallop. (B) Electric organ discharge (EOD) rate recorded from one fish in response to a scallop (F1) presented at time = 0 s. Tick marks below the EOD rate curve represent the time of each pulse in the stimulus. The red vertical line represents the time of the minimum IPI in the stimulus. (C) Latency to fish's maximum EOD rate vs. latency to minimum IPI of the stimulus for natural and time-reversed scallops. Each point represents the average across seven fish in response to each natural scallop

in (A). Error bars represent S.E.M. Lines are the results of a linear regression (natural scallops: r^2=0.72, p=0.033; time-reversed scallops: r^2=0.81, p=0.014.) (D) Same as (B) for a start-shifted version of the F1 scallop. This stimulus consisted of the ninth through eleventh IPIs of the F1 scallop followed by the first through eighth IPIs. (E) The latency to fish's maximum EOD rate vs. the latency to the minimum IPI for start-shifted sequences of all six natural scallops. Each point represents the average across seven fish and error bars represent S.E.M.

scallop consisting of 11 IPIs, one start-shifted version consisted of the second through eleventh IPIs followed by the first IPI. If fish's responses indeed depend on when the minimum IPI occurs in the signal, we should observe a relationship between the latency of the minimum IPI and the latency of fish's maximum EOD rate. We recorded the time of fish's responses to all possible start-shifts of all six natural scallops (Fig. 1D). Response latencies were positively correlated with the latencies of the minimum IPI in the stimulus for minimum IPI latencies longer than ~0.2 s (linear regression, r^2=0.84-0.98, p=0.000003-0.0096 across all six natural scallops) (Fig. 1E). This means that as long the minimum IPI occurred ~200 ms or later after the start of the sequence, the timing of fish's responses tracked the time of the minimum IPI. These results further demonstrate fish's behavioral sensitivity to the temporal structure of scallops.

Next we sought to test the temporal precision of scallop detection by asking by how much we could change the scallop pattern before affecting the strength of fish's behavioral responses. To test how changes in the order of scallop IPIs affected behavioral responses, we generated time-reversed and randomized sequences (Fig. 2A). Randomized sequences of scallop IPIs were generated independently for each stimulus presentation. We recorded fish's responses to natural, time-reversed, and randomized sequences of all six scallops presented at the same intensity (291 mV/cm), and found no differences in fish's maximum EOD rate in response to the three types of sequences (mean across all sequences = 18.6 $\pm$ 0.2 Hz; repeated-measures ANOVA, $F_{(2,12)}$=0.72, p=0.51).

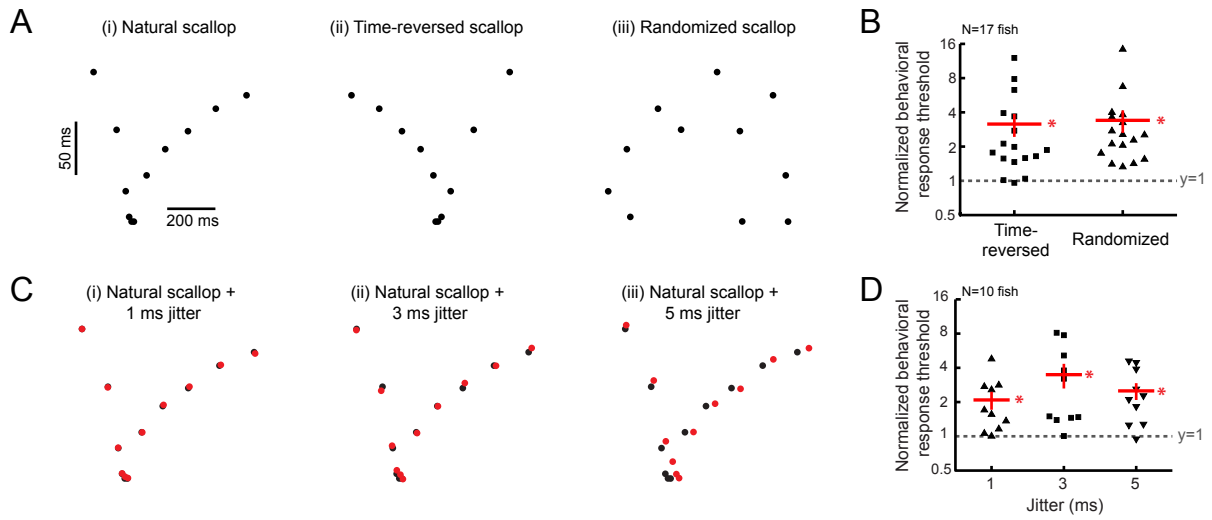

Figure 2. Temporal manipulations of natural scallops increase behavioral response thresholds. (A) Time-reversed (ii) and a randomized (iii) version of the natural M2 scallop (i). Each point represents the IPI vs. time of each pulse in the sequence. (B) Behavioral response thresholds for time-reversed and randomized sequences normalized to the thresholds for natural scallops. Each point represents the average of one fish's normalized thresholds for manipulations of all six natural scallops. Red horizontal bars represent the average across all fish and error bars represent S.E.M. *, $p < 0.01$, single-sample t-test against 1. (C) Examples of a natural scallop (M2; black) and one sequence (red) with each of three different amounts of jitter added. (D) Behavioral response thresholds for jitter-added sequences normalized to the thresholds for natural scallops. *, $p < 0.02$, single-sample t-test against 1.

Next we measured behavioral response thresholds for natural, time-reversed, and randomized scallops in 17 fish. We varied stimulus intensity in 1 dB increments until the fish no longer responded with an increase in EOD rate that exceeded the prestimulus mean EOD rate + 3SD. The lowest intensity that evoked a response from the fish was defined as the behavioral response threshold. We hypothesized that behavioral response thresholds would be more sensitive to temporal manipulations of scallops than the isointensity responses.

Behavioral responses thresholds for natural scallops ranged from 0.6-22.7 mV/cm (N=17 fish). Because response thresholds were variable across days within and also across fish, we normalized thresholds for time-reversed and randomized sequences to those for natural scallops. We found that behavioral response thresholds were on average ~3 times higher for time-reversed and randomized sequences than for natural sequences (single-sample t-test against 1; time-reversed: $t_{(16)}$=3.0, p=0.0088; randomized: $t_{(16)}$=3.1, p=0.0063) (Fig. 2B). This means that time-reversed and randomized signals had to be ~3 times more intense than natural signals to elicit a response. These results reveal that the IPI order, and not just overall IPI composition, of natural scallops is important for fish's responses.

Each individual produces its own scallop pattern that is slightly different from other individuals' scallops (Serrier and Moller, 1989; Carlson and Hopkins, 2004). This suggests that the electrosensory system cannot use a single template for recognizing scallops, but instead must be able to handle slight intra-individual variation. To investigate how changing the precise IPIs in natural scallops affects behavioral responses, we added jitter to each pulse in a natural scallop. To do so, we randomly drew a value from a Gaussian distribution centered around 0 and with SD of 1, 3, or 5 ms, and added this value to the time of each pulse in the natural scallop (Fig. 2C). Jitter values were added independently to each pulse in a stimulus during each presentation such

that the jittered stimulus was slightly different on each presentation. The overall effect resulted in IPIs that were sometimes shorter and sometimes longer than those in the natural scallop.

We first recorded fish's responses to natural and jittered sequences of all six scallops presented at the same intensity (291 mV/cm). There were no differences in fish's maximum EOD rate in response to natural, 1 ms jitter-added, 3 ms jitter-added, and 5-ms jitter-added sequences (mean across all sequences = 18.7 $\pm$ 0.2 Hz; repeated-measures ANOVA, $F_{(3,18)}$=0.98, p=0.42).

Next we measured behavioral response thresholds to natural and jitter-added sequences. Thresholds to natural scallops ranged from 0.6-6.2 mV/cm (N=10 fish). We found that behavioral response thresholds were elevated 2-3-fold for jittered sequences compared to natural sequences (single-sample t-test against 1; 1 ms jitter: $t_{(9)}$=2.9, p=0.018; 3 ms jitter: $t_{(9)}$=2.9, p=0.017; 5 ms jitter: $t_{(9)}$=3.6, p=0.0060) (Fig. 2D). These results reveal that fish are behaviorally sensitive to the precise intervals in scallops.

Interval-selective midbrain neurons respond differently to scallops

The IPIs in electric communication signals are precisely encoded at the periphery and preserved by the ascending electrosensory system until activity reaches the midbrain posterior exterolateral nucleus (ELp), where single neurons are selective for particular IPIs (see Baker et al., 2013 for review). To begin to understand how this population of IPI-selective neurons contributes to fish's behavioral sensitivity to scallop temporal structure, we obtained *in vivo* intracellular whole-cell recordings from 56 ELp neurons during electrosensory stimulation with scallop stimuli (Fig. 3). IPI tuning was classified as high-pass (n=20) (e.g., Fig. 3A), band-stop

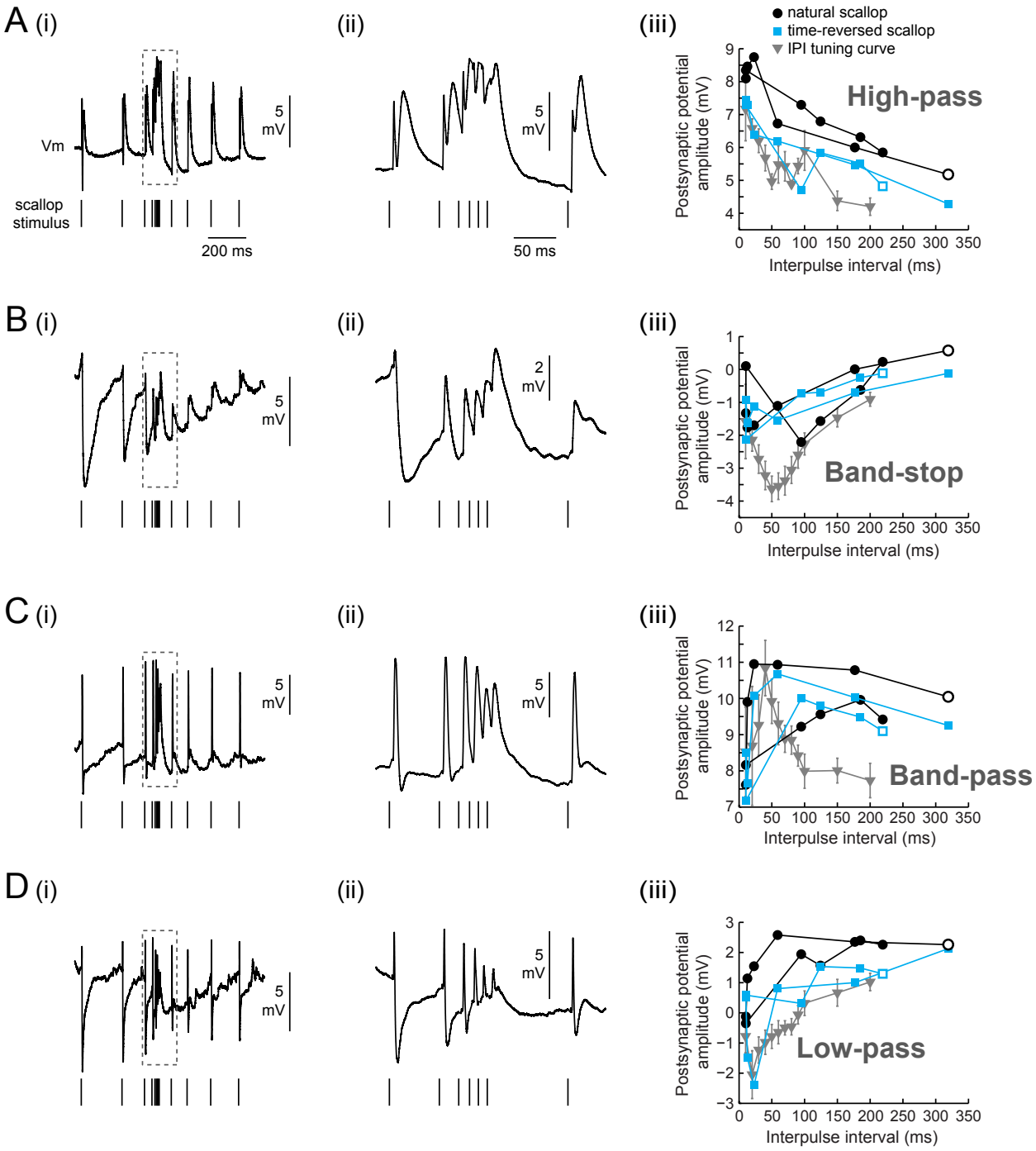

Figure 3. Interval-selective midbrain neurons respond differently to scallops. (A) (i) Intracellular membrane potential (*Vm*) recording from a high-pass neuron in response to a natural scallop (M3). The trace represents the membrane potential averaged over 10 stimulus presentations. Tick marks below the recording trace denote the time of each electric pulse in the stimulus. (ii) Close-up of the recording in (i) during the shortest IPIs in the scallop (dashed box in (i)). (iii) Postsynaptic potential (PSP) amplitudes in response to IPI tuning curve, natural scallop, and time-reversed scallop stimuli. The black curve reflects the responses shown in (i-ii). Open symbols indicate the response to the first IPI in the natural and time-reversed scallop stimuli. (B-D) Same as (A) for a band-stop (B), band-pass (C), and low-pass (D) neuron.

(*n*=8) (e.g., Fig. 3B), band-pass (*n*=7) (e.g., Fig. 3C), low-pass (*n*=16) (e.g., Fig. 3D), complex (*n*=3), or all-pass (*n*=2).

Neurons responded differently to the same scallop sequences depending on their IPI tuning (Fig. 3) (Carlson, 2009). High-pass neurons produced the largest postsynaptic potential (PSP) amplitudes during the shortest IPIs in the scallop (Fig. 3A). Band-stop neurons produced the largest PSP amplitudes during the shortest and longest IPIs in the scallop (Fig. 3B). Band-pass neurons produced the greatest PSP amplitudes in response to intermediate IPIs in the scallop (Fig. 3C). Low-pass neurons produced the largest PSP amplitudes in response to the longest IPIs of the scallop (Fig. 3D). In some neurons, the PSP amplitudes depended on direction of IPI change, such that response amplitudes to the same IPIs were slightly different for natural and time-reversed sequences of the same scallop (Fig. 3A, B, D). This wide variety of response properties arises from a combination of synaptic mechanisms, including temporal summation and short-term depression, as well as intrinsic membrane properties (George et al., 2011; Baker and Carlson, 2014; Kohashi and Carlson, 2014). Thus ELp neurons act as temporal filters for electric communication signals.

Responses of single interval-selective neurons are sensitive to changes in the order of intervals in scallops

We recorded the intracellular responses of ELp neurons to natural, time-reversed, randomized, and jittered sequences of the same six scallops that we used in the behavior experiments. For each neuron, we measured the PSP amplitudes evoked by each pulse on every stimulus presentation, and then used the PSP amplitudes in response to the second through last pulse in discriminant function analysis (DFA). We used responses to all six stimulus sequences

(natural, time-reversed, randomized, jitter: 1 ms, jitter: 3 ms, and jitter: 5 ms) to define discriminant functions. We then used these functions to classify the neuron's responses to 10 independent presentations of the natural scallop.

To test whether subthreshold responses of individual neurons could be used to distinguish natural from time-reversed and randomized scallops, we used the discriminant functions to classify responses to each of 10 presentations of the natural scallop as one of these three sequences (Fig. 4A, B). Across all neurons, responses to natural scallops were correctly classified with a probability of 0.63 ± 0.03, which was significantly more frequently than predicted by chance (single-sample *t*-test against 0.33, $t_{(55)}=11$, $p<0.000001$) (Fig. 4C). Responses to natural scallops were incorrectly classified as time-reversed (single-sample *t*-test against 0.33, $t_{(55)}=-9.1$, $p<0.000001$) and randomized (single-sample *t*-test against 0.33, $t_{(55)}=-7.1$, $p<0.000001$) sequences significantly less frequently than predicted by chance (Fig. 4C).

Interestingly, classification performance depended on IPI tuning (one-way ANOVA, $F_{(3)}=3.2$, $p=0.032$) (Fig. 4D). Band-stop responses were significantly better than high-pass (Tukey post-host test, $p=0.044$) and low-pass (Tukey post-hoc test, $p=0.025$) responses in classifying natural vs. time-reversed and randomized scallops. Nevertheless, neurons in all tuning classes correctly classified natural scallops significantly more frequently than expected by chance (single-sample *t*-test against 0.33, high-pass: $t_{(19)}=6.4$, $p=0.000004$; band-stop: $t_{(7)}=11$, $p=0.000011$; band-pass: $t_{(6)}=3.4$, $p=0.016$; low-pass: $t_{(15)}=5.6$, $p=0.000052$) (Fig. 4D). These results demonstrate that the IPI selectivity of ELp neurons results in responses that can be used to distinguish changes in the order of IPIs in natural temporal patterns.

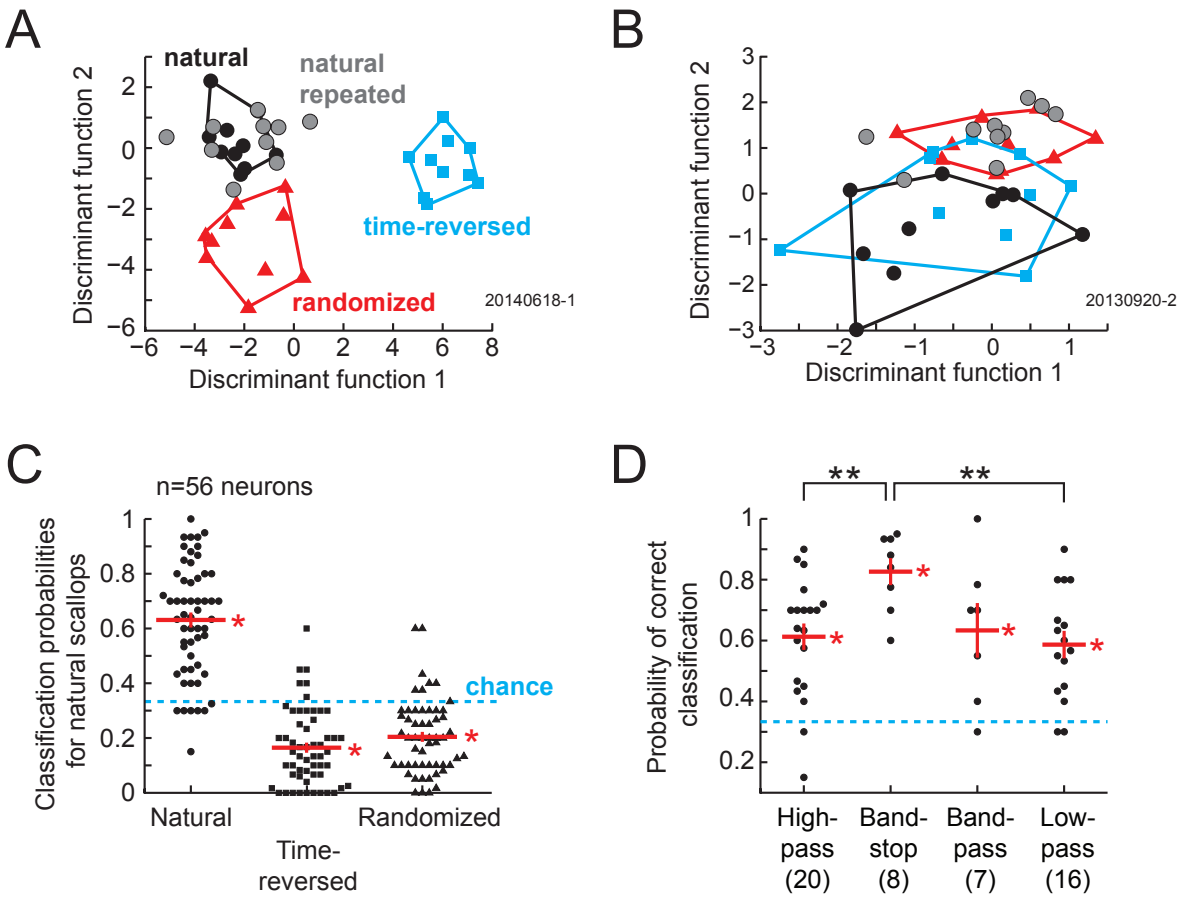

Figure 4. The responses of single neurons are sensitive to changes in the order of intervals in scallops. (A) Discriminant function analysis (DFA) results for responses to natural, time-reversed, and randomized scallop (F2) sequences in a high-pass neuron with high classification accuracy. PSP amplitudes evoked by the second through last pulse in each of 10 stimulus presentations of natural, time-reversed, randomized, and jittered sequences were used to define the discriminant functions. We then used these functions to classify responses to 10 additional presentations of the natural scallop (grey circles) as natural, time-reversed, or randomized sequences based on Mahalanobis distances from group centroids. All 10 of this neuron's responses to the repeated natural scallop were correctly classified as belonging to the natural sequence. Each point reflects the neuron's responses to one stimulus presentation. The neuron's ID is given in the bottom right corner of the plot. (B) Same as (A) for a low-pass neuron with low classification accuracy. One of 10 of this neuron's responses to the repeated natural scallop was correctly classified. (C) Probabilities of classification of natural scallop responses as natural, time-reversed, and randomized sequences for all neurons. *, single-sample t-test against chance (0.33), $p<0.000001$. (D) Probability of correct classification by IPI tuning. Complex ($n=3$ neurons) and all-pass ($n=2$ neurons) were excluded from this analysis. *, single-sample t-test against chance (0.33), $p<0.02$. **, one-way ANOVA, Tukey post-hoc test, $p<0.05$. Red horizontal bars in (C, D) represent the average across neurons and error bars represent S.E.M.

Responses of single band-stop neurons are sensitive to changes in the precise intervals in scallops

Next, we used the previously defined discriminant functions to classify responses to each of 10 presentations of natural scallops as natural or jittered sequences (Fig. 5A, B). In general, the responses of single ELp neurons could not be used to correctly identify natural sequences significantly more frequently than predicted by chance (single-sample *t*-test against 0.25, $t_{(55)}$=-0.21, p=0.83) (Fig. 5C). However, classification accuracy again depended on IPI tuning (one-way ANOVA, F(3)=4.3, p=0.01), with band-stop neurons performing significantly better than band-pass (Tukey post-hoc test, p=0.011) and low-pass (Tukey post-hoc test, p=0.022) neurons (Fig. 5D). Indeed, only band-stop neurons correctly classified natural scallops more frequently than predicted by chance (single-sample *t*-test against 0.25, $t_{(7)}$=3.8, p=0.0070). These results demonstrate that the responses of only one IPI tuning class can be used to distinguish changes in the precise intervals in natural temporal patterns.

Spikes increase discriminability of responses to natural versus jittered scallops

We have shown that subthreshold PSP amplitudes in single neurons can be used to discriminate between natural timing patterns and some artificial versions of these patterns. However, these subthreshold changes in membrane potential are not transmitted to downstream neurons; only spiking activity is. To investigate how spiking may affect the discriminability of single-neuron responses, we counted the number of spikes elicited by each pulse during every presentation of natural, time-reversed, randomized, and jittered scallop sequences. Thirteen neurons produced spikes often enough to provide sufficient variation for DFA to work. For each neuron, we used the spike counts in response to the second through the last pulse of natural,

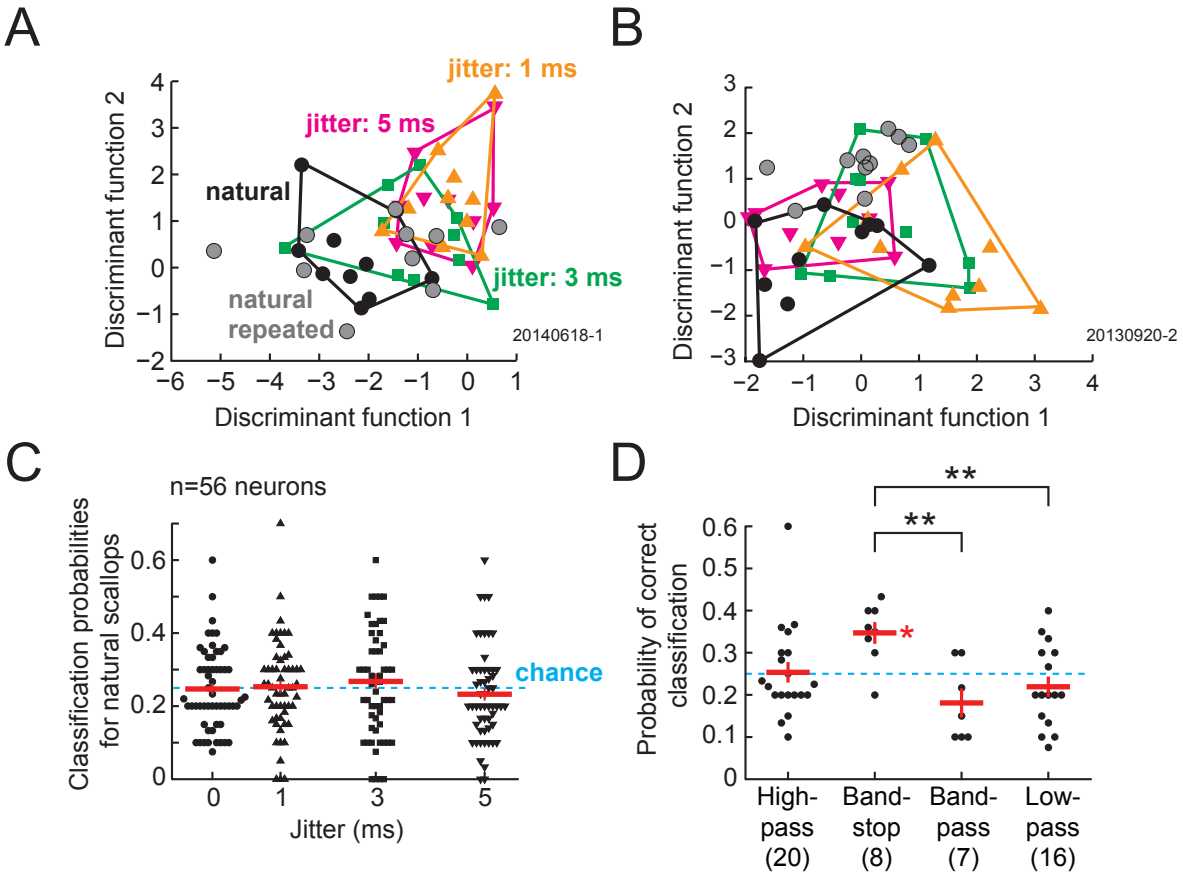

Figure 5. The responses of single band-stop neurons are sensitive to changes in the precise intervals in scallops. (A) DFA results for responses to natural and jittered scallop (F2) sequences in a high-pass neuron with high classification accuracy (same neuron as in Fig. 4A). PSP amplitudes evoked by the second through last pulse in each of 10 stimulus presentations of natural, time-reversed, randomized, and jittered sequences were used to define the discriminant functions. We then used these functions to classify responses to 10 additional presentations of the natural scallop (grey circles) as natural or jittered sequences based on Mahalanobis distances from group centroids. Five of 10 of this neuron's responses to the repeated natural scallop were correctly classified. Each point reflects the neuron's responses to one stimulus presentation. The neuron's ID is given in the bottom right corner of the plot. (B) Same as (A) for a low-pass neuron with low classification accuracy (same neuron as in Fig. 4B). One of 10 of this neuron's responses to the repeated natural scallop was correctly classified. C) Probabilities of classification of natural scallop responses as natural and jittered sequences for all neurons. (D) Probability of correct classification by IPI tuning. Complex (n=3 neurons) and all-pass (n=2 neurons) were excluded from this analysis. *, single-sample t-test against chance (0.25), $p<0.01$. **, one-way ANOVA, Tukey post-hoc test, $p<0.03$. Red horizontal bars in (C, D) represent the average across neurons and error bars represent S.E.M.

time-reversed, randomized, and jittered sequences to define the discriminant functions that maximized the separability of the responses to each manipulation. We then used these functions to classify responses to 10 independent presentations of the natural scallop.

Spiking activity was no better than subthreshold PSPs at classifying natural vs. time-reversed and randomized scallops (paired *t*-test, $t_{(13)}$=-0.76, p=0.46) (Fig. 6B). On average, the responses of spiking neurons correctly classified natural scallop sequences with a probability of 0.55 $\pm$ 0.07, which was significantly more frequent than predicted by chance (single-sample *t*-test against 0.33, $t_{(12)}$=3.2, p=0.0078). Classification accuracy for natural vs. time-reversed and randomized sequences was not correlated with the average number of spikes per sweep over all stimuli (Spearman R=-0.085, $t_{(11)}$=-0.28, p=0.78).

In contrast, spikes resulted in significantly better classification performance than PSP amplitudes for natural vs. jittered scallops (paired *t*-test, $t_{(13)}$=2.3, p=0.037) (Fig. 6C). In this subset of neurons, using spikes resulted in correct classification of natural sequences with a probability of 0.25 $\pm$ 0.05, compared to 0.17 $\pm$ 0.05 using PSPs. However, classification accuracy using spikes was equal to that predicted by chance. Classification accuracy for natural vs. jittered sequences was not correlated with average spikes per sweep over all stimuli (Spearman R=-0.44, $t_{(11)}$=-1.6, p=0.13). These results demonstrate that spiking activity can enhance the discriminability of single-neuron responses to natural vs. jittered temporal patterns.

Pooling classification probabilities of multiple neurons improves accuracy

We have shown that the responses of individual ELp neurons can be used to correctly classify natural vs. time-reversed and randomized scallop sequences, but that the responses to natural vs. jittered sequences are generally less discriminable. However, the electrosensory

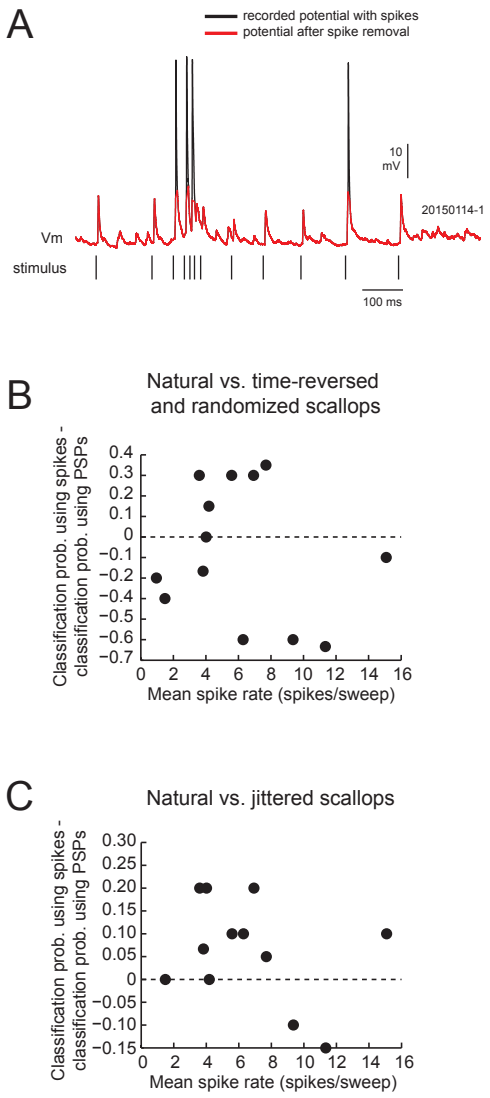

Figure 6. Spikes increase discriminability of responses to natural versus jittered sequences. (A) Intracellular recording of the membrane potential (*Vm*) from a high-pass neuron in response to a natural scallop (F2). The recorded potential is shown in black, and the potential after spike removal is shown in red. (B) The difference in correct classification probability using spikes and PSPs vs. the mean spike rate over all stimuli for natural vs. time-reversed and randomized sequences. (C) The difference in correct classification probability using spikes and PSPs vs. the mean spike rate over all stimuli for natural vs. jittered sequences.

system does not have to rely solely on the output of any one ELp neuron to detect scallops. Rather, downstream neurons could integrate the output of multiple ELp neurons to identify temporally patterned communication signals. Therefore, we wanted to study how classification performance would be affected if we pooled the responses of multiple ELp neurons together. We used Bayesian updating with single-neuron classification probabilities to estimate the probability of correct classification of natural vs. time-reversed and randomized sequences for all possible combinations of two, three, four, and five neurons. We used the single-neuron classification probabilities for the natural scallop to which we had responses from the most neurons (M3, *n*=35 neurons).

The probability of correct classification of natural vs. time-reversed and randomized scallop sequences increased as the responses of more neurons were combined (Fig. 7A). Combining the classification probabilities of five neurons resulted in an average correct classification probability of 0.96. These data were well fit with the logarithmic function, $y=0.18\ln(x)+0.67$ ($r^2=0.99$) (Fig. 7A). According to our fit, 100% accuracy would be possible with between six and seven neurons.

The probability of correct classification of natural vs. time-reversed and randomized scallop sequences increased from 0.66 ± 0.05 using single neurons (*n*=35 neurons) to 0.82 ± 0.01 using pairs (*n*=591 pairs) of neurons. To determine whether the IPI tuning of constituent neurons may affect classification, we compared the probability of correct classification for pairs consisting of all possible tuning compositions (Fig. 7B). Band-stop neurons formed pairs that tended to have the highest probability of correct classification (Fig. 7B). This finding is consistent with band-stop neurons having significantly greater correct classification probabilities than neurons of other tuning types (Fig. 4D). In general, pairs of neurons of different tuning

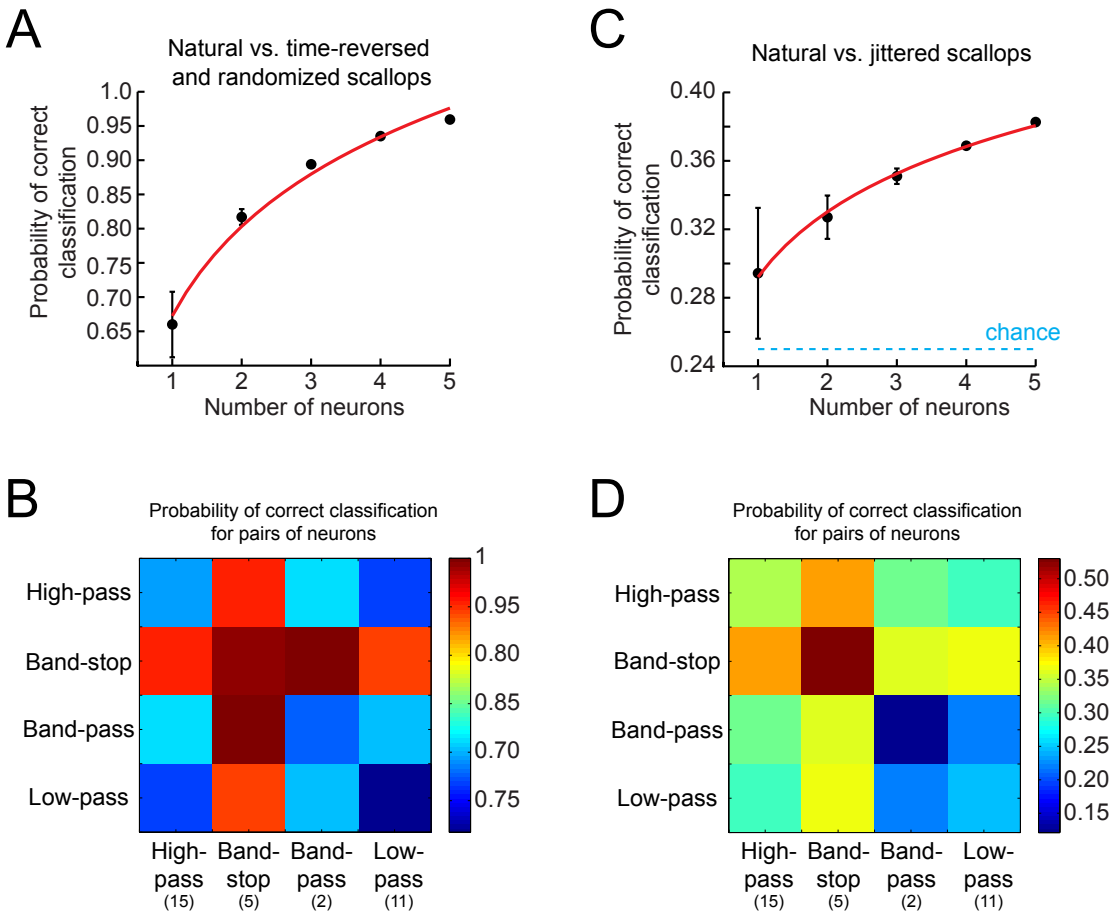

Figure 7. Pooling classification probabilities of multiple neurons improves accuracy. (A) Probability of correct classification vs. number of neurons in a group for natural vs. time-reversed and randomized scallop sequences. We used Bayesian updating to estimate classification probabilities for all possible combinations of single-neuron probabilities from the responses of 35 neurons to the same scallop (M3). The red line represents the function $y=0.19*\ln(x)+0.67$ ($r^2=0.99$). (B) Color map of classification accuracy of natural vs. time-reversed and randomized scallop sequences for all possible pairs of neurons by IPI tuning. We excluded results of pairs formed by one complex neuron and one all-pass neuron from these data. (C) Same as (A) for classification of natural vs. jittered scallop sequences. The red line represents the function $y=0.06*\ln(x)+0.29$ ($r^2=1.0$). (D) Same as (B) for classification accuracy of natural vs. jittered scallop sequences.

classes had significantly higher correct classification probabilities for natural vs. time-reversed and randomized sequences than pairs of neurons of the same tuning class (independent *t*-test, $t_{(522)}$=-2.5, p=0.014).

Pooling probabilities from groups of neurons also improved classification accuracy for natural vs. jittered scallops (Fig. 7C). However, using the classification probabilities of even five neurons resulted in a probability of correct classification of only 0.38. The relationship between classification probabilities and the number of neurons in a group was well fit with the function, $y=0.06\ln(x)+0.29$ (r^2=1.0) (Fig. 7C). This equation predicts that a group of even 100 neurons would result in classification probability of 0.57, which is still lower than the single-neuron correct classification probability of natural vs. time-reversed and randomized scallops.

Pooling responses from just two neurons resulted in correct classification of natural vs. jittered sequences significantly more frequently than that predicted by chance (single-sample *t*-test, $t_{(589)}$=6.1, p<0.000001). Band-stop neurons tended to form pairs with the highest classification probabilities (Fig. 7D), but there was no significant difference in the probability of correct classification of natural vs. jittered sequences for pairs of similarly vs. dissimilarly tuned neurons (independent *t*-test, $t_{(522)}$=-0.34, p=0.73). Collectively, these results indicate that, even though pooling classification probabilities of multiple ELp neurons improves accuracy, responses to natural sequences are still less discriminable from responses to jittered sequences than from responses to time-reversed and randomized sequences.

Responses of single interval-selective neurons are sensitive to individual variation in scallops

Next we wanted to understand how single-neuron sensitivity to manipulated scallops relates to sensitivity to natural variation in scallops. In 15 neurons, we collected responses to 10 repetitions of four natural scallops, each from a different individual. We used the PSP amplitudes evoked by the second through last pulse in each scallop to define discriminant functions that maximally separated responses to the four scallops. We then used these functions to classify responses to 10 independent presentations of each of the same four natural scallops (Fig. 8A).

On average, the probability of correct classification across neurons was 0.64 ± 0.05, which was significantly higher than that predicted by chance (single-sample *t*-test against 0.25, $t_{(14)}=8.8$, $p<0.000001$). The probability of correct classification for all scallops was significantly higher than chance (single-sample *t*-test, F1: $t_{(14)}=7.6$, $p=0.000003$; F2: $t_{(14)}=4.7$, $p=0.00037$; M2: $t_{(14)}=4.2$, $p=0.00086$; M3: $t_{(14)}=7.4$, $p=0.000003$), with no significant differences in correct classification probability across the four scallops (repeated-measures ANOVA, $F_{(3,42)}=1.9$, $p=0.14$).

Correct classification probability for different individuals' scallops was positively correlated with correct classification probability for natural vs. time-reversed and randomized scallops (Spearman R=0.66, $t_{(13)}=3.2$, $p=0.0069$). In contrast, there was no relationship between correct classification probability for different individuals' scallops and correct classification probability for natural vs. jittered scallops (Spearman R=0.35, $t_{(13)}=1.3$, $p=0.20$). Therefore, neurons that were good at discriminating natural from time-reversed and randomized scallops were also good at discriminating among scallops from different individuals.

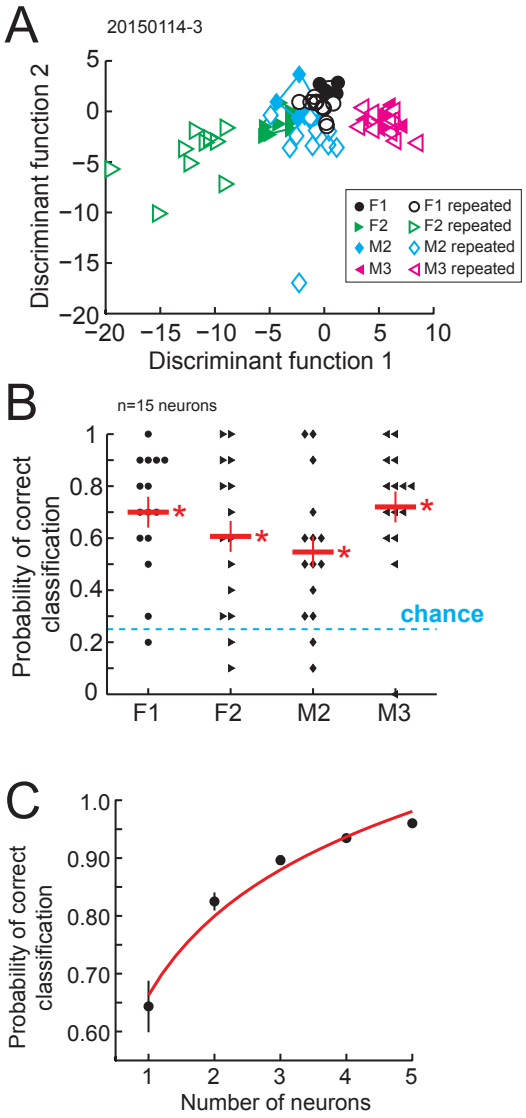

Figure 8. The responses of single neurons are sensitive to individual variation in scallops. (A) DFA results for responses to natural scallop sequences from four different individuals (F1, F2, M2, M3) in a high-pass neuron with high classification accuracy. PSP amplitudes evoked by the second through last pulse in each of 10 stimulus presentations of the four scallops were used to define the discriminant functions. We then used these functions to classify responses to 10 additional presentations of each natural scallop (open symbols) as one of the four natural scallops based on Mahalanobis distances from group centroids. All 10 repetitions of the F2 and M3 scallops were correctly classified, and seven of 10 repetitions of the F1 and M2 scallops were correctly classified. Each point reflects the neuron's responses to one stimulus presentation. The neuron's ID is given in the upper left corner of the plot. (B) Probabilities of correct classification by scallop. Each point represents the probability for one neuron. Red horizontal bars in represent the average across neurons and error bars represent S.E.M. *, single-sample t-test vs. chance (0.25), $p<0.001$. (C) Probability of correct classification vs. number of neurons in a group for natural scallops. We used Bayesian updating to estimate classification probabilities for all possible combinations of single-neuron probabilities from the responses of 15 neurons to the same four scallops. The red line represents the function, $y=0.20\ln(x)+0.67$ ($r^2=0.97$).

Pooling the responses of multiple neurons further enhanced the discriminability of natural scallops (Fig. 8C). Combining the classification probabilities of five neurons resulted in an average correct classification probability of 0.96. These data were well fit with the logarithmic function, $y=0.20\ln(x)+0.67$ ($r^2=0.97$) (Fig. 8C). According to our fit, 100% accuracy would be possible with between five and six neurons. These results are very similar to those obtained for the discrimination of natural vs. time-reversed and randomized scallops in single neurons.

DISCUSSION

Our results demonstrate that fish are behaviorally sensitive to millisecond timing variations in natural scallop patterns. This sensitivity is due at least in part to a population of midbrain neurons that serve as temporal filters for electric communication signals. The output of single interval-selective neurons can be used to correctly discriminate natural scallop patterns from changes in the order of IPIs, demonstrating that the order of IPIs, and not just overall IPI composition, is important for scallop detection. Although the subthreshold responses of single neurons are less sensitive to small changes in the precise IPI durations within a scallop, spikes could improve discriminability. Furthermore, the discriminability of natural scallop patterns from artificial variations could be improved by pooling the responses over multiple neurons. Remarkably, there is enough information present in the subthreshold responses of single neurons to distinguish among scallops produced by different individuals. Collectively, these results provide an illustration of how a population of interval-selective neurons can contribute to the detection of behaviorally relevant temporal patterns in sensory stimuli.

Although we had a limited sample size on which to test sensitivity to natural scallop variation, correct classification probabilities for scallops from different individuals were correlated with those for natural vs. time-reversed and randomized scallops. Thus we can infer that the observed range of single-neuron sensitivities to natural vs. time-reversed and randomized scallops reasonably reflects the ELp population's sensitivity to individual variation in scallop patterns. The ability of single ELp neurons to provide enough information to discriminate among scallops from different individuals is in line with similar findings in auditory and electrosensory pathways. The spiking responses of auditory receptors and higher-order neurons in the grasshopper, as well as those of songbird field L neurons, can be used to discriminate among

conspecific songs produced by different individuals (Machens et al., 2003; Wang et al., 2007; Ronacher et al., 2008). Likewise, the spiking responses of hindbrain electrosensory neurons in wave-type weakly electric fish, which evolved their electric sense independently of mormyrids, can be used to discriminate between courtship signals from different individuals (Marsat and Maler, 2010). However, to our knowledge all previous studies of neural discrimination have used spike trains recorded from extracellular recordings. Here we show that subthreshold PSPs can be used to discriminate among natural and artificial temporal sequences in communication signals.

From a purely information-theoretic perspective, graded membrane potential changes in response to sensory stimuli contain more information than spikes (de Ruyter van Steveninck and Laughlin, 1996; Juusola and French, 1997; Haag and Borst, 1998; Dhingra and Smith, 2004). Accordingly, spike threshold has been shown to play an important role in sharpening single-neuron stimulus selectivity in visual, auditory, and somatosensory cortices (Priebe and Ferster, 2008). As responses become more sharply tuned for particular stimulus features, their ability to provide enough information to discriminate among different stimuli might be expected to decline. However, in the fly visual system, spikes have been shown to improve discriminability if they amplify particular characteristics of the graded responses (Kretzberg et al., 2001). Therefore, it cannot be taken as a given that graded, subthreshold responses will always outperform spiking responses on stimulus discrimination measures.

In our recordings, just under one-quarter (n=13/56) of ELp neurons fired spikes regularly enough to allow DFA. We found that spikes significantly improved discrimination of natural vs. jittered scallops, but not discrimination of natural vs. time-reversed and randomized scallops. Classification performance for natural vs. jittered stimuli using PSPs was much lower than that

for natural vs. time-reversed and randomized scallops, suggesting that spikes could increase discriminability of stimuli that are not well discriminated by PSPs.

Discriminability based on PSPs improved when we pooled the classification probabilities of multiple neurons. For pairs of neurons, we found an effect of IPI tuning, with pairs consisting of two neurons in different IPI tuning classes performing better than pairs with similar IPI tuning. Several studies have reported that a population of neurons with heterogeneous response properties can result in better discrimination performance than a population of neurons with homogeneous response properties (Shamir and Sompolinsky, 2006; Chelaru and Dragoi, 2008; Osborne et al., 2008; Holmstrom et al., 2010; Marsat and Maler, 2010; but see Schneider and Woolley, 2010). However, a combination of heterogeneity and homogeneity in olfactory mitral bulb cells provided the most benefits to stimulus encoding, and the optimal combination of heterogeneous vs. homogeneous neural responses depended on the stimulus (Tripathy et al., 2013).

ELp neurons exhibit a great deal of diversity in responses to IPIs. We classify these responses into six categories (i.e., high-pass, low-pass, band-pass, band-stop, complex, and all-pass) based on quantitative measures of PSP amplitudes evoked by IPIs (Carlson, 2009; George et al., 2011; Baker and Carlson, 2014). However, even within these tuning classes, responses are variable with respect to parameters such as bandwidth, best IPI, sensitivity to direction of IPI change, and intrinsic excitability (Carlson, 2009; George et al., 2011; Ma et al., 2013; Baker and Carlson, 2014; Kohashi and Carlson, 2014). Given that neural heterogeneity increases discriminability in a variety of other systems, it is likely that such diversity in ELp enhances the ability of population responses to detect and classify temporally patterned communication signals.

The improvement in classification probability by pooling responses over many neurons suggests that downstream neurons could integrate the output of multiple ELp neurons to achieve high discriminability between natural temporal patterns. Our method of pooling probabilities considered the responses of each neuron with equal weights. However, neurons could achieve even better performance than predicted here by adjusting synaptic weights accordingly (Shamir and Sompolinsky, 2006; Barbour et al., 2007). For instance, a neuron receiving one input with high classification accuracy and another input with low classification accuracy could assign a stronger weight to the better performing input. One such mechanism that could facilitate changes in synaptic weights is spike-timing-dependent plasticity (Feldman, 2012). Therefore, the ability of single ELp neurons to detect natural, behaviorally relevant temporal patterns could be enhanced by integrating responses from multiple neurons of different IPI tuning classes, and/or by adjusting the relative synaptic weights of different ELp neurons onto downstream targets.

How and where such integration of ELp responses might take place remains an open question. ELp sends projections to the midbrain isthmic granule nucleus, which in turn projects back to ELp as well as to the valvula cerebellum (Haugede-Carre, 1979; Finger et al., 1981). ELp also projects to the subpraæeminential nucleus, inferior olive, and the medioventral nucleus of the midbrain, which is hypothesized to be involved in spatial analysis of signaling fish (Haugede-Carre, 1979; Friedman and Hopkins, 1998). Future *in vivo* electrophysiology experiments will be necessary to understand the roles of the isthmic granule nucleus, the subpraæeminential nucleus, and the inferior olive in electric communication signal analysis.

We found that single-neuron responses were sensitive to individual variation in scallop patterns. PSP amplitudes from single neurons could be used to discriminate among scallops from different individuals with a probability of 0.64 ± 0.05, with discriminability improving even

further when responses of multiple neurons were combined. Therefore, the information necessary to resolve individual differences in scallops is present in the population output of ELp. However, whether fish behaviorally discriminate individual differences in scallops remains to be determined. The individually stereotyped EOD waveform contains identifying information such as species, sex, and dominance status, and can even be used to identify individuals in some species (Graff and Kramer, 1992; Friedman and Hopkins, 1996; Carlson, 2002; Hanika and Kramer, 2005). Combining the stereotyped EOD waveform with individually characteristic scallop pattern could facilitate individual recognition. Another potential function of stereotyped scallop patterns could be to signal information such as fitness. Since scallops are hypothesized to play a role in aggressive encounters (Carlson and Hopkins, 2004), these individually distinctive temporal patterns could be used to "size up" a competitor. Whether discrimination of inter-individual differences in scallops would provide any benefit to the fish remains to be seen.

Here we explored how a population of neurons encodes one particular electric communication signal. However, mormyrids produce at least three additional types of temporal patterns during social encounters called accelerations, rasps, and creaks, which all consist of a larger number of IPIs than scallops (Carlson and Hopkins, 2004; Wong and Hopkins, 2007). The ability of single ELp neurons to distinguish between individual scallops consisting of only 10 IPIs suggests that these neurons would likely also be able to distinguish between different classes of communication signals (Carlson and Hopkins, 2004). Furthermore, neurons with different IPI tuning properties have been shown to respond differently to accelerations and rasps (Carlson, 2009). Since ELp neurons are involved in detecting more than just scallop sequences, it is possible that neurons whose responses poorly discriminated scallop variation may instead be better suited to discriminate between (or among) accelerations or rasps. It will be necessary to

investigate population coding of these additional communication displays to gain a fuller understanding of how interval-selective neurons in ELp mediate the detection of the full range of behaviorally relevant temporal patterns in communication signals.

REFERENCES

Baker CA, Carlson BA (2014) Short-term depression, temporal summation, and onset inhibition shape interval tuning in midbrain neurons. J Neurosci 34:14272-14287.

Baker CA, Kohashi T, Lyons-Warren AM, Ma X, Carlson BA (2013) Multiplexed temporal coding of electric communication signals in mormyrid fishes. J Exp Biol 216:2365-2379.

Barbour B, Brunel N, Hakim V, Nadal JP (2007) What can we learn from synaptic weight distributions? Trends Neurosci 30:622-629.

Bell CC, Grant K (1989) Corollary discharge inhibition and preservation of temporal information in a sensory nucleus of mormyrid electric fish. J Neurosci 9:1029-1044.

Bennett MVL (1965) Electroreceptors in mormyrids. Cold Spring Harb Sym 30:245-262.

Carlson BA (2002) Electric signaling behavior and the mechanisms of electric organ discharge production in mormyrid fish. J Physiology-Paris 96:405-419.

Carlson BA (2009) Temporal-pattern recognition by single neurons in a sensory pathway devoted to social communication behavior. J Neurosci 29:9417-9428.

Carlson BA, Hopkins CD (2004) Stereotyped temporal patterns in electrical communication. Anim Behav 68:867-878.

Carlson BA, Kawasaki M (2006) Stimulus selectivity is enhanced by voltage-dependent conductances in combination-sensitive neurons. J Neurophysiol 96:3362-3377.

Carlson BA, Hasan SM, Hollmann M, Miller DB, Harmon LJ, Arnegard ME (2011) Brain evolution triggers increased diversification of electric fishes. Science 332:583-586.

Chelaru MI, Dragoi V (2008) Efficient coding in heterogeneous neuronal populations. P Natl Acad Sci USA 105:16344-16349.

Cooley WW, Lohnes PR (1971) Multivariate Data Analysis. New York: John Wiley & Sons.

de Ruyter van Steveninck RR, Laughlin SB (1996) The rate of information transfer at graded-potential synapses. Nature 379:642-645

Dhingra NK, Smith RG (2004) Spike generator limits efficiency of information transfer in a retinal ganglion cell. J Neurosci 24:2914-2922.

Diehl RL, Lindblom B (2004) Explaining the structure of feature and phoneme inventories. In: Speech processing in the auditory system (Greenberg S, Ainsworth W, Popper A, Fay R, eds), pp pp. 101-162. New York: Springer.

Edwards CJ, Alder TB, Rose GJ (2002) Auditory midbrain neurons that count. Nat Neurosci 5:934-936.

Feldman DE (2012) The spike-timing dependence of plasticity. Neuron 75:556-571.

Finger TE, Bell CC, Russell CJ (1981) Electrosensory pathways to the valvula cerebelli in mormyrid fish. Exp Brain Res 42:23-33.

Fortune ES, Rose GJ (1997a) Passive and active membrane properties contribute to the temporal filtering properties of midbrain neurons in vivo. J Neurosci 17:3815-3825.

Fortune ES, Rose GJ (1997b) Temporal filtering properties of ampullary electrosensory neurons in the Torus semicircularis of Eigenmannia: Evolutionary and computational implications. Brain Behav Evolut 49:312-323.

Fortune ES, Rose GJ (2000) Short-term synaptic plasticity contributes to the temporal filtering of electrosensory information. J Neurosci 20:7122-7130.

Fortune ES, Rose GJ (2003) Voltage-gated Na+ channels enhance the temporal filtering properties of electrosensory neurons in the torus. J Neurophysiol 90:924-929.

Friedman MA, Hopkins CD (1996) Tracking individual mormyrid electric fish in the field using electric organ discharge waveforms. Anim Behav 51:391-407.

Friedman MA, Hopkins CD (1998) Neural substrates for species recognition in the time-coding electrosensory pathway of mormyrid electric fish. J Neurosci 18:1171-1185.

George AA, Lyons-Warren AM, Ma X, Carlson BA (2011) A diversity of synaptic filters are created by temporal summation of excitation and inhibition. J Neurosci 31:14721-14734.

Gittelman JX, Li N, Pollak GD (2009) Mechanisms underlying directional selectivity for frequency-modulated sweeps in the inferior colliculus revealed by in vivo whole-cell recordings. J Neurosci 29:13030-13041.

Goel A, Buonomano DV (2014) Timing as an intrinsic property of neural networks: evidence from in vivo and in vitro experiments. Philos T R Soc B 369:20120460.

Graff C, Kramer B (1992) Trained weakly-electric fishes Pollimyrus isidori and Gnathonemus petersii (Mormyridae, Teleostei) discriminate between waveforms of electric pulse discharges. Ethology 90:279-292.

Grothe B (1994) Interaction of excitation and inhibition in processing of pure-tone and amplitude-modulated stimuli in the medial superior olive of the moustached bat. J Neurophysiol 71:706-721.

Haag J, Borst A (1998) Active membrane properties and signal encoding in graded potential neurons. J Neurosci 18:7972-7986.

Hanika S, Kramer B (2005) Intra-male variability of its communication signal in the weakly electric fish, Marcusenius macrolepidotus (South African form), and possible functions. Behaviour 142:145-166.

Haugede-Carre F (1979) Mesencephalic exterolateral posterior nucleus of the mormyrid fish Bryenomyrus niger: efferent connections studied by the HRP method. Brain Res 178:179-184.

Holmstrom LA, Eeuwes LBM, Roberts PD, Portfors CV (2010) Efficient encoding of vocalizations in the auditory midbrain. J Neurosci 30:802-819.

Juusola M, French AS (1997) The efficiency of sensory information coding by mechanoreceptor neurons. Neuron 18:959-968.

Kohashi T, Carlson BA (2014) A fast BK-type KCa current acts as a postsynaptic modulator of temporal selectivity for communication signals. Front Cell Neurosci 8:286.

Kretzberg J, Warzecha AK, Egelhaaf M (2001) Neural coding with graded membrane potential changes and spikes. J Comput Neurosci 11:153-164.

Loftus-Hills JJ, Littlejohn MJ (1971) Pulse repetition rate as basis for mating call discrimination by two sympatric species of Hyla. Copeia:154-156.

Lyons-Warren AM, Kohashi T, Mennerick S, Carlson BA (2013) Retrograde fluorescent labeling allows for targeted extracellular single-unit recording from identified neurons in vivo. J Vis Exp 76:e3921.

Ma XF, Kohashi T, Carlson BA (2013) Extensive excitatory network interactions shape temporal processing of communication signals in a model sensory system. J Neurophysiol 110:456-469.

Machens CK, Schutze H, Franz A, Kolesnikova O, Stemmler MB, Ronacher B, Herz AVM (2003) Single auditory neurons rapidly discriminate conspecific communication signals. Nat Neurosci 6:341-342.

Marsat G, Maler L (2010) Neural heterogeneity and efficient population codes for communication signals. J Neurophysiol 104:2543-2555.

Osborne LC, Palmer SE, Lisberger SG, Bialek W (2008) The neural basis for combinatorial coding in a cortical population response. J Neurosci 28:13522-13531.

Pluta SR, Kawasaki M (2010) Temporal selectivity in midbrain electrosensory neurons identified by modal variation in active sensing. J Neurophysiol 104:498-507.

Pollack G (2000) Who, what, where? Recognition and localization of acoustic signals by insects. Curr Opin Neurobiol 10:763-767.

Priebe NJ, Ferster D (2008) Inhibition, spike threshold, and stimulus selectivity in primary visual cortex. Neuron 57:482-497.

Ronacher B, Wohlgemuth S, Vogel A, Krahe R (2008) Discrimination of acoustic communication signals by grasshoppers (Chorthippus biguttulus): Temporal resolution, temporal integration, and the impact of intrinsic noise. J Comp Psychol 122:252-263.

Rose G, Capranica RR (1983) Temporal selectivity in the central auditory system of the leopard frog. Science 219:1087-1089.

Rose GJ, Fortune ES (1996) New techniques for making whole-cell recordings from CNS neurons in vivo. Neurosci Res 26:89-94.

Rose GJ, Leary CJ, Edwards CJ (2011) Interval-counting neurons in the anuran auditory midbrain: factors underlying diversity of interval tuning. J Comp Physiol A 197:97-108.

Sakai M, Chimoto S, Qin L, Sato Y (2009) Neural mechanisms of interstimulus interval-dependent responses in the primary auditory cortex of awake cats. BMC Neurosci 10.

Schneider DM, Woolley SMN (2010) Discrimination of communication vocalizations by single neurons and groups of neurons in the auditory midbrain. J Neurophysiol 103:3248-3265.

Serrier J, Moller P (1989) Patterns of electric organ discharge activity in the weakly electric fish Brienomyrus niger L. (Mormyridae). J Exp Biol 48:235-244.

Shamir M, Sompolinsky H (2006) Implications of neuronal diversity on population coding. Neural Comput 18:1951-1986.

Tripathy SJ, Padmanabhan K, Gerkin RC, Urban NN (2013) Intermediate intrinsic diversity enhances neural population coding. P Natl Acad Sci USA 110:8248-8253.

Trussell LO (1999) Synaptic mechanisms for coding timing in auditory neurons. Annu Rev Physiol 61:477-496.

Wang L, Narayan R, Grana G, Shamir M, Sen K (2007) Cortical discrimination of complex natural stimuli: Can single neurons match behavior? J Neurosci 27:582-589.

Wong RY, Hopkins CD (2007) Electrical and behavioral courtship displays in the mormyrid fish Brienomyrus brachyistius. J Exp Biol 210:2244-2252.

Xu-Friedman MA, Hopkins CD (1999) Central mechanisms of temporal analysis in the knollenorgan pathway of mormyrid electric fish. J Exp Biol 202:1311-1318.

Chapter 4

Oscillatory phase reset: a novel mechanism for peripheral sensory coding

This chapter contains a version of a manuscript currently under review:

Baker C.A., Huck K.R., and Carlson B.A. Peripheral sensory coding through oscillatory phase reset in weakly electric fish. (under review at *eLIFE*)

Author contributions for the above submission:

C.A.B. and B.A.C. designed research; C.A.B., K.R.H., and B.A.C. performed research; C.A.B. and K.R.H. analyzed data; C.A.B. and B.A.C. wrote the manuscript.

ABSTRACT

Here we address how evolutionary divergence in sensory perception relates to differences in the physiological coding of sensory stimuli. Evolutionary changes in the electrosensory systems of mormyrid fishes enabled some species to detect subtle variations in electric communication signals. Species sensitive to waveform variation have peripheral sensory receptors that respond to an electric pulse with a single, time-locked spike. These receptors encode signal waveform into spikes at signal onset in some receptors, and spikes at signal offset in other receptors. This coding scheme preserves the precise timing cues necessary for waveform discrimination. In contrast, the receptors of species insensitive to waveform variation produce spontaneous potentials that continuously oscillate at frequencies of 1-3 kHz. However, it was previously unknown how these oscillatory receptors encode electric communication signals. Using extracellular recordings, we found that oscillating receptors responded to an electric pulse by resetting the phase of their oscillations. These phase resets did not preserve the precise timing information necessary for signal waveform discrimination, but they did encode the information necessary for detecting and locating signal sources. In addition, we found that a species that independently evolved waveform sensitivity also evolved spiking receptors. Thus, different perceptual capabilities correspond to different mechanisms for the peripheral encoding of stimuli. Futhermore, whereas spiking receptors were most sensitive to stimulus frequencies matching the power spectra of signals produced by conspecific individuals, oscillating receptors were most sensitive to frequencies that were only found in the collective signals of large groups of individuals. During behavioral playback experiments, a species with oscillating receptors responded more strongly to group communication signals than did a species in the same genus with spiking receptors. High-frequency receptor oscillations may therefore be an adaptation for

detecting group communication signals. Our findings provide the first evidence for peripheral sensory coding through an oscillatory phase-reset mechanism.

INTRODUCTION

Evolutionary change in sensory systems can have profound effects on sensory perception and behavior (Carlson and Arnegard, 2011; Carlson, 2012; Baldwin et al., 2014). Recently, we documented a striking example of evolutionary change in the electrosensory systems of weakly electric fish (Carlson et al., 2011). Modifications in the anatomy of sensory receptors and the associated brain pathway that processes electric communication signals resulted in a newfound ability to detect subtle variations in these signals. This perceptual expansion led to a dramatic increase in the rates of signal evolution and species diversification. However, how these anatomical and perceptual differences relate to physiological differences in the underlying information processing mechanisms was unknown. Here we investigate how evolutionary change in sensory perception relates to differences in peripheral sensory coding mechanisms.

Mormyrid fish communicate by producing a stereotyped, species-specific electric organ discharge (EOD) at variable interpulse intervals (see Carlson, 2002 for review). Some species can detect subtle variation in EOD waveforms, whereas others cannot (Carlson et al., 2011). Mormyrids have peripheral sensory receptors in their skin, called knollenorgans, that detect electric signals. In species sensitive to EOD waveform variation, these receptors are broadly distributed across the fish's head, back, and underbelly (Carlson et al., 2011). These receptors fire a single, time-locked spike in response to an electric pulse in all species that have been studied (Bennett, 1965; Harder, 1968; Hopkins and Bass, 1981; Lyons-Warren et al., 2012). Spiking receptors encode electric pulse duration into spike-timing differences, with some receptors responding to pulse onset and others to pulse offset (Hopkins and Bass, 1981). These timing differences are then compared in the midbrain (Friedman and Hopkins, 1998; Lyons-Warren et al., 2013).

The frequency sensitivity of spiking receptors tends to match peak frequencies in the power spectra of conspecific EODs (Hopkins, 1981; Bass and Hopkins, 1984; Lyons-Warren et al., 2012). Peripheral sensory receptors whose maximal sensitivity corresponds to a principal feature present in the signal they detect are considered "matched filters" (Wehner, 1987). Spiking receptors thus appear to be matched filters for conspecific EODs. Theoretically, matched filters in the periphery should reduce signal-processing demands on the central nervous system.

In contrast, species insensitive to EOD waveform variation have receptors that produce spontaneously oscillating potentials at frequencies of 1-3 kHz (Harder, 1968). These receptors are clustered into three groups, called rosettes, on each side of the head (Harder, 1968; Lavoue et al., 2004; Lavoue et al., 2010; Carlson et al., 2011). It is not known how oscillatory receptors encode electric communication signals.

Oscillations (~0.5-600 Hz) in neural activity are widespread throughout the brains of many animals, including humans, and have been hypothesized to play a role in sleep, attention, memory, motor output, and sensory coding (Buzsaki and Draguhn, 2004; Thut et al., 2012; Canavier, 2015). Oscillations could facilitate multiplexed signal coding, in which spikes carry information depending on the phase of the oscillation during which they occur (Thut et al., 2012). Another effect of oscillations could be to enhance communication between neural populations during periods of synchronized excitability (Thut et al., 2012). Additional hypothesized functions include signal gating, feature binding, and cross-modal integration (Thut et al., 2012), although a clear functional role for electrical oscillations has remained elusive (Canavier, 2015).

To gain insight into the neural basis of differences in perceptual abilities among species, here we investigate for the first time how oscillating receptors encode electric stimuli. Using

extracellular recordings, we compare spiking and oscillating receptor responses to electric pulses. Our findings reveal a novel phase-reset mechanism for signal detection in oscillating receptors. This is the first demonstration of information coding by oscillatory phase resets at the periphery. These phase resets did not encode pulse waveform, explaining why species with oscillating receptors cannot behaviorally discriminate EOD waveform variation. Furthermore, we provide physiological and behavioral evidence that oscillating receptors respond most strongly to communication signals with fast temporal patterns that can only be produced by large groups of conspecifics, suggesting that oscillating receptors may be specialized for group signal detection.

MATERIALS AND METHODS

Animals. Fifteen *Brevimyrus niger* (standard length [SL] = 5.9-8.6 cm), seventeen *Pollimyrus adspersus* (SL = 6.2-8.6 cm), twenty *Petrocephalus microphthalmus* (SL = 6.3-8.0 cm), twenty *Petrocephalus tenuicauda* (SL = 5.5-9.0 cm), and five *Petrocephalus soudanensis* (SL = 8.0-10.0 cm) contributed data to this study. We used fish of both sexes. All fish were acquired through the aquarium trade except for *P. microphthalmus,* which were obtained from Lac Zilé, Gabon. EODs and receptor frequency tuning data from *Brienomyrus brachyistius* came from a previously published study (Lyons-Warren et al., 2012). In the lab, we housed fish in conspecific-only group tanks with 12h:12h light:dark cycle, water conductivity of 200-400 μS/cm, and temperature of 25-29°. We fed the fish live black worms four times per week. Species of the genus *Petrocephalus* are extremely difficult to obtain. Therefore, to minimize the number of fish used in our physiological recordings, we collected just enough data to detect a robust pattern, which in some cases happened at a low sample size (e.g. n=3 in Fig. 5, 6). All procedures were in accordance with the guidelines established by the National Institutes of Health and were approved by the Institutional Animal Care and Use Committee at Washington University in St. Louis.

Receptor recordings. Extracellular recordings from single receptors were obtained using previously reported methods (Bennett, 1965; Hopkins and Bass, 1981; Lyons-Warren et al., 2012). Briefly, we anesthetized fish in 300 mg/L tricaine methanesulfonate (MS-222, Sigma-Aldrich, St. Louis, MO) and then paralyzed and electrically silenced fish with 20-80 μL of 0.1 mg/mL gallamine triethiodide (Flaxedil, Sigma-Aldrich). We then placed the fish in a 20 x 12.5 x 45 cm chamber filled with freshwater and positioned the fish on a plastic platform with lateral supports. We respirated the fish with freshwater through a pipette tip in the fish's mouth while

monitoring the fish's electromotor output using a pair of electrodes placed next to the fish's tail (Carlson, 2002). Flaxedil silences the EOD, but external electrodes can be used to record fictive EOD motor commands from spinal electromotor neurons. After the fish had completely recovered from anesthesia, as indicated by the return of fictive EODs, we began the recording session. After receptor recordings, fish were allowed to recover completely from paralysis before being returned to their home tank.

We used electrodes made from borosilicate capillary glass (o.d. = 1 mm, i.d. = 0.5 mm; A-M Systems, Everett, WA, USA). We bent the last ~1 cm of the electrode to a 30 degree angle and polished the tip using the flame from a Bunsen burner. We filled the electrode with tank water and placed it in an electrode holder with a Ag-AgCl wire connected to the headstage of the amplifier. We placed the electrode next to, but not quite touching, individual receptors. The fish remained completely under water for the entire recording session. Extracellular activity was referenced to ground, amplified 10 times (Neuroprobe Model 1600, A-M Systems), digitized at a rate of 97.7 kHz (RP2.1, Tucker-Davis Technologies, Alachua, FL, USA), and saved using custom software in Matlab 7.0 (MathWorks, Natick, MA, USA). Spiking responses and some oscillating responses were also low-pass filtered (cut-off frequency = 100 kHz) during recording.

We obtained simultaneous recordings from pairs of oscillating receptors using the same glass electrodes as single-receptor recordings. Extracellular activity was referenced to ground, amplified 100 times, band-pass filtered (0.3 – 20 kHz) (Model 1800, A-M Systems), digitized at a rate of 97.7 kHz (RP2.1, Tucker-Davis Technologies), and saved in Matlab. We selected one spontaneously oscillating receptor in each rosette, for a total of 14 possible pairs across six rosettes. In one *P. tenuicauda*, we collected five one-second simultaneous recordings of spontaneous activity in 13 pairs of rosettes. We were unable to see the left and right

nackenrosettes at the same time under our microscope in this fish, so we could not obtain simultaneous recordings from this pair of rosettes. In another *P. tenuicauda*, we obtained simultaneous recordings from six pairs of rosettes.

For differential recordings, we used a differential electrode consisting of a pair of Ag-AgCl wires separated by 5 mm. Each wire had a diameter of 0.635 mm and uninsulated tip length of 2 mm. We oriented the electrode pair perpendicular to the skin, with the recording electrode next to the skin and reference electrode farther away. Electrical activity was amplified 100 times and band-pass filtered (0.3-5 kHz) (Model 1800, A-M Systems), digitized at a rate of 97.7 kHz (RP2.1, Tucker-Davis Technologies), and saved using custom software in Matlab 7.0.

Stimulus delivery. All stimuli were generated in Matlab, digital-to-analog converted at a rate of 195.31 kHz (RP2.1, Tucker-Davis Technologies), and attenuated (PA5, Tucker-Davis Technologies) before delivery to the current input of the amplifier (Neuroprobe Model 1600, A-M Systems). The amplifier then delivered constant-current stimuli through the monopolar recording electrode referenced to ground (Lyons-Warren et al., 2012). We used a bridge balance to minimize the stimulus artifact.

To study how receptors encode electric pulse waveform, we recorded responses to 10 or 25 repetitions of monopolar square pulses of durations ranging from 0.01 to 5 ms. We used both positive and negative polarities at an intensity within the behaviorally relevant range that reliably elicited responses from each receptor (10-18 nA in *P. adspersus*, 18 nA in *B. niger*, 32 nA in *P. microphthalmus*, and 45-100 nA in *P. tenuicauda*).

We also delivered previously recorded conspecific EOD waveforms. For each receptor, we randomly selected an EOD stimulus from a library of 10 conspecific EOD waveforms. We

presented 10 repetitions of both normal (head-positive) and reversed polarity waveforms at intensities ranging from 6-312 nA.

To measure frequency tuning in spiking receptors, we presented 15 repetitions of 90-ms duration sinusoidal stimuli of frequencies ranging from 0.1-50 kHz with 5 ms cosine-squared on- and off-ramps. Because we could not separate a continuously oscillating response from a continuously oscillating stimulus artifact, we had to use different stimuli to measure frequency tuning in oscillating receptors. We presented 10 repetitions of single-cycle bipolar sine wave stimuli of frequencies ranging from 0.2-84 kHz to measure frequency tuning of oscillating receptors. We also delivered single-cycle bipolar sine wave stimuli at durations equal to multiples (¼, ½, 1, 2, 4) of each receptor's spontaneous oscillation period. We used both positive (peak leading trough) and negative (trough leading peak) polarities at three stimulus intensities (10, 32, and 100 nA) in *P. tenuicauda*. In *P. soudanensis* we used positive and negative polarity stimuli at 32 nA.

To study how spiking and oscillating receptors encode interpulse intervals (IPIs) in communication signals, we presented 10 repetitions of a pair of monopolar square pulses, with each pulse 0.2 ms in duration. We used IPIs ranging from 0.3 to 13 ms. For oscillatory receptors, we also used IPIs equal to multiples (¼, ½, 1, 2, 4, 8) of each oscillating receptor's intrinsic oscillation period. We used both positive and negative polarities at an intensity that reliably elicited responses in each receptor (6-10 nA in *P. adspersus*, 7-10 nA in *B. niger*, 18 nA in *P. microphthalmus*, and 10-100 nA in *P. tenuicauda*).

Data analysis. To quantify the responses of spiking receptors, we detected spikes by finding the peak voltage that crossed a manually set threshold specific to each receptor. We measured interspike intervals as the difference in time between consecutive spikes. To measure

the responses of oscillating receptors, we first median filtered the recordings using a filter width of 0.1 ms. Next we detected the first seven oscillatory peaks after stimulus offset on each stimulus sweep, which allowed us to measure the first six post-stimulus oscillation periods. Imperfections in artifact balancing had no impact on the detection and measurement of spiking responses. However, sometimes it was unclear whether the first post-stimulus oscillatory peak was contaminated by artifact. To assess whether the stimulus artifact affected the first post-stimulus oscillation peak, we compared the first post-stimulus period to the average of the following five post-stimulus periods. If the first period was less than 85% or more than 115% of the average of the next five periods, we concluded that the artifact interfered with the first post-stimulus peak and instead used the second post-stimulus peak for all measurements.

The time between the first and second post-stimulus peaks represented the post-stimulus oscillation period. We measured the oscillation amplitude by first averaging the voltage values of the first two post-stimulus oscillatory peaks, and then subtracting the voltage value at the intervening oscillatory trough. Next we calculated the angle (φ, in radians) of the oscillatory phase reset as

$$\varphi = \frac{lat}{p}, \tag{4.1}$$

where *lat* is the latency of the first post-stimulus peak (time of peak minus time of stimulus offset) and *p* is the first post-stimulus period. We then used these values across repetitions to calculate the vector strength (*r*), a measure of phase-locking, according to

$$r = \sqrt{\left(\frac{\sum \cos(\varphi)}{n}\right)^2 + \left(\frac{\sum \sin(\varphi)}{n}\right)^2}, \tag{4.2}$$

where *n* is the number of stimulus repetitions. The vector strength is a normalized measure of phase-locking that equals 1 when the constituent angles are perfectly in phase with one another, and 0 when the constituent angles are completely random relative to one another.

We recorded spontaneous activity of each receptor five times for one second each. For a given spiking receptor, we measured the interspike intervals on each repetition and then averaged across recordings. For oscillating receptors, we averaged the fast Fourier transform (FFT) of the oscillatory activity across five repetitions, and then used the peak of the averaged FFT as the receptor's spontaneous oscillation frequency. We used the inverse of the spontaneous oscillation frequency as the spontaneous oscillation period. We measured the spontaneous oscillation amplitude of each receptor by subtracting the voltage at each oscillatory trough from the voltage of the preceding oscillatory peak, and then averaging these amplitude values across the spontaneous recordings. If spontaneous activity was recorded more than once from the same receptor, we averaged measurements across all recordings.

We measured frequency tuning in spiking receptors following previously described methods (Lyons-Warren et al., 2012). We defined a response as at least one more spike/sweep during the 90 ms stimulus period than during the 90 ms prestimulus period. We determined a receptor's threshold by finding the lowest intensity at which the receptor responded to a given frequency. The frequency with the lowest threshold was defined as the receptor's best frequency. We generated normalized tuning curves by setting threshold intensities as dB relative to the threshold intensity at the best frequency. For oscillating receptors, we generated tuning curves by plotting vector strength versus stimulus frequency. We defined the best frequency as the frequency with the highest vector strength. In three of eight oscillating receptors, the best frequencies in response to positive and negative polarity stimuli differed slightly. In these cases,

we determined the receptor's best frequency by averaging the best frequencies to each stimulus polarity.

To study how spiking receptors encode electric pulse waveform, we averaged the time of the first spike that occurred after stimulus onset (positive polarity stimuli) or stimulus offset (negative polarity stimuli). The difference in average spike times elicited by the two polarity stimuli was defined as the spike-timing difference. Since receptors on opposite sides of the body experience stimuli of opposite polarities, this procedure is equivalent to measuring the difference in spike times between receptors on opposite sides of the body evoked by the same stimulus (Hopkins, 1981). For a comparable measurement in oscillatory responses, we subtracted the average time of the first peak that occurred after the offset of the negative polarity pulse from the average time of the first peak that occurred after the onset of the positive polarity pulse for pulse durations longer than 0.5 ms. For shorter stimulus durations ($\leq$0.5 ms), we measured the difference in the times of the first oscillatory peaks that occurred after stimulus offset for each stimulus polarity. This procedure is equivalent to measuring the difference in oscillatory peak times between receptors on opposite sides of the body evoked by the same stimulus. To quantify the degree of oscillation amplitude enhancement, we first measured all prestimulus oscillation amplitudes on each recording trace, and then averaged across all repetitions of the same stimulus. Next we measured the poststimulus oscillation amplitude on each recording trace and averaged across all repetitions of the same stimulus. Lastly, we divided the mean poststimulus oscillation amplitude by the mean prestimulus oscillation amplitude for each pulse duration.

Since the peak power frequency of a single-cycle bipolar sine wave is slightly lower than the inverse of the wave's duration, we used Welch's power spectral density in Matlab to compute

the power spectrum of each single-cycle sine wave. We took the peak of the power spectrum as the frequency of each stimulus.

We measured the difference in the phases of oscillatory resets evoked by opposite polarity stimuli by first averaging the recorded potential across stimulus repetitions, and then measuring the first post-stimulus period and the latency of the first post-stimulus peak. We used these values to calculate the difference in the phase ($\Delta\varphi$) of oscillatory reset between responses to opposite polarity pulses according to

$$\Delta\varphi = \frac{lat_N - lat_P}{\left(\frac{p_N + p_P}{2}\right)} \times 360° \tag{4.3}$$

where lat_N is the latency of the first peak, and p_N is the first period, respectively, evoked by the negative polarity stimulus, and lat_P is the latency of the first peak, and p_P is the first period, respectively, evoked by the positive polarity stimulus.

To measure spiking responses to paired pulses, we measured the interspike intervals between the spikes elicited by the onset (positive polarity stimuli) or offset (negative polarity stimuli) of each pulse. If no spikes occurred in response to the second pulse, no interspike intervals were recorded. For clarity, stimulus artifacts were removed from the recording traces shown in Figs. 5A and B by drawing a straight line from the times of stimulus onset or offset plus 0.03 ms. In oscillating receptors, the stimulus artfact at the shortest IPIs tested obscured responses to the first pulse in the pair. To circumvent this issue, we first averaged oscillatory responses across stimulus presentations. Next we measured the time interval between the first oscillatory peak that followed a single pulse and the first oscillatory peak that followed the second pulse in the pair. This method is equivalent to measuring the time interval between the first peaks following each pulse in the pair. We also measured the vector strength and

poststimulus oscillation amplitude following the second pulse in the pair. We normalized mean poststimulus oscillation amplitudes by dividing by the mean poststimulus oscillation amplitude following a single pulse of 0.2 ms with the same polarity.

EOD recording and analysis. EODs were amplified 20-100 times, band-pass filtered (1 Hz – 50 kHz) (BMA-200, CWE Inc., Ardmore, PA, USA), digitized at a rate of 195 kHz (RP2.1, Tucker Davis Technologies), and saved using custom software in Matlab 7.0. We measured total EOD durations using previously defined criteria (Carlson et al., 2000). EOD power spectra were computed using Welch's power spectral density estimate in Matlab.

IPI recordings. To measure the IPIs generated by single fish and groups of fish, we recorded 20 minutes of electrical activity from a species with spiking receptors (*P. microphthalmus*) and a congeneric species with oscillating receptors (*P. tenuicauda*). For single-fish recordings, fish were removed from their home tank and placed into a 15 x 17 x 31 cm plastic chamber with a single recording electrode in which the positive and negative terminals were separated by 20 cm. Fish were allowed to acclimate for at least 10 minutes before the recordings. For group recordings, we placed four vertically oriented electrodes suspended with the reference terminal up (16.5 cm from the top of the tank) in the home tank (61 x 76 x 61 cm) of each species. Each electrode was located one-third of the distance between tank walls (i.e., at the vertices of nine equally sized rectangles). We placed the electrodes in the tank and allowed fish to acclimate to them overnight before starting the recordings. We amplified electrical activity 100 times before band-pass filtering (0.1 Hz – 20 kHz) (Model 1700, A-M Systems) and digitizing at 97.7 kHz (RX8, Tucker-Davis Technologies). We detected EODs as points where the rectified recorded potential exceeded a threshold of 0.6 mV. Data were saved using custom Matlab software. For the histograms shown in Fig. 7B, C, E and F, we used the recording from

just one of the four electrodes. Single-fish and group tank recordings took place between 1700 and 1900.

Behavioral playback experiments. To test whether species with different receptor physiologies exhibited different behavioral responses to IPIs, we recorded fish's EOD output in response to a train of 10 conspecific EODs at a constant IPI (0.3-100 ms) using previously described methods (Carlson et al., 2011). Briefly, we removed one fish from its group tank and placed it into a 10 gallon tank with a cylindrical plastic chamber (5 cm diameter x 13.2 cm) in the middle of the tank. If the fish was not inside the chamber at the end of a 30-minute acclimation period, we guided the fish into the chamber with nets. Netted caps were then placed over each end of the chamber to keep the fish inside during the experiment. Fish were then allowed an additional five-minute acclimation period before starting the experiment. A pair of electrodes oriented horizontally along the inside walls of the chamber delivered the stimulus, and a pair of electrodes oriented vertically at either end of the chamber recorded the fish's EOD output. For each fish, we randomly selected a conspecific EOD waveform stimulus from a library. To generate the IPI train stimuli, we first defined the start and end of the EOD as the first and last points, respectively, where the absolute value of the waveform exceeded 0.5% of the maximum peak-to-peak amplitude. We then concatenated 10 identical EODs together, adding zero padding as necessary in between EODs to achieve the desired IPIs. If the duration of the EOD was longer than the IPI, we truncated the EOD at the IPI. We presented only normal (head-positive) polarity stimuli. All stimuli were generated in Matlab, digital-to-analog converted at a rate of 195.31 kHz (RX8, Tucker-Davis Technologies), and attenuated (PA5, Tucker-Davis Technologies) before delivery to the analog stimulus isolator (Model 2200, A-M Systems).

To record fish's EOD output, we amplified electrical activity 100 times before band-pass filtering (0.1 Hz – 20 kHz) (Model 1700, A-M Systems) and digitizing at 97.7 kHz (RX8, Tucker-Davis Technologies). We collected a fish's responses to 20 repetitions of each IPI train and to a single EOD stimulus, with one minute between trials to reduce habituation. We randomized stimulus order. To quantify responses, we recorded the time of each EOD produced by the fish, and then computed the spike-density function (SDF) by convolving each EOD time with a Gaussian of 200 ms width (Carlson and Hopkins, 2004). We then averaged the SDF across stimulus repetitions. Next we measured the fish's baseline response by averaging the resulting EOD rate over a window starting 200 ms after the start of the 5 sec prestimulus period and ending 200 ms before stimulus onset. Because mormyrids can respond to electric stimuli with increases or decreases in their EOD rate (Moller et al., 1989; Post and von der Emde, 1999; Carlson et al., 2011), we measured the maximum and minimum of the SDF that occurred between stimulus onset and one second following stimulus offset. We subtracted the baseline discharge rate from these two values to get the maximum increase in EOD rate and the maximum decrease in EOD rate in response to the stimulus.

Statistics. We used circular statistics to measure mean angles $\pm$ S.E.M. of phase modulations of oscillatory receptor responses (Batschelet, 1981). We used the parametric second-order Hotelling test for paired circular data to compare oscillatory phase modulations elicited by normal and reversed polarity EODs (Zar, 1999). We used repeated-measures ANOVA in Statistica 6.1 (StatSoft, Tulsa, OK, USA) to compare behavioral responses to IPI stimuli across two species. We used Spearman's rank test in Statistica 6.1 to compare spontaneous oscillation amplitudes and frequencies, as well as spontaneous and stimulus-evoked oscillation amplitudes in response to square pulses in oscillatory receptors.

RESULTS

Spontaneous receptor activity

We obtained extracellular recordings of spontaneous activity from the sensory receptors of five species of mormyrids (Fig. 1). This sample included three species with broadly distributed receptors, including *Petrocephalus microphthalmus*, whose receptor physiology was previously unknown. *P. microphthalmus* is behaviorally sensitive to EOD waveform variation, but it appears to have evolved this ability independently of other species with broadly distributed receptors (Carlson et al., 2011). Our extracellular recordings revealed that the receptors of *P. microphthalmus* indeed fire spikes (Fig. 1A), just like other mormyrids with broadly distributed receptors and EOD waveform sensitivity. Across three species, spiking receptors had median spontaneous interspike intervals ranging from 0.7 to 195 ms (Fig. 1B).

We recorded spontaneous oscillations from rosette receptors of two species (Fig. 1C, D). In *Petrocephalus tenuicauda*, the amplitude of oscillatory activity varied from 0.04-6.1 mV. We only measured the frequency of spontaneous activity if the oscillation amplitude was at least 2.5 times baseline noise ($\geq$ 0.1 mV). Forty-nine of 69 (71%) receptors in *P. tenuicauda* met these criteria (see example in Fig. 1C). These receptors had a median oscillation frequency of 1.7 kHz.

We recorded spontaneous activity from three rosette receptors in *Petrocephalus soudanensis*. These receptors had spontaneous oscillation amplitudes of 0.09, 0.4, and 1.9 mV, and frequencies of 2.1, 2.6, and 2.5 kHz, respectively. Thus, receptors of *P. soudanensis* tended to have shorter spontaneous oscillation periods than those of *P. tenuicauda* (Fig. 1D).

Oscillating receptors are organized into three rosette clusters on each side of the head (Harder, 1968; Lavoue et al., 2004; Lavoue et al., 2010; Carlson et al., 2011). The augenrosette is found near the eye, the nackenrosette dorsal to the gill cover, and the kehlrosette ventral to the

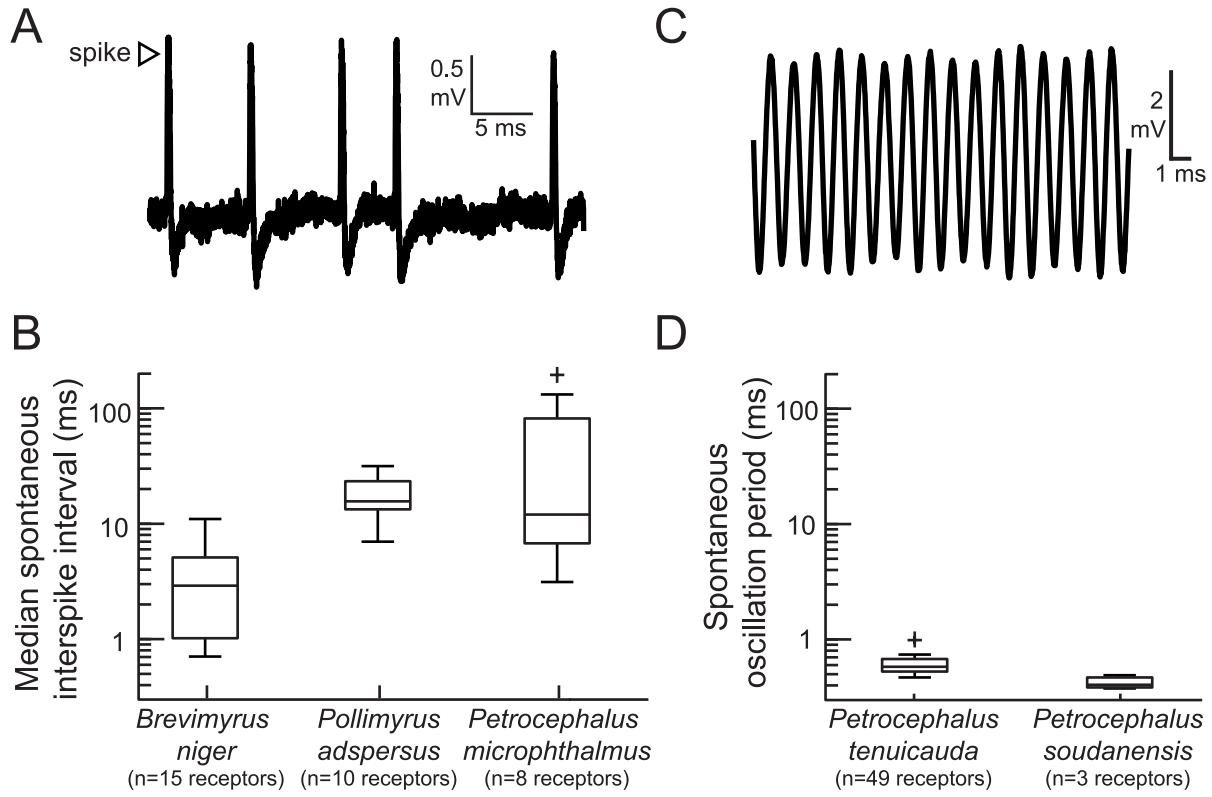

Figure 1. The peripheral sensory receptors of some mormyrid species fire spikes, whereas the receptors of other species produce spontaneously oscillating potentials. (A) An extracellular recording of spontaneous spikes from a receptor of *Petrocephalus microphthalmus*. (B) Box plots of spontaneous interspike intervals in the receptors of three species. (C) An extracellular recording of spontaneously oscillating receptor potentials in *Petrocephalus tenuicauda*. (D) Box plots of spontaneous oscillation periods in the receptors of two species.

gill cover (Fig. 2A). In one *P. tenuicauda*, we obtained spontaneous recordings from every receptor of the right augenrosette (Fig. 2B). Spontaneous oscillation amplitudes ranged from 0.04-5.2 mV. Spontaneous oscillation amplitude was largest in the center of the rosette, and progressively decreased towards the periphery. Spontaneous oscillation frequencies ranged from 1.0-2.1 kHz. Oscillation frequency and amplitude were not significantly correlated (Spearman R=0.27, $t_{(22)}$=1.3, p=0.21), although frequencies tended to be highest near the center of the rosette (Fig. 2B).

Spontaneous oscillations of different receptors are not synchronized

To determine whether the oscillations of receptors in different rosettes were synchronized with one another, we collected simultaneous recordings from pairs of receptors in two *P. tenuicauda*. In one fish, we recorded from 13 pairs of receptors, each located in a different rosette (see Fig. 2C). To assess the degree of synchrony between receptors, we computed the cross-correlation, which measures the correlation between two waveforms as a function of the relative delay between them. In general, oscillatory activity was not synchronized across receptors (see example in Fig. 2D). Across all 13 pairs, maximum cross-correlation coefficients ranged from 0.02-0.8. The plot of cross-correlation coefficient vs. time lag has peaks at the relative delays at which the two recordings are in phase with one another, and troughs at the relative delays at which the two recordings are perfectly out of phase with one another (Fig. 2D). These peaks and troughs are regularly spaced, creating a continuous beat pattern. These beats are present in the plot because the frequencies of the two constituent signals are different, and their phases are not synchronized, leading to a rhythmic pattern of constructive and destructive interference. This is the behavior expected for two independent oscillators, and it was observed

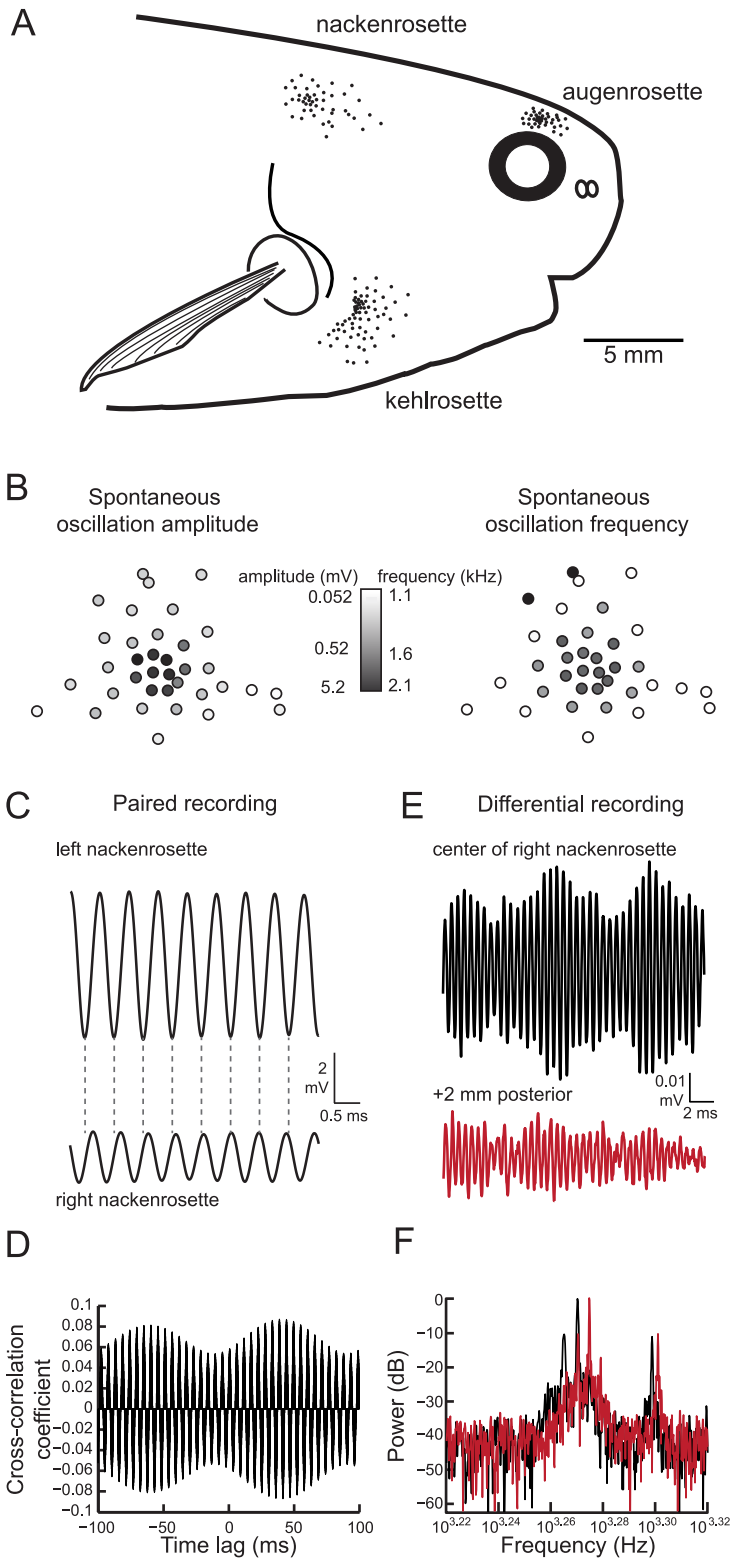

Figure 2. Oscillatory activity is not synchronized across receptors. (A) Receptor locations on the right side of one *P. tenuicauda* are illustrated as black dots (receptor size not to scale). (B) An approximate map of all 32 receptors in the right augenrosette of one *P. tenuicauda*. This map comes from a different fish

than shown in (A). (C) Simultaneous extracellular recordings from a receptor in the left nackenrosette and a receptor in the right nackenrosette of one *P. tenuicauda*. Vertical dashed lines indicate the times of troughs in the top recording trace for comparison with the bottom recording trace. (D) The cross-correlation coefficient vs. time lag for the paired recording in (C), for time lags between -100 and 100 ms. (E) Differential extracellular recordings from a position centered over the right nackenrosette (black) and a position 2 mm posterior (red) in one *P. tenuicauda*. The recording and reference terminals of the electrode were separated by 5 mm. (F) Power spectra for the differential recordings shown in (E). Only the frequency range where peaks occurred is shown (~1.7-2.1 kHz).

in every pair-wise recording. In another *P. tenuicauda*, we recorded from six pairs of receptors and found similar results, with maximum cross-correlation coefficients ranging from 0.05-0.2.

To determine whether the oscillations of individual receptors within rosettes were synchronized, we recorded spontaneous activity with a differential electrode pair centered over a single rosette. The differential electrode allowed us to record local field potentials resulting from multiple receptors. Beats were present in these recordings (see example in Fig. 2E), indicating that our electrode was in fact recording activity from multiple sources with different frequencies. Indeed, at least three distinct peaks were present in the power spectrum of this recording (black trace in Fig. 2F). Recording activity at a position 2 mm posterior to this location led to the loss of two of these peaks and the addition of two new peaks in the power spectrum, suggesting that the electrode was recording activity from a distinct, but overlapping population of receptors compared to the previous location (red traces in Fig. 2E and F). Qualitatively similar results were seen in differential recordings from additional rosettes. Therefore, in agreement with a previous report (Harder, 1968), the oscillatory activity of individual receptors is not correlated within or across rosettes.

Electric pulses elicit time-locked spikes in spiking receptors, and phase resets in oscillating receptors

To understand how receptors encode electric stimuli, we recorded receptor responses to monopolar square pulse stimuli (Fig. 3). We delivered both positive and negative polarity pulses to mimic the stimulation that receptors on opposite sides of the body would naturally experience in response to the same stimulus (Hopkins and Bass, 1981). As shown previously, spiking receptors responded with a single time-locked spike in response to inward current transients (Bennett, 1965), which occur at the onset of a positive polarity pulse and at the offset of a negative polarity pulse (Fig. 3A, B). The probablility that a spiking receptor would respond depended on pulse duration, with pulses longer than ~0.02 ms reliably eliciting a spike (Fig. 3C). Spike probability was high for pulse durations within the range of total durations of conspecific EODs (horizontal bars in Fig. 3C).

Oscillating receptors responded to monopolar square electric pulses with phase resets and amplitude increases (Fig. 3E, F). The degree of amplitude enhancement relative to prestimulus amplitudes depended on pulse duration (Fig. 3G). Phase resets and amplitude increases occurred both in receptors with high-amplitude spontaneous oscillatory activity as well as in receptors with little to no spontaneous oscillations. At the stimulus duration that elicited the maximum oscillation amplitude in each receptor, there was a positive correlation between spontaneous and stimulus-evoked oscillation amplitudes (Spearman R=0.90, $t_{(3)}$=3.6, p=0.037).

Spiking receptors encode pulse duration, whereas oscillating receptors do not

Spiking receptors encoded square pulse duration into differences in spike times between receptors. For instance, the differences in spike times elicited by each polarity of a square pulse

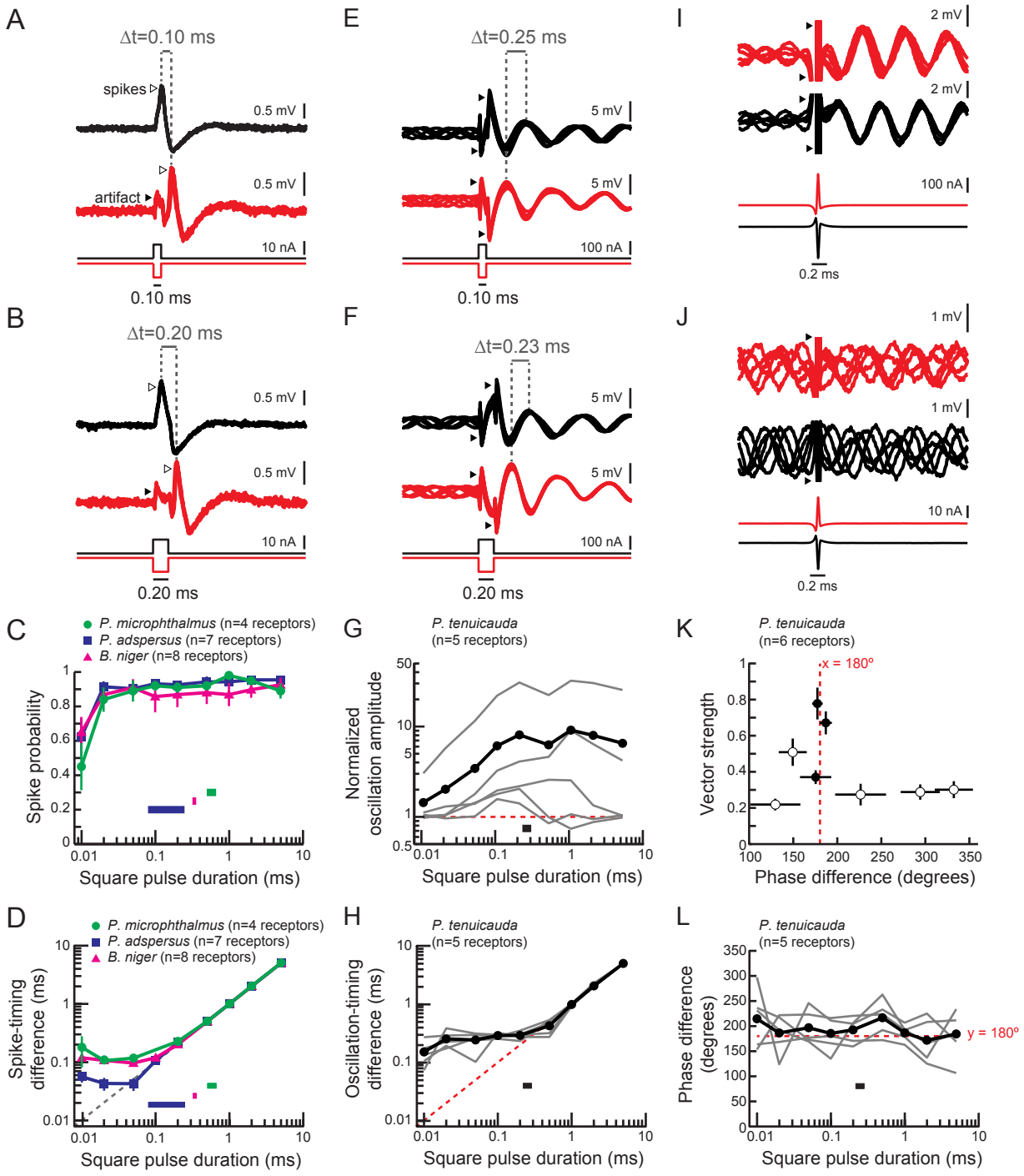

Figure 3. Spiking receptors encode pulse duration, whereas oscillating receptors do not. (A) Extracellular recordings from a spiking receptor in *B. niger* to positive polarity (black) and negative polarity (red) monopolar square pulses of 0.10 ms duration. A single time-locked spike occurs at the onset of a positive polarity pulse, and at the the offset of a negative polarity pulse. Spikes are indicated by open arrowheads and the stimulus artifact is indicated by closed arrowheads. Traces from five stimulus repetitions are superimposed. The difference in the times (Δt) of spikes to positive and negative polarity stimuli is 0.10 ms. (B) Responses of the same receptor as shown in (A) for a monopolar square pulse of 0.20 ms

duration. The spike-timing difference (Δt) is 0.20 ms. (C) Spike probability vs. square pulse duration for responses to positive polarity stimuli for spiking receptors of three species. Horizontal bars indicate the behaviorally relevant ranges of total durations measured in 10 conspecific electric organ discharge (EOD) waveforms. (D) Spike-timing differences between responses to positive and negative polarity stimuli vs. square pulse duration for the same receptors in (C). (E) Responses of an oscillating receptor in *P. tenuicauda* to positive (black) and negative (red) polarity monopolar square pulses of 0.10 ms duration. The difference in the time of oscillatory peaks (Δt) elicited by opposite polarity stimuli is 0.25 ms. (F) Responses of the same receptor as shown in (E) for a monopolar square pulse of 0.20 ms duration. The oscillation timing difference (Δt) is 0.23 ms. (G) Evoked oscillation amplitudes normalized to prestimulus oscillation amplitudes vs. square pulse duration for oscillating receptors. Curves for each receptor are shown in grey, and the averages across receptors are shown in black. The horizontal bar indicates the range of total durations of 10 conspecific EODs. (H) Oscillation-timing differences between responses to positive and negative polarity stimuli vs. square pulse duration for the same receptors shown in (G). (I) Extracellular recordings from an oscillating receptor in *P. tenuicauda* in response to a head-positive ("normal polarity") conspecific EOD waveform (black) and the reversed polarity waveform (red). Stimulus intensity was 316 nA. Traces from five stimulus repetitions are superimposed. (J) Same as (I) for EOD stimuli at 32 nA. (K) Vector strength vs. phase difference of oscillatory responses to opposite polarity conspecific EODs in *P. tenuicauda*. Each point represents the mean of responses from 6 receptors. Vector strength was averaged across stimulus polarity within each receptor before averaging across receptors. Error bars represent S.E.M. Closed circles indicate phase resets that were significantly different for normal vs. reversed polarity EODs (Hotelling test for paired circular data, $F>F_{crit}=6.9$, $p<0.05$). The stimulus intensities that evoked significantly different phase resets for opposite polarity EODs were 56, 178, and 316 nA. One intervening intensity (100 nA) did not result in significantly different phase resets. No stimulus intensities below 56 nA elicited oscillatory resets to significantly different phases. (L) Phase differences between responses to positive and negative polarity stimuli vs. square pulse duration for oscillatory responses to monopolar square electric pulses.

of durations 0.10 and 0.20 ms were exactly 0.10 and 0.20 ms, respectively (Fig. 3A and B). Across all spiking receptors, this spike-timing difference perfectly matched pulse duration for pulses longer than ~0.1 ms, and as short as 0.05 ms in *Pollimyrus adspersus* (Fig. 3D). At shorter durations, however, the spike-timing differences no longer accurately reflected pulse duration. Importantly, spike-timing differences precisely represented square pulse duration over the behaviorally relevant ranges for total EOD duration in each species (horizontal bars in Fig. 3D), indicating that spiking receptors can faithfully encode the waveform durations found in conspecific signals. These results confirm previous studies on the encoding of pulse waveform by spiking receptors (Hopkins and Bass, 1981; Lyons-Warren et al., 2012). Such precise coding of timing cues mediates the demonstrated ability of species with spiking receptors to detect EOD

waveform variation (Hopkins and Bass, 1981; Arnegard et al., 2006; Machnik and Kramer, 2008; Feulner et al., 2009; Carlson et al., 2011).

In oscillatory receptors, the phase resets elicited by square pulses depended on stimulus polarity (Fig. 3E, F). Positive and negative polarity square pulses elicited phase resets that differed by ~180° (Fig. 3E, F). This phase difference was constant regardless of pulse duration, both throughout and beyond the behaviorally relevant range (Fig. 3L). To determine whether oscillating receptors could encode pulse duration in a manner similar to the spike-timing differences of spiking receptors, we measured the difference in times of oscillatory peaks evoked by opposite polarity pulses (Fig. 3E, F). For pulse durations exceeding receptors' intrinsic oscillation periods (~0.5 ms), the phase could be reset in response to each stimulus edge. In these instances, we measured the oscillation-timing difference elicited by the onset of a positive polarity pulse and the offset of a negative polarity pulse. These oscillation-timing differences precisely reflected square pulse duration (Fig. 3H). However, pulses of shorter durations (≤0.5 ms) did not elicit phase resets to each stimulus edge, since these durations are shorter than receptors' intrinsic oscillation periods. For these stimulus durations, we measured the oscillation-timing differences after stimulus offset (e.g. Fig. 3E, F). We found that oscillation-timing differences did not accurately encode pulse durations shorter than ~1 ms (Fig. 3H), reflecting phase resets to the leading edge of the pulse that differ by ~180° regardless of pulse duration (Fig. 3E, F, L). This means that oscillatory responses could not encode pulse durations found in conspecific EODs (black bar in Fig. 3H). These observations help shed light on the inability of fish with oscillating receptors to resolve slight EOD waveform variation. Species with oscillating receptors cannot detect waveform variation because the necessary cues are not encoded at the

periphery. However, oscillating receptors would be able to encode the direction of the stimulus based on which receptors reset to a peak first, owing to differences in polarity.

To confirm that oscillatory phase differences of ~180° also occurred in response to natural EOD waveforms, we presented previously recorded conspecific EODs at varying intensities to oscillating receptors (Fig. 3I, J). We measured the vector strength and phase differences for responses to opposite polarity stimuli. The vector strength is a measure of phase-locking that ranges from 0 (phase is random across repetitions) to 1 (identical phase across repetitions). At each intensity, we compared the phases elicited by each polarity using the parametric second-order Hotelling test for paired circular data (Zar, 1999). At intensities (56, 178, 316 nA) for which the phase resets evoked by opposite polarity EODs were significantly different, phase differences were always ~180° (filled circles in Fig. 3K). Stimulus intensities of 100 nA and less than 56 nA did not elicit oscillatory resets to significantly different phases (open circles in Fig. 3K; see example in Fig. 3J).

Frequency sensitivity of spiking receptors is matched to the power spectra of conspecific EOD waveforms

Spiking receptors have been reported to be most sensitive to the frequencies occuring in conspecific EOD waveforms (Hopkins, 1981; Bass and Hopkins, 1984; Lyons-Warren et al., 2012). To confirm this finding in our test species, we compared the frequency sensitivity of individual spiking receptors to the power spectra of conspecific EODs (Fig. 4A, B, D). We collected threshold frequency tuning curves as described previously (Lyons-Warren et al., 2012). We defined a spiking response to a constant-frequency stimulus as at least one more spike/sweep during the 90 ms stimulus than during the 90 ms prestimulus period. We decreased the intensity

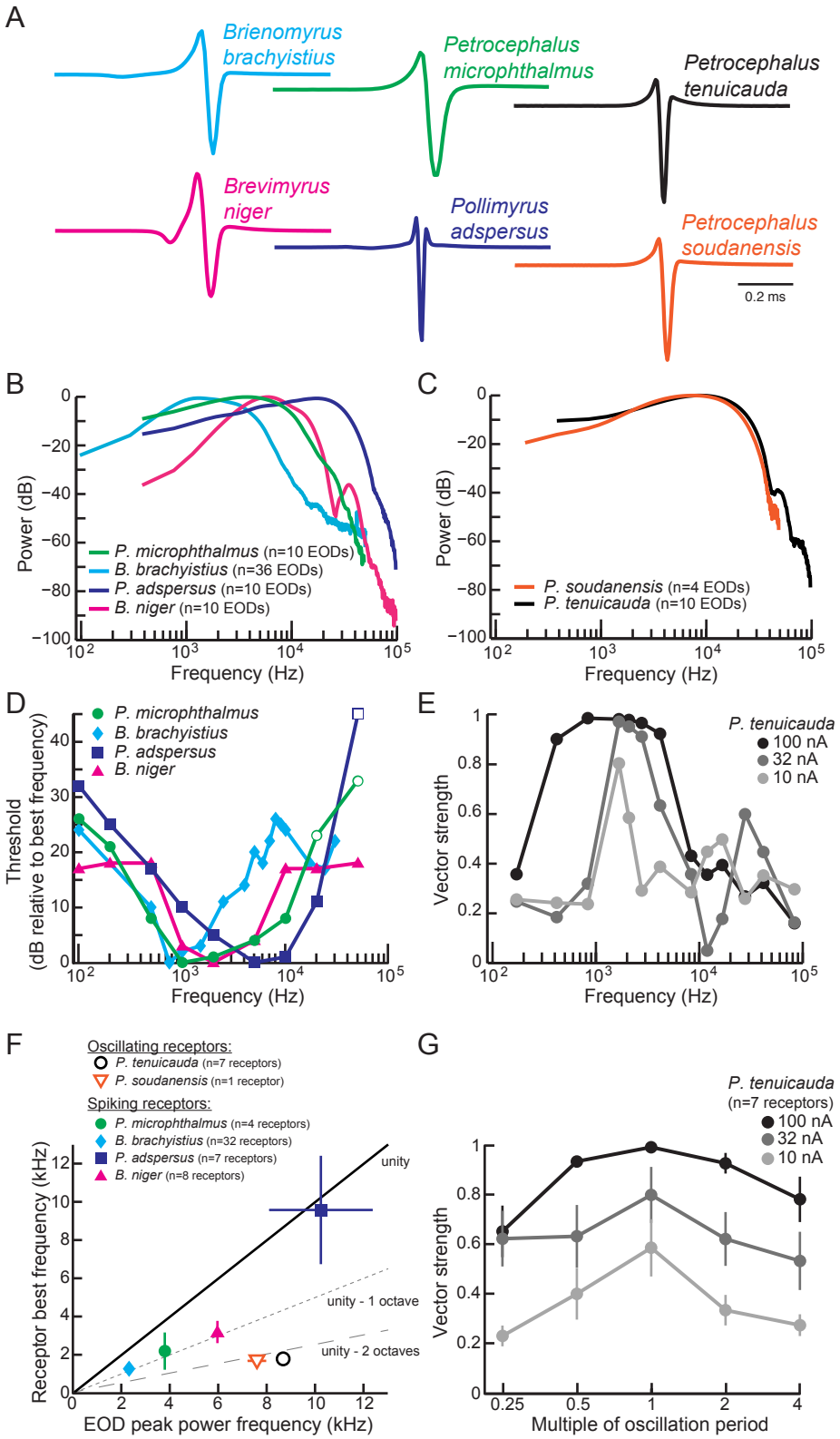

Figure 4. Frequency sensitivity of spiking receptors is matched to conspecific EOD power spectra, whereas frequency sensitivity of oscillating receptors is not. (A) Representative EODs from four species with spiking receptors (*B. brachyistius*, *P. microphthalmus*, *B. niger*, and *P. adspersus*), and two species

with oscillating receptors (*P. tenuicauda* and *P. soudanensis*), plotted head-positive up with normalized peak-to-peak heights. (B-C) Average power spectra of EODs from species with spiking receptors (B) and of species with oscillating receptors (C). (D) Frequency tuning curves for representative spiking receptors from four species. Constant-frequency stimuli were 90 ms in duration. Threshold was determined as the lowest intensity stimulus that elicited a spiking response. Thresholds were defined as dB relative to the threshold at each receptor's best frequency. Open symbols indicate stimuli for which there was no response from the receptor at the intensity shown, but responses to higher intensities were not recorded. (E) Frequency tuning curves for a representative oscillating receptor from *P. tenuicauda* at three intensities. Stimuli were single-cycle bipolar sine waves with positive polarity (peak preceding trough). Vector strength was used as a measure of phase-locking across responses. Vector strength equals 1 when the phase of the oscillatory reset is the same for each stimulus presentation and 0 when the phase of oscillatory reset is completely random for each stimulus presentation. (F) Average receptor best frequency vs. average conspecific EOD peak power frequency for all six species studied. Best frequencies were averaged across responses to positive and negative (trough preceding peak) polarity stimuli in oscillating receptors. We used the best frequencies at 10 nA in *P. tenuicauda*. Closed symbols denote species with spiking receptors and open symbols denote species with oscillating receptors. (G) Vector strength of oscillating responses to positive polarity single-cycle bipolar sine stimuli at multiples of receptors' spontaneous oscillation periods at three intensities in *P. tenuicauda*. Each point in (F) and (G) represents the average across receptors where appropriate, and error bars represent S.E.M.

of the stimulus until the receptor no longer produced a response. We defined a receptor's threshold as the lowest intensity that elicited a response. We defined a receptor's best frequency as the frequency with the lowest threshold.

In general, spiking receptors had the lowest thresholds in the frequency range approximately corresponding to the frequencies with the highest power in conspecific EODs (compare Fig. 4D with Fig. 4B). For spiking receptors, best frequencies varied widely across species and correlated with the peak power frequencies of conspecific EODs. On average, the best frequencies of spiking receptors were within one octave of the peak power frequencies of conspecific EODs (filled symbols in Fig. 4F). These findings support the interpretation of spiking receptors as matched filters for conspecific EODs.

Frequency sensitivity of oscillating receptors is not matched to the power spectra of conspecific EOD waveforms

To test whether the frequency sensitivity of oscillating receptors is also matched to the power spectra of conspecific EOD waveforms, we collected frequency tuning curves in two species. Due to the oscillatory nature of both stimulus artifact and response, we could not use the same 90 ms constant-frequency stimuli that we used to characterize frequency tuning in spiking receptors. Instead, we presented single-cycle bipolar sine waves at three intensities and measured the vector strength of phase resets at stimulus offset. We defined an oscillating receptor's best frequency as the frequency that elicited the largest vector strength.

In general, oscillating receptors were most sensitive to frequencies well below the peak power frequency in conspecific EODs (compare Fig. 4E with black trace in Fig. 4C). On average, the best frequencies of oscillating receptors were more than two octaves below the peak power frequencies of conspecific EODs (open symbols in Fig. 4F). These data indicate that, in contrast to spiking receptors, oscillating receptors do not represent matched filters for conspecific EODs.

At stimulus intensities of 10 nA, where tuning was sharpest, the best frequencies (0.8-2.5 kHz) of these receptors roughly corresponded to their intrinsic oscillation frequencies (1.5-2.0 kHz), suggesting that their frequency tuning resulted from resonance with their intrinsic oscillations. To test this hypothesis, we also delivered single-cycle bipolar sine waves at multiples of each unit's intrinsic oscillation period. Indeed, oscillatory responses were strongest for stimulus durations matching each receptor's spontaneous oscillation period (Fig. 4G).

Spiking receptors encode interpulse intervals into interspike intervals

Electric communication signals consist of the EOD produced at variable interpulse intervals (IPIs). Whereas the stereotyped EOD waveform can contain identifying information such as species and sex, the interpulse intervals convey behavioral state (see Carlson, 2002 for review). Spiking receptors have previously been reported to respond to IPIs as short as 2 ms (Bell and Grant, 1989). To investigate IPI coding in the three species with spiking receptors included in this study, we presented receptors with a pair of 0.2 ms duration monopolar square pulses at a range of IPIs (Fig 5A, B).

The probability that a receptor fired a spike in response to the second pulse in the pair decreased at the shortest intervals tested (Fig. 5B, C). The minimum IPI at which spikes could reliably be elicited varied slightly across species (Fig. 5C). Importantly, receptors of all species reliably fired spikes at the reported minimum IPIs produced by individual fish (~8 ms) (Hopkins, 1986; Carlson, 2002).

In agreement with previous studies (Bell and Grant, 1989; Baker et al., 2013), spiking receptors encoded IPIs into interspike intervals within receptors, with the interspike intervals exactly matching the IPI (Fig. 5A, D). This relationship held for IPIs as short as 1 ms in *P. adspersus* and *P. microphthalmus*, and as short as 0.3 ms in *Brevimyrus niger*. Shorter IPIs failed to evoke spikes in response to the second pulse due to receptors' refractory periods (Fig. 5B, C), which is why data points below these values are missing from Fig. 5D. These findings demonstrate that spiking receptors can faithfully encode the IPIs generated by individual signaling fish into interspike intervals within single receptors.

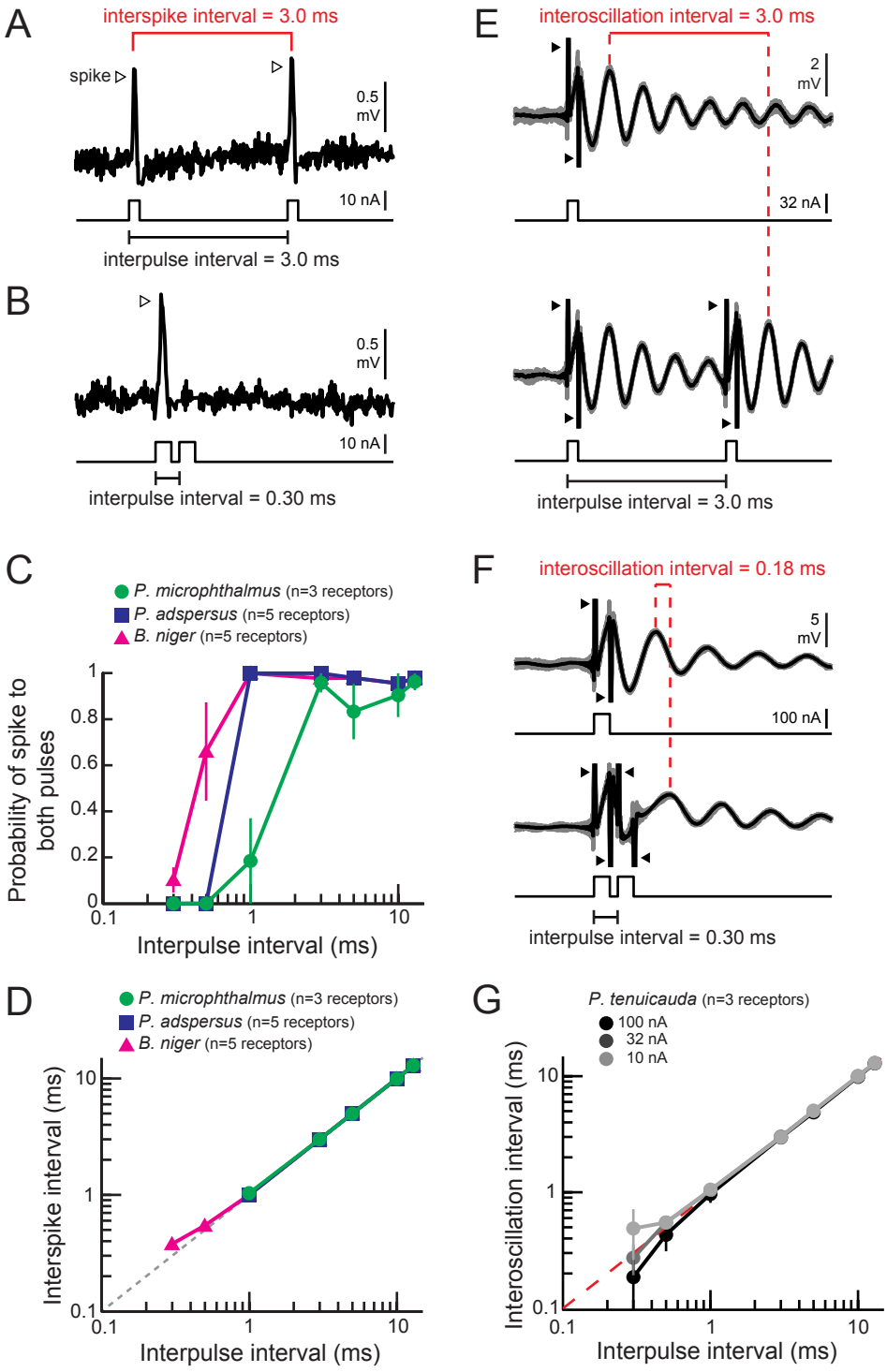

Figure 5. Spiking and oscillating receptors encode interpulse intervals into interspike and interoscillation intervals, respectively. (A) Extracellular recording from a spiking receptor in *B. niger* in response to a pair of positive polarity monopolar square pulses of 0.2 ms duration and 3.0 ms interpulse interval. The time interval between spikes elicited by the pulse pair was 3.0 ms. (B) Same as (A) for 0.30 ms interpulse interval. A spike occurred in response to the first pulse only. Stimulus artifact was removed from

recordings in (A-B). (C) The probability that a receptor fired spikes to both positive polarity pulses in a pair vs. interpulse interval for spiking receptors from three species. (D) Interspike interval vs. positive polarity interpulse intervals for the same spiking receptors shown in (D). The receptors of *P. adspersus* and *P. microphthalmus* did not fire spikes in response to both pulses when interpulse intervals were shorter than 1 ms, so there are no data points at these intervals. (E) Extracellular recordings from an oscillating receptor in *P. tenuicauda* in response to a single pulse (top) and to a pair of pulses with 3.0 ms interpulse interval (bottom). Responses to each stimulus presentation are shown in grey and the average across stimulus presentations is shown in black. The interoscillation interval, defined as the time interval between the first poststimulus oscillatory peak evoked by the single pulse and that evoked by the second pulse in the pair, was 3.0 ms. The interoscillation interval was measured from the average trace. (F) Same as (E) for 0.30 ms interpulse interval. The interoscillation interval was 0.18 ms. (G) Interoscillation interval vs. interpulse interval for the responses of oscillating receptors of *P. tenuicauda* to positive polarity stimuli. Each point in (C), (D), and (G) represents the mean across receptors and error bars represent S.E.M.

Oscillating receptors encode interpulse intervals into interoscillation intervals and amplitude increases

Oscillating receptors responded to paired pulses with phase resets and amplitude increases in response to each pulse in the pair (bottom panels in Fig. 5E, F). At the shortest intervals (0.3 ms) tested, the stimulus artifact of the second pulse obscured the oscillatory response to the first pulse (Fig. 5F). Thus, to investigate how oscillating receptors encode IPIs, we measured interoscillation intervals as the time between the first oscillatory peak following a single-pulse stimulus and the first oscillatory peak following the second pulse in the paired stimulus (Fig. 5E, F). This method was equivalent to measuring the time interval between oscillatory peaks evoked by each pulse in the pair, but it allowed us to measure the interoscillation intervals at the shortest intervals where the oscillatory response is obscured by stimulus artifact. Interoscillation intervals accurately represented the IPI for intervals of ~1 ms and longer (Fig. 5E, G). At shorter IPIs, the interoscillation interval did not reliably match the IPI (Fig. 5F, G). Importantly, interoscillation intervals accurately encoded IPIs over the range produced by individual fish (≥8 ms) (Hopkins, 1986; Carlson, 2002).

Interestingly, the amplitude of oscillations evoked by a pair of pulses also depended on the IPI (Fig. 6A, B). To facilitate comparisons across and within receptors, we normalized oscillation amplitudes evoked by the second pulse in the pair to those evoked by a single pulse. At the highest intensity tested, oscillation amplitudes were attenuated relative to single-pulse responses for IPIs below 1 ms (black curve in Fig. 6C). As stimulus intensity decreased, however, oscillation amplitudes became selectively enhanced in response to 0.5 ms IPIs (Fig. 6C). At the lowest intensity tested, oscillation amplitudes evoked by 0.5 ms IPIs were about 40% greater than those evoked by single pulses (light grey curve in Fig. 6C). Phase-locking, as measured by the vector strength of oscillatory responses to the second pulse in the pair, also depended on IPI and stimulus intensity (Fig. 6E). As the intensity decreased, responses became more sharply selective for IPIs around 0.5 ms, which is near the intrinsic oscillation periods (0.47-0.99 ms) of receptors in the species tested. This is suggestive of resonance, in which stimulating an oscillating receptor with a pair of pulses separated by the receptor's intrinsic oscillation period results in stronger responses.

To test this hypothesis, we presented receptors with IPIs equal to multiples of their intrinsic oscillation periods (Fig. 6D, F). As stimulus intensity decreased, oscillatory responses became more selective for IPIs equal to the intrinsic oscillation period (Fig. 6D). In contrast, oscillation amplitudes were attenuated relative to single-pulse responses for IPIs shorter than the intrinsic oscillation period (Fig. 6D). At the lowest intensity tested, the vector strength was also highest for IPIs matching receptors' intrinsic oscillation periods (light grey curve in Fig. 6F).

Collectively, these results indicate that, while oscillating receptors encode IPIs into interoscillation intervals, the oscillations also exhibit the interesting property of enhanced responses for IPIs matching their intrinsic oscillation periods. These oscillatory periods,

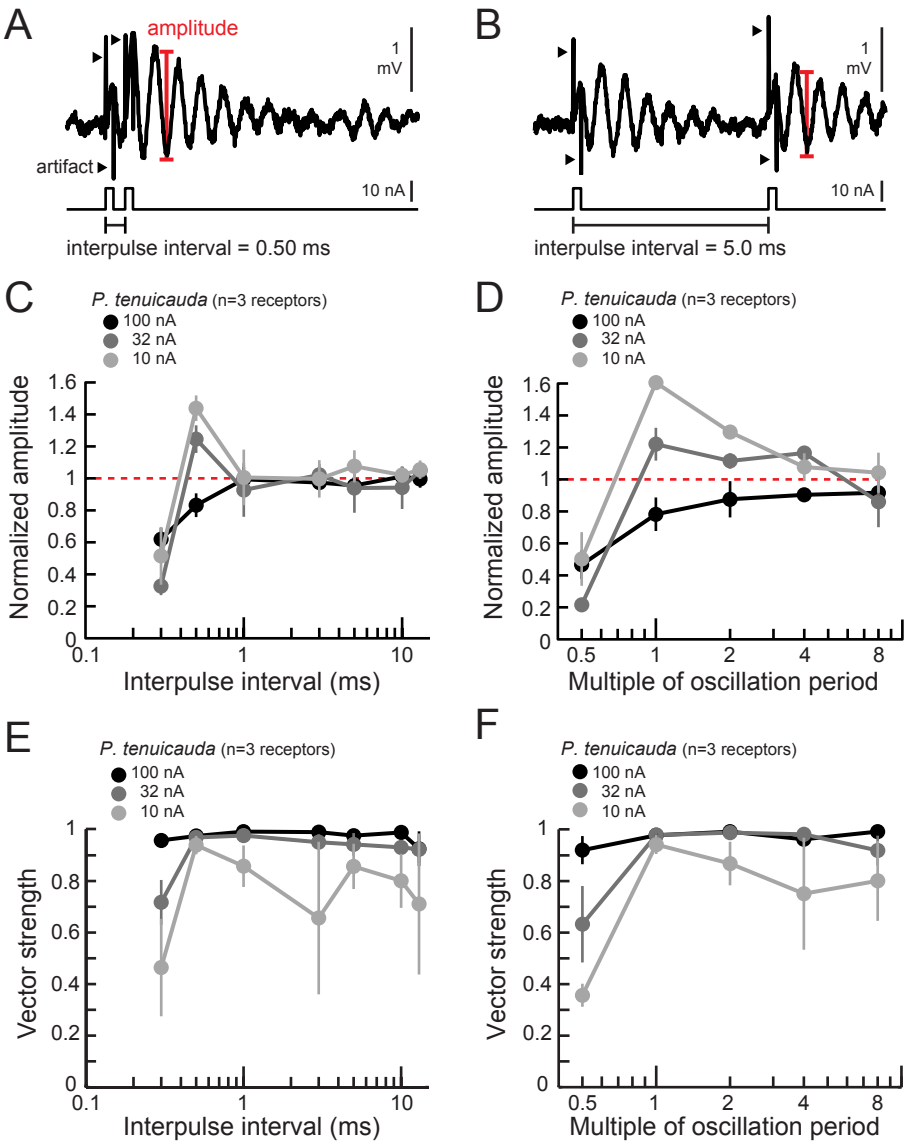

Figure 6. Oscillating receptors produce enhanced oscillation amplitudes at submillisecond interpulse intervals matching their intrinsic oscillation periods. (A) An extracellular recording from an oscillating receptor in *P. tenuicauda* in response to a pair of monopolar square pulses of 0.2 ms duration and 0.50 ms interpulse interval. We measured the oscillation amplitude for each stimulus repetition as the mean voltage of the first two poststimulus oscillatory peaks minus the voltage at the intervening trough. We then averaged amplitudes across all repetitions of the same stimulus. (B) Same as in (A) for an interpulse interval of 5.0 ms. (C) Oscillation amplitude evoked by the second pulse in pair normalized to the amplitude evoked by a single pulse vs. interpulse interval for the responses of oscillating receptors in *P. tenuicauda* at three stimulus intensities. Data shown are for positive polarity pulses. (D) Same as (C) for interpulse intervals corresponding to multiples of oscillating receptors' intrinsic oscillation periods. (E) Vector strength vs. interpulse interval for oscillating responses to positive-polarity stimuli at three intensities in the same receptors shown in (C, D). (F) Same as (E) for interpulse intervals corresponding to multiples of oscillating receptors' intrinsic oscillation periods. Each point in (C-F) represents the mean across receptors and error bars represent S.E.M.

however, are at least one order of magnitude shorter than the IPIs that could be produced by a single fish. Why would some species of mormyrids have receptors that are maximally sensitive to signals too short to be produced by individual fish?

Oscillating receptors produce the strongest responses at submillisecond IPIs present in communication signals recorded from a group of fish

Even though the minimum IPI a single fish can produce is approximately 8 ms, a large group of signaling fish may collectively produce much shorter IPIs. Could the high-frequency oscillations in rosette receptors be tuned to these shorter IPIs? To test this hypothesis, we first recorded 20 minutes of electric signaling from individual fish of a species with spiking receptors (*P. microphthalmus*) (e.g., Fig. 7A) and from individual fish of a species from the same genus with oscillating receptors (*P. tenuicauda*) (e.g., Fig. 7D). We recorded EOD times as the times at which the rectified recorded potential crossed a predefined threshold. We then calculated IPIs as the time between successive EODs (insets in Fig. 7A, D). Next we recorded electrical activity from group tanks of each of the same two species (Fig. 7B, E). Indeed, group signals contained much shorter IPIs than single-fish signals (compare Fig. 7B with 7A, and Fig. 7E with 7D; note different time scales).

To determine whether spiking and oscillating receptors could encode the very short IPIs in group signals, we compared receptor response strengths with the IPIs recorded from a group of the corresponding species (Fig. 7C, F). The spiking receptors of *P. microphthalmus* responded faithfully to intervals of ~3 ms and longer (Fig. 7C). However, these receptors could not respond to the submillisecond intervals present in signals recorded from a group of this species (Fig. 7C). In contrast, oscillating receptors responded most strongly to 0.5 ms IPIs, which are found only in

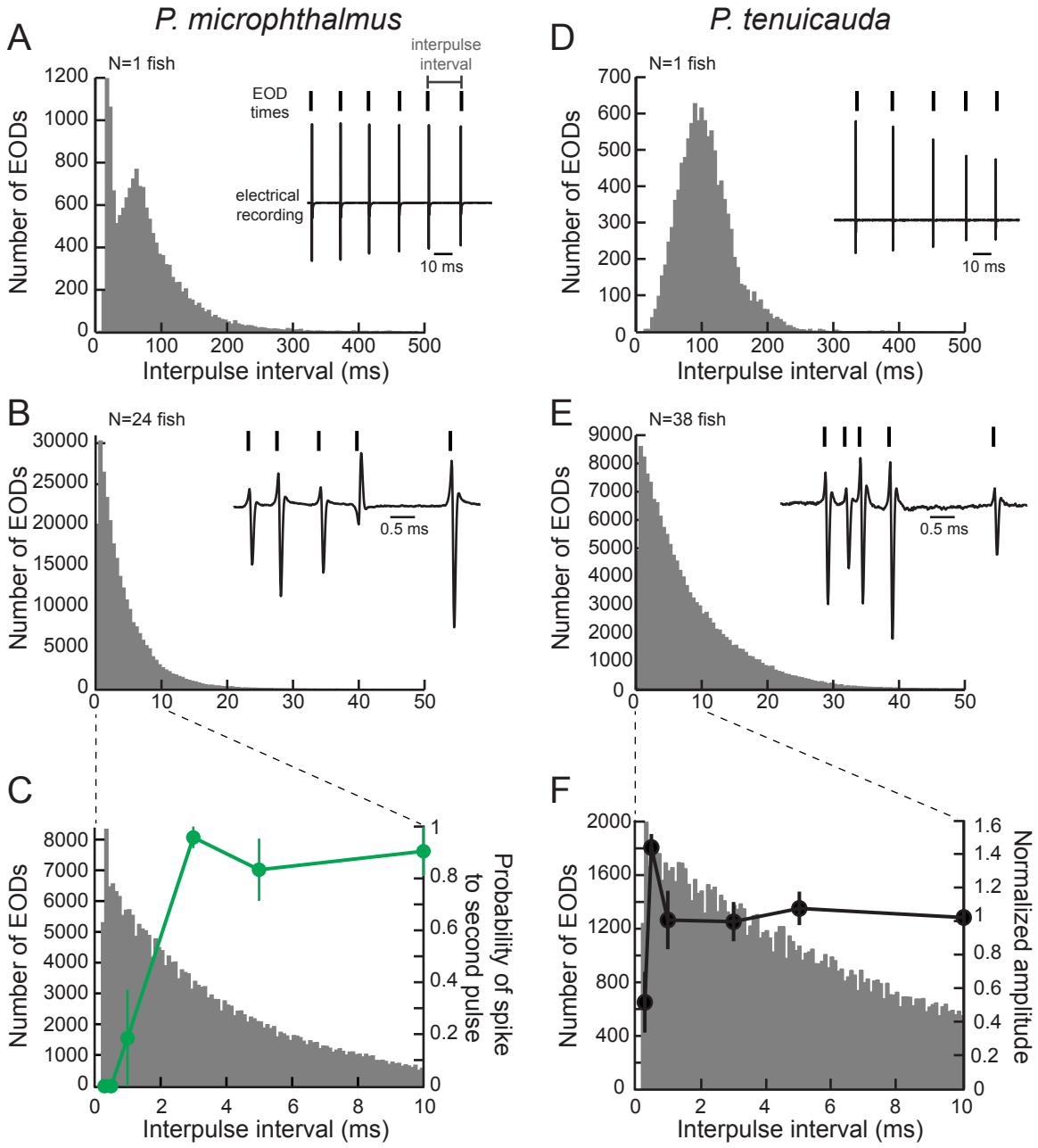

Figure 7. Oscillating receptors are most sensitive to submillisecond interpulse intervals occurring in group communication signals. (A) A histogram of the interpulse intervals recorded over 20 minutes from a single fish with spiking receptors (*P. microphthalmus*). Inset, illustration of interpulse interval calculation. We recorded the electric signaling activity from a single fish and recorded the time of each EOD as the time at which the rectified potential crossed a predefined threshold (tick marks above electrical recording trace). We measured the interpulse intervals as the time between successive EODs. (B) Same as in (A) for a recording from a group tank of 24 *P. microphthalmus*. Inset, electrical recording from the same group of fish illustrating submillisecond interpulse intervals. EOD polarity and amplitude depend on fish's orientation and location relative to the recording electrode. (C) Spike probability of three *P. micropthalmus* receptors (green; *y*-axis on right; same data as in Fig. 5C) vs. interpulse interval superimposed on the interpulse interval histogram from (B). Note the expanded data range in the *x*-axis.

Each point represents the mean across three receptors and error bars represent S.E.M. (D-E) Same as in (A-B) for a congeneric species with oscillating receptors (*P. tenuicauda*). (F) Normalized oscillation amplitudes of three *P. tenuicauda* receptors (black; *y*-axis on right; same data as in Fig. 6C at 10 nA) vs. interpulse interval superimposed on the interpulse interval histogram from (E). Note the expanded data range in the *x*-axis. Each point represents the mean across three receptors and error bars represent S.E.M.

group signals (Fig. 7F). These IPIs are too short for spiking receptors to encode (compare Fig. 7C and F). Thus, one advantage for species with high-frequency, oscillating receptors may be the ability to detect very short IPIs in group communication signals that spiking receptors cannot encode due to refractoriness.

Behavioral responses of a species with oscillating receptors reveal tuning to submillisecond IPIs

If oscillating receptors facilitate detection of communication signals produced by a group of individuals, then species with oscillating receptors should exhibit selective behavioral responses to submillisecond IPIs, and species with spiking receptors should not. To test this hypothesis, we performed behavioral playback experiments in which we presented a single fish with a train of 10 conspecific EODs at constant IPIs ranging from 0.3–100 ms (Fig. 8). We recorded the fish's electric signaling activity, and then compared the fish's EOD output evoked by IPI stimuli to that evoked by a single conspecific EOD.

In general, mormyrids respond to electric signals by increasing or decreasing their rate of EOD production (Moller et al., 1989; Post and von der Emde, 1999; Carlson et al., 2011; Lyons-Warren et al., 2012). Accordingly, we measured the maximum increase in EOD rate and the maximum decrease in EOD rate that occurred between stimulus onset and 1 s after stimulus offset. We found that behavioral responses depended on the IPI of the stimulus (Fig. 8). A species with oscillating receptors produced the strongest EOD rate increases at the shortest and

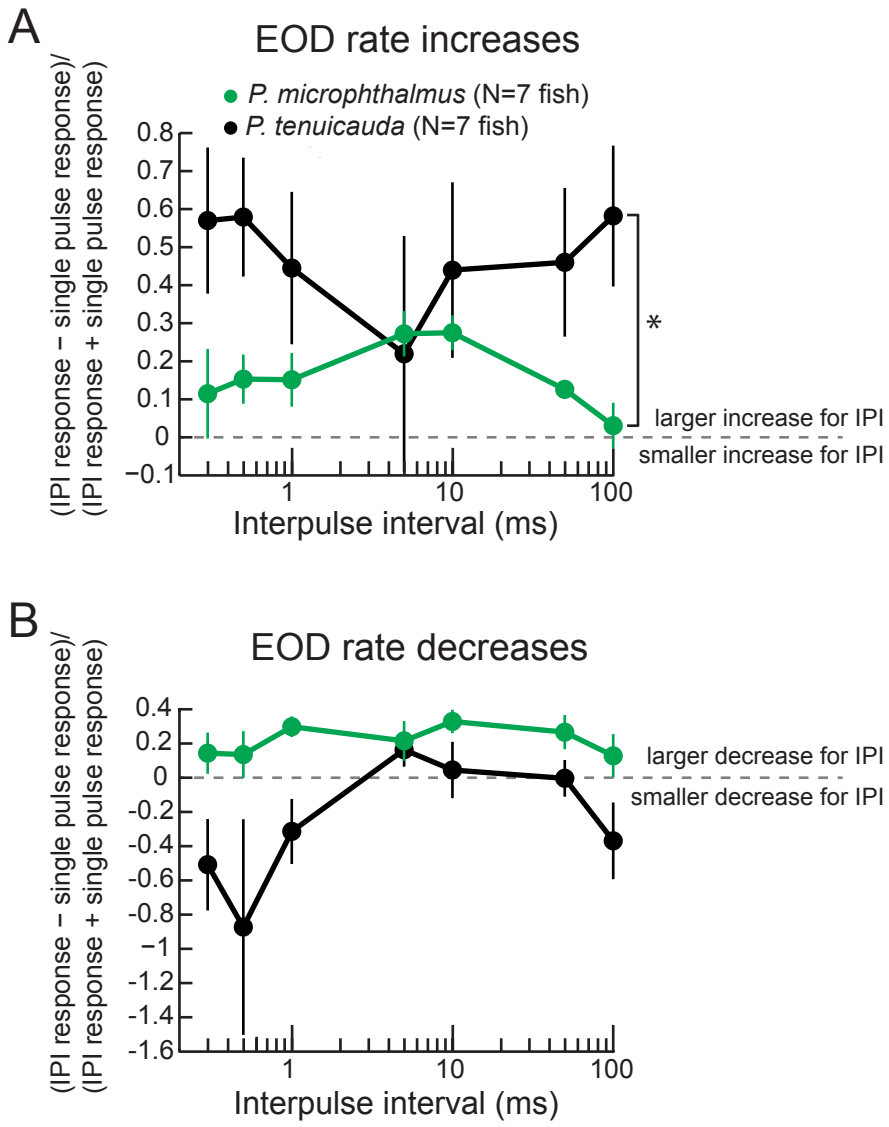

Figure 8. Behavioral responses reveal tuning to submillisecond interpulse intervals (IPIs) in a species with oscillating receptors. (A) A normalized measure of EOD rate increases to constant interpulse interval trains of conspecific EODs vs. interpulse interval during behavioral playback experiments. *, repeated-measures ANOVA, interaction between species and interpulse interval, $p<0.01$. (B) Same as (A) for EOD rate decreases. Each point represents the mean across fish and error bars represent S.E.M.

longest IPIs tested (*P. tenuicauda* in Fig. 8A). The shortest IPIs ($\leq$ 5 ms) correspond to those found only in signals recorded from groups of fish.

The pattern of behavioral responses of a congeneric species with spiking receptors (*P. microphthalmus* in Fig. 8A) was significantly different (repeated-measures ANOVA, interaction between species and IPI, $F_{(6,12)}$=3.4, p=0.0048) from that of the species with oscillating receptors. The species with spiking receptors produced the greatest EOD rate increases for IPIs in the intermediate range of those tested, which roughly correspond to the minimum IPI produced by individual fish.

In general, the species with oscillating receptors tended to produce weaker EOD rate decreases in response to the IPI stimuli than to single pulses (negative y-values in Fig. 8B). In contrast, the species with spiking receptors tended to produce stronger EOD rate decreases for IPI stimuli than for single EODs (positive y-values in Fig. 8B). Accordingly, there was a significant effect of species in a repeated-measures ANOVA ($F_{(1)}$=18, p=0.0012). However, there was no interaction effect between species and IPI for EOD rate decreases ($F_{(6,12)}$=1.0, p=0.43).

These results lend support to our hypothesis that the high-frequency activity of oscillating receptors may mediate detection of submillisecond IPIs that are only present in the communication signals produced by a large group of individuals. These very short IPIs elicit stronger responses in oscillating receptors and greater EOD rate increases in species with oscillatory receptors. Since spiking receptors cannot encode these submillisecond IPIs, we propose that these oscillations are an adapation for detecting large groups of conspecifics.

DISCUSSION

Here we describe for the first time a novel mechanism for peripheral sensory coding, in which sensory receptors with spontaneous, high-frequency oscillatory activity encode stimuli into phase resets. These resets provide information about pulse timing and polarity, but not signal waveform, consistent with the inability of these fish to behaviorally detect EOD waveform variation (Carlson et al., 2011). Further, oscillating receptors are most sensitive to submillisecond IPIs that match their oscillation period (0.47-0.99 ms). This sensitivity is remarkable for two reasons. First, these submillisecond IPIs are too short for spiking receptors to reliably encode. Second, these IPIs are much shorter than those produced by individual fish, suggesting increased sensitivity to the communication signals produced by groups of individuals. Indeed, playback experiments demonstrated that a species with oscillating receptors responded strongly to submillisecond IPIs matching in the range of enhanced receptor sensitivity. Thus, this novel peripheral coding mechanism may represent an adaptation for detecting communication signals from large groups of fish.

Oscillatory electrical activity is widespread in neural networks (Buzsaki and Draguhn, 2004). Resets in the phase of ongoing oscillations have also been widely reported, and are hypothesized to play a role in attention, memory, cross-modal integration, motor control, and speech processing (Axmacher et al., 2006; Llinas, 2009; Gross et al., 2013; Thorne and Debener, 2014; Frey et al., 2015). Functionally, phase resets could serve to align ongoing activity to an event or periodic stimulus, or to facilitate coupling between independent oscillators (Canavier, 2015). Many studies have linked phase resets in ongoing cortical oscillations to perceptual performance, suggesting an important role for phase resets in sensory processing (Thorne and Debener, 2014). However, whether these phase resets encode specific information about a

sensory stimulus or instead serve a modulatory function remains to be determined (Lakatos et al., 2009). Futhermore, all phase resets previously described occur in central circuits and involve oscillations of much lower frequencies (<100 Hz) than those (1-3 kHz) in the sensory receptors we describe here (Harder, 1968; Thut et al., 2012; Canavier, 2015). Using *in vivo* extracellular recordings of single receptors, we demonstrate that phase resets in the periphery enable detection of and entrainment to very fast temporal patterns in communication signals. Sensitivity to temporal patterns has previously been shown to involve network interactions in a wide range of central circuits (Klug et al., 2012; Buonomano, 2014). Here we show that electrical oscillations in sensory receptors can act as peripheral filters for temporal patterns.

Spiking receptors are most sensitive to stimulus frequencies near those in conspecific EODs (Hopkins, 1981; Bass and Hopkins, 1984; Lyons-Warren et al., 2012), consistent with these receptors functioning as matched filters (Wehner, 1987). Moreover, the precisely timed spikes in these receptors enable discrimination of waveform variation (Hopkins and Bass, 1981; Carlson et al., 2011), which would facilitate signaler identification. In fact, studies on species with spiking receptors have revealed sensitivity to individual differences in conspecific EODs (Graff and Kramer, 1992; Hanika and Kramer, 2005). Collectively, these results support the hypothesis that spiking receptors are specialized for detecting communication signals produced by individual fish, and encoding the information necessary to identify the sender.

In contrast, oscillating receptors exhibit matched filters not for EOD waveforms, but for IPI patterns in group signals. A receptor's oscillation frequency is predictive of its frequency tuning. However, oscillating receptors are tuned to much lower frequencies than the peak power frequencies of conspecific EODs. Furthermore, these oscillation frequencies confer enhanced sensitivity to IPIs that can only be produced by groups of fish. Therefore, the oscillatory

encoding mechanism may result in fundamentally different functionality than the spiking mechanism. Whereas spiking receptors are specialized for detecting signals from individuals, oscillating receptors appear specialized for detecting signals from a large group.

These differences in receptor physiology and tuning may relate to differences in social behavior. Species in the lineage with oscillatory receptors have been reported to school as adults and prefer open water (Nichols and Griscom, 1917; Hopkins, 1980, 1981; Chapman et al., 1996; Lavoue et al., 2004; Lavoue, 2012), unlike other species, which have generally been described as solitary and territorial, and prefer areas with dense vegetation and detritus (Nichols and Griscom, 1917; Hopkins, 1980, 1981; Hopkins and Bass, 1981; Chapman et al., 1996; Friedman and Hopkins, 1996; Lavoue, 2012). In single-species lab tanks, *P. tenuicauda* and *P. soudanensis* form open-water shoals and schools, respectively, while *B. niger*, *P. adspersus*, and *B. brachyistius* are generally solitary and seek shelter, which they aggressively defend against intruders (unpub. obs.). Thus, the increased sensitivity of peripheral receptors for communication signals produced by groups of conspecifics may mediate the detection and localization of shoals or schools in fish's native habitats. In addition, the inability of fish in this lineage to detect subtle EOD variation is associated with reduced EOD diversity among species compared to other mormyrids (Lavoue et al., 2008; Carlson et al., 2011). However, *P.microphthalmus* presents an important exception to the apparent relationship between behavior and sensitivity to EOD variation. These fish, with spiking receptors and associated sensitivity to EOD waveform variation, form schools both in laboratory and natural settings (Lavoue et al., 2004). Field studies will be necessary to more fully understand how behavioral and ecological differences between species may have selected for different peripheral coding strategies and the perceptual abilities they confer.

Electrical oscillations appear to be a common feature of electroreceptors. Indeed, the spiking receptors of mormyrids exhibit damped oscillations in spike probability following an electrical stimulus (Bennett, 1965, 1967; Roth and Szabo, 1972). However, these oscillations are too small to be recorded at the pore of the receptor and do not appear to occur spontaneously. Instead, these oscillations likely help establish electrical tuning to frequencies in conspecific EOD waveforms (Bennett, 1967). Similarly, oscillations in other types of electroreceptors, including the tuberous receptors of wave-type gymnarchid and gymnotiform electric fish, are hypothesized to confer electrical tuning to a fish's own EOD frequency for electrolocation and communication (Bennett, 1965, 1967; Hopkins, 1976; Viancour, 1979; Watson and Bastian, 1979; Kawasaki, 2001, 2005). Spontaneous, noisy oscillations in paddlefish ampullary electroreceptors are hypothesized to contribute to prey detection (Neiman and Russell, 2001; Neiman and Russell, 2011).

Oscillatory electrical activity also occurs in non-mammalian auditory hair cells, where it serves as a frequency tuning mechanism (Fettiplace and Fuchs, 1999). Of particular relevance are frog saccular hair cells, in which differences in spontaneous spiking vs. oscillatory electrical activity are linked to differences in the density of three types of potassium channels (Rutherford and Roberts, 2009). Pharmacology and/or intracellular recordings from receptor sensory cells will be necessary to determine whether similar mechanisms contribute to high-frequency oscillations in some mormyrid species and spikes in other species. Importantly, the oscillations observed in rosette receptors of mormyrids are distinct from oscillations in hair cells and other electroreceptors due to their larger amplitudes and higher frequencies, as well as the fact that they use phase resets to encode information. The phase resets reported here are the first to be observed in any oscillating sensory receptor.

The entirety of our knowledge of the coding of electric communication signals in mormyrids had been limited to species with broadly distributed receptors (see Baker et al., 2013 for review), which fire spikes in all species that have been studied. The sensitivity of these fish to EOD waveform variation is due in part to the precise encoding of timing cues in EODs by spiking receptors. Receptors on one side of the body fire spikes at pulse onset, and receptors on the other side of the body fire spikes at pulse offset (Hopkins and Bass, 1981). These spike-timing cues in receptors on opposite sides of the body are compared in a midbrain region called the anterior exterolateral nucleus (ELa), in which excitation and inhibition from different receptive fields establish single-neuron selectivity for stimulus pulse durations (Friedman and Hopkins, 1998; Lyons-Warren et al., 2013). These duration-selective neurons project to the posterior exterolateral nucleus (ELp), where single-neuron selectivity for interpulse intervals arises (Carlson, 2009). Notably, species with receptors organized into rosettes have a smaller exterolateral nucleus (EL) that is not subdivided into anterior and posterior regions (Carlson et al., 2011). In all three species that have been studied, rosette receptors produce high-frequency oscillations (Harder, 1968, this study). How electric communication signals are processed centrally in the EL of these species remains unknown.

Central processing of oscillatory receptor inputs could play a role in distinguishing self-generated stimuli from external stimuli while selectively maximizing sensitivity to external stimuli. In the absence of an electric stimulus, the spontaneous oscillations across receptors are asynchronized. When the fish emits its own EOD, receptors in all rosettes will experience stimuli of identical polarity based on the direction of current flow through the receptors (Hopkins, 1986). This means that oscillations in all receptors will reset to the same phase in synchrony. In this case, subtracting the oscillatory responses of receptors on opposite sides of the body would result

in cancellation. In contrast, in the presence of an external electric stimulus, receptors on opposite sides of the body will experience opposite polarity stimuli, and will reset to opposite phases. In this case, subtraction of opposite-phase responses would increase oscillation amplitudes relative to single-receptor oscillations, thus potentially increasing sensitivity to external signals.

The electrosensory system could implement such a subtraction mechanism if oscillatory receptors on one side of the body mediate excitation, and receptors on the opposite side mediate inhibition onto central neurons. In response to the fish's own signals, excitation would arrive coincidentally with inhibition, thus cancelling responses. This proposed mechanism would also provide the information necessary to locate external signal sources. Stimuli coming from one direction would elicit maximal excitation from one side of the body and minimal inhibition from the other side of the body, whereas stimuli from the other direction would elicit minimal excitation and maximal inhibition. The directionality would presumably be reversed in the opposite hemisphere, leading to a reversed directional preference. Given the excitatory-inhibitory interactions found in the ELa circuit of species with broadly distributed receptors (Friedman and Hopkins, 1998; Lyons-Warren et al., 2013), such an excitatory-inhibitory interaction could occur in a homologous circuit within the midbrain EL.

The mormyrid family contains two subfamilies called Mormyrinae and Petrocephalinae (Sullivan et al., 2000). The majority of mormyrine species have broadly distributed receptors, ELa/ELp, and behavioral sensitivity to EOD waveform variation (Carlson et al., 2011). In contrast, most petrocephaline species have receptors organized into rosettes as well as an EL midbrain region, and they are not sensitive to EOD waveform variation (Carlson et al., 2011). Although the available evidence indicates that EL is ancestral to ELa/ELp, it remains unclear whether spiking or oscillating receptors are ancestral (Carlson et al., 2011). The sister taxon to

mormyrids, *Gymnarchus*, has synchronously oscillating tuberous electroreceptors tuned to their own wave-type EOD frequencies (Kawasaki, 2005). The knollenorgan receptors in mormyrids are also tuberous, suggesting that oscillations may be the ancestral condition in mormyrids.

The only petrocephaline that has both broadly distributed receptors and ELa/ELp is *P. microphthalmus*, and it can also detect EOD waveform variation (Carlson et al., 2011). Therefore, this represents a striking case of parallel evolution in which a perceptual ability arose twice independently, once in Mormyrinae and once in *P. microphthalmus* (Carlson et al., 2011). Here we demonstrate that the broadly distributed receptors of *P. microphthalmus* fire spikes, and that these spiking receptors display similar physiological properties to the spiking receptors of three mormyrine species, which are likewise similar to spiking receptors previously described in at least seven additional mormyrine species (Bennett, 1965; Harder, 1968; Hopkins, 1981; Arnegard et al., 2006). Thus, we demonstrate correlated evolutionary changes in peripheral sensory physiology, neuroanatomy, and perception. These results suggest that parallel, independent evolution of a perceptual ability relates to parallel, independent evolution of its sensory basis.

In addition to describing the sensory basis for a major perceptual difference among species, our results provide the first illustration of information coding by modulations of ongoing oscillations at the periphery. These results lay the groundwork for future investigations into 1) the cellular mechanisms responsible for generating continuous high-frequency oscillations and phase resets in sensory receptors, 2) cellular and network mechanisms for central processing of oscillatory modulations, and 3) differences in ecology and/or social behavior among species with different peripheral coding strategies.

REFERENCES

Arnegard ME, Jackson BS, Hopkins CD (2006) Time-domain signal divergence and discrimination without receptor modification in sympatric morphs of electric fishes. J Exp Biol 209:2182-2198.

Axmacher N, Mormann F, Fernandez G, Elger CE, Fella J (2006) Memory formation by neuronal synchronization. Brain Res Rev 52:170-182.

Baker CA, Kohashi T, Lyons-Warren AM, Ma XF, Carlson BA (2013) Multiplexed temporal coding of electric communication signals in mormyrid fishes. J Exp Biol 216:2365-2379.

Baldwin MW, Toda Y, Nakagita T, O'Connell MJ, Klasing KC, Misaka T, Edwards SV, Liberles SD (2014) Evolution of sweet taste perception in hummingbirds by transformation of the ancestral umami receptor. Science 345:929-933.

Bass AH, Hopkins CD (1984) Shifts in frequency tuning of electroreceptors in androgen-treated mormyrid fish. J Comp Physiol 155:713-724.

Batschelet E (1981) Circular statistics in biology. London ; New York: Academic Press.

Bell CC, Grant K (1989) Corollary discharge inhibition and preservation of temporal information in a sensory nucleus of mormyrid electric fish. J Neurosci 9:1029-1044.

Bennett MVL (1965) Electroreceptors in mormyrids. Cold Spring Harb Symp Quant Biol 30:245-262.

Bennett MVL (1967) Mechanisms of electroreception. Bloomington: University Indiana Press.

Buonomano DV (2014) Neural dynamics based timing in the subsecond to seconds range. In: Neurobiology of Interval Timing (Merchant H, de Lafuente V, eds), pp 101-117. New York: Springer Science + Business Media.

Buzsaki G, Draguhn A (2004) Neuronal oscillations in cortical networks. Science 304:1926-1929.

Canavier CC (2015) Phase-resetting as a tool of information transmission. Curr Opin Neurobiol:206-213.

Carlson BA (2002) Electric signaling behavior and the mechanisms of electric organ discharge production in mormyrid fish. J Physiology-Paris 96:405-419.

Carlson BA (2009) Temporal-pattern recognition by single neurons in a sensory pathway devoted to social communication behavior. J Neurosci 29:9417-9428.

Carlson BA (2012) Diversity matters: The importance of comparative studies and the potential for synergy between neuroscience and evolutionary biology. Arch Neurol-Chicago 69:987-993.

Carlson BA, Hopkins CD (2004) Stereotyped temporal patterns in electrical communication. Anim Behav 68:867-878.

Carlson BA, Arnegard ME (2011) Neural innovations and the diversification of African weakly electric fishes. Commun Integr Biol 4:720-725.

Carlson BA, Hopkins CD, Thomas P (2000) Androgen correlates of socially induced changes in the electric organ discharge waveform of a mormyrid fish. Horm Behav 38:177-186.

Carlson BA, Hasan SM, Hollmann M, Miller DB, Harmon LJ, Arnegard ME (2011) Brain evolution triggers increased diversification of electric fishes. Science 332:583-586.

Chapman LJ, Chapman CA, OgutuOhwayo R, Chandler M, Kaufman L, Keiter AE (1996) Refugia for endangered fishes from an introduced predator in Lake Nabugabo, Uganda. Conserv Biol 10:554-561.

Fettiplace R, Fuchs PA (1999) Mechanisms of hair cell tuning. Annu Rev Physiol 61:809-834.

Feulner PGD, Plath M, Engelmann J, Kirschbaum F, Tiedemann R (2009) Magic trait electric organ discharge (EOD). Commun Integr Biol 2:329-331.

Frey JN, Ruhnau P, Weisz N (2015) Not so different after all: The same oscillatory processes support different types of attention. Brain Research doi:10.1016/j.brainres.2015.02.017.

Friedman MA, Hopkins CD (1996) Tracking individual mormyrid electric fish in the field using electric organ discharge waveforms. Anim Behav 51:391-407.

Friedman MA, Hopkins CD (1998) Neural substrates for species recognition in the time-coding electrosensory pathway of mormyrid electric fish. J Neurosci 18:1171-1185.

Graff C, Kramer B (1992) Trained weakly-electric fishes Pollimyrus isidori and Gnathonemus petersii (Mormyridae, Teleostei) discriminate between wave-forms of electric pulse discharges. Ethology 90:279-292.

Gross J, Hoogenboom N, Thut G, Schyns P, Panzeri S, Belin P, Garrod S (2013) Speech rhythms and multiplexed oscillatory sensory coding in the human brain. PLoS Biol 11:e1001752.

Hanika S, Kramer B (2005) Intra-male variability of its communication signal in the weakly electric fish, Marcusenius macrolepidotus (South African form), and possible functions. Behaviour 142:145-166.

Harder W (1968) Die beziehungen zwischen electrorezeptoren, elektrischem organ, seitenlinienorganen und nervensystem bei den Mormyridae (Teleostei, Pisces). Z Vgl Physiol 59:272-318. German.

Hopkins CD (1976) Stimulus filtering and electroreception - tuberous electroreceptors in three species of gymnotoid fish. J Comp Physiol 111:171-207.

Hopkins CD (1980) Evolution of electric communication channels of mormyrids. Behav Ecol Sociobiol 7:1-13.

Hopkins CD (1981) On the diversity of electric signals in a community of mormyrid electric fish in West-Africa. Am Zool 21:211-222.

Hopkins CD (1986) Behavior of Mormyridae. New York, NY: John WIley & Sons.

Hopkins CD, Bass AH (1981) Temporal coding of species recognition signals in an electric fish. Science 212:85-87.

Kawasaki M (2001) Cutaneous electrical oscillation in a weakly electric fish, Gymnarchus niloticus. J Comp Physiol A 187:597-604.

Kawasaki M (2005) Physiology of tuberous eletrosensory systems. In: Electroreception (Bullock TH, Hopkins CD, Popper AN, Fay RR, eds). New York: Springer.

Klug A, Borst JGG, Carlson BA, Kopp-Scheinpflug C, Klyachko VA, Xu-Friedman MA (2012) How do short-term changes at synapses fine-tune information processing? J Neurosci 32:14058-14063.

Lakatos P, O'Connell MN, Barczak A, Mills A, Javitt DC, Schroeder CE (2009) The leading sense: supramodal control of neurophysiological context by attention. Neuron 64:419-430.

Lavoue S (2012) Petrocephalus Marcusen, 1854 (Osteoglossomorpha: Mormyridae) of the Bangweulu-Mweru ecoregion (Luapula River system, Congo basin), with the description of a new species. J Nat Hist 46:2159-2178.

Lavoue S, Hopkins CD, Toham AK (2004) The Petrocephalus (Pisces, Osteoglossomorpha, Mormyridae) of Gabon, Central Africa, with the description of a new species. Zoosystema 26:511-535.

Lavoue S, Sullivan JP, Arnegard ME (2010) African weakly electric fishes of the genus Petrocephalus (Osteoglossomorpha: Mormyridae) of Odzala National Park, Republic of the Congo (Lekoli River, Congo River basin) with description of five new species. Zootaxa:1-52.

Lavoue S, Arnegard ME, Sullivan JP, Hopkins CD (2008) Petrocephalus of Odzala offer insights into evolutionary patterns of signal diversification in the Mormyridae, a family of weakly electrogenic fishes from Africa. J Physiology-Paris 102:322-339.

Llinas RR (2009) Inferior olive oscillation as the temporal basis for motricity and oscillatory reset as the basis for motor error correction. J Neurosci 162:797-804.

Lyons-Warren AM, Hollmann M, Carlson BA (2012) Sensory receptor diversity establishes a peripheral population code for stimulus duration at low intensities. J Exp Biol 215:2586-2600.

Lyons-Warren AM, Kohashi T, Mennerick S, Carlson BA (2013) Detection of submillisecond spike timing differences based on delay-line anticoincidence detection. J Neurophysiol 110:2295-2311.

Machnik P, Kramer B (2008) Female choice by electric pulse duration: attractiveness of the males' communication signal assessed by female bulldog fish, Marcusenius pongolensis (Mormyridae, Teleostei). J Exp Biol 211:1969-1977.

Moller P, Serrier J, Bowling D (1989) Electric organ discharge displays during social encounter in the weakly electric fish Brienomyrus niger L (Mormyridae). Ethology 82:177-191.

Neiman A, Russell DF (2001) Stochastic biperiodic oscillations in the electroreceptors of paddlefish. Phys Rev Lett 86:3443-3446.

Neiman AB, Russell DF (2011) Sensory coding in oscillatory electroreceptors of paddlefish. Chaos 21:047505.

Nichols JT, Griscom L (1917) Fresh-water fishes of the Congo basin obtained by the American Museum Congo expedition, 1909-1915. Bulletin of the American Museum of Natural History 37:653-756.

Post N, von der Emde G (1999) The "novelty response" in an electric fish: response properties and habituation. Physiol Behav 68:115-128.

Roth A, Szabo T (1972) The receptor potential and its functional relationship to nerve impulse analyzed in a sense organ by means of thermal and electrical stimuli. J Comp Physiol 80:285-308.

Rutherford MA, Roberts WM (2009) Spikes and membrane potential oscillations in hair cells generate periodic afferent activity in the frog sacculus. J Neurosci 29:10025-10037.

Sullivan JP, Lavoue S, Hopkins CD (2000) Molecular systematics of the African electric fishes (Mormyroidea : Teleostei) and a model for the evolution of their electric organs. J Exp Biol 203:665-683.

Thorne JD, Debener S (2014) Look now and hear what's coming: on the functional role of cross-modal phase reset. Hearing Res 307:144-152.

Thut G, Miniussi C, Gross J (2012) The functional importance of rhythmic activity in the brain. Curr Biol 22:R658-R663.

Viancour TA (1979) Electroreceptors of a weakly electric fish. 2. Individually tuned receptor oscillations. J Comp Physiol 133:327-338.

Watson D, Bastian J (1979) Frequency-response characteristics of electroreceptors in the weakly electric fish, Gymnotus carapo. J Comp Physiol 134:191-202.

Wehner R (1987) "Matched filters" - neural models of the external world. J Comp Physiol A 161:511-531.

Zar JH (1999) Biostatistical analysis, 4th Edition. Upper Saddle River, N.J.: Prentice Hall.

Chapter 5

Conclusions and future directions

SUMMARY AND SIGNIFICANCE

The temporal patterns of spikes play important information coding roles in sensory processing, motor control, and spatial navigation (Lestienne, 2001; Huxter et al., 2003; Tang et al., 2014). However, how neural circuits process these kinds of timing codes was not well understood. I addressed this question using a combination of behavior and *in vivo* electrophysiology in mormyrid weakly electric fishes. Some mormyrid species decode temporally patterned electric communication signals with midbrain neurons that are selective for particular time intervals (Carlson, 2009). In this dissertation, I demonstrated that short-term depression and temporal summation of excitation and inhibition contribute to single-neuron interval-selectivity. I showed that using only depression or only summation to establish interval-selectivity would result in less diversity in tuning properties across the population, which would presumably negatively impact the circuit's ability to detect behaviorally relevant variation in communication signals. I also showed that the responses of single interval-selective neurons were sensitive enough to be able to discriminate between a particular communication display produced by different individuals. Finally, I described how a subset of mormyrid species establishes temporal sensitivity at the periphery through ongoing electrical oscillations. These oscillations were most sensitive to timing patterns produced by only large groups of fish. A species with oscillating receptors also exhibited strong behavioral responses to group temporal patterns, suggesting that oscillating receptors may be specialized for detecting communication signals produced by a large group of conspecifics, which is a novel function for a sensory receptor. In summary, I have demonstrated how temporal pattern recognition can be mediated by excitatory-inhibitory interactions in central neurons, as well as a novel mechanism for temporal pattern recognition in the periphery.

FUTURE DIRECTIONS

EOD coding in ELp. Spiking knollenorgan electroreceptors use temporal multiplexing to encode communication signals. Electric organ discharge (EOD) waveform is encoded into spike-timing differences between receptors, which are then decoded by duration-selective neurons in the anterior exterolateral nucleus (ELa). Interpulse intervals (IPIs) are encoded into interspike intervals within receptors, which are then decoded by interval-selective neurons in the posterior exterolateral nucleus (ELp). ELa sends its only output to ELp, which means that information about IPI arriving in ELp has already been filtered for waveform. The ELa projections to ELp are topographical, suggesting the potential for some gradient in pulse duration coding in ELp (Friedman and Hopkins, 1998). To more fully understand central processing of electric communication signals, it will be necessary to understand how the responses of ELp neurons depend on pulse duration as well as IPI. *In vitro* calcium imaging of ELp responses to a range of pulse durations and IPIs would be the best approach to elucidate how population output reflects EOD waveform and IPI. Understanding how the combination of EOD and IPI are encoded is applicable to understanding how the knollenorgan pathway handles communication signals coming from more than one fish.

Cellular mechanisms underlying differences in excitatory and inhibitory effects in ELp. I have shown that ELp neurons receive excitation and inhibition with a range of strengths and durations, as well as degrees and time courses of short-term depression (Baker and Carlson, 2014). It remains to be determined whether these differences reflect presynaptic variation, postsynaptic variation, or some combination. In particular, ELp neurons exhibit large dendritic arbors (Xu-Friedman and Hopkins, 1999; George et al., 2011; Ma et al., 2013). It is becoming clear that dendritic structure can influence synaptic integration, such that the same temporal

pattern of inputs can have different postsynaptic effects depending on dendritic location (e.g., Branco and Hausser, 2011). Therefore, it will be interesting to determine how the observed differences in excitation and inhibition in high- and low-pass ELp neurons arise. For instance, is the longer onset inhibition in low-pass neurons due to asynchronous inputs that spread out in time, differences in postsynaptic GABA receptor properties, and/or differences in dendritic filtering? Do ion channel densities, kinetics, or composition vary along dendritic branches? GABA and glutamate uncaging experiments *in vitro* would be necessary to understand the contribution of dendritic filtering to IPI sensitivity in ELp.

Processing of electric communication signals downstream from ELp. ELp sends projections to the isthmic granule nucleus (IG), the subpraæeminential nucleus, the inferior olive, and the medioventral nucleus (MV). IG in turn sends a feedback projection to ELp. The medioventral nucleus is hypothesized to play a role in spatial analysis of communication signals (Haugede-Carre, 1979; Friedman and Hopkins, 1998), and the inferior olive is hypothesized to play a role in the timing and learning of motor output (De Zeeuw et al., 1998). However, how the targets of ELp contribute to the processing of communication signals is completely unknown.

The function of the IG-ELp feedback remains to be determined. One putative role for this pathway could be the modulation of ELp responses depending on social environment. For instance, modulation via IG could be a way for fish to selectively tune out or tune into signals coming from a particular individual when multiple signalers are present.

A general feature of sensory circuits is the parallel processing of information (Gasser and Erlanger, 1929; Nassi and Callaway, 2009; Recanzone and Cohen, 2010; Rossler and Brill, 2013). Furthermore, as information ascends within a pathway, it is represented by fewer neurons that are more selective for particular stimulus features (Barlow, 1972). Given these principles, I

hypothesize that at some stage in the electrosensory pathway, single neurons may be selective for different classes of communication signals, with some cells responding only to scallops, some only to accelerations, and some only to rasps. Furthermore, since EOD waveform can contain identifying information, higher-level neurons could even be selective for scallops from dominant males, who have longer EODs than submissive males, as just one example. *In vivo* electrophysiological recordings from downstream targets will be essential to understanding how the population code for EOD and IPI established in ELp is transformed and used to guide behavior.

Do fish use individually stereotyped scallops to recognize individuals? Scallop sequences are individually stereotyped (Serrier and Moller, 1989; Carlson and Hopkins, 2004), and here I have shown that single ELp neurons are sensitive to individual variation in scallop patterns. Whether fish use this information remains unknown. Each individual's EOD waveform is also stereotyped, and in some species, individuals can be identified on the basis of EOD alone (Crawford, 1992; Friedman and Hopkins, 1996). Therefore, combining the stereotyped EOD waveform with individually characteristic scallop patterns could facilitate individual recognition.

Scallops have been hypothesized to play a role in aggressive encounters (Carlson and Hopkins, 2004). We studied scallop detection in *Brienomyrus brachyistius*, which is highly territorial and aggressive. Territorial animals often respond more strongly to encounters with a stranger than with a known neighbor (Ydenberg et al., 1988). Therefore, advertising and recognizing individual identity could help prevent escalations between territorial neighbors that do not present a threat (Temeles, 1994). In mormyrids, the ability to use both EOD waveform and IPI patterns to gain information about the sender could facilitate neighbor-stranger recognition. Individual recognition could be tested in the lab by observing fish's reactions to a

known neighbor's electric signals and to a stranger's electric signals. Increased aggression towards communication signals from strangers would provide evidence for individual recognition. The separability of the EOD and IPI would allow further testing of the role of each component to such recognition.

Species recognition in species with rosette receptors. The stereotyped EOD waveform has been hypothesized to play a role in species recognition (reviewed in Baker et al., 2013). Species with broadly distributed receptors, which fire spikes in all species studied, have been shown to exhibit behavioral sensitivity to subtle EOD waveform variation (Carlson et al., 2011). In contrast, species with rosette receptors are behaviorally insensitive to EOD waveform variation (Carlson et al., 2011). In all species studied, rosette receptors produce continuously oscillating potentials that do not encode the timing cues necessary to resolve waveform variation (Chapter 4, Harder, 1968). Accordingly, these species also exhibit less variation in EOD waveform (Lavoue et al., 2008). Therefore, these fish must use other cues to recognize conspecifics, such as IPI (Carlson and Arnegard, 2011) or even vision. The lineage with rosette receptors evolved an enhanced visual system relative to other mormyrids (Stevens et al., 2013), and they tend to have black spots on their skin that may be species-specific (Lavoue et al., 2008; Lavoue et al., 2010). These findings suggest that species with oscillating receptors may rely more heavily on vision for species recognition than species with spiking receptors. Whether species with rosette receptors may use IPIs for species recognition could be tested by observing behavioral responses to playback of natural and shuffled IPI sequences recorded from conspecifics and heterospecifics. Whether these species may also or instead use vision for species recognition could be tested by observing behavioral responses to an electrically silenced conspecific or heterospecific behind a clear enclosure.

IPI coding in EL. Species with rosette receptors do not have ELa and ELp; instead, they have a smaller exterolateral (EL) region that is not subdivided (Carlson et al., 2011). How electric communication signals are processed in EL is completely unknown. ELa is distinguishable from ELp due to the abundance of heavily myelinated axons from the nucleus of the electrosensory lateral line lobe (nELL) that serve as delay lines to small cells (Friedman and Hopkins, 1998). Small cells integrate this delayed excitation with direct inhibition to establish selectivity for stimulus pulse duration (Friedman and Hopkins, 1998; Lyons-Warren et al., 2013). This processing contributes to fish's behavioral sensitivity to subtle EOD waveform variation (Carlson et al., 2011). In contrast, species with rosette receptors and EL cannot detect subtle waveform variation (Carlson et al., 2011), which is at least partly due to the fact that phase resets in oscillating receptors do not encode the timing cues necessary to resolve waveform variation (Chapter 4). Therefore, it is reasonable to conclude that EL likely lacks the axonal delay lines from nELL that contribute to duration selectivity. Whether EL contains large cells, small cells, and multipolar cells remains to be determined. However, since EL is smaller than ELa/ELp, species with EL may also be less sensitive to precise temporal patterns than species with ELp. Anatomical studies using tracers and immunohistochemistry will be necessary to reveal EL circuitry. Further, analysis of temporal patterns in the communication signals of species with EL will be necessary to determine whether they also use displays consisting of distinct IPI patterns.

Coevolution of sensory receptors and central pathways. In Chapter 4, I demonstrated that evolution of the perceptual ability to resolve slight EOD waveform variation was correlated with evolution of peripheral sensory physiology and central neuroanatomy. Receptor recordings from several additional species will be important for further understanding the coevolution of peripheral receptors and associated central neuroanatomy. Mormyrids can be subdivided into two

subfamilies, Mormyrinae and Petrocephalinae. All but two species in the Petrocephalinae subfamily have rosette receptors; the remaining two have broadly distributed receptors (Carlson et al., 2011). One of these two species, *Petrocephalus microphthalmus*, also has ELa/ELp, and I showed that its receptors also fire spikes, in line with other species with distributed receptors and ELa/ELp. *Petrocephalus zakoni* is the only other petrocephaline species known to have broadly distributed receptors; however, it also has the smaller, undivided EL midbrain region (Carlson et al., 2011). In addition, all known species in the genus *Myomyrus* (Mormyrinae subfamily) have an intermediate receptor distribution, with one cluster of receptors on each side of the head and several broadly distributed receptors, along with a smaller, undivided EL (Carlson et al., 2011). Whether *Myomyrus* spp. and *P. zakoni* are sensitive to EOD variation is unknown. Studies of EOD perception and receptor physiology in these species will be essential to more completely understanding the relationship between peripheral encoding, neuroanatomy, and perception.

CONCLUSIONS

In this thesis I have demonstrated two divergent mechanisms for temporal pattern recognition. One approach is to precisely encode timing patterns in the periphery and then use excitatory-inhibitory interactions in central neurons to extract behaviorally relevant temporal cues. An alternative approach is to use electrical oscillations to establish temporal pattern sensitivity in the periphery. Previously, the filtering of temporal information was thought to be a purely central processing problem. In my thesis I have shown that temporal pattern recognition can also arise from peripheral filtering through a novel oscillatory phase reset mechanism. These results are broadly relevant to understanding information processing, sensory coding, and the evolution of sensory circuits.

REFERENCES

Baker CA, Carlson BA (2014) Short-term depression, temporal summation, and onset inhibition shape interval tuning in midbrain neurons. J Neurosci 34:14272-14287.

Baker CA, Kohashi T, Lyons-Warren AM, Ma XF, Carlson BA (2013) Multiplexed temporal coding of electric communication signals in mormyrid fishes. J Exp Biol 216:2365-2379.

Barlow HB (1972) Single units and sensation: a neuron doctrine for perceptual psychology? Perception 1:371-394.

Branco T, Hausser M (2011) Synaptic integration gradients in single cortical pyramidal cell dendrites. Neuron 69:885-892.

Carlson BA (2009) Temporal-pattern recognition by single neurons in a sensory pathway devoted to social communication behavior. J Neurosci 29:9417-9428.

Carlson BA, Hopkins CD (2004) Stereotyped temporal patterns in electrical communication. Anim Behav 68:867-878.

Carlson BA, Arnegard ME (2011) Neural innovations and the diversification of African weakly electric fishes. Commun Integr Biol 4:720-725.

Carlson BA, Hasan SM, Hollmann M, Miller DB, Harmon LJ, Arnegard ME (2011) Brain evolution triggers increased diversification of electric fishes. Science 332:583-586.

Crawford JD (1992) Individual and sex specificity in the electric organ discharges of breeding mormyrid fish (Pollimyrus isidori). J Exp Biol 164:79-102.

De Zeeuw CI, Simpson JI, Hoogenraad CC, Galjart N, Koekkoek SKE, Ruigrok TJH (1998) Microcircuitry and function of the inferior olive. Trends Neurosci 21:391-400.

Friedman MA, Hopkins CD (1996) Tracking individual mormyrid electric fish in the field using electric organ discharge waveforms. Anim Behav 51:391-407.

Friedman MA, Hopkins CD (1998) Neural substrates for species recognition in the time-coding electrosensory pathway of mormyrid electric fish. J Neurosci 18:1171-1185.

Gasser HS, Erlanger J (1929) The role of fiber size in the establishment of a nerve block by pressure or cocaine. Am J Physiol 88:581-591.

George AA, Lyons-Warren AM, Ma X, Carlson BA (2011) A diversity of synaptic filters are created by temporal summation of excitation and inhibition. J Neurosci 31:14721-14734.

Harder W (1968) Die beziehungen zwischen electrorezeptoren, elektrischem organ, seitenlinienorganen und nervensystem bei den Mormyridae (Teleostei, Pisces). Z Vgl Physiol 59:272-318. German.

Haugede-Carre F (1979) Mesencephalic exterolateral posterior nucleus of the mormyrid fish Bryenomyrus Niger: efferent connections studied by the HRP method. Brain Res 178:179-184.

Huxter J, Burgess N, O'Keefe J (2003) Independent rate and temporal coding in hippocampal pyramidal cells. Nature 425:828-832.

Lavoue S, Sullivan JP, Arnegard ME (2010) African weakly electric fishes of the genus Petrocephalus (Osteoglossomorpha: Mormyridae) of Odzala National Park, Republic of the Congo (Lekoli River, Congo River basin) with description of five new species. Zootaxa:1-52.

Lavoue S, Arnegard ME, Sullivan JP, Hopkins CD (2008) Petrocephalus of Odzala offer insights into evolutionary patterns of signal diversification in the Mormyridae, a family of weakly electrogenic fishes from Africa. J Physiol-Paris 102:322-339.

Lestienne R (2001) Spike timing, synchronization and information processing on the sensory side of the central nervous system. Prog Neurobiol 65:545-591.

Lyons-Warren AM, Kohashi T, Mennerick S, Carlson BA (2013) Retrograde fluorescent labeling allows for targeted extracellular single-unit recording from identified neurons in vivo. J Vis Exp 76:e3921.

Ma XF, Kohashi T, Carlson BA (2013) Extensive excitatory network interactions shape temporal processing of communication signals in a model sensory system. J Neurophysiol 110:456-469.

Nassi JJ, Callaway EM (2009) Parallel processing strategies of the primate visual system. Nat Rev Neurosci 10:360-372.

Recanzone GH, Cohen YE (2010) Serial and parallel processing in the primate auditory cortex revisited. Behav Brain Res 206:1-7.

Rossler W, Brill MF (2013) Parallel processing in the honeybee olfactory pathway: structure, function, and evolution. J Comp Physiol A 199:981-996.

Serrier J, Moller P (1989) Patterns of electric organ discharge activity in the weakly electric fish Brienomyrus niger L. (Mormyridae). J Exp Biol 48:235-244.

Stevens JA, Sukhum KV, Carlson BA (2013) Independent evolution of visual and electrosensory specializations in different lineages of mormyrid electric fishes. Brain Behav Evolut 82:185-198.

Tang C, Chehayeb D, Srivastava K, Nemenman I, Sober SJ (2014) Millisecond-scale motor encoding in a cortical vocal area. PLoS Biology 12:e1002018.

Temeles EJ (1994) The role of neighbors in territorial systems: when are they "dear enemies"? Anim Behav 47:339-350.

Xu-Friedman MA, Hopkins CD (1999) Central mechanisms of temporal analysis in the knollenorgan pathway of mormyrid electric fish. J Exp Biol 202:1311-1318.

Ydenberg RC, Giraldeau LA, Falls JB (1988) Neighbors, strangers, and the asymmetric war of attrition. Anim Behav 36:343-347.